UNIVERSITY OF SOUTHAMPTON
FACULTY OF ENGINEERING, SCIENCE AND MATHEMATICS
SCHOOL OF ELECTRONICS AND COMPUTER SCIENCE

Adaptive Detection in Ultrawide Bandwidth Wireless Communication Systems

by

Qasim Zeeshan Ahmed
BE, MSc

A doctoral thesis submitted in partial fulfilment of the
requirements for the award of Doctor of Philosophy
at the University of Southampton

June 2009

SUPERVISOR: Doctor Lie-Liang Yang
BEng, MEng, PhD, Senior Member IEEE
School of Electronics and Computer Science
University of Southampton
Southampton SO17 1BJ
United Kingdom

𝔇edicated to my caring parent, younger brother and loving wife.

UNIVERSITY OF SOUTHAMPTON

FACULTY OF ENGINEERING AND APPLIED SCIENCE

SCHOOL OF ELECTRONICS AND COMPUTER SCIENCE

ABSTRACT

Doctor of Philosophy

Adaptive Detection in Ultrawide Bandwith Wireless Communication Systems

by Qasim Zeeshan Ahmed

The main motivation of this thesis is to design low-complexity high-efficiency pulse-based ultra-wide bandwidth (UWB) systems with reasonable bit-error-rate (BER) performance. The thesis starts with proposing a new pulse-based UWB system, namely the hybrid direct-sequence time-hopping (DS-TH) UWB system. This novel pulse-based UWB system is capable of inheriting the advantages of both the pure direct-sequence (DS)-UWB and pure time-hopping (TH)-UWB systems, while avoiding their disadvantages. Furthermore, this hybrid DS-TH UWB scheme can be easily converted to the pure DS-UWB or pure TH-UWB scheme. The BER performance of the hybrid DS-TH UWB systems employing either correlation or minimum mean-square error (MMSE) detection is investigated. From our studies it can be found that both the correlation and MMSE detectors have the capability to make use of the multipath diversity. The correlation detector does not have the capability to remove multiuser interference (MUI) and inter-symbol interference (ISI), while the MMSE detector is capable of mitigating efficiently both the ISI and MUI. While for single-user scenario the correlation detector is near-optimum and has low-complexity, it is shown that for multi-user scenarios the MMSE detector must be employed in order to achieve a reasonable BER performance. However, in this case the complexity of the hybrid DS-TH UWB system is found to be extreme. Furthermore, in order to implement MMSE detection, the signature waveforms, delays and complete channel knowledge of all the active users are required to be known by the receiver, which make the MMSE detection impractical. In practical channels obtaining the channel knowledge is highly challenging, since the received UWB signals usually consist of a huge number of resolvable multipaths and the energy conveyed by each resolvable multipath is usually very low.

In order to mitigate the above mentioned problems of the MMSE detection, then, in this thesis a range of training-based adaptive detectors are investigated in the context of the hybrid DS-TH UWB systems. In detail, in this thesis a brief introduction to the literature of adaptive detection is first provided, followed by the philosophies of least mean-square (LMS), normalised least-mean squares (NLMS) and recursive least square (RLS) algorithms. In our study decision directed (DD) approaches are also introduced to the adaptive detectors to improve the BER performance and spectral-efficiency

of the hybrid DS-TH UWB systems. Our studies show that the complexity of the adaptive LMS and adaptive NLMS detectors may be even lower than that of the conventional correlation detector. For the RLS adaptive detector, our studies show that, if it is initialised properly, it is capable of attaining a faster convergence rate than the LMS and NLMS adaptive detectors. In this case, the RLS adaptive detector requires less number of training bits, and hence provides higher spectral-efficiency than the LMS and NLMS adaptive detectors for the hybrid DS-TH UWB systems. Furthermore, the RLS adaptive detector is more robust and has more degrees of freedom than the LMS and NLMS adaptive detectors. However, the complexity of the RLS adaptive detector is still too high to be implemented in practical UWB systems.

In order to further reduce the complexity of the RLS adaptive detector, rank-reduction techniques are introduced. With the aid of reduced-rank techniques, the filter size can be efficiently reduced, which in turn reduces the number of parameters required to be estimated. Consequently, the convergence speed, tracking ability and robustness of the RLS adaptive detector can be improved. In this thesis, three classes of reduced-rank techniques are investigated associated with the RLS adaptive detector, which are derived based on the principles of principal components analysis (PCA), cross-spectral metric (CSM) and Taylor polynomial approximation (TPA), respectively. Our study and simulation results show that, given a sufficient rank of the detection subspace on which the RLS adaptive detector is operated, the reduced-rank RLS adaptive detector is capable of achieving a similar BER performance as the corresponding full-rank RLS adaptive detector, while with a detection complexity that is significantly lower than that of the full-rank RLS adaptive detector. Furthermore, our studies shown that the TPA-based reduced-rank RLS adaptive detector constitutes one of the highly efficient detection schemes for the pulse-based UWB systems. The TPA-based reduced-rank RLS adaptive detector is usually capable of attaining the full-rank BER performance with a very low rank, which is typically in the range of $5 - 8$, regardless of the system size in terms of the spreading factor, number of resolvable multipaths and the number of users supported by the UWB systems.

Finally, in this thesis we summarise our discoveries and provide discussion on the possible future research issues.

Acknowledgements

There are many people I would like to acknowledge for making my experience in the University of Southampton one of the most important and rewarding period of my life. First, I would like to thank my supervisor, Dr. Lie-Liang Yang, for his guidance and support through all these years. I am grateful to Prof. Sheng Chen for his discussion and comments on the issues about minimum bit error rate adaptive detection. I am also grateful to other faculty members and researchers of the department, in particular to Prof. Lajos Hanzo, Dr. Soon Xin Ng, Dr. Robert Maunder, Dr. Jos Akhtman, Dr. Osamah Alamri and Dr. Wei Liu, who have made my learning experience at the University of Southampton more than enjoyable. I am also thankful to Denise Harvey for her patience and help on various administrative issues.

I also owe many personal thanks to all my other colleagues in the Communications Research Group, particularly to Dr. Andreas Wolfgang, Dr. Sohail Ahmed, Dr. Bin Hu and Dr. Ming Jiang, for their help. I am also deeply indebted to many friends of mine both in and outside Southampton for sharing my joys and sorrows.

The financial support by the Ministry of Sciences and Technology (MOST), Pakistan, is gratefully acknowledged.

I would like to thank my beloved parents for their continued love, their unfailing support and their understanding. I am also grateful to my elder sister and younger brother for their support and taking care of me. Special thanks to my wife for her love and support. Finally, I appreciate all my teachers and friends who made my life more colourful and enjoyable.

Declaration of Authorship

I, **Qasim Zeeshan Ahmed**,
declare that the thesis entitled

Adaptive Detection in Ultrawide Bandwidth Wireless Communication Systems

and the work presented in this thesis are both my own, and have been generated by me as the results of my own original research. I confirm that:

- this work was done wholly or mainly while in candidature for a research degree at this University;
- where any part of this thesis has previously been submitted for a degree or any other qualification at this University or any other institution, this has been clearly stated;
- where I have consulted the published work if others, this is always clearly attributed;
- where I have quoted form the work of others, the source is always given. With the exception of such quotations, this thesis is entirely my own work;
- I have acknowledged all main sources of help;
- where the thesis is based on work done by myself jointly with others, I have made clear exactly what was done by others and what I have contributed myself;
- parts of this work have been published, as seen in List of Publications.

Signed: .....
Dated: .....

List of Publications

1) **Q. Z. Ahmed** and L.-L. Yang, "Performance of hybrid direct-sequence time-hopping ultrawide bandwidth systems in nakagami-m fading channels," in *IEEE 18th International Symposium on Personal, Indoor and Mobile Radio Communications, PIMRC*, (Athens, Greece), pp. 1–5, Sept. 2007.

2) **Q. Z. Ahmed**, W. Liu and L.-L. Yang, "Least Mean Square Aided Adaptive Detection in Hybrid Direct-Sequence Time-Hopping Ultrawide Bandwidth Systems," in *IEEE 67th Vehicular Technology Conference, VTC-Spring*, (Marina Bay, Singapore), pp. 1–5, May 2008.

3) **Q. Z. Ahmed** and L.-L. Yang, "Reduced-rank detection for hybrid direct-sequence time- hopping UWB systems in nakagami-m fading channels," in *IEEE 68th Vehicular Technology Conference, VTC-Fall*, (Calgary, Canada), pp. 1–5, Sept. 2008.

4) **Q. Z. Ahmed** and L.-L. Yang, "Normalised Least Mean-Square Aided Decision-Directed Adaptive Detection in Hybrid Direct-Sequence Time-Hopping UWB Systems," in *IEEE 68th Vehicular Technology Conference, VTC-Fall*, (Calgary, Canada), pp. 1–5, Sept. 2008.

5) **Q. Z. Ahmed** and L.-L. Yang, "Low-Complexity Reduced-Rank Adaptive Detection in Hybrid Direct-Sequence Time-Hopping Ultrawide Bandwidth System," appearing in *IEEE 69th Vehicular Technology Conference, VTC-Spring*, (Barcelona, Spain), pp. 1–5, April. 2009.

6) **Q. Z. Ahmed** and L.-L. Yang and S. Cheng, "Low-Complexity Reduced-Rank Adaptive Detection in Hybrid Direct-Sequence Time-Hopping Ultrawide Bandwidth System," appearing in *IEEE International Conference in Communications, ICC*, (Dresden, Germany), pp. 1–5, May. 2009.

7) R. A. Riaz, M. El-Hajjar, **Q. Z. Ahmed**, S. Cheng and L. Hanzo, "Convergence Analysis of Iteratively Detected Time-Hopping and DS-CDMA Ultrawide Bandwidth Systems by EXIT Charts," in *IEEE 67th Vehicular Technology Conference, VTC-Spring*, (Marina Bay, Singapore), pp. 1127–1131, May 2008.

8) R. A. Riaz, M. El-Hajjar, **Q. Z. Ahmed**, S. Cheng and L. Hanzo, "EXIT Chart Aided Design of DS-CDMA UltraWideBand Systems Using Iterative Decoding," in *IEEE 68th Vehicular Technology Conference, VTC-Fall*, (Calgary, Canada), pp. 1–5, Sept. 2008.

9) **Q. Z. Ahmed** and L.-L. Yang, "Performance of Hybrid Direct-Sequence Time-Hopping Ultrawide Bandwidth Systems Employing Adaptive Multiuser Detection," submitted to *IET Communications*.

10) **Q. Z. Ahmed** and L.-L. Yang, "Reduced-rank adaptive detection in Hybrid Direct-Sequence Time-Hopping Ultrawide Bandwidth Systems," submitted to *IEEE Transactions on Wireless Communications* (Revised).

11) **Q. Z. Ahmed** and L.-L. Yang and S. Cheng, "Minimum Bit error rate detector for Hybrid Direct-Sequence Time-Hopping Ultrawide Bandwidth Systems," to be submitted to *IEEE Transactions on Wireless Communications*.

List of Symbols

General Notation

- $\boldsymbol{A}^*$: Complex Conjugate of matrix $\boldsymbol{A}$.
- $\boldsymbol{A}^T$: Transpose of the matrix $\boldsymbol{A}$.
- $\boldsymbol{A}^H$: Hermitian of the matrix $\boldsymbol{A}$.
- $\hat{\boldsymbol{x}}$: Estimate of x.
- $\Re(x)$: Real part of x.

List of Symbols

$\psi(t)$: Basic signal pulse waveform.

T_ψ: Duration of basic signal pulse or width of time-slot.

E_ψ: Energy of basic signal pulse.

$S_\psi(f)$: Normalised power spectral density of basic signal pulse.

E_b: Energy per bit.

$\gamma_\psi(\tau)$: Normalized auto-correlation function of basic signal pulse.

$b_i^{(k)}$: The ith data bit transmitted by user k.

N_c: Number of chips per bit or DS spreading factor.

N_ψ: Number of time-slots per chip or TH spreading factor.

K: Total number of active users.

T_c: Chip duration.

T_b: Bit duration.

$s^{(k)}(t)$: Transmitted signal of the kth user.

$[d_0^{(k)}, d_1^{(k)}, \cdots, d_{N_c-1}^{(k)}]$: DS spreading sequence assigned to the kth user.

$[c_0^{(k)}, c_1^{(k)}, \cdots, c_{N_\psi-1}^{(k)}]$: TH-pattern assigned to the kth user.

N_0: Single-sided power spectral density of Additive white Gaussian noise (AWGN).

$\psi_{rec}(t)$: Received time-domain pulse waveform.

$r(t)$: Received signal.

$n(t)$: Additive white Gaussian noise (AWGN).

$\boldsymbol{y}_i$: Received observation vector.

σ^2: Noise variance.

$\boldsymbol{C}_k$: Spreading matrix of the k user.

$\boldsymbol{C}_i^{(k)}$: Spreading matrix corresponding to the ith bit of the kth user.

$\boldsymbol{H}_k$: Channel matrix of the kth user.

$\boldsymbol{w}_k$: Optimum weight vector of the kth user.

$\boldsymbol{R}_{y_i}$: Auto-correlation matrix of the $\boldsymbol{y}_i$.

$\boldsymbol{r}_{y_i b_i}$: Cross-correlation vector between the $\boldsymbol{y}_i$ and b_i.

γ_i: Signal to interference noise ratio.

L: Number of resolvable multipaths.

Λ: Cluster arrival rate in UWB channels.

λ: Ray arrival rate in UWB channels.

Γ: Cluster decay factor in UWB channels.

γ: Ray decay factor in UWB channels.

$h(t)$: Channel impulse response.

μ: Step-size for adaptive algorithms.

λ_{RLS}: Forgetting factor of RLS adaptive detector.

δ_{RLS}: Initialisation constant of RLS adaptive detector.

Contents

Chapter 1

Introduction

1.1 Research Background and Motivation

With the development of consumer electronics, personal computing and wireless communications, people have become more and more interested in connecting together different devices to form a network [1–5]. For example, a personal area network (PAN) can now easily be formed by using cables to connect all the devices, in order to achieve communications between them. However, in the cable-connected networks the mobility, flexibility and scalability of the connected devices are very low, since the devices are required to be connected at particular positions with special interface plugs [5]. For this sake, in recent years wireless techniques have drawn great attention for implementation of certain networks in order to improve their mobility, flexibility and scalability. Among the various wireless techniques, UWB technique is the one which has been proposed for future short-range indoor wireless communications [1, 6–8], in order to achieve the integration of consumer electronics, personal computing and mobile devices [1–5]. Specifically, the applications of the UWB techniques can be broadly divided into the following three categories.

- **High data rate (HDR) services:** For supporting HDR services, the UWB systems are expected to support a data rate in the range from 110 Mbps to more than 1 Gbps [5, 6]. The HDR UWB systems are operated in the frequency band from 3.1 GHz to 10.6 GHz. They can be built at low-cost with a coverage range less than 10 m. The major applications of the HDR UWB systems include file transfer, video streaming, high quality audio streaming, etc. Recently, Orthogonal Frequency-Division Multiplexing (OFDM)- based UWB schemes have been adopted for providing HDR services [3, 6].

- **Low data rate (LDR) services:** When considering LDR services, low complexity and low power consumption are usually the main concern of the UWB systems. In this type of UWB systems, the amount of data transfered is usually very small, while the battery life of the devices is of great importance [6, 9]. The LDR applications of UWB include wireless sensor networks and tagging [10,11], as well as the communications scenarios where, exact location is particular significant [11]. It has been recognized that the pulsed-based UWB schemes are well suitable for the LDR applications [6].

- **Imaging:** Imaging is also one of the major applications of UWB systems. The major characteristics of imaging include accurate ranging and high-precision geolocation. The applications of UWB systems for imaging include ground penetration radar, through and in-wall imaging, security devices, etc. [6,12]. These applications are suitable for providing alternatives for some harsh environments, where global positioning system (GPS) fails [6]. Additionally, the UWB techniques can provide imaging applications for medical instruments, such as x-rays and body screening scans.

Although the research for the theory and applications of UWB communications has been carried out for many years, however, design of a practical UWB system still faces a lot of challenges. Specifically, when designing UWB systems demanding high spectral-efficiency and high flexibility, the following issues should be considered with emphasis.

- In UWB communications, a low-complexity receiver that is capable of achieving a reasonable bit-error-rate (BER) performance is highly important, since UWB devices are usually required to be simple and light weight. In UWB communications, the multipath delay profile (MDP) is generally sparse [13], resulting in that a large number of low-power resolvable multipaths are required to be processed at the receiver, in order to make the UWB radio energy-efficient and achieve a good BER performance. The UWB receivers are required to be able to mitigate efficiently the ISI. They are required to be efficient when the UWB system supports multiple users, which generate MUI. Furthermore, the UWB receivers are expected to be able to cope with the interfering signals generated by the other existing UWB systems, narrowband and wideband interferers;

- In UWB communications channel estimation becomes highly challenging [14], not only because the number of resolvable multipaths is high, but also because each multipath channel conveys very low power. Furthermore, the number of parameters, such as delays, amplitudes,

phases, etc. associated with each resolvable multipaths, required to be estimated at the receiver is extremely high, which makes the channel estimation unaffordably complex for a low-complexity UWB device;

- Since UWB signals usually have very wide bandwidth, they are unavoidably overlapping with the other existing radios. Hence, the interference inflicted by the UWB systems on the existing wireless systems operated in the same frequency-band should be as low as possible;

- Synchronization is another major issue for UWB systems. The huge bandwidth of the UWB signals make them have a fine time resolution, which results in that a large space is required to be searched during the synchronization stage. Generally, an UWB system requires a fast and accurate synchronization step. However, due to the large search space, low power constraint, huge number of low-power multipaths and very low duty cycle, the synchronization process in UWB communications becomes slow and complicated. In addition to the above-mentioned synchronization issues, in UWB systems a very fast analog-to-digital converter (ADC) is also required to sample the received signals constituted by nano-second pulses, which also makes the implementation of UWB system highly challenging [15];

- Finally, in UWB communications the characteristics of the basic UWB pulses are much more complicated than that of the basic pulses used in narrowband systems. The basic UWB pulses characteristics strongly affect the design of transmitter and receiver filters, signal bandwidth, BER performance of the UWB system in Gaussian and/or multipath fading environments.

Due to the above-mentioned issues, this thesis motivates to propose and investigate a generalized pulse-based UWB scheme, namely the hybrid direct-sequence time-hopping UWB (DS-TH UWB) system. As our forthcoming discourse shown, both the pure direct-sequence UWB (DS-UWB) and time-hopping UWB (TH-UWB) constitute special examples of our proposed hybrid DS-TH UWB scheme. In this thesis, we focus on studying the achievable performance of the hybrid DS-TH UWB systems, when the UWB systems are operated in Gaussian or multipath fading environments. We motivate to design the low-complexity receivers for the hybrid DS-TH UWB systems. These low-complexity receivers are expected to be free from channel estimation and are operated without requiring the knowledge, such as the number of resolvable multipaths, the multipaths' strength, etc. Furthermore, these low-complexity receivers are expected to be capable of achieving a reasonable BER performance in the presence of MUI and ISI, when communicating over UWB channels. To be more specific, the work carried out in this thesis can be summarised as follows.

1.2 Thesis Outline

In this thesis, pulse-based UWB systems, namely the pure TH-UWB, pure DS-UWB and hybrid DS-TH-UWB systems are investigated. The thesis is structured as follows:

- **Chapter 2:** In this chapter an overview is provided for the various UWB systems in the context of their advantages and disadvantages. Specifically, the UWB systems reviewed include the TH-UWB, DS-UWB, multiband OFDM-UWB, etc. Additionally, in this chapter the time-domain pulses proposed for UWB communications are reviewed and their characteristics are compared. The stochastic tapped-delay-line (STDL) channel propagation model for modelling UWB indoor channels is analyzed. The differences between the UWB channels and the conventional narrowband/wideband channels are addressed. Furthermore, the Saleh-Valenzuela (S-V) channel model for UWB indoor wireless communications is discussed in detail. Note that, in this thesis the S-V UWB indoor channel model is invoked for the BER performance evaluation of the various pulse-based UWB systems in the following chapters.

- **Chapter 3:** Since both the TH-UWB and DS-UWB schemes have their unique advantages and disadvantages, a hybrid DS-TH UWB scheme using both DS spreading and TH is proposed in Chapter 3, in order to take the advantages of both the DS-UWB and TH-UWB schemes, while avoiding simultaneously their disadvantages. It can be shown that the hybrid DS-TH UWB systems are capable of providing more degrees-of-freedom than the pure DS-UWB or pure TH-UWB systems. Specifically, in this chapter the error performance of the hybrid DS-TH UWB systems is investigated associated with various low-complexity detection schemes, which include the conventional correlation detector and minimum mean-square error (MMSE) detector, respectively, when communicating over UWB indoor wireless channels. The complexity of the hybrid DS-TH UWB systems employing both the correlation detector and MMSE detector are analyzed. From the simulation results obtained in this chapter, we can find that there is a trade-off between the DS spreading and TH spreading invoked in the hybrid DS-TH UWB systems, especially, when the single-user correlation detector is considered. The best BER performance of a hybrid DS-TH UWB system can be achieved by appropriately choosing the DS and TH spreading factors. Furthermore, when the hybrid DS-TH UWB systems support multiple users, multiuser receiver, such as MMSE receiver, is required for enhancing the BER performance, but at a cost of increase of system complexity.

- **Chapter 4:** In this chapter we first demonstrate that the MMSE multiuser detector is difficult to be implemented practically in a pulse-based UWB system, due to its high computational complexity and requiring that the receiver has the ideal knowledge about the channel state information (CSI) associated with all the users as well as the spreading sequences of all the users, which may not be available in practical communication environments. For this sake, in this chapter we propose to employ adaptive detection for the pulse-based UWB systems with the aid of training sequences. In this chapter different training-based adaptive detectors are proposed and also studied in the context of different UWB systems. Specifically, the adaptive detectors based on the algorithms of least mean-square (LMS), normalised least mean-squares (NLMS) and recursive least-square (RLS), etc., are investigated in conjuction with the hybrid DS-TH UWB systems. Furthermore, in this chapter the complexity of these adaptive detectors are analyzed when considering communications over UWB channels.

- **Chapter 5:** Since in UWB systems a high spreading factor might be used and since there usually exists a large number of multipaths in UWB channels, the filter length of the adaptive detectors considered in Chapter 4 may hence be very long, yielding high complexity of detection. Furthermore, according to the adaptive filtering theory, a large number of filter taps makes the convergence of an adaptive filter slow [16]. Therefore, in this chapter rank-reduction techniques are employed for further reducing the complexity of detection in UWB systems, in order to make the UWB systems practically implementable. Specifically, in this chapter three classes of reduced-rank techniques are investigated, which are derived based on the principles of principal components analysis (PCA), cross-spectral metric (CSM) and Taylor polynomial approximation (TPA), respectively. Our study and simulation results in this chapter show that, given a sufficiently high rank of the detection subspace, the above-mentioned reduced-rank detection schemes are capable of achieving a similar BER performance as the corresponding full-rank detection scheme, while with a detection complexity that is significantly lower than that of the full-rank detection scheme. Furthermore, it can be shown that the TPA-based reduced-rank detection scheme results in a better BER performance than the PCA- or CSM- assisted reduced-rank detection, when the same rank of detection subspace is assumed, provided that the rank of the detection subspace is lower than that of the signal subspace, as defined in Chapter 5.

- **Chapter 6:** Finally, in Chapter 6 we summarise our conclusions obtained in this thesis and present possible future research directions.

1.3 Novel Contributions

The novel contributions of this thesis can be summarised as follows.

- A hybrid DS-TH UWB scheme is proposed for the pulse-based UWB systems. This novel pulse-based UWB scheme is capable of inheriting the advantages of both the pure DS-UWB and pure TH-UWB schemes, while simultaneously circumventing their disadvantages. Furthermore, it can be shown that the hybrid DS-TH UWB scheme is capable of providing more degrees-of-freedom than the pure DS-UWB or pure TH-UWB system. The increased degrees-of-freedom of the hybrid DS-TH UWB can be exploited for enhancing the UWB system's performance and/or for providing flexibility for design and reconfiguration of UWB systems. In this thesis one of our major objectives is to design low-complexity detectors with acceptable detection performance in UWB communications. Therefore, in this thesis the detection schemes considered are the low-complexity detection schemes, which are the single-user correlation detector and minimum mean square error multiuser detectors (MMSE-MUD).

  - **Single-User Correlation Detector:** It has the lowest complexity. However, when it is employed for detection in UWB systems, the complexity of the correlation detector increases at least linearly with the number of multipaths collected at receiver. Furthermore, as the number of users increases, the BER performance of the UWB systems using correlation detector becomes worse, as the correlation detector does not have the capability to mitigate MUI and ISI. However, given the channel conditions, signal-to-noise ratio (SNR) value and the total spreading factor, there exist optimum combinations of DS and TH spreading factors, which result in that the hybrid DS-TH UWB system achieves the lowest BER.

  - **Multiuser MMSE Detector:** MMSE detector is one of the multiuser detectors, which has a higher complexity than the correlation detector. The complexity of the MMSE detector can be maintained to be a constant, since the MMSE detector has the ability to combine automatically all the multipaths falling in the same window. Furthermore, the MMSE detector has the capability to mitigate both the MUI and ISI. Our study in this thesis shows that the BER performance of the pure DS-UWB, pure TH-UWB and hybrid DS-TH UWB systems is similar, when the MMSE detector assuming ideal CSI and signature codes is employed.

- Generally, ideal channel knowledge is very hard to acquire in the pulse-based UWB commu-

nications systems, since the received UWB signals are usually constituted by many multipath components and each multipath component conveys very low energy. Furthermore, the complexity of the MMSE detector is mainly determined by the inversion opeartion of the autocorrelation matrix, which might be very large due to the employment of a high spreading factor and existance of a large number of multipaths. According to the principles of adaptive filtering, adaptive detectors may be employed for solving the complexity issue in UWB systems, since the adaptive detectors can be operated without requiring to invert the autocorrelation matrix. Furthermore, with the help of training sequences, the adaptive detectors can also be operated without requiring the knowledge about the user signatures as well as the UWB channels. Therefore, in Chapter 4 a range of adaptive detectors operated based on the principles of LMS, NLMS and RLS are proposed and investigated in the context of the pulse-based UWB systems. The performance of the adaptive detectors are investigated and compared in terms of their convergence speed, BER performance, robustness and computational complexity. From our study and performance results, the following main conclusions can be derived.

- **LMS-Aided Adaptive Detector:** The complexity of the LMS-aided adaptive detector is lower than that of the RAKE-receiver. The BER performance of the LMS-aided adaptive detector at higher SNR value is similar as that of the ideal MMSE detector, which employs perfect CSI. However, the LMS-aided adaptive detector does not perform well in the low SNR region. In comparison with the NLMS- and RLS-aided adaptive detectors, our study shows that the LMS-aided adaptive detector has a relatively lower convergence speed.
- **NLMS-Aided Adaptive Detector:** The NLMS-aided adaptive detector has a slightly higher complexity than the LMS-aided adaptive detector. However, its complexity is still lower than that of the RAKE receiver. By contrast, the BER performance of the NLMS-aided adaptive detector is better than that of the LMS-aided adaptive detector. Furthermore, the NLMS-aided adaptive detector is more robust to noise amplification problem than the LMS-aided adaptive detector. Additionally, the NLMS-aided adaptive detector converges faster than the LMS-aided adaptive detector.
- **RLS-Aided Adaptive Detector:** The RLS-aided adaptive detector has lower complexity than the MMSE-MUD using full channel knowledge, but has significantly higher complexity than the single-user RAKE receiver. Our study and performance results show that the BER performance of the RLS-aided adaptive detector is much better than the LMS- or NLMS-aided adaptive detector. Furthermore, the RLS-aided adaptive detec-

tor has more degrees-of-freedom than the LMS- or NLMS-aided adaptive detector. These degrees-of-freedom may be used for controlling the convergence rate and the mean square error (MSE) of the RLS-aided adaptive detector. It can be shown that the RLS-aided adaptive detector is generally more robust and also converges faster than the LMS- and NLMS-aided adaptive detectors.

- Finally, in this thesis reduced-rank techniques are proposed and investigated in the context of the adaptive detectors for the hybrid DS-TH UWB systems. It can be shown that the reduced-rank techniques are capable of providing a flexible trade-off between the achievable BER performance and the computational complexity. Specifically, the effects of the reduced-rank techniques on the performance of the hybrid DS-TH UWB systems can be summarised as follows.

  - **Convergence Speed:** For the training-based adaptive detectors, it is desirable that the convergence speed is high, so that the overhead incurred for the training could be minimised. As analysed previously, in pulse-based UWB systems, the length of the adaptive detector affects the convergence speed: the convergence speed increases as the length of the adaptive filter becomes short. When the reduced-rank techniques are employed, the length of the adaptive filters can be shortened. Hence, employing the reduced-rank techniques may enhance the convergence speed of the adaptive filters invoked. Furthermore, faster convergence results in shorter training sequences, hence enhancing the spectral-efficiency of the UWB systems.

  - **BER Performance:** In conventional adaptive detectors, there exists a trade-off between the convergence speed and the MSE achieved, where higher convergence speed usually leads to higher MSE and ultimately results in worse BER performance. As above-mentioned, applying reduced-rank techniques enhances the convergence speed of the adaptive detectors. However, in the reduced-rank adaptive detectors faster convergence usually does not lead to higher MSE value. The reduced-rank adaptive detectors are capable of achieving the same MSE performance as the adaptive detectors without using reduced-rank techniques. Furthermore, the reduced-rank adaptive detectors are capable of achieving similar BER performance as the full-rank adaptive detectors.

  - **Robustness:** With the employment of reduced-rank detections, the number of parameters to be estimated is reduced. Hence, the reduced-rank adaptive detectors are more robust to MUI and ISI than the conventional adaptive detectors without using reduced-rank techniques.

- **Computational Complexity:** The number of parameters need to be updated in a reduced-rank adaptive detector is significantly lower than that of a corresponding conventional adaptive detector. Hence, the complexity of the adaptive detector may be reduced by employment of reduced-rank techniques.

In this thesis, a range of reduced-rank schemes are investigated, which are derived based on the principles of PCA, CSM and TPA, respectively. From our study and simulation results, we can have the following observations.

- **Principal Component Analysis (PCA):** PCA is derived based on the eigen-decomposition technique. In this technique, U, which is a value that may be significantly lower than the rank of the original observation space, eigenvectors corresponding to the U number of largest eigen-values of the autocorrelation matrix concerned are used to form a detection subspace. Our study shows that, if the rank U of the detection subspace is lower than the rank of the signal subspace determined by the number of signals invoked, BER floors are likely to occur. However, when the rank U of the detection subspace reaches the rank of the signal subspace, full-rank BER performance of the UWB systems can be achieved.
- **Cross Spectral Metric (CSM):** CSM is also derived based on the eigen-decomposition technique. Our study and simulation result show that, if the rank U of the detection subspace is lower than the rank of the signal subspace, the CSM-based rank-reduction scheme outperforms the PCA-based rank-reduction scheme. However, CSM-based reduced-rank adaptive detectors cannot approach the BER performance of the corresponding full-rank adaptive detector. This performance loss is mainly the result of time-varying channels, since in this case the detection subspace cannot be updated correspondingly with the time-varying channels.
- **Taylor Polynomial Approximation (TPA):** The TPA-based reduced-rank scheme does not depend on the eigen-decomposition and can achieve a similar BER performance as a corresponding full-rank scheme with a rank that is significantly lower than that of signal subspace. Given a rank of the detection subspace, the TPA-based reduced-rank scheme is usually capable of achieving the lowest BER among the three types of reduced-rank schemes considered. Furthermore, the implementation complexity of the TPA-based reduced-rank scheme does not scale with the size of the UWB system, including the total spreading factor and the number of users supported.

Chapter 2

Overview of Ultrawide Bandwidth Communications and Systems

Channel capacity of a communications system depends on the bandwidth occupied and the signal-to-noise ratio SNR achieved at the receiver. According to Shannon [17], channel capacity increases linearly with the increase of bandwidth but increases only logarithmically with the increase of SNR. Furthermore, according to [18], the channel capacity increases linearly with the SNR, if the channel bandwidth is infinite. Therefore, in order to achieve a higher channel capacity without incurring a higher SNR, wider bandwidth can be employed by the communications systems. For this sake, in recent years a lot of attention in wireless communications has been drawn to the UWB communications, where the instantaneous bandwidth is significantly higher than the minimum bandwidth required to deliver the information [1, 19]. According to the Federal Communications Commission (FCC) in the United States [1, 7, 8, 19], a wireless system can be referred to as an UWB system, either when the frequency bandwidth of the system is at least 20 percent of the center frequency, or when the system's frequency bandwidth is higher than 500 megahertz (MHz) and the center frequency is above 6 gigahertz (GHz).

In recent years UWB techniques have drawn a lot of interest in both research and industry communities [1, 3, 7, 8]. The potential strength of UWB techniques lies in their use of extremely wide transmission bandwidth, which results in that the UWB radios employ a range of merits when compared against the conventional narrowband and wideband radios. Specifically, the UWB radios employ the merits, such as, accurate position location and ranging [7, 10, 20–22], lack of significant fading [13, 23], high multiple-access capability [24], high data rate [13, 19, 21], covert communica-

tions [19, 23, 25, 26], possibly easier material penetration [24, 27, 28], etc. However, due to the highly dispersive UWB channels, UWB communications may be mainly suitable for short-range communications, such as for applications in wireless sensor networks (WSN) and PAN [29]. One of the major applications of UWB techniques is for alleviating the problem of increasingly scarce spectrum resources by re-using the spectrum already allocated to the other systems without degrading their quality-of-services (QoS) noticeably [30].

2.1 A Brief History of UWB Communications

The history of UWB communications goes back to the first wireless transmission made on 12 December 1901 by Marconi with the help of a Spark Gap Emitter, which actually generated UWB signals, as the instantaneous bandwidth of the sparks was significantly higher than the data rate transmitted [1, 31, 32]. However, the actual work in UWB communications was not started until the early 1960s. The research of UWB communications in 1960s was led by Harmuth at Catholic University in America, Ross and Robins at Sperry Rand Corporation and van Etten at the United States Air Force (USAF) Rome Air Development Center [1, 33]. In UWB communications, matched-filtering (MF) was first introduced by Harmuth, Ross and Robbins [33] and the UWB was referred to as baseband radio [1]. The system design and antenna concept were developed based on Van Etten's empirical testing [33]. The fundamental concept in UWB communications was to characterize the UWB system as a linear time-invariant (LTI) system with the aid of time-domain response rather than frequency-domain response. However, until 1960, there was no convenient means to observe and measure the waveforms that had a duration of sub-nanoseconds [31]. The major break through in UWB communications was achieved, when the sampling oscilloscope was invented by Tektronix and Hewlett-Packard in 1960s [1,31,33]. The sampling oscilloscope helped to display and integrate UWB signals, which made it possible to design simple circuits necessary for generation of sub-nanosecond pulses [1, 33]. During the same period, in Lawrence Livermore National Laboratories (LLNL) and Los Alamos National Laboratories (LANL) research in pulse transmitters, receivers and antennas was performed [33]. In 1970s the basic design for UWB systems was available along with the design of the basic components such as, pulse train generator, pulse train modulator, pulse receiver and wideband antennas, etc. However, the commercial success for UWB communications did not come into practice until 1974, when Moray designed an impulse radar, which was capable of penetrating the ground and was used by Geophysical Survey System [33]. In 1994, McEwan at LLNL developed the first Micropower Impulse Radar, which was a compact, inexpensive and low-power UWB

system [1, 33].

According to literature, UWB systems can be implemented by pulse-based or multi-carrier-based techniques. In the forthcoming section, a brief discussion of these two approaches is provided.

2.2 Pulse-Based UWB System

Pulse-based UWB system is also referred to as an impulse radio [34]. It is a carrier-less or a base-band modulation system, where signals are transmitted with the assistance of trains of time-shifted pulses [1, 34, 35]. As the pulse-duration of UWB signals is on the order of nano-seconds (ns), the bandwidth occupied by the pulse-based UWB signals transmitted is typically several GHz. In UWB communications, pulses should be designed properly in order to improve the efficiency of communications. Hence, the basic pulses proposed in literature are reviewed in Section 2.2.1. In this Section the basic requirements for the UWB pulses are also discussed. In Section 2.2.2 different types of UWB pulses are analyzed, which include the Gaussian pulses (GP), Traingular enveloped sinusoidal monocycle (TESM), pulses based on Prolate spheroidal (PS) functions, Modified hermite polynomial based pulses (HP) and Gaussian modulated sinusoidal pulses (GMSP). Section 2.2.3 presents the typical UWB signals transmitted. In Section 2.2.4 we discuss the advantages and disadvantages of different types of modulation schemes that may be employed by UWB systems. Finally, in Section 2.2.5 different kinds of multiple access (MA) schemes available for pulse-based UWB system are considered. Let us first review the basic pulses for UWB communications.

2.2.1 Basic Signal Pulses for UWB Communications

The basic UWB signal pulse $\psi(t)$ is usually defined in the time-domain. Let the duration or the width of the pulse be T_ψ. It has been found that the UWB system's performance is related to the width T_ψ of the basic pulse and the performance usually degrades, when the pulse width increases [36]. This is mainly because, when using a wider pulse, the corresponding UWB system may suffer higher interference from narrowband systems, if there are narrowband systems overlaying with the UWB systems. For example, a Gaussian pulse with $T_\psi = 1$ ns has a center frequency of 1 GHz, while a Gaussian pulse with $T_\psi = 2$ ns has only a center frequency of 500 MHz. In this case, when decreasing the pulse duration T_ψ, the UWB spectrum moves towards higher frequencies, which eventually expand beyond the range of the interfering frequencies [36]. Let the energy of a basic signal pulse is denoted by E_ψ, which is given by

$$E_\psi = \int_{-\infty}^{\infty} [\psi(t)]^2 dt \tag{2.1}$$

The auto-correlation function of a basic signal pulse $\psi(t)$ is defined as

$$\gamma_{\psi}(\tau) \triangleq \frac{1}{E_{\psi}} \int_{-\infty}^{\infty} \psi(t)\psi(t-\tau)dt \tag{2.2}$$

where τ is assumed to be in the interval $[0, T_{\psi}]$. Let us below discuss the requirements for design of basic UWB pulses.

2.2.1.1 Requirements for Design of Basic UWB Pulses

The shape of the basic UWB pulse strongly affects the design of transmitter and receiver filters, signal bandwidth, BER, performance in Gaussian and/or multipath fading environments [37–39]. The basic pulse may be selected from a range of time domain-pulses, including rectangular pulses, raised-cosine pulses, prolate spheroidal function based pulses, Gaussian pulses, sinusoidal pulses, etc. However, the pulse shape and width determine the spectrum of the transmitted signal, which should be optimised in some sense. Specifically, when designing the basic pulses for UWB systems the following requirements should be satisfied.

- **No DC Component**: In UWB systems, the transmitted pulse is differentiated after passing through antenna [40]. Therefore, the first major requirement for the UWB basic pulse is that the transmitted UWB signals should contain no DC component. This implies that the integration of a basic pulse over its duration, should go to zero [41], yielding

$$\int_{0}^{T_{\psi}} \psi(t)dt = 0 \tag{2.3}$$

  Since there is no DC component, the transmitted power may hence be decreased [42].

- **Radiation or High Power Efficiency**: Radiation efficiency is defined as the ratio of the power radiated to the total power supplied to the radiator at a given frequency [40]. For achieving effective radiation, the basic pulse should not contain a DC component as above-mentioned. Note that, this requirement may not be necessary for the systems using carrier frequencies [40]. It is well-known that one of the main advantages of UWB systems is that they can co-exist with the conventional narrowband or wideband systems. Specifically, by spreading the transmitted power as wide in frequency as possible, the power spectral density (PSD) of UWB signals can be very low. Consequently, UWB systems impose little interference on the other narrowband/wideband systems. Therefore, UWB pulses must have high power efficiency. The

conventional Nyquist pulse shaping requires linear amplifiers, which are usually not power efficient [43]. Therefore, the Nyquist pulses such as rectangular and raised cosine pulses have not been considered for UWB applications. Additionally, in UWB communications the pulses, which have their main lobes containing the majority of signal power are preferred. In this case, the side lobes have relatively lower power, and thus causing less adjacent channel interference [37].

- **Derivative**: In UWB systems the frequency of the basic signal pulse spans several GHz, making the wavelength of the pulse even smaller than the distance between transmitter and receiver. This phenomena is known as the far zone in radio systems. Hence, in the pulse-based UWB systems, electric field is usually more appropriately defined by differentiation operator [40]. Specifically, in pulse-based UWB systems, a pulse is differentiated when it passes through an antenna. Since there are transmitter and receiver the received pulse is hence the second order derivative of the transmitted pulse, after it passed both the transmitter and receiver antennas. Consequently, in the pulse-based UWB systems, the time-domain pulse must have a second order derivative.

  As mentioned previously in this section, in order to avoid the narrowband interference, the width T_ψ of the pulse should be small so as to achieve a high bandwidth of the UWB signal. The study in UWB, has also shown that increasing the order of the derivative of the radiated pulse waveform shifts the PSD of the transmitted UWB signal towards higher frequencies [36]. In this case, the chances to interfere with the existing narrowband systems which are usually allocated in the relatively low frequency region, can be avoided. Furthermore, it has been shown in [36] that, when high data rate is required, short pulses with higher order derivative should be employed. However, as shown in [36, 44], when the data rate is not high and there is no narrowband interference, relatively wider pulses with low order derivatives usually perform better than the shorter pulses with high order derivative.

- **Matched Filtering**: In wireless communications, the conventional MF or correlator multiplies the received signal with a locally generated replica of the transmitted signal and then integrates the result over a certain range. The locally generated signal replica is the same as the transmitted signal. In UWB systems, however, the conventional MF is hard to use, since the shape of the transmitted pulses may be changed due to the differentiation operations generated by the antennas [12, 45]. In order to employ the MF-assisted detector in UWB systems, alternatively, an integrator can be applied before the transmit antenna and another one is applied after receive

antenna [46]. By doing this, the original pulse shape is recovered after the second integrator and the MF matched to the original pulse shape can then be employed.

- **Power Spectral Density**: The PSD of UWB signals is an important measure of the interference caused by UWB signals to the conventional narrowband/wideband systems or vica versa. The PSD of UWB signals consists of two components: the continuous component that is due to the shape of the pulse and the discrete components which are generated by the periodical transmission of the pulse sequences. In UWB communications the discrete spectrum lines are usually the main interference sources in comparison with the continuous PSD component. However, in practice, the continuous PSD component is often used for making the UWB signals spectrum meet the frequency emission mask [47]. Furthermore, it is possible to shift away or reduce part of spectral lines in some particular part of the spectrum by careful design of the modulation and spreading sequences involved [40].

2.2.2 Time-Domain Pulses for UWB Systems

A range of basic pulses have been proposed and considered for pulse-based UWB systems. Some of these basic pulses are defined and their relevant properties are discussed in this section. Table 2.1 summarises the typical characteristics and properties of various time-domain pulses that are considered below.

2.2.2.1 Gaussian Pulse and Its Higher Derivatives

The Gaussian pulse (GP) is modified from the conventional Gaussian probability density function (PDF), which is expressed as [49]

$$\psi(t) = \exp\left(-\frac{[t-\mu]^2}{2\sigma^2}\right) \tag{2.4}$$

where μ and σ are the centre and standard deviation of the GP, respectively. For the GP, the pulse width T_ψ is related to the standard deviation by $T_\psi = 2\pi\sigma$ [1]. The nominal center frequency can be given as $f_0 = 1/T_\psi$ and the -3 dB bandwidth is 116% of the nominal center frequency [7]. The time-domian pulse of (2.4) is plotted in Fig. 2.1 for different σ values where ps stands for pico-seconds. It can be shown from Fig. 2.1 that the time dispersion of the pulse increases as the standard deviation increases. Furthermore, the GP has a DC component, which can be readily observed from Fig. 2.1, since the pulse amplitude is always positive.

Monocycle	Gaussian Pulse (GP) and higher Derivatives	Triangle Enveloped Sinusoidal Monocycle (TESM)	Prolate Spheroidal Functions (PS)	Modified Hermite Polynomial Based Pulses (HP)	Gaussian Modulated Sinusoidal Pulses (GMSP)
DC-Component	Even order have a DC component	Do not have a DC component	Not available	Even order have a DC component	Do not have a DC component
Generation	Difficult [46]	Simple [46]	No closed form expression [37]	Very complex	Not simple
Transmitted/ received signal	Very different [46]	Identical [46]	Very different	Very different	Very different
Processing	Complicated [46]	Simple [46]	Complex	Complex	Complex
Integrability	Low [46]	High [46]	Not available	Not available	Not available
Side lobe	113.5 dB below the main lobe [46]	30 dB below the main lobe [46]	Large side lobe [37]	Large side lobe [37]	60 dB below the main lobe
BER rate	Best [37]	Not available	As good as GP [37]	Worse than GP [37]	As good as GP [42]
Falls into FCC limits	5th and 7th derivative [48]	Not available	Can design to fit in [37]	Frequency shift is required [37]	Easily meet [42]

Table 2.1: Summary of the UWB time-domain pulses and their basic characteristics.

The normalised PSD of the GP having the time-domian pulse of (2.4) is given by [48]

$$S_{\psi}(f) = \left[\exp\left(-\frac{[2\pi f\sigma]^2}{2}\right)\right]^2 \tag{2.5}$$

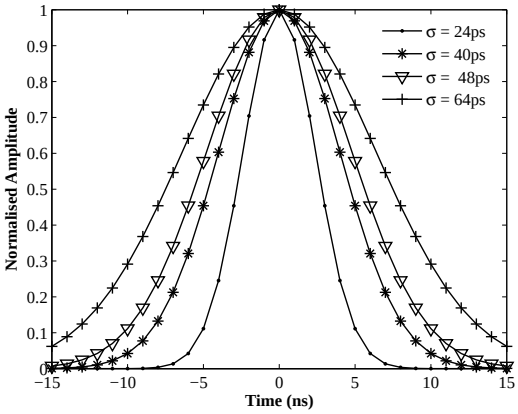

Figure 2.1: Time-domain representation of the Gaussian pulses.

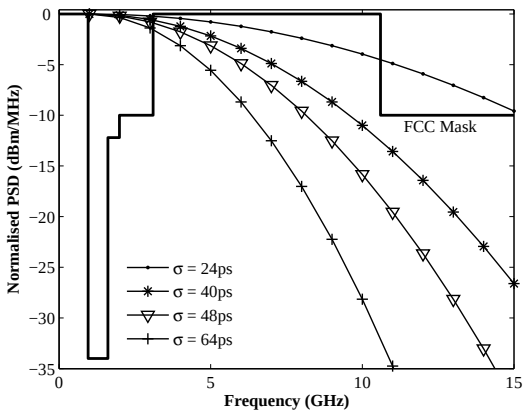

Figure 2.2: PSD of the Gaussian pulses shown in Fig.2.1.

which is plotted in Fig. 2.2 for different σ values. From Fig. 2.2 it can be observed that the GP's bandwidth becomes lower as the standard deviation increases. In Fig. 2.2 the FCC mask [37] is also plotted. It can be shown that the PSD of the GP defined by (2.4) does not fulfill the FCC's requirement, regardless of the standard deviation value used. Therefore, the GP cannot satisfy all the requirements of the basic UWB pulses as described in Section 2.2.1.1.

From Fig. 2.2 we can see that the FCC mask may be satisfied by shifting the centre of the PSD of the GP. However, it is well-known that the impulse radio is a carrierless system, which makes the complexity of implementation low. Shifting the centre of the PSD of the GP through carrier modulation introduces carrier phase rotation, which hence increases the complexity of implementation [48]. Additionally, when shifting the pulse to a higher frequency region the penetration capability of the corresponding UWB signals reduces [8].

As mentioned previously, applying a higher order derivative on the GP can shift the resultant pulse towards a higher frequency region. It can be shown that the nth order derivative of the GP exists, which can be determined recursively by the following formula [48]

$$\psi^{(n)}(t) = -\frac{(n-1)}{\sigma^2}\psi^{(n-2)}(t) - \frac{t}{\sigma^2}\psi^{(n-1)}(t) \tag{2.6}$$

The pulses shown in Fig. 2.3 are obtained by the 4th-, 5th-, 6th- and 7th-order of derivatives of the GP. From these figures we can observe that the even number of derivatives, i.e., the 4th- and 6th-order, of the GP generates DC components. By contrast, the time-domain pulses derived from

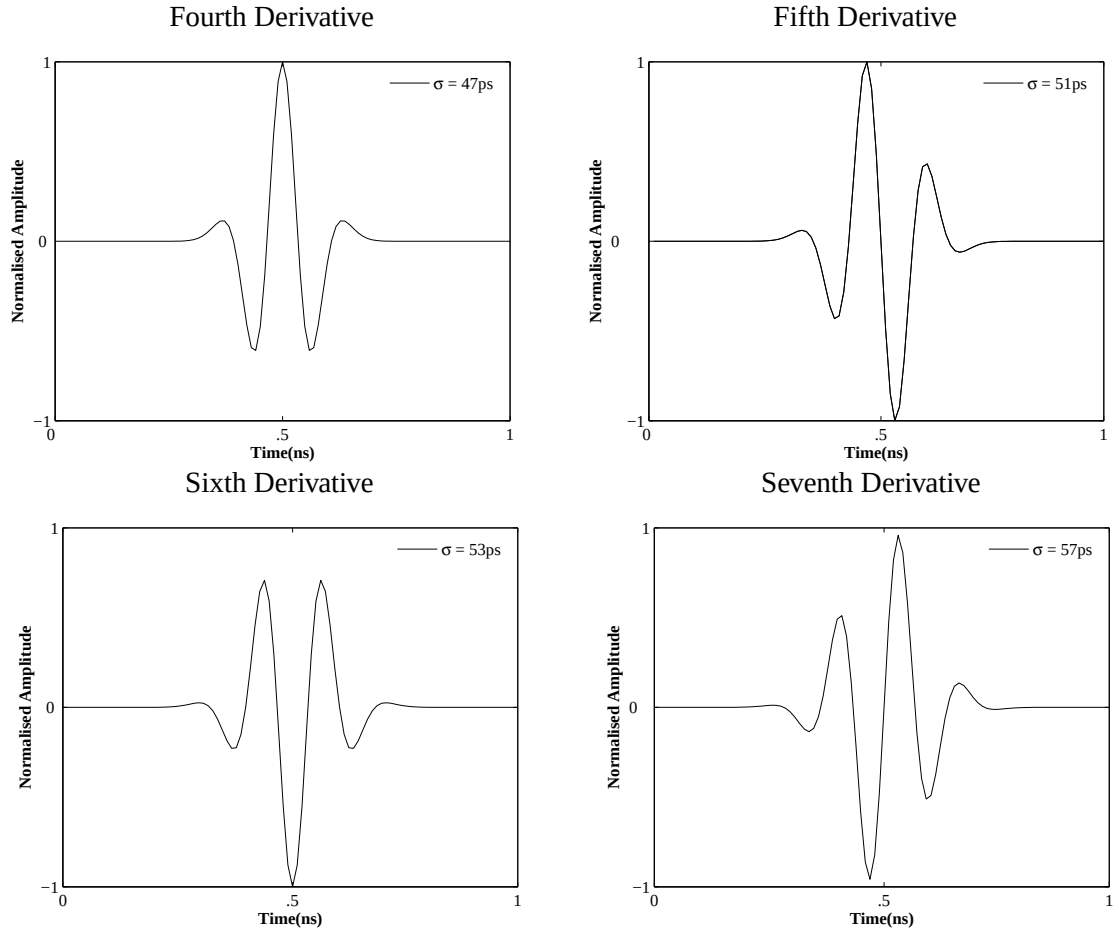

Figure 2.3: Different order of derivatives of the Gaussian pulse.

the odd number of derivatives, i.e., the 5th- and 7th-order, have no DC components. Hence, in our forthcoming discourse only the odd-order derivatives of the GP are considered.

It can be derived that the normalised PSD of the nth-order derivative of the GP can be expressed as [48]

$$S_{\psi}^{(n)}(f) = \frac{(2\pi f\sigma)^{2n} \exp\left\{-(2\pi f\sigma)^2\right\}}{n^n \exp(-n)} \tag{2.7}$$

which is shown in Fig. 2.4 for different values of σ and different values of n. Note that, the FCC mask for indoor UWB systems as shown in Fig. 2.4 is defined in [37]. Additionally, in Fig. 2.4 the PSD was normalised by the peak value allowed by the FCC, which was -41 dBm/MHz. Explicitly, Fig. 2.4 shows that that the 5th-order or higher-order derivative of the GP is capable of satisfying the requirement of the FCC mask.

Fig. 2.5 shows the normalised PSD of the time-domain pulses derived by the higher-order derivatives of the GP for the outdoor UWB systems. As shown in Fig. 2.5, the 7th-order or higher-order

derivative complies with the FCC limits for the outdoor UWB systems. Furthermore, as shown in Figs. 2.4 and 2.5, in order to maintain the signal bandwidth as wide as possible, the time-domain pulses derived by the 5th- and 7th-order derivatives should be employed for indoor and outdoor UWB systems, respectively. This is because, as the derivative increases, the standard deviation increases. Consequently, the pulse width T_ψ is increased and correspondingly the bandwidth of the UWB pulse decreases.

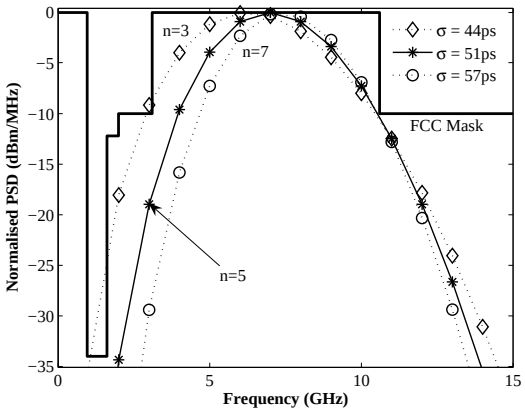

Figure 2.4: Power spectral density of the time-domain pulses formed by the higher-order derivatives of the Gaussian pulse for indoor UWB systems.

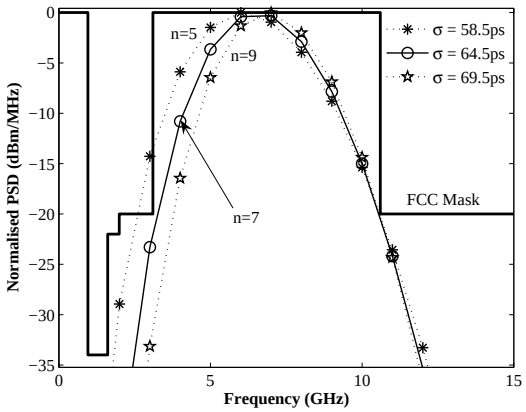

Figure 2.5: Power spectral density of the time-domain pulses formed by the higher-order derivatives of the Gaussian pulse for outdoor UWB systems.

Another interesting thing about the Gaussian monocycle is higher the order of the derivative of the Gaussian monocycle, the lower is the achievable BER performance [8]. However, this BER performance improvement is achieved at the expense of more strict receiver synchronisation. As shown in Fig. 2.3 the gradient of higher order Gaussian monocycle changes more rapidly with the time, which makes the synchronisation more difficult.

The most common method for generating the GP is passing a baseband rectangular pulse stream through a filter with a Gaussian impulse response, which can be obtained by the 8th-order Bessel filters, if their cut-off frequency are accurately set [50, 51]. However, the Bessel filter in practice are difficult to implement. Furthermore, a rectangular pulse passed becomes smeared, when it is passed through a Bessel filter, even when this Bessel filter is ideal. Specifically, a rectangular pulse of 0.2 ns of width may be extended to 0.7 ns [46] of width, when it passes through an ideal Bessel filter. This implies that, when using the Bessel filter to generate GP, the original pulse is required to be very narrow and should have small rise and fall time, which is sometimes unattainable in practice [46].

Due to the above-mentioned reasons, GP is usually difficult to generate practically. Additionally, the MF for the GP is difficult to implement, since in UWB communications the received signal is significantly different from the transmitted signal. In this case, it is difficult to recreate a signal that is identical to the received signal carrying the information [46], which hence makes the processing further complicated.

2.2.2.2 Triangle Enveloped Sinusoidal Monocycle

The triangle enveloped sinusoidal monocycle (TESM) is defined as

$$\psi(t) = \begin{cases} -\frac{t+2T}{T}, & -2T < t < -T \\ \frac{t}{T}, & -T < t < T \\ \frac{t-2T}{T}, & T < t < 2T \\ 0, & \text{otherwise} \end{cases} \tag{2.8}$$

where the pulse width is $T_\psi = 4T$. In Fig. 2.7, the TESM is plotted for the pulse width $T_\psi = 1$ ns. From (2.8) we can find that the first order derivative of the TESM pulse is not continuous. Hence, the second order derivative of the TESM pulses does not exist. Therefore, integrators are required before the transmitter antenna and after receiver antenna, in order to recover the received pulse. Consequently, MF-based receiver can be employed, which makes low-complexity detection possible. Additionally, from Fig. 2.7, it is apparent that the TESM does not have DC components.

The PSD of the TESM is given by [46]

$$S_\psi(f) = \frac{T^2}{4}\left[\text{sinc}^4\left(\frac{2\pi(fT-1)}{4}\right) + \text{sinc}^4\left(\frac{2\pi(fT+1)}{4}\right)\right] \tag{2.9}$$

which is plotted in Fig. 2.8. From Fig. 2.8, it can be observed that the side lobes of the PSD are about 30 dB lower than the main lobe. However, these side lobes do not degrade the system performance significantly, since the magnitude of these side lobes are still much lower than that of the main lobe [46].

The generation of TESMs is simple. For example, Fig. 2.6 represents an approach for generation of TESMs. To be more specific, the oscillator generates a sinusoidal signal at point 1 in Fig. 2.6, which is then passed through a comparator. The comparator transforms the sinusoidal signal into a square wave, as seen at point 2 in Fig. 2.6. The square wave is then integrated to create a triangular wave. In Fig. 2.6, the switch permits the transmitter to send the pulses at a desired rate. Therefore, the signal at point 3 is triangle enveloped at the desired pulse rate. Then, the traingular envelopes are

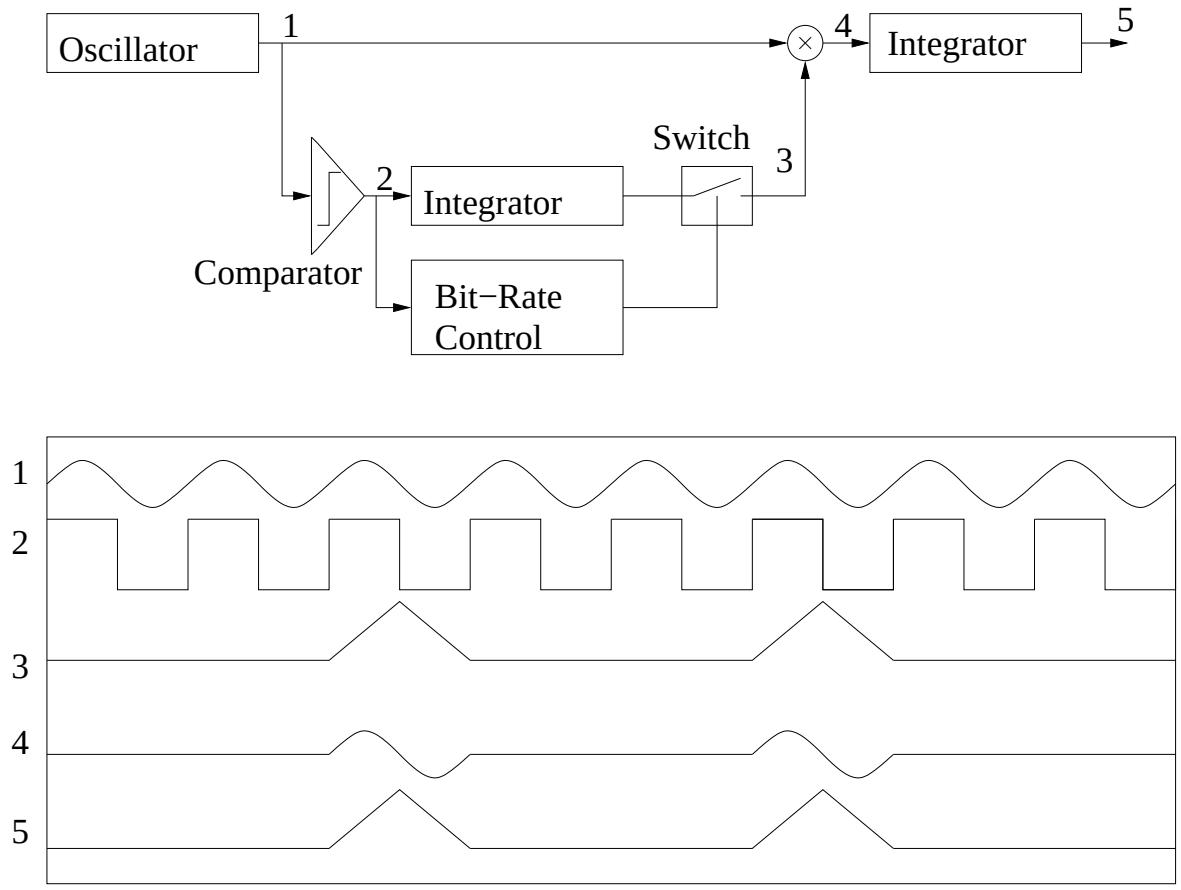

Figure 2.6: Triangular sinusoidal monocyclic pulses

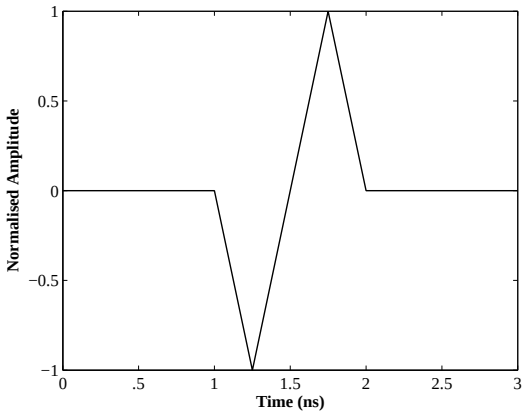

Figure 2.7: A triangle-enveloped sinusoidal monocycle

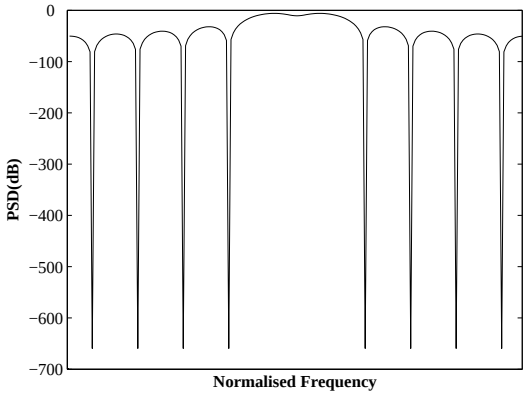

Figure 2.8: PSD of a triangle-enveloped sinusoidal monocycle

multiplied with the original sinusoid in order to generate the sinusoidal pulses as shown in point 4 of Fig. 2.6. The resulted signal is then integrated, leading to the final TESMs pulses as shown in point 5.

2.2.2.3 Prolate Spheroidal Functions

The idea of generating the UWB basic pulse by Prolate Spheroidal (PS) functions was presented in [47]. Fig. 2.9 represents the block diagram illustrating the principles of generating the basic UWB pulse using PS functions. As observed in Fig. 2.9 the basic pulse $\psi(t)$ is passed through a bandpass filter having an impulse response $h(t)$, which has the desired frequency mask $H(f)$. According to Fig. 2.9, the output of the filter is the convolution of $\psi(t)$ with $h(t)$, which can be expressed as

$$y(t) = \int_{-T_\psi/2}^{T_\psi/2} \psi(\tau) h(t-\tau) d\tau \tag{2.10}$$

In order for the pulse generated to be used for the UWB communications, according to the princi-

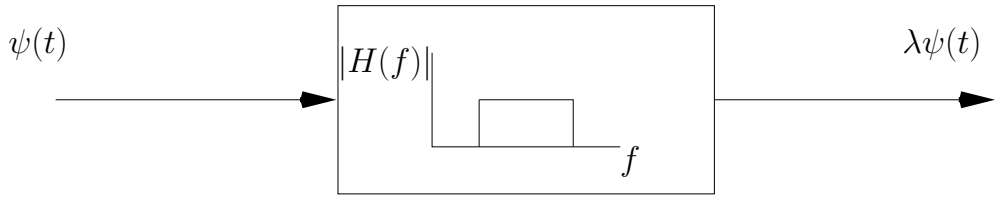

Figure 2.9: Block diagram generating the basic UWB pulses through Prolate Sphedorial functions.

ples of UWB communications, we should have $y(t) = \lambda\psi(t)$, where λ is the attenuation constant. According to FCC limits $h(t)$ is given as [47]

$$h(t) = 2f_U \text{sinc}(2f_U t) - 2f_L \text{sinc}(2f_L t) \tag{2.11}$$

where $f_L = 3.1$ GHz and $f_U = 10.6$ GHz. It has been shown that a closed-form solution to (2.10) is extremely difficult to find. For this sake, an algorithm has been proposed in [47] which obtains a numerical solution through the discretisation of (2.10). To be more specific, when using $(N+1)$ samples per pulse width T_ψ, (2.10) can be written as

$$\lambda\psi[n] = \sum_{m=-N/2}^{N/2} \psi[m] h[n-m], \quad n = -\frac{N}{2}, \cdots, \frac{N}{2} \tag{2.12}$$

where $y(t) = \lambda\psi(t)$ was assumed. When expressed in matrix form, (2.12) can be

$$\lambda \underbrace{\begin{pmatrix} \psi[-\frac{N}{2}] \\ \psi[-\frac{N}{2}+1] \\ \vdots \\ \psi[0] \\ \vdots \\ \psi[\frac{N}{2}] \end{pmatrix}}_{\psi} = \underbrace{\begin{pmatrix} h[0] & h[-1] & \dots & h[-N] \\ h[1] & h[0] & \dots & h[-N+1] \\ \vdots & \vdots & \vdots & \vdots \\ h[\frac{N}{2}] & h[\frac{N}{2}-1] & \dots & h[-\frac{N}{2}] \\ \vdots & \vdots & \vdots & \vdots \\ h[N] & h[N-1] & \dots & h[0] \end{pmatrix}}_{\mathbf{H}} \underbrace{\begin{pmatrix} \psi[-\frac{N}{2}] \\ \psi[-\frac{N}{2}+1] \\ \vdots \\ \psi[0] \\ \vdots \\ \psi[\frac{N}{2}] \end{pmatrix}}_{\psi} \tag{2.13}$$

where $\mathbf{H}$ is a Toeplitz matrix and ψ is the eigenvector of $\mathbf{H}$ and λ is a eigenvalue corresponding to ψ. Explicitly, λ and ψ can be found by the eigenanalysis of $\mathbf{H}$. Let the eigenvalues of $\mathbf{H}$ be $\lambda_1 \geq \lambda_2 \geq \cdots \geq \lambda_N$ and their corresponding eigenvectors be $\boldsymbol{\psi}_1, \boldsymbol{\psi}_2, \cdots, \boldsymbol{\psi}_N$. Then, any eigenvalue and its eigenvector satisfies (2.13). However, it has been shown in [47] that the eigenvalue chosen affects the desired power spectrum and that high-valued eigenvalue is usually preferred. Therefore, for our case of (2.13), we can choose λ_1 and its corresponding eigenvector $\boldsymbol{\psi}_1$, in order to form the UWB pulse $\psi(t)$.

Note that, when the matrix $\mathbf{H}$ is a Hermitian matrix, then its eigenvalues are real and their corresponding eigenvectors are orthogonal. In this case, multiple synchronous orthogonal UWB pulses may be generated, which can be used to transmit high information rate without interference in an UWB systems [47].

The UWB basic pulses generated using the PS functions can meet the FCC masks without frequency shift. However, this type of UWB basic pulses cannot be generated based on closed-form expression, which makes the implementation of the PS-based pulses more complicated in comparison with the Gaussian monocycles [37–39]. Additionally, decreasing the pulse width T_ψ of the PS-based pulses increases the amplitude of the dominant sidelobes of the PSD, which results in strong adjacent channel interference [37–39]. However, it seems that the UWB system using the PS-based pulses is capable of virtually achieving the same BER performance as the UWB system using GPs, for different lengths of the repetition codes [37, 38].

2.2.2.4 Modified Hermite Polynomial Based Pulses

A set of orthogonal pulses based generated on the Hermite polynomials (HP) has been proposed for UWB communications [52]. Using the modified HP functions, a set of orthogonal pulses having

almost invariant pulse width T_ψ can be obtained. The modified HP pulses can be employed by the UWB systems, when pulse shape modulation is used as data modulation [7]. Specifically, the nth order modified HP pulse is given by [52]

$$\psi^n(t) = \exp\left(-\frac{t^2}{4}\right) h_{e_n}(t) \tag{2.14}$$

where h_{e_n} is defined as

$$h_{e_n}(t) = (-1)^n \exp\left(\frac{t^2}{4}\right) \frac{d^n}{dt^n}\left[\exp\left(-\frac{t^2}{2}\right)\right] \tag{2.15}$$

In Fig. 2.10, the 0th, 1st, 2nd and 3rd orders of HP pulses are depicted. From Fig. 2.10, we can

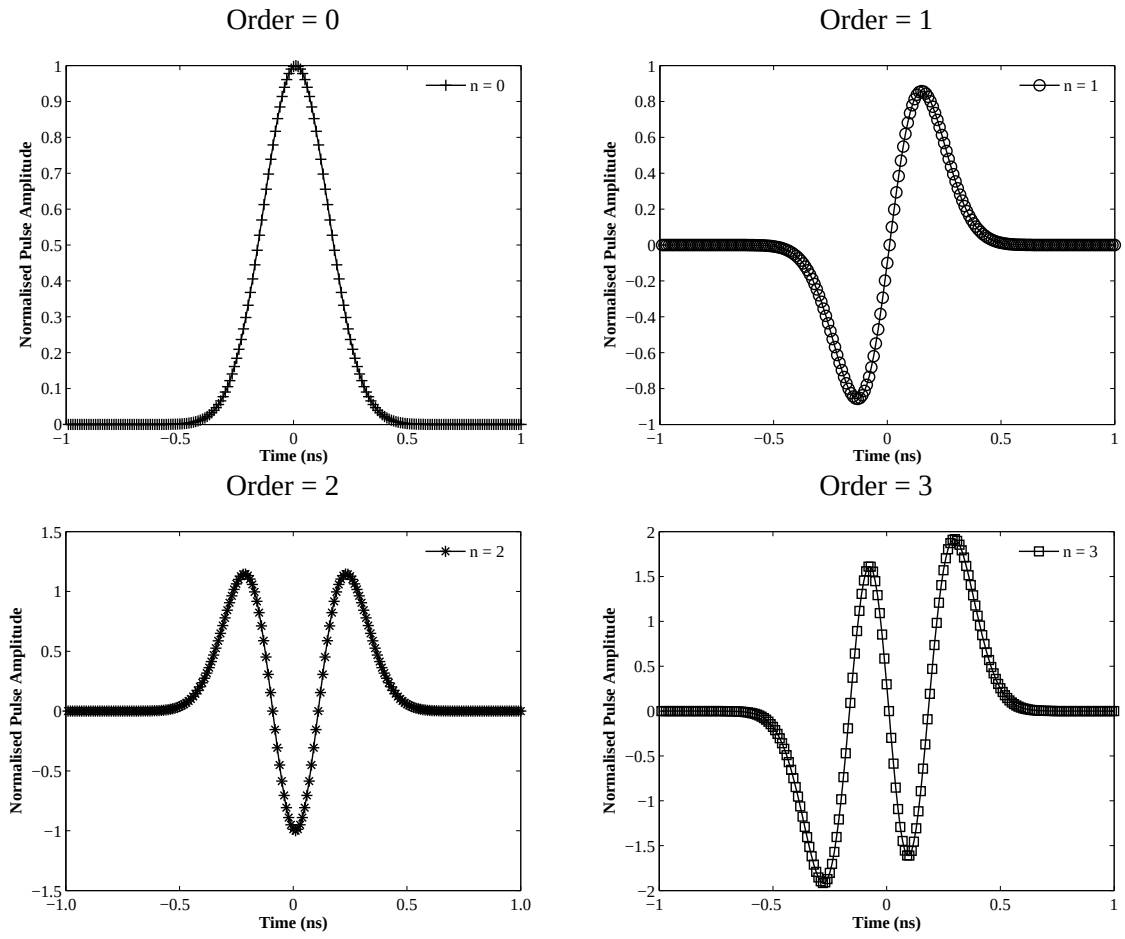

Figure 2.10: Illustration of the nth order modified Hermite polynomials pulses for $n = 0, 1, 2$ and 3.

observe that, as the GPs shown in Fig. 2.3 the HP pulses with even orders have a DC component,

while the HP pulses with odd orders do not have a DC component. Hence, the HP pulses with even orders are not suitable for UWB communications. Additionally, in the UWB communications using the HP pulses, the transmitted and received pulses are different, after the antennas at the transmitter and receiver differentiate the transmitted pulses. Hence, MF-based detection is hard to implement.

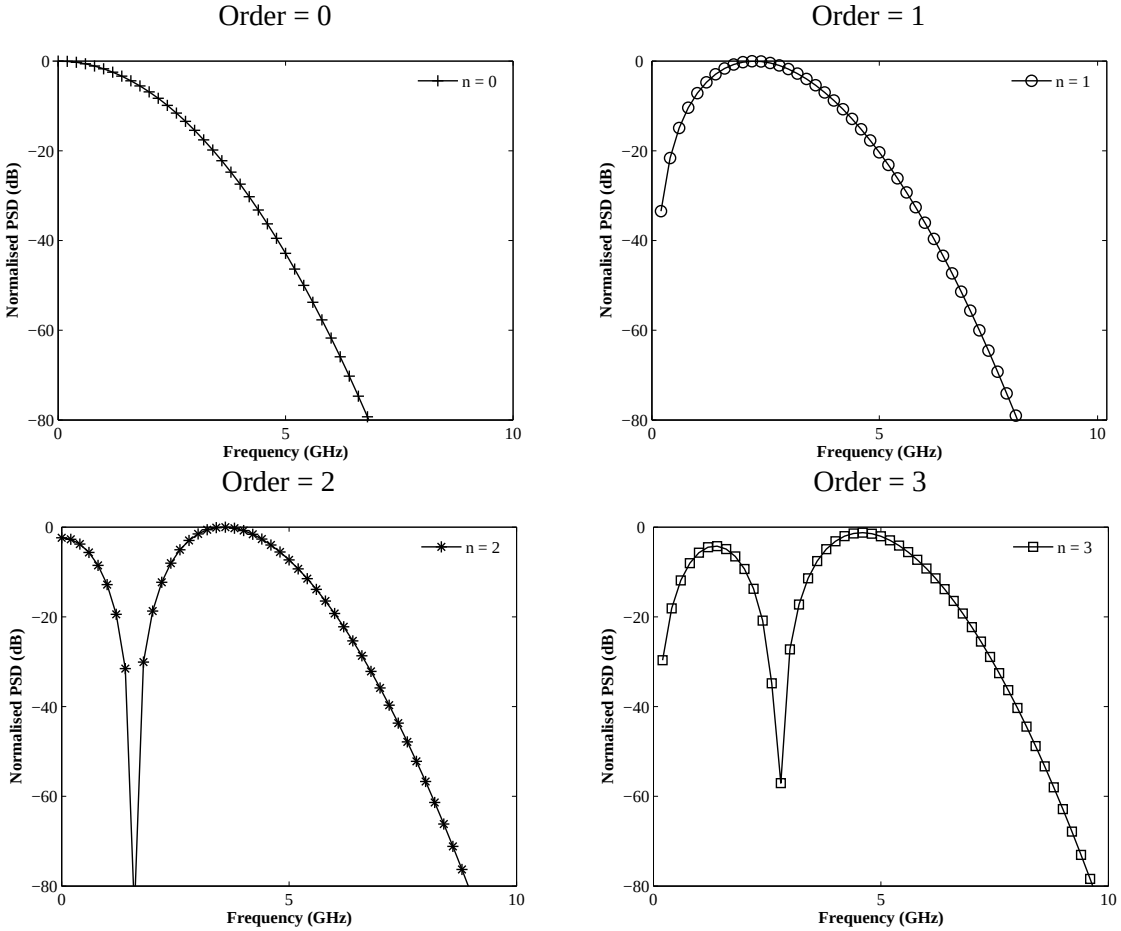

Figure 2.11: PSD of the normalised Hermite polynomial pulses having the orders of $n = 0$,1,2 and 3.

The transfer function of HP pulses can be expressed as [52]

$$H_{n+1}(f) = \frac{1}{4\pi}\Big\{4\pi n H_{n-1}(f) - j8\pi^2 f H_n(f)\Big\} - j2\pi f H_n(f) \tag{2.16}$$

which shows that the transfer functions of different orders HP pulses can be computed recursively. With the aid of (2.16), the PSD of a HP pulse can be readily obtained, which is given by $|H_n(f)|^2$. In Fig. 2.11 of the HP pulses is demonstrated for $n = 0, 1, 2$ and 3. Explicitly, a frequency shift is required for the HP pulses of order 0 and 1 in order to meet the FCC spectral mask. By contrast, for

the pulses with higher order, there exist large sidelobes, which need to be removed using bandpass filters. Therefore, in the UWB systems using the HP pulses, different kinds of operations are required for the HP pulses to meet the FCC spectral mask [37–39], which inevitably increases the complexity of the UWB systems.

The orthogonality of the HP pulses is one of the most desirable properties, since it enable optimum detection with low-complexity at receiver [7]. However, the orthogonality can only be retained when the user signals are synchronously transmitted, which in UWB communications due to multipath fading is very difficult [8]. Furthermore, it has been found in [37] that the GPs generally outperform the HP pulses for all SNR values. It has also been found that the MA capability of the UWB scheme using single HP pulse is worse than that of the UWB scheme using either the GP or the PS pulse, when assuming that all these pulses are constrained to meet the FCC spectral mask [37, 39].

2.2.2.5 Gaussian Modulated Sinusoidal Pulses

The Gaussian modulated sinusoidal pulse (GMSP) is defined by [1]

$$\psi(t) = \left(\frac{8k}{\pi}\right)^2 \frac{1}{\sqrt{1+\exp(2\pi^2 f_c^2/k)}} \exp(-k^2t^2)\cos(2\pi f_c t) \tag{2.17}$$

where f_c denotes the desired frequency for the pulse, which is $f_c = 6.85$ GHz for the FCC spectral mask. In (2.17) the parameter k determines the pulse duration, which increases as the value of k decreases. Fig. 2.12 depicts the time-domain GMSP. Explicitly, the GMSP does not contain a DC component.

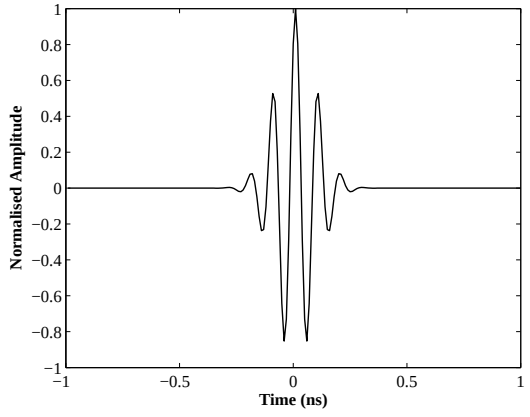

Figure 2.12: Time domain of the Gaussian modulated sinusoidal pulse.

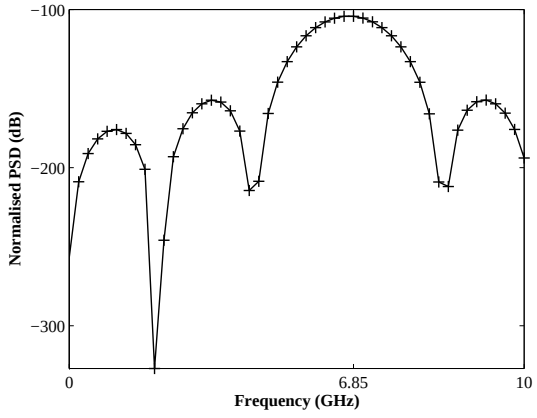

Figure 2.13: Power spectral density of the Gaussian modulated sinusoidal pulses.

The frequency response of the GMSP of (2.17) can be expressed as

$$\psi(f) = \left(\frac{8k}{\pi}\right)^2 \frac{1}{\sqrt{1+\exp(2\pi^2 f_c^2/k)}} \left[\sqrt{\frac{\pi}{k^2}} \exp\left(-\pi^2 f^2/k^2\right) * \frac{1}{2}[\delta(f-f_c)+\delta(f+f_c)]\right] \tag{2.18}$$

where $*$ represents the convolution operation. The normalised PSD of $\psi(f)$ is plotted in Fig. 2.13 for $f_c = 6.85$ GHz. It can be shown that the GMSP pulse can easily be designed to meet the FCC limits, which can be achieved by changing the pulse width, i.e., the value of k or by changing the centre frequency of f_c. Furthermore, it can be observed from Fig. 2.13 that the side lobes are about 60 dB lower than the main lobe. Therefore, the main lobe contains most of the power transmitted, which implies that the UWB systems using the GMSP may cause less interference to the systems working in the same frequency band.

These GMSP pulses are generated with the Gaussian pulses described in Section 2.2.2.1. Hence, generation of the GMSP is not simple, as analysed in Section 2.2.2.1. Furthermore, as the pulse shape of the GMSPs changes after passing them through the transmitter/receiver antennas, MF-based detection is hard to implement. Note that, it has been shown in [42] that the BER performance of the UWB systems using GMSP pulses is similar as that of the UWB systems using Gaussian pulses for the same effective bandwidth.

So far, we have provided a review for a range of basic pulses that may be employed in the UWB communications. In the public literature, there are also other techniques for designing the basic pulses. For example, in [53] an approach has been proposed for designing the basic pulses for UWB communications systems. The pulses generated are time-limited in order to make the implementation simple. Furthermore, it has been shown [53] that this class of pulses are capable of achieving the same BER performance as the class of gaussian monocycles or PS pulses. However, the basic pulses generated by the approach of [53] has more degrees-of-freedom, which can be adjusted so that the corresponding spectral meets the FCC spectral mask. Additionally, reference [39] shows that an appropriate sinc-pulse can be defined as

$$\psi(t) = \text{sinc}(Wt)\cos(2\pi f_c t) \tag{2.19}$$

where $f_c = 6.85$ GHz is the center frequency, $W = 3.75$ GHz and $\text{sinc}(\cdot)$ is given as

$$\text{sinc}(x) = \begin{cases} \frac{\sin(\pi x)}{\pi x}, & x \neq 0 \\ 1, & x = 0 \end{cases} \tag{2.20}$$

The sinc pulse defined by (2.19) complies well with the required spectral emission constraints, and achieves better BER performance than the Gaussian monocycles, PS-based pulses or the pulses generated using the approach proposed in [53]. After discussion of the basic requirements for UWB pulses and review of various classes of UWB pulses, let us now consider the transmission of pulses in UWB systems.

2.2.3 Signalling in UWB Systems

In pulse-based UWB systems, each information-conveying symbol is transmitted by a number of frames [14, 34]. Without data modulation, the general form of an uniform pulse train with a constant amplitude of one can be represented as

$$s(t) = \sum_{n=0}^{N_f-1} \psi(t - nT_f) \tag{2.21}$$

where $s(t)$ denotes the transmitted signal at time t, N_f denotes the number of pulses transmitted and T_f denotes the duration of a frame. The uniform-pulse train is depicted in Fig. 2.14, where the pulse starts at $t = 0$ and is repeated every T_f seconds. Hence, T_f can be viewed as the average time-duration between the transmission of two pulses. Explicitly, the uniform pulse train cannot be

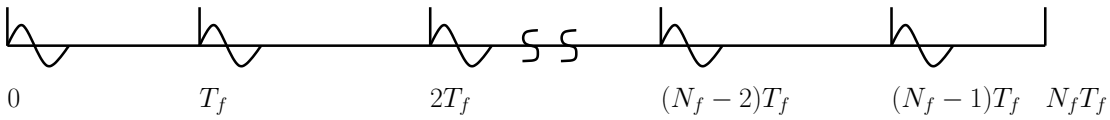

Figure 2.14: Illustration of an uniform pulse train.

employed for implementing MA communications due to the following reasons.

1) Firstly, when multiple users transmit information using the same pulse train, strong interference exists among these users [24];

2) Secondly, when the same uniform pulse train is employed for supporting multiple users, it becomes difficult for the receiver to distinguish between the users. This is because, in this case, the signals transmitted by different users are highly correlated, making the detection very difficult [34];

The above-mentioned problems existing in the pulse-based UWB systems using uniform pulse train may be efficiently solved by employing proper data modulation techniques and MA schemes.

Additionally, since FCC has imposed no restriction on data modulation techniques and MA schemes, different kinds of modulation techniques and different types of MA schemes may hence be employed for the pulse-based UWB systems [54]. Below we consider some of the modulation techniques that may be employed for pulse-based UWB communications. Then some MA schemes, that may be employed for the pulse-based UWB systems are discussed.

2.2.4 Data Modulation Techniques for UWB Systems

As UWB systems communicate in power-limited regime and there are different types of applications that may be supported by UWB systems, a number of facts must be considered, when choosing a data modulation techniques. Specifically, when choosing the modulation schemes for UWB systems, we should take into account the following issues.

- First, UWB systems usually co-exist with the conventional narrowband/wideband systems operating in the same frequency band, the UWB signals hence impose interference on these conventional systems [55]. Therefore, in order to minimise the interference by the UWB systems, the PSD of the UWB systems needs to be very low [1]. As mentioned previously, the PSD of UWB signals consists of two components: the continuous spectral waveforms, which are due to the shape of the pulse, and the discrete spectral lines, which are due to the periodical transmission of the pulse sequence [40]. Since the magnitude of the discrete spectral lines are usually higher than that of the continuous spectral waveforms, the discrete spectral lines constitute the major source inflicting interference on the other narrowband or wideband systems operating in the same frequency band as the UWB systems [23, 36]. Therefore, in order to reduce the interference caused by the discrete spectral lines, the transmitted power of the UWB systems may need to be further reduced. However, as UWB systems are usually operated in the power-limited regime, reducing the transmission power may result in difficult detection of the information at the receiver side. Furthermore, it is desirable that in UWB systems, the mean of the data modulation scheme is zero. Otherwise, the discrete spectral lines will appear at a regular interval [4], yielding interference on the other systems. Additionally, due to the constraint on the total transmitted power, the data modulation schemes should be power-efficient, in order for the UWB systems to attain a reasonably low BER and to support a relatively high data rate [34, 56, 57].

- Second, in the conventional communication systems, signal inversion causes little or no harm in addition to fading in multipath channels, as the phase error due to signal inversion can be

easily detected and corrected [58]. However, in UWB communications this phenomena requires special attention, since many pulse modulation schemes depend on the signal's polarity. For example, when employing binary pulse position modulation (PPM) using a single correlator for detection, the outputs are positive when it is applied to the in-phase pulses and negative when is applied to the shifted pulses. In multipath channels, the positions of the pulses will be shifted, thus, the detection of the signals might not be correct. Therefore, special techniques must be developed to assure the right polarity of the transmitted signal.

- Finally, when choosing a data modulation scheme for a particular type of UWB systems, the data rate supported, affordable complexity, intersymbol interference ISI generated, spectral characteristics, robustness against narrowband interference, BER performance, etc. [34, 45, 58–61] are required to be taken into account. Specifically, for high data-rate applications, BER performance, complexity and system flexibility are the key criteria [62], that need to be considered when choosing the corresponding modulation schemes.

For pulse-based UWB systems, basic modulation schemes considered in the literature include the on-off keying (OOK), PPM, pulse amplitude modulation (PAM), pulse shape modulation (PSM), etc. Table 2.2 shows some of the characteristics of these modulation schemes, which are now discussed in a little more detail in the following subsections.

Modulation Schemes	Complexity	Pulse Negation	Discrete Spectral Lines	BER Performance	M-ary Scalability
OOK	Lowest [45]	Not required	Yes	Worse than PPM [45]	Not scalable
PPM	Higher than OOK [45]	Not required	Yes	Better than OOK [45]	Scalable
PAM	Higher than PPM [45]	Required	No	3-dB better than PPM [63]	Scalable
PSM	Higher than PPM	Required	No	Worse than PPM [58]	Scalable

Table 2.2: Summary of the data modulation schemes for pulse-based UWB systems.

2.2.4.1 On-Off Keying

OOK is one of the data modulation schemes that are preferred for pulse-based UWB systems [45, 63]. In the OOK modulation scheme, a pulse is transmitted for an information bit '1' while there is no transmission for an information bit '0' [45]. The OOK modulation scheme employs the following advantages for UWB communications. Firstly, with the OOK modulation, only a low-complexity energy detector is required at the receiver [45]. Hence, the OOK modulation scheme may make the UWB communications systems simple. Secondly, when the OOK is employed, no pulse negation is required as negating ultra-short pulses is difficult to implement [14, 25]. The OOK has the disadvantage that there are discrete spectral lines in the PSD of the transmitted UWB signals, since the mean of the OOK modulation scheme is not zero [56]. Furthermore, it has been shown that, for the same communications environment, the PPM and PAM schemes are capable of achieving better BER performance than the OOK scheme [45]. Additionally, the OOK scheme is not suitable for M-ary modulation.

2.2.4.2 Pulse Position Modulation

PPM is one of the modulation techniques that are suitable for UWB communications supporting power-limited applications [14]. With the PPM, no negation of UWB pulses is required [64, 65]. It has also been shown in [66] that the PPM can be readily scaled to implement the M-ary PPM (MPPM). The scalability of the PPM can improve the MA capability of the corresponding UWB systems, when a given number of users and a given data transmission rate are supported [66]. This is because, with the higher value of M, it is possible to improve the probability of detection of the MPPM-based systems supporting a fixed number of users, or for a fixed probability of error, to increase the number of users supported by keeping the transmitted signal power constant [67]. Another advantage of using PPM is that noncoherent detection can be employed, since in the PPM-based UWB systems information is extracted from the location of the transmitted pulses and hence no phase estimation is necessary. The disadvantages of using PPM is that discrete spectral lines may exist in the PSD of the transmitted signal, due to the non-zero mean of the PPM modulated signals [14]. However, in the PPM-based UWB systems, the discrete spectral lines introduce cyclostationarity, which can be exploited for finding the timing-offset of the system [14].

2.2.4.3 Pulse Amplitude Modulation

With the development of microelectronics and signal processing, negation of ultra-short pulses becomes easier and practical. Consequently, modulation schemes with zero mean have become more attractive [45]. Pulse-Amplitude Modulation (PAM) is a data modulation scheme with zero mean. Hence, in UWB systems using the PAM data modulation, there are no discrete spectral lines in the PSD, resulting in a smooth PSD [45, 56]. The PAM is suitable for implementation of M-ary PAM, which is capable of improving the MA capability of the UWB systems for a given data rate. It has been shown that the binary PAM has 3 dB of SNR gain over the binary PPM, when communicating over multipath fading channels [60, 63, 68]. It has also been shown that the multiple-access-interference (MAI) of the UWB systems using the PPM has a higher impact on the BER performance than that of the UWB system using the PAM [68, 69]. However, as the value of M increases, the impact of MAI on the BER performance decreases for the UWB system using PAM. By contrast, the impact of the MAI on the BER performance of the UWB systems using the PPM retain the same, when the value of M increases [68]. Although the PAM has certain advantages over the PPM, however, according to [4], amplitude modulation is usually not desirable for UWB communications. This is because, in amplitudes modulations the smaller amplitudes are more susceptible to noise interference than the larger amplitudes. Furthermore, the PAM has a higher peak-to-average power ratio (PAPR) than the PPM. Hence, the PAM scheme might not be power-efficient for UWB communications [4].

2.2.4.4 Pulse Shape Modulation

It has been recognised that the PSM is an alternative modulation technique for UWB communications, where different pulse shapes are used to carry information [7, 70]. In order to implement the PSM modulation a set of pulses is required, where the number of pulses used determines the modulation order of the PSM. In the PSM, orthogonal pulses can be employed to remove the discrete spectral lines, in order to reduce the possible interference of the UWB systems on the other narrowband/wideband systems operated in the same frequency band. However, in practice it is difficult to maintain the orthogonality of the transmitted pulses in ad-hoc communications environments, where signals transmitted by different users are hard to synchronise [8]. Furthermore, the orthogonality of the transmitted signals may be destroyed by the dispersive multipath fading channels [71].

Below we consider some other issues related to the pulse-based UWB communications. As an example, we assume that the UWB systems employ the MPPM. In the case, when the M-ary symbol $X_n \in [0, M-1]$ is transmitted within the nth frame, an additional time-shift of $X_n T_\psi$ is added

to the transmitted pulse. Hence, for the UWB systems using MPPM the transmitted signal can be represented as

$$s(t) = \sum_{n=0}^{N_f-1} \psi(t - nT_f - X_n T_\psi) \tag{2.22}$$

where T_ψ denotes the width of the basic UWB pulse, T_f represents the frame-duration and N_f represents the number of frames invoked for transmitting one symbol. Fig. 2.15, illustrates the time-shift caused by the data-modulation, where $X_n = 1$ was assumed. As shown in Fig. 2.15, the basic UWB pulse in the $(N_f - 4)$th frame is shifted by T_ψ seconds, due to $X_n = 1$.

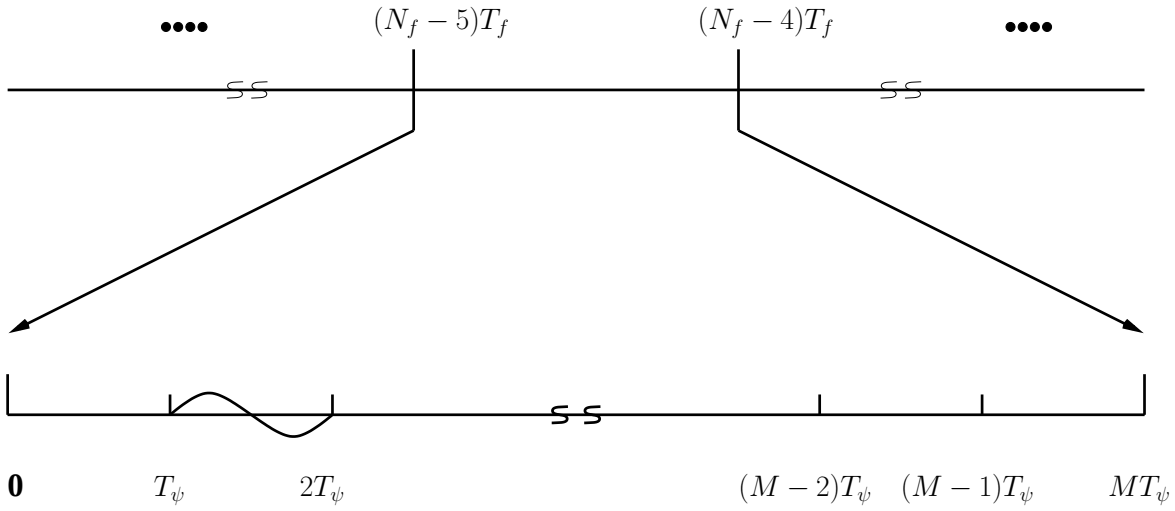

Figure 2.15: Illustration of M-ary pulse position modulation in pulse-based UWB systems.

Let us now provide an overview of the MA schemes for the pulse-based UWB systems using MPPM.

2.2.5 Multiple-Access Schemes for UWB Systems

UWB systems are typical spread-spectrum systems. Hence, UWB systems may be implemented by invoking various spread-spectrum techniques. It can be shown that many spread-spectrum techniques, such as frequency-hopping (FH) [72], time-hopping (TH), direct-sequence (DS), etc., may be employed to implement UWB systems. In this thesis our focus is mainly on the UWB systems based on TH and DS, i.e., the TH-UWB and DS-UWB. Hence, below we provide an overview for the TH-UWB and DS-UWB systems.

2.2.5.1 Time-Hopping UWB System

Time-hopping multiple-access (THMA) technique for UWB communications system was first introduced by Robert A. Scholtz in 1993 [1,34,35]. In this type of spread-spectrum technique an additional time-shift is imposed on the transmitted pulses in the pulse train due to the TH [73]. Furthermore, in TH-UWB the discrete spectral lines, which are generated in the pulse-based UWB due to using uniform pulses, can be smoothed to a certain level by choosing the proper TH codes [63]. THMA can be classified into fast TH (FTH) and slow TH (STH). In the FTH systems, a symbol is transmitted with the aid of N_f frames, each frame consists of a UWB pulse and the position of this UWB pulse is determined jointly by the TH code and the data modulation technique employed. By contrast, in the STH systems, a symbol is transmitted by N_f frames but only a single UWB pulse is transmitted by these frames. In the STH system, the selection of the frame for transmission depends upon the TH code while the position of the pulse in the selected frame is determined by the data modulation scheme employed. To be more specific, the FTH and STH schemes can be explained as follows.

- **Fast Time Hopping:** In FTH-UWB systems a symbol is transmitted by invoking several frames. The transmitter schematic of the FTH-UWB system using MPPM is shown in Fig. 2.16. For the sake of supporting multiple users, in the FTH-UWB systems each user is assigned a unique TH pattern, which is also referred to as a TH address code, in order to distinguish among different users. Assume that N_f is the number of frames invoked for transmitting one symbol, and that the TH code of user k can be expressed as $\boldsymbol{t}_m^{(k)} = [t_m^{(k)}(0), t_m^{(k)}(1), \cdots, t_m^{(k)}(N_f - 1)]$, where m is related to the mth symbol transmitted by user k. Then, for a given M-ary transmitted symbol $X_m^{(k)}$ of user k, $X_m^{(k)}$ is first combined with the kth user's TH code based on the operation

$$\boldsymbol{Y}_m^{(k)} = (X_m^{(k)} \cdot \mathbf{1}) \oplus \boldsymbol{t}_m^{(k)} = [y_m^{(k)}(0), y_m^{(k)}(1), \cdots, y_m^{(k)}(N_f - 1)] \tag{2.23}$$

  where $\mathbf{1}$ is an all-one vector of length N_f and $\oplus$ denotes the addition operation in $GF(Q)$, which denotes a Galois field having Q elements, where $Q \geq M$ represents the number of time-slots per frame. As shown in Fig. 2.16, each element in $\boldsymbol{Y}_m^{(k)}$ imposes an extra delay for the corresponding pulse. Consequently, as shown in Fig. 2.16 the transmitted signal for the kth user can be expressed as

$$s^{(k)}(t) = \sum_{m=0}^{\infty} \sum_{n=0}^{N_f-1} \psi(t - mT_s - nT_f - y_m^{(k)}(n)T_\psi) \tag{2.24}$$

  where T_s is the symbol duration and $T_s = N_f T_f$.

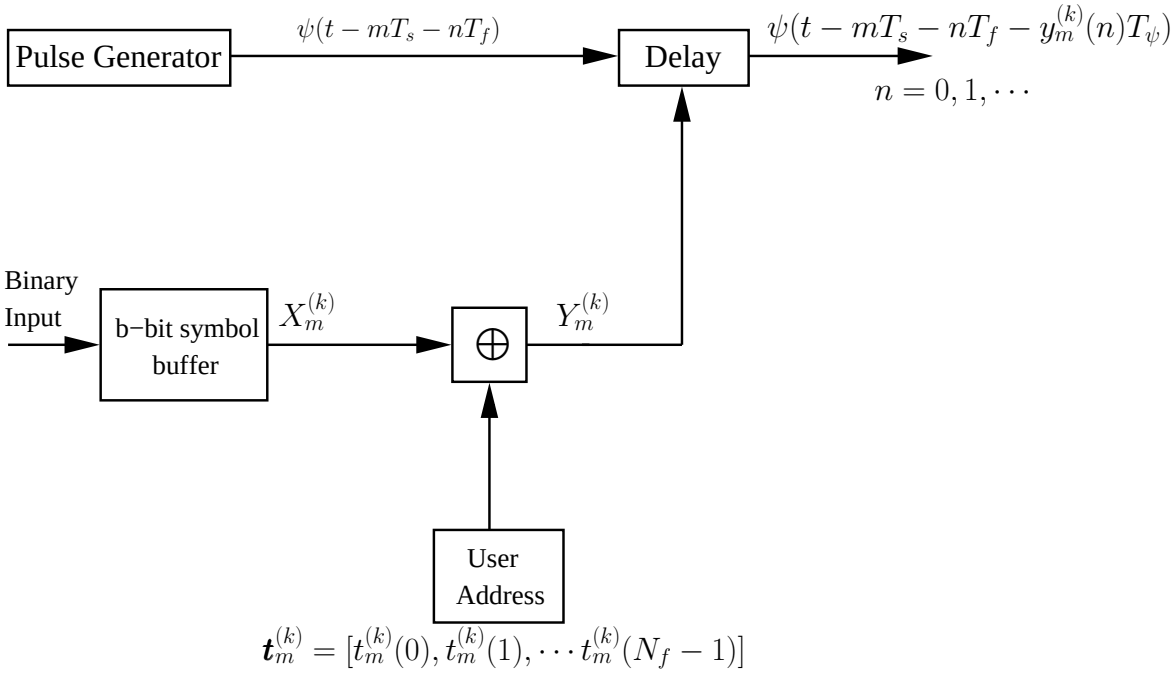

Figure 2.16: Schematic block diagram of fast time-hopping ultrawide bandwidth systems using M-ary pulse position modulation.

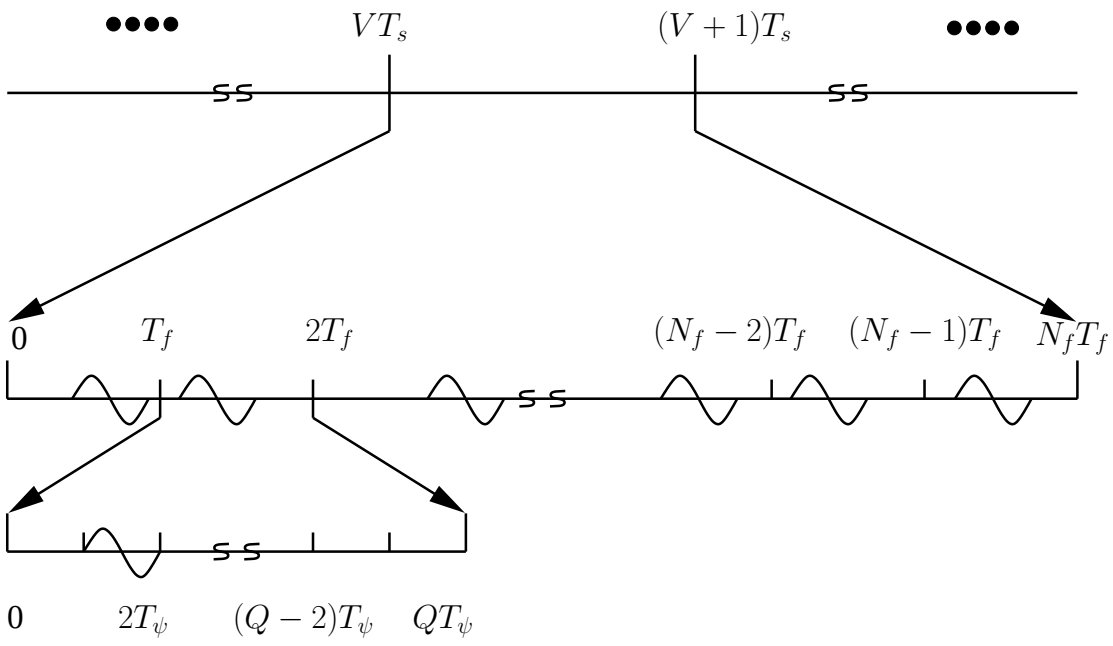

Figure 2.17: Illustration of the transmitted signals in the fast time-hopping ultrawide bandwidth using M-ary pulse position modulation.

Fig. 2.17 illustrates the transmitted UWB signal in the Vth symbol duration. As shown in Fig. 2.17, the Vth symbol duration is first divided into N_f number of frames having a frame duration T_f. Then, each frame is further divided into Q number of time-slots of duration T_ψ. As shown in Fig. 2.17, during each frame a pulse is transmitted and the pulse position at the time slot level is jointly determined by the TH address code and the symbol value of the transmitted data according to (2.23).

- **Slow Time Hopping:** In the STH-UWB system, only a single UWB pulse is transmitted in a symbol duration, which consists of N_f number of frames. The operation of the STH-UWB systems may be further augmented by referring to Fig. 2.18. As shown in Fig. 2.18, during a signalling interval duration T_s, b message bits of the kth user are loaded into a b-bit buffer, yielding a M-ary symbol of value $X_m^{(k)}$. The M-ary symbol $X_m^{(k)}$ is temporarily stored in the buffer, and awaits for its time-slot for its transmission. As shown in Fig. 2.18, the transmitter generates an UWB basic pulse expressed as $\psi(t - mT_s)$ for the mth symbol duration. The pseudo-noise (PN) code generator generates a TH pattern for user k. Let the kth user's TH pattern be $\{t_m^{(k)}\}$, where $0 \leq t_m^{(k)} \leq (N_f - 1)$. As shown in Fig. 2.18, for the mth symbol, the TH operation applies an additional shift of $t_m^{(k)} T_f$ to the basic UWB pulse $\psi(t - mT_s)$, locating the pulse at $\psi(t - mT_s - t_m^{(k)} T_f)$. Let us assume that a frame is divided into M number of time-slots to implement MPPM. Then, when the desired time-slot arrives the data-modulation imposes a further delay of $X_m^{(k)} T_\psi$ on the transmitted UWB pulse. Consequently, the transmitted signal for the kth user in the STH-UWB scheme can be expressed as

$$s^{(k)}(t) = \sum_{m=0}^{\infty} \psi(t - mT_s - t_m^{(k)} T_f - X_m^{(k)} T_\psi) \tag{2.25}$$

which shows that, for the mth symbol, a pulse is transmitted at the $X_m^{(k)}$th time-slot of the $t_m^{(k)}$th frame within the mth symbol duration. Fig. 2.19 shows the transmitted UWB signal in the Vth symbol duration. As shown in Fig. 2.19, the Vth symbol duration is first divided into N_f number of frames having a frame duration T_f. Then, each frame is further divided into M number of time-slots of duration T_ψ. In Fig. 2.19 we used $t_m^{(k)} = 1$. Therefore, the first frame is activated and the position of the pulse in this frame is determined by the M-ary symbol $X_m^{(1)} = 1$.

Note that, when designing the TH-UWB systems, the following issues must be taken into account.

- If the value of Q in the FTH-UWB or the value of N_f in the STH-UWB is small, catastrophic

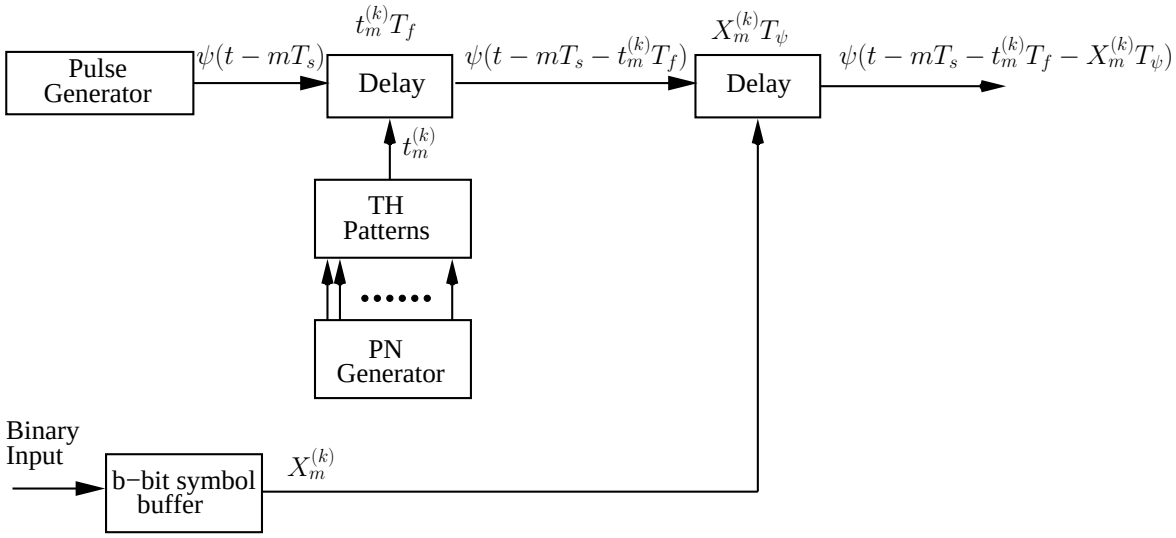

Figure 2.18: Schematic block diagram of slow time-hopping ultrawide bandwidth system using M-ary pulse position modulation.

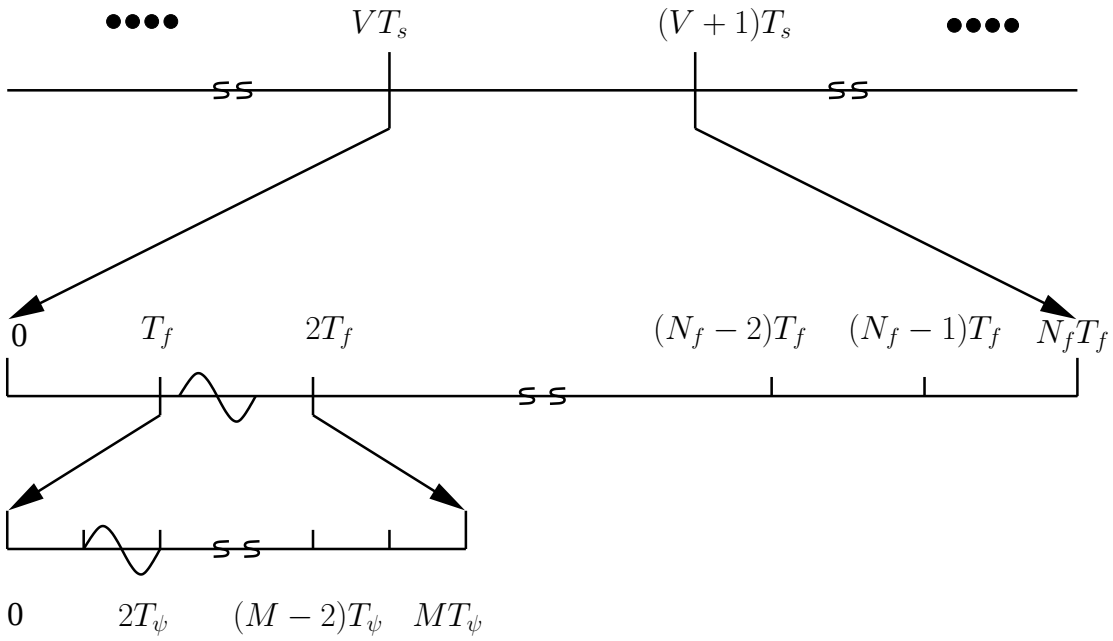

Figure 2.19: Illustration of the transmitted signals in slow time-hopping ultrawide bandwidth using M-ary pulse position modulation.

collision (hit) among the users may occur at a high probability. Usually, the higher the value of Q in the FTH-UWB or the higher value of N_f in the STH-UWB, the lower is the probability of hit;

- When the FTH-UWB has a large value of Q or when the STH-UWB has a large value of N_f, the MAI may be modelled more accurately by the Gaussian random process [34];

- Finally, the ratio QT_ψ/T_f in the FTH-UWB or MN_fT_ψ/T_s in STH-UWB represents the fraction of a frame time duration over which the TH is allowed. This ratio is usually kept less than one, in order to avoid interpulse interference (IPI) [35], which is generated due to the overlap among the successive transmitted pulses from the same user. Furthermore, the receiver could utilise this time after TH to read the output and reset the correlator, etc. [34].

Recently, pseudo-chaotic time-hopping (PCTH) assisted PPM has been proposed for UWB modulation and for implementation of MA transmission [23, 74, 75]. In the PCTH, the principle of symbolic dynamics is exploited to generate an aperiodic spreading sequence, which is dependent on the input data. The PCTH enhances the UWB systems by removing most of the periodic components from the transmitted signal, hence resulting in a low probability of intercept [23]. Furthermore, with the PCTH, the discrete spectral lines of the UWB signals can be effectively removed. Hence, less interference may be inflicted by the UWB systems on the wireless systems operated in the same frequency band [23, 74]. Additionally, the PCTH-based systems have the advantage of high immunity to interception, making them useful for high-security communications [8].

2.2.5.2 Direct-Sequence UWB System

Direct-sequences (DS) spread-spectrum is a famous spread-spectrum technique and a lot of research has already been carried out associated with the DS code-division-multiplexing access (CDMA). In DS-UWB, a data bit is transmitted with the aid of multiple chips and the chip duration is usually set to equal the width T_ψ of the basic UWB pulse. Therefore, in DS-UWB system the frame duration T_f, chip-duration T_c and the pulse width T_ψ are all the same [36, 76, 77]. In UWB systems, since the data rate supported may range from tens of megabits per second to hundreds of megabits per second [29], the number of chips per bit-duration in UWB systems is expected to be in a range from tens to several hundreds. In DS-UWB systems the conventional DS-CDMA-related techniques may be applied [78–80].

In DS-UWB the transmitted signal of the kth user can be represented as

$$s^{(k)}(t) = \sum_{m=0}^{\infty} \sum_{n=0}^{N_c-1} c_n^{(k)} \psi(t - mT_s - nT_c) \tag{2.26}$$

where m indicates the mth symbol, T_s denote the symbol duration, while $c_n^{(k)}$ assumes a value of $+1$ or -1 with equal probability, when random spread sequences are assumed. Furthermore, in (2.26), N_c is the number of chips per symbol, representing the spreading factor. The transmitted DS-UWB signal of (2.26) can be explained with the help of Fig. 2.20, where the Vth symbol duration is considered. As shown in the Fig. 2.20, the Vth symbol duration is divided into N_c number of chips having a chip-duration of $T_c = T_\psi$, and associated with each chip a UWB pulse is transmitted.

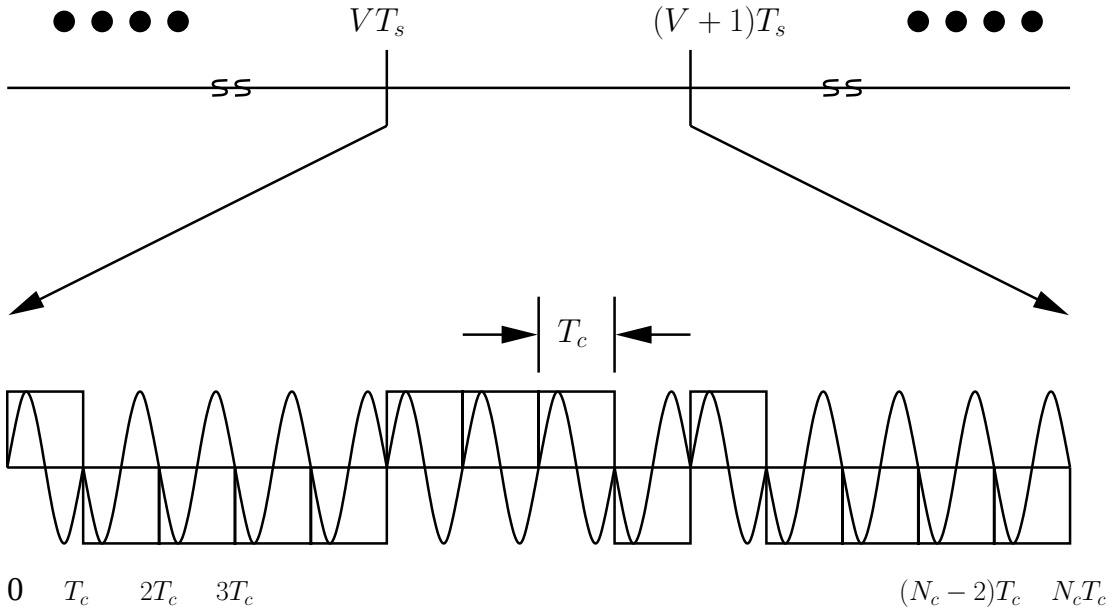

Figure 2.20: Illustration of direct-sequence ultrawide bandwidth signals.

In the DS-UWB systems the M-ary bi-orthogonal keying (MBOK) can be employed [81, 82]. As the MBOK uses bi-orthogonal sequences, the mean of the transmitted DS-UWB signals is zero. Hence, there are no discrete spectral lines present in the PSD of the DS-UWB signals. Furthermore, the MBOK is a power-efficient modulation scheme, which may boost the data-rate supported by the DS-UWB system. However, when there is a large number of multipaths, which generate severe ISI, the BER performance of the MBOK-assisted DS-UWB system may be significantly degraded [81]. The problem caused by the multipaths may be mitigated with the rake reception or high-efficiency

equalisation techniques at a cost of higher complexity.

2.2.5.3 Comparison between TH-UWB and DS-UWB Systems

Both TH-UWB and DS-UWB systems have their advantages and disadvantages, which are summarised as follows.

- **Duty-Cycle:** As above mentioned, in a FTH-UWB system a data-symbol is transmitted with the help of N_f frames, each of which is further divided into Q number of time-slots. Since every frame transmits one UWB pulse by activating one time-slot per frame, the duty-cycle of the FTH-UWB is hence $1/Q$. In a STH-UWB system a data-symbol is transmitted within the time-duration of N_f frames, with each frame being divided into M time-slots. Therefore, the duty-cycle of the STH-UWB approaches $1/MN_f$, since only one UWB pulse is transmitted within the symbol-duration of N_f frames. Finally, in a DS-UWB system each symbol-duration is divided into N_c chips having the chip duration equalling to the width of the basic UWB pulse. Since in DS-UWB a pulse is transmitted associated with each chip, the duty-cycle of the DS-UWB hence approaches unity. From the above discussion, it can be implied that, for the systems using the same spreading factor, the duty-cycle of the TH-UWB systems is much lower than that of the DS-UWB systems. It has been shown in [9] that, for a low-rate wireless personal area network (LR-WPAN), equipments with exceptionally long battery life are highly important. Therefore, low consumption of power for data transmission is important [83]. Since low duty-cycle is a key requirement for low average power consumption, the TH-UWB schemes are hence more suitable for LR-WPAN applications than the DS-UWB schemes [9]. Additionally, references [55, 60, 84, 85] have shown that lower duty-cycle usually causes less interference to the Universal Mobile Telecommunications System (UMTS) systems operating in the same frequency band as the UWB systems.

- **Inter-Chip Interference and Inter-Symbol Interference:** It is well-established that UWB signals with huge bandwidth have the characteristics of fine resolution, yielding a high number of resolvable multipaths [13, 86]. Due to the large number of multipaths and continuous transmission, strong ICI and ISI exist in the DS-UWB systems. It has been shown that the BER performance of the DS-UWB systems communicating over multipath fading channels degrades due to ICI and ISI, when the ICI and ISI are not efficiently mitigated [87, 88]. By contrast, due to the discontinuous transmission in the TH-UWB systems, the TH-UWB systems hence have the robustness against multipath fading [36]. In TH-UWB systems, the symbol duration is usu-

ally very large in comparison with the width of the basic UWB pulse, as a result, the ICI and ISI in the TH-UWB systems can be effectively mitigated [35].

- **Multiuser Interference (MUI):** A DS-UWB system can accommodate a large number of users simultaneously [78]. However, the DS-UWB system may conflict severe multiuser interference (MUI), when the spreading sequences assigned to different users are not orthogonal and when the DS-UWB systems experience multipath fading [89]. By contrast, in the TH-UWB systems, as the number of users supported increases, the chance that two or more users transmit at the same time-slot increases, also yielding MUI. In both the DS-UWB and TH-UWB systems, the MUI may be efficiently mitigated with the aid of the advanced multiuser detection techniques [78, 89, 90]. However, in [80, 91–93] it has been shown that the DS-UWB system can support a larger number of users as compared to TH-UWB system.

- **Interference to The Systems Operated in The Same Frequency Band:** Since an UWB system occupies a huge bandwidth, it is common that an UWB system co-exists with the other narrowband or wideband systems operated in the same frequency band [15]. In DS-UWB systems the discrete spectral lines of the PSD are closely placed, but the magnitudes of the discrete spectral lines are usually low [94]. By contrast, the discrete spectral lines of the PSD in the TH-UWB systems are relatively higher than that of the PSD in the DS-UWB systems. Consequently, the TH-UWB systems may impose higher interference on the existing narrowband or wideband systems than the DS-UWB systems do. In the TH-UWB systems the interference caused by the discrete spectral lines of PSD can be reduced to a sufficiently low level [63, 95–102] by properly design of the spreading codes, pulse width, pulse shape, etc. It has been shown in [21, 36, 93] that the DS-UWB usually causes less in-band interference to the systems operated in the same frequency band, when compared with the TH-UWB.

- **Interference Imposed on UWB Systems by Other Systems:** When there are narrowband and/or wideband systems operated in the same frequency band of the UWB systems, the UWB systems also experience interference imposed by these narrowband and/or wideband systems [15, 103, 104]. Since narrowband and wideband systems usually transmit at higher power than the UWB systems operated in the same band, they may cause higher interference on the UWB systems. Specifically, in a cellular environment, cellular phones may transmit at a power of 30 dBm, which results in a PSD that is 10^7 times higher than that of the UWB systems [62]. It has been demonstrated in [36, 55] that the error performance of the TH-UWB systems is slightly better than that of the DS-UWB systems in the presence of the interference

caused by the global system for mobiles (GSM) and UMTS.

2.3 Multi-Carrier UWB System

Multi-carrier techniques have also been proposed for implementation of UWB communications, where the UWB frequency band is divided into many sub-bands and each sub-band is associated with a subcarrier [62, 105, 106]. For UWB communications, the bandwidth of the multicarrier systems should be at least a bandwidth of 500 MHz, in order to comply with the FCC's definition for UWB systems [1]. It is well-known that in multi-carrier communications, orthogonal frequency divison multiplexing (OFDM) is an attractive modulation scheme, since the OFDM uses fast Fourier transform (FFT) techniques to implement low-complexity multi-carrier modulation/demodulation. Furthermore, the OFDM scheme can capture efficiently the energy dispersed over a huge number of multipaths in UWB channels [62, 105, 106]. Additionally, OFDM scheme has a high flexibility to achieve the spectral regulations by FCC [107].

In [62] an OFDM-UWB scheme has been proposed. In this OFDM-UWB scheme the whole system bandwidth for UWB systems is divided into 14 sub-bands each having a bandwidth of approximately 528 MHz, so that it is convenient for frequency plan and design of the pre-select filters [62]. Note that, the pre-select filters are employed in order to attenuate the out-of-band signals, from global positioning system (GPS), GSM system etc. [62, 106]. In the above-mentioned OFDM-UWB system, over the 528 MHz of bandwidth, there are a total of 128 sub-carriers, which are constituted by 122 sub-carriers carrying useful signals and 6 null-tones [106]. Out of the 122 sub-carriers, 100 of which are devoted to data transmission, 12 of which are assigned for transmitting pilots, while the remaining of which provide guard bands. In this OFDM-UWB system quadrature phase-shift keying (QPSK) baseband modulation is employed [106]. Multiple users are supported through spread-spectrum techniques by assigning different users different time-frequency codes.

In the OFDM-UWB scheme, guard-interval and cyclic-prefix (CP) are added before each transmitted data block. The guard-interval is set in order to provide a sufficient time for the transmitter and receiver to switch between different center frequencies [62]. By contrast, the CP is added for mitigating the ISI caused by multipath fading and the length of the CP may be chosen to minimise the impact of ISI, while maximising the captured energy [62]. In [108] it has been shown that, instead of using CP, zero-padding (ZP) can also be employed for mitigating the ISI. The ZP technique has advantage of reducing ripples in the PSD, which is usually generated due to the redundancy or structure added by CP.

Note that, when designing an OFDM-UWB system, the size of the FFT invoked plays an important role. It has been pointed out that, when using a FFT size of 256, the complexity becomes extreme for portable and handheld devices [62]. The research results in [62] show that a FFT size of 128 with a CP of 60.6 ns is generally desirable for an OFDM-UWB system to achieve a reasonable balance between performance and complexity.

Let us below provide some comparisons between the pulse-based UWB and the multi-carrier UWB.

2.4 Comparison of Pulse-Based UWB Schemes and Multi-Carrier UWB Schemes

Both the pulse-based UWB schemes and the multi-carrier UWB schemes have their specific advantages and disadvantages, which are dependent on the specific communications environments. Some of the comparisons between these two UWB arrangements are summarised as follows.

- **Coexistence with other systems:** As previously discussed, UWB systems are generally deployed to co-exist with the other narrowband/wideband systems operated in the same frequency band, in order to reuse the spectrum resources. Therefore, the UWB systems deployed in certain areas should impose as low interference as possible on the existing narrowband/wideband systems operated in the same frequency band as the UWB systems. Similarly, it is desirable that the interference imposed by the co-existing narrowband/wideband systems on the UWB systems is also as low as possible.

  - **Interference inflicted by UWB systems on the other systems:** In order to reduce the interference inflicted by the UWB systems on the systems operated in the same frequency band, the PSD of the UWB signals should be as low as possible. It is well-recognized that the PAPR of the transmitted signals in single-carrier systems is significantly lower than that of the transmitted signals in multi-carrier systems [109]. Therefore, the multi-carrier UWB systems may inflict more interference on the other systems operated in the same frequency band than the single-carrier systems. Another disadvantage of the multi-carrier UWB, which is caused by its high PAPR, is the increased battery drain [107]. Since in some battery operated UWB applications, such as in LR-WPAN, battery life is critical [9, 83], hence, in this type of applications the pulse-based UWB scheme are preferred.

- ❖ **Interference imposed by the other systems on UWB systems:** It can be shown that in the presence of narrowband interference (NBI), the bandwidth efficiency and overall capacity of the OFDM-UWB systems degrades [107]. However, in the OFDM-UWB systems the NBI caused by narrowband systems may be avoided by choosing an appropriate carrier frequency [1]. By contrast, in the pulsed-based UWB systems, the interference caused by the narrowband systems may be efficiently mitigated by choosing an appropriate processing gain [34] and/or designing a proper pulse shape [97].

- **Position and ranging:** For accurate positioning and ranging, UWB signals are required to have high time-resolution [110]. The time-resolution of a wireless signal is dependent on the basic pulse duration; wireless signals having shorter pulse-duration have higher time-resolution, and the capability to provide more accurate positioning and ranging. Since the pulse-based UWB signals use much shorter pulse duration than the multi-carrier UWB signals, therefore, the pulse-based UWB signals are capable of providing much more accurate positioning and ranging than the multi-carrier UWB signals. For example, in the ad-hoc networks, where accurate positioning is important, pulse-based UWB schemes may play an important role [30].

- **Bit error-rate performance:** The BER performance of a wireless system is dependent on many factors, such as the amount of energy collected, noise level, interference level, detection approach, etc. In UWB systems the transmitted energy is dispersed over a large number of multipaths. Hence, in order to achieve a good BER performance, the energy conveyed by a large number of multipaths is required to be collected. For the pulse-based UWB schemes, a RAKE receiver with a large number of fingers may be employed, in order to collect the energy conveyed by the multipaths. However, the complexity of the RAKE receiver increases with the increase of the number of fingers in the RAKE receiver [111]. By contrast, in the multi-carrier UWB arrangement, the frequency band is divided into many sub-bands that experience flat fading. Therefore, the energy dispersed over the multipaths can be collected in the frequency domain without requiring complex equalisation [107]. It has been shown in [62] that the multi-band OFDM-UWB system with a bandwidth of 528 MHz and a CP of 60.6 ns is capable of capturing approximately 95% of the transmitted energy. By contrast, a DS-UWB system using a RAKE receiver having 16-fingers can only capture 56% of the transmitted energy [62].

- **Transmitter design:** In order to reduce the cost of an UWB device, the UWB transceivers should be as simple as possible. The transmitter in a pulse-based UWB system consists of only a simple pulse generator and a modulator [110], and hence, is very simple. By contrast, in a multi-

carrier UWB system, FFT, digital-to-analog converters (DAC), multiple frequency generators and fast FH synthesisers required. Hence, the transmitter of the OFDM-UWB systems may be much more complex than that of the pulse-based UWB systems [110]. Furthermore, when designing the OFDM-UWB transmitter, different trade-offs need to be taken into account. For example, when considering the FFT size, larger size of FFT results in higher complexity of handheld and portable devices, while smaller size of FFT yields larger portion of overhead due to the CP [62].

- **Receiver design:** When designing a receiver for the UWB systems, complexity of the receiver is one of the most important issues to be considered. When using RAKE receivers the complexity of a pulsed-based UWB system increases linearly with the number of fingers of the RAKE receiver [109, 112]. By contrast, the complexity of the multi-carrier OFDM-UWB system depends logarithmically on the FFT size [62].

- **Timing jitter and synchronization:** As above-mentioned, the multiband OFDM-UWB arrangement utilise relatively long pulse duration, which can mitigate the effect of timing jitter on the achievable BER performance of the system. By contrast, the timing jitter may impose severe impact on the BER performance of the pulse-based UWB systems [113]. Additionally, using shorter pulse-duration requires more strict synchronization [32], since more precise timing is required. It has been shown in [40] that using a higher order of monocycle in the pulse-based UWB systems has the potential for achieving a better BER performance, as a result that a higher order of monocycle results in a lower variance of synchronization error.

Let us now look into the UWB channel model in detail.

2.5 Ultrawide Bandwidth Channel Modelling

Channel modelling constitutes one of the highly important areas that have drawn wide research since the start of wireless communications [1, 7, 13, 29, 43, 114–116]. Wireless channel models that can closely simulate the real-world wireless channels are highly attractive, since, in this case, a lot of research in wireless communications may be carried out based on the wireless channel models instead of the real-world wireless channels, which might be expensive, time-consuming and sometimes impractical. In this section we provide an overview for UWB wireless channel modelling, with the emphasis on its differences from the conventional narrow-band and wideband channels. The UWB

channel models considered in this section, will be applied in the upcoming chapters in the context of various pulse based UWB systems.

This section is structured as follows. Section 2.5.1 compares different types of channel models and summarises their main characteristics. Section 2.5.2 describes the UWB channel model in detail. The impact of both the large-scale fading and small-scale fading on the UWB channels is considered, especially, with the emphasis on small-scale fading. The modified Saleh-Valenzuela (S-V) channel model for modelling of UWB channels is analyzed in detail.

2.5.1 Typical Wireless Channel Models

A lot of work have already been done in the context of wireless channel modelling. Dependent on the bandwidth of the transmitted radio signals, wireless channels can be classified as narrowband, wideband and ultrawide bandwidth (UWB) channels. The typical characteristics of the above-mentioned three types of wireless channels can be described as follows.

- **Narrowband Channel:** The bandwidth of the transmitted signal is significantly less than the coherence bandwidth of the wireless channel. The channel exhibits frequency non-selective or flat fading [114]. All the received multipath component signals of a transmitted symbol arrive at the receiver within a symbol duration. The delays associated with the individual multipath components do not yield big impact on the performance of the system [29]. The multipath component signals are added together at the receiver to form the received signal. If the number of multipath components are sufficiently large, then the amplitude of the received signal can be modelled using Rayleigh or Rician distribution depending on whether there exists a line-of-sight (LOS) propagation path between the transmitter and receiver [1, 13, 29, 117].

- **Wideband Channel:** Wideband channels are typical frequency-selective fading channels, since the coherence bandwidth of wideband channels is usually less than the bandwidth of the transmitted wideband signals [114]. In wideband systems, the delays assisted with the multipath components have effect on the system performance [29]. In order to make use of the multipath components, the delay spread of a wideband channel is divided into bins, where the size of each bin is equal to the inverse of the bandwidth of the transmitted wideband signal. In frequency-selective wideband channel modelling, it is usually assumed that each delay bin contains many multipath components. If there are enough multipath components in a delay bin, the overall amplitude statistics of these multipath components can be modelled as Rayleigh or Rician distribution if there exists no or one LOS propagation path between the transmitter and

the receiver [29, 114].

- **Ultrawide Bandwidth Channel:** Like wideband channels, UWB channels are typical frequency-selective fading channels. In UWB channels, the bandwidth of the transmitted signal is extremely higher than the coherence bandwidth of the corresponding wireless channels. As a result, the size of the delay bins becomes extremely small. In this case, there is a possibility that no multipath components or only a few multipath components fall within a delay bin. Consequently, in UWB channel modelling it becomes necessary to characterise the likelihood that there are empty bins containing no signals [29]. Since, as above-mentioned, there are usually no or only a few multipath components falling within a resolvable delay bin, central-limit theorum may no longer be valid [29]. Hence, in UWB channels, the amplitude statistics of the signals within a delay bin may not be modelled using Rayleigh or Rician distribution [29], which will be explored in detail in our forthcoming discourse in this chapter.

2.5.2 UWB Channel Modelling

In UWB systems, it is possible to resolve the multipath components generated by the objects separated by only several feet, hence the fading margin can be significantly reduced. Low fading margin and low PSD make UWB systems best suitable for short-range communications [118]. Recent results indicate that UWB systems are viable candidates for short-range MA communications in dense multipath environments. The UWB systems have the potential of providing a high order of diversity, since the UWB signals employ the capability of fine delay resolution [119, 120]. Since various UWB schemes have been considered for providing short-range high-speed wireless communications, in recent years a lot of measurements have been carried out in order to model the UWB channels, especially the indoor UWB channels [29, 121–130]. In [131], a detailed overview of UWB indoor channels has been presented.

In this section an overview of the UWB channel models given in the literature is provided. As the channel modelling for the conventional narrowband and wideband channels, the UWB channel modelling can also be characterised in the context of the large-scale and small-scale fading. However, it has been shown that, in UWB communications, it is the small-scale fading that plays an important role in indoor short range wireless communications.

2.5.2.1 Large-Scale Fading

In UWB communications the impact of the channel on the transmitted signal over a large distance (greater than 1m) is referred to as large-scale fading [1]. Large-scale fading includes the average attenuation effect due to the distance between the transmitter and receiver and large objects in the propagation path. In traditional channel modelling the large-scale fading is also called as path-loss, which is measured as [43]

$$PL(d) = \overline{PL}(d_o) + 10\eta \log_{10}\left(\frac{d}{d_o}\right) + X_\sigma, \qquad d \geq d_o \tag{2.27}$$

where $PL(d)$ is the path-loss at a distance d, $\overline{PL}(d_o)$ is the average path-loss at a given distance or referenced distance of d_o, e.g. $d_o = 1m$, η is the path-loss exponent and X_σ takes into account the shadowing, which is a Gaussian distributed random variable (in dB) with a standard deviation σ (also in dB) [43]. The average path-loss, path-loss exponent and the standard deviation σ are statistically dependent on the communications environments. Therefore, they are usually modelled as random variables obeying certain distributions [118]. The path-loss exponent η depends upon the carrier frequency, antenna height and propagation environments [114]. It has been found to have a normal distribution $N[\mu_\eta, \sigma_\eta]$ associated with a mean μ_η and a standard deviation σ_η. Hence, the path-loss exponent can be expressed as [118]

$$\eta = \mu_\eta + \eta_1 \sigma_\eta \tag{2.28}$$

where η_1 is a Gaussian variable having mean zero and unit variance.

The shadow fading term X_σ given in (2.27) is environmental specific and can be modelled as [118]

$$X_\sigma = \eta_2(\mu_\sigma + \eta_3 \sigma_\sigma) \tag{2.29}$$

where η_2 and η_3 are also zero mean Gaussian distributed random variables and σ_σ has a normal distribution where the mean and the variance is determined statistically from the measured data. It is found that in shadow fading the standard deviation σ_σ is independent of the carrier frequency [132]. Upon substituting (2.28) and (2.29) into (2.27), finally, the propagation path-loss, can be expressed as

$$PL(d) = \overline{PL}(d_o) + 10\mu_\eta \log_{10}\left(\frac{d}{d_o}\right) + 10\eta_1\sigma_\eta \log_{10}\left(\frac{d}{d_o}\right) + \eta_2\mu_\sigma + \eta_2\eta_3\sigma_\sigma \tag{2.30}$$

Note that, in (2.30) the first two terms represent the median path-loss, while the rest three terms represent the random variations about the median path-loss [118].

2.5.2.2 Small-Scale Fading: Saleh-Valenzuela Channel Model

In wireless communications small-scale fading is caused by the small objects in the communications environments which result in that the receiver receives many versions of the transmitted signal, which arrive at the receiver with different phases and also slightly different time delays [43]. In UWB communications, small-scale fading refers to the fading within an area of one square metre $1m^2$ [1]. Therefore, it is the major parameter of interest in indoor communications. The main small-scale fading model adopted for indoor UWB communications is the modified Saleh-Valenzuela (S-V) model [29], which is now described in detail.

In UWB Communications, it has been recognised that the multipath components arrive at the receiver in clusters [13, 29, 133]. In wireless communications, generally, the number of resolvable multipaths is a function of the measured bandwidth of the transmitted signals and the communications environment [13], which can be formulated approximately as

$$L \approx [WT_m] + 1 \tag{2.31}$$

where L denotes the number of resolvable multipath components, $W = 1/T_\psi$ is the bandwidth of the radio signals, while T_m represents the maximum delay-spread of the wireless communications channel. In UWB indoor communications, the delay-spread T_m spans several nanoseconds, yielding possibly many resolvable multipaths, which generates ISI, if the transmitted UWB pulses are closely positioned in time [29]. However, the ISI may be mitigated by properly designing of the basic pulse waveform or by employing advanced signal processing or/and equalisation techniques for detection [29].

In UWB channels the multipath arrivals can be classified into two categories: cluster arrival and ray arrival within a cluster. Therefore, for the UWB channels, four parameters are required in order to describe the S-V channel model. The four parameters determining the S-V model for UWB channels are as follows:

- Λ: Cluster arrival rate,
- λ: Ray arrival rate within a cluster,
- Γ: Cluster decay factor,
- γ: Ray decay factor within a Cluster.

Let us below explain these parameters in more details.

1) **Cluster Arrival Rate (Λ):** In indoor UWB communications, the clusters are formed by the building structure [133]. The cluster arrival can be modelled as a Poisson process with a mean cluster arrival rate of Λ [1, 29, 133]. Therefore, the probability of having v clusters within a time-duration of T can be given as

$$P_v = \frac{(\Lambda T)^v}{v!} \exp(-\Lambda T) \tag{2.32}$$

Note that, for convenience, we can assume that the first cluster is always present. Furthermore, according to the principles of Poisson process, the inter-arrival time of the clusters can be described by a random variable obeying the exponential PDF

$$p(T_v|T_{v-1}) = \Lambda \exp[-\Lambda(T_v - T_{v-1})], \quad v > 0 \tag{2.33}$$

where, for UWB communications, the value of $1/\Lambda$ is typically in the range of 10 ns to 50 ns [13]. In the S-V model, the clusters usually overlap one another, making it difficult for the naked eye to observe the start and end of the cluster [7]. As the number of clusters is a function of bandwidth and environment, there are usually one till five number of clusters present in an UWB indoor channel [1, 118, 124, 134].

2) **Ray Arrival Rate within A Cluster (λ):** In indoor UWB communications, rays are formed by the objects within the vicinities of the transmitter and receiver [133]. Ray arrival within a cluster can also be modelled by a Poisson process, where the inter-arrival of two adjacent rays is a random variable obeying the exponential PDF given by

$$P(\tau_{u,v}|\tau_{u-1,v}) = \lambda_v \exp[-\lambda_v(\tau_{u,v} - \tau_{u,v-1})], \quad u > 0, v = 1, 2, \cdots \tag{2.34}$$

where $\tau_{u,v}$ denotes the arrival time of the uth multipath in the vth cluster, while λ_v is the mean arrival rate of the rays (multipaths) in the vth cluster. Typically, each cluster may contain many multipaths, implying $\lambda >> \Lambda$ [133]. For some UWB communications environments where the ray arrival rate of the later clusters is higher than that of the earlier clusters [13, 127], the ray arrival can be modelled as a mixture of two Poisson processes given as [13, 135, 136].

$$\begin{aligned} P(\tau_{u,v}|\tau_{u-1,v}) &= \alpha\lambda_1 \exp[-\lambda_1(\tau_{u,v} - \tau_{u,v-1})] \\ &+ (1-\alpha)\lambda_2 \exp[-\lambda_2(\tau_{u,v} - \tau_{u,v-1})], \quad u > 0, v = 1, 2, \cdots \end{aligned} \tag{2.35}$$

where $0 \leq \alpha \leq 1$ is the mixture coefficient, while λ_1 and λ_2 are the ray arrival rates of the first and second Poisson processes. In UWB communications, one of the two ray arrival rates is usually higher than the other one in the mixture model. Hence, the duration of the process having a higher ray arrival rate is shorter than the duration of the process having a lower ray arrival rate. However, the former case usually results in stronger multipath components than the later case [137].

3) **Cluster Decay Factor (Γ):** The decay factor is derived from the observed power decay profile of the UWB channels [29]. In S-V model, the average power of clusters usually decays exponentially with the delay [137]. For a block of data, the power and arrival time delay of the first arrived cluster are normalised to one and a time delay zero, respectively. All the other clusters of the same block of data are expressed relative to the first cluster [136]. It has been found that the cluster decay factor Γ increases, if the building walls are more reflective [133].

4) **Ray Decay Factor within A Cluster (γ):** The average power of the resolvable multipaths within a cluster also decays exponentially, which is reflected by the value of the ray decay factor of a cluster [137]. In UWB communications, the multipath decay factor or the so-called intra-cluster decay rate is found to be dependent linearly on the arrival time of the cluster [135]. Specifically, the decay factor of the vth cluster can be described as

$$\gamma_v \propto u_\gamma T_v + \gamma_0, \quad v = 0, 1, \cdots, V-1 \tag{2.36}$$

where γ_0 represents the decay factor of the zeroth cluster, u_γ is a constant, while T_v devoted the arrival time of the vth cluster. Within a cluster, the arrival time of the first ray is set to zero and its corresponding amplitude is set to one. All the other rays within a cluster are then adjusted accordingly relative to the first ray according to the exponential distribution [136]. In UWB communications, it has been found that we have typically, $\Gamma > \gamma$, which indicates that the expected power of the rays within a cluster decays slower than the expected power of the first rays of the clusters [136].

UWB channels are typical time-varying frequency-selective fading channels, which can be modelled using tapped-delay line approach [1, 124, 138]. Specifically, in [124–126] an indoor UWB channel model has been presented based on statistical analysis of the data collected from an UWB propagation experiment, performed in typical office buildings. The channel model is obtained based on the measurements carried out within the frequency-range from 300 MHz - 1 GHz and using the UWB

basic pulse having 2 ns of delay resolution. Hence, the resultant UWB channel model constitutes a representative channel model suitable for low-frequency (LF) UWB systems. In the context of this LF-UWB channel model [124, 131], the measurement data shows that the direct path always falls in the first resolvable path, which is usually the strongest path. The power of the subsequent resolvable paths decays exponentially with the increase of delay. The analysis in the context of the LF-UWB channel [124] shows that the well-established tapped-delay-line model [49], is well suitable for the LF-UWB channel modelling. Furthermore, the statistics analysis in [124] shows that the best-fit distribution of the small-scale magnitude statistics is the Nakagami-m distribution or the Gamma distribution, when power is considered. It has been shown [124] that the parameters of the Gamma distribution vary from path to path. The value of the fading parameter in the Nakagami-m/ or Gamma distribution ranges from 1 and 6, which decreases as the excess delay increases.

In contrast to the UWB channel model considered in [124, 131], which is suitable for the frequency range from 300 Mhz-1 GHz, channel model proposed in [29, 121–123] is suitable for the frequency band ranged from 3.1 GHz to 10.6 GHz. Correspondingly, this UWB channel model can be viewed as a representative channel model for high-frequency (HF) UWB systems. To be more specific, the measurements in the context of [121–123, 139] have been carried out in both the residential and office areas, where both LOS signals and non-LOS signals exist, resulting in that the delay-spread ranges from 5 ns to about 40 ns. The measurement data shows that in the above-mentioned HF-UWB channels the first resolvable multipath at the receiver is not necessarily the strongest one. The power delay profile is generally sparse, where some of the resolvable multipaths do not carry any significant power, or even empty [29]. In the HF-UWB channels, multipaths arrive at the receiver in clusters rather than in continuum as in narrowband channels. Hence, in [29, 121, 122] a double exponential decay UWB channel model has been introduced for characterising the power delay profile of the HF-UWB channels, where one corresponds to the clusters, while the other one corresponds to the multipaths within a cluster. Furthermore, the measurement data shows that the signal amplitudes do not follow Rayleigh distribution. Instead, a lognormal or Nakagami distribution may be employed to measurement data. Furthermore, it has been found that both the lognormal and Nakagami distributions can fit the measurement data equally well.

Based on the above-mentioned properties in association with the UWB channels, in this thesis the conventional statistical tapped-delay-line (STDL) channel model is introduced and modified for our investigation in the forthcoming discourses. Specifically, the S-V model is employed, which has the

channel impulse response (CIR) of the S-V model and can be represented as [1, 133, 137]

$$h(t) = \sum_{v=1}^{\infty} \sum_{u=1}^{\infty} \beta_{u,v} \delta(t - T_v - \tau_{u,v}) \tag{2.37}$$

where $\beta_{u,v}$ denotes the fading gain of the uth multipath in the vth cluster, T_v denotes the arrival time of the vth cluster and $\tau_{u,v}$ is the arrival time of the uth multipath in vth cluster and is relative to T_v. In UWB communications in order to capture all or most of the transmitted signal energy, the receiver may require to process a huge number of resolvable multipaths [140]. In order to reduce the complexity, L out of the total number of resolvable multipaths may be used for detection. It has been shown that using L multipaths for detection may achieve an error performance close to that achieved by a receiver that processes all the resolvable multipath components provided the value of L is sufficiently high [141].

In practice, the received UWB signals can only have a limited number of clusters, where each cluster contains a limited number of resolvable multipaths. In this case, the CIR of (2.37) can be reduced to

$$h(t) = \sum_{v=1}^{V} \sum_{u=1}^{U} \beta_{u,v} \delta(t - T_v - \tau_{u,v}) \tag{2.38}$$

where V represents the number of clusters and U denotes the number of resolvable multipaths in each of the V clusters. Therefore, for the UWB channels having the CIR of (2.38), the total number of resolvable multipaths can be as high as $L = UV$. Note that, as we mentioned previously, the parameters $\beta_{u,v}$, T_v and $\tau_{u,v}$ may be time-varying, due to the relative motion between the transmitter and receiver. However, for the sake of convenience, we assume that the fading rate is significantly lower than the data rate conveyed. Under this assumption, the parameters $\beta_{u,v}$, T_v and $\tau_{u,v}$ may be treated as time invariant random variables, when data block of interest are relatively short [133]. In (2.38), we define the average power of a multipath component at a given delay $T_v + \tau_{u,v}$ is relative to the average power of the first resolvable multipath as

$$\overline{\beta_{u,v}^2} = \overline{\beta_{1,1}^2} \exp\left(-\frac{T_v}{\Gamma}\right) \exp\left(-\frac{\tau_{u,v}}{\gamma}\right), \quad u = 1, 2, \cdots, U, \quad v = 1, 2, \cdots, V \tag{2.39}$$

where $\overline{\beta_{1,1}^2}$ denotes the average power of the first resolvable multipath in the first cluster, while $\overline{\beta_{u,v}^2}$ denotes the average power by the uth multipath in the vth cluster. Furthermore, in order to carry out comparison among different scenarios, the total average power received is normalised to unity, i.e.,

we have

$$\sum_{u=1}^{U}\sum_{v=1}^{V}\overline{\beta_{u,v}^2}=1 \tag{2.40}$$

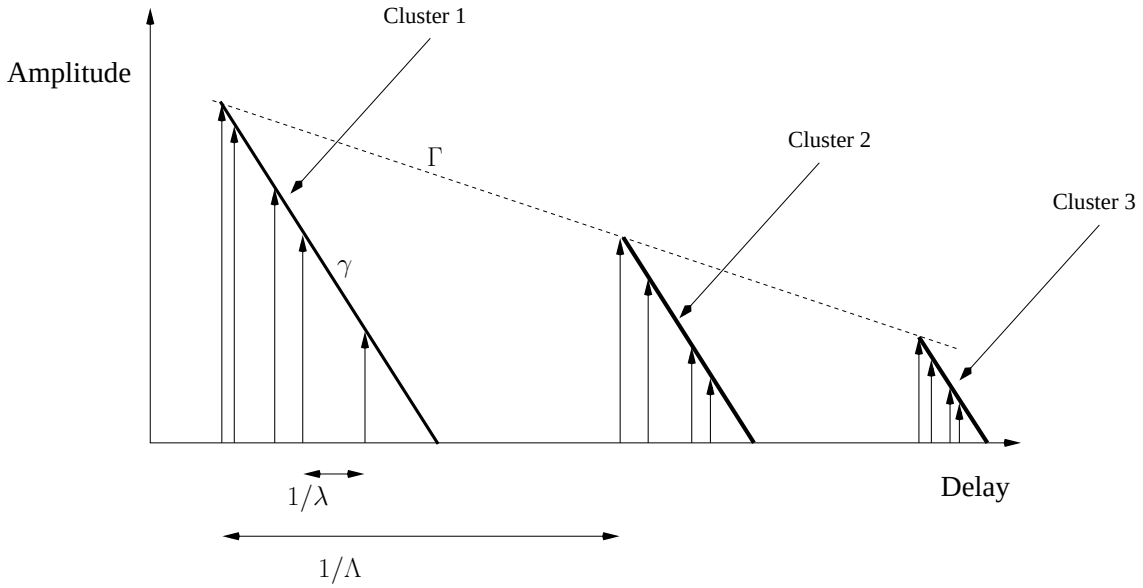

Figure 2.21: Illustration of the Saleh Valenzuela UWB channel model, which contains three clusters and each cluster may contain different number of resolvable multipaths.

Figure 2.21 shows conceptually the CIR of the S-V UWB channel model [13]. As discussed previously in this section, in UWB communications the empirical distribution of the fading amplitudes of the multipaths differs remarkably from the Rayleigh distribution. Instead, the measurement data matches to the lognormal or Nakagami distribution, which has been validated using Kolmogorov-Smirnov testing with a significance level 1% [29]. Specifically, in this thesis, we mainly assume that the fading amplitudes of the UWB channels follow the Nakagami-m distribution, which can be expressed as

$$\begin{aligned} P(\beta_{u,v}) &= M\left(\beta_{u,v}, m, \Omega_{u,v}\right) \\ &= \frac{2m^m\beta_{u,v}^{2m-1}}{\Gamma(m)\Omega_{u,v}^m}\exp(-m/\Omega_{u,v})\beta_{u,v}^2 \end{aligned} \tag{2.41}$$

where $m \geq 1/2$ is the fading parameter, determining the severity of fading, which is equal to $m = \mathbf{E}^2[(\beta_{u,v}^2)]/\mathbf{Var}[(\beta_{u,v})^2]$, $\Gamma(m)$ is the Gamma-function and $\Omega_{u,v} = \mathbf{E}[(\beta_{u,v})^2]$ is the second moment of the fading amplitude of the uth multipath in vth cluster. The Nakagami-m PDF of (2.41)

employs the following properties.

1) Lognormal distribution can be approximated by the Nakagami distribution associated with a relatively high value of m of the fading parameter [29].

2) Rayleigh distribution is valid in some UWB communications environments, even when the time resolution is fine [13]. For example, Rayleigh fading has been observed in industrial environments, where dense multipath scattering objects exist, resulting in numerous multipath components [117]. The Nakagami-m distribution of (2.41) is reduced to the Rayleigh distribution, when the fading parameter m is set to one, i.e, when $m = 1$.

3) Nakagami-m distribution is a generalised distribution, which often gives the best fit to land-mobile and indoor-mobile multipath propagation environments, as well as to scintillating ionospheric radio links [142]. With the aid of (2.41), it can be shown that different propagation scenarios can be modelled by the Nakagami-m distribution by simply changing the value of m in the Nakagami-m distribution. Furthermore, the Nakagami-m distribution offers features of analytical convenience [142].

Finally, four typical UWB channel models proposed in literature [29] are summarised in Table 2.3. Our simulation results provided in the following chapters were also obtained based on these typical channel models.

2.6 Summary and Conclusions

In this chapter an overview of UWB systems has been presented. It can be shown that UWB systems employ a lot of merits in comparison with conventional narrowband/wideband systems, as the instantaneous bandwidth of the UWB systems is significantly higher than the minimum bandwidth required to deliver the information. Therefore, in recent years a lot of interest has been drawn in both the research communities and industry.

UWB systems can be implemented by pulse-based or multi-carrier-based techniques. Pulse-based UWB system, can be a carrier-less or a base-band modulation system, where signals are transmitted with the assistance of trains of time-shifted pulses. When designing pulse-based UWB systems the following issues needs to be considered.

- The shape of the basic UWB pulse has a strong impact on the design of transmitter and receiver filters, signal bandwidth, BER, etc. The pulse is usually required to have no DC-component,

Channel Characteristics	Channel Model-1	Channel Model-2	Channel Model-3	Channel Model-4
Λ [1/nsec] (Cluster arrival rate)	0.0233	0.4	0.0667	0.0667
λ [1/nsec] (Ray arrival rate)	2.5	0.5	2.1	2.1
Γ (Cluster decay factor)	7.1	5.5	14	24
γ (Ray decay factor)	4.3	6.7	7.9	12
Communication environments	LOS (0-4 m)	NLOS (0-4 m)	NLOS (4-10 m)	Extreme NLOS

Table 2.3: Typical ultrawide bandwidth channel models, where LOS and NLOS stands for line of sight and non-line of sight, respectively.

in order to yield high power efficiency. The second order derivative of the pulse should exist so that matched-filtering could be employed at the receiver for achieving low complexity detection. Furthermore, it is required to have a low PSD, so that the interference inflicting to the co-existing communications systems is low. In order to meet the above-mentioned requirements in this chapter a range of UWB pulses for pulse-based UWB systems have been analyzed in detail. Specifically, the basic characteristics of GP, TESM, PS, HP and GMSP etc. UWB pulses have been summarized in Table 2.1.

- As FCC has imposed no restriction on data modulation scheme, different kinds of data modulation schemes may be employed for pulse-based UWB systems. Therefore, when considering a data modulation scheme for pulse-based UWB systems, the data rate supported, affordable complexity, ISI generated, spectral characteristics, robustness against narrowband interference, BER performance, etc., are required to be taken into account. Generally, it is desirable that the data modulation scheme has zero mean so that there are no discrete spectral lines in the PSD. Furthermore, the data modulation scheme is expected to be scalable to M-ary communications, in order to improve the MA capability of the UWB systems. Specifically, in Table 2.2

the characteristics for OOK, PPM, PSM and PAM, etc., data modulation schemes have been summarized and compared.

- As shown in our discussion, in pulse-based UWB systems, different types of MA schemes may be employed. As UWB systems are typical spread-spectrum systems, TH, FH, DS, etc., spread-spectrum techniques can hence be employed. The MA schemes have been overviewed in detail in Section 2.2.5. It can be shown that each MA scheme has some advantages and also some disadvantages for UWB applications.

For the multicarrier UWB schemes, the UWB frequency band is divided into many sub-bands with each sub-band having at least a bandwidth of 500 MHz. It has been realised that OFDM is an attractive transmission scheme for the multi-carrier UWB systems. In the OFDM-UWB systems the whole available bandwidth is divided into 14 sub-bands with each sub-band having a total of 128 subcarriers. Out of 128 subcarriers, 100 are used for data transmission, 12 are used for transmitting pilots, 10 are used to provide guard bands and the rest are null-tones without transmitting information at all. In the OFDM-UWB systems, QPSK baseband modulation is employed and multiple users are supported by spread-spectrum techniques by assigning each user a user specific time-frequency spreading code.

Finally, in this chapter the modelling of UWB channels has been considered. It can be shown that the UWB channels have the following characteristics.

- The UWB channels are significantly different from the conventional narrowband and wide-band channels. Therefore, the results obtained for modelling the conventional narrowband and wideband channels cannot be applied directly for modelling the UWB channels.

- In the context of the large-scale fading, in UWB communications the path-loss is found to be environmental specific, both the average path-loss and the path-loss exponent are environmental specific.

- Since UWB communications are mainly for indoor and short-range communications, hence the modelling of their small-scale fading is more interested. In UWB communications, the widely recognised channel model adopted for modelling the small-scale fading is the modified S-V model, which is a STDL model. The S-V channel model is characterised by four parameters, namely, the cluster arrival rate (Λ), the ray arrival rate within a cluster (λ), the cluster decay factor (Γ) and the ray decay factor within a cluster (γ), respectively.

- The measurement data shows that the amplitude statistics in UWB channels follows the log-normal or Nakagami distribution, or in some specific cases, the Rayleigh distribution. Usually, the Nakagami distribution is preferred, since both the Rayleigh and log-normal distributions can be approximated by the Nakagami distribution. Furthermore, the Nakagami distribution can often result in closed-form analytical results.

Chapter 3

Hybrid Direct-Sequence Time-Hopping Ultrawide Bandwidth Systems

3.1 Introduction

In Chapter 2 pulse-based UWB schemes were discussed and it was realised that like other spread-spectrum systems, UWB systems do not rely only on the spreading sequence or hopping pattern to produce a wide bandwidth signal. Instead, it is the extremely short duration of the basic UWB pulses that results in the UWB systems having ultra-wide bandwidth [56, 92, 143, 144]. As discussed in Chapter 2, UWB communication has initially been implemented with the aid of time-hopping pulse-position modulation (TH-PPM) techniques without carrier modulation [34, 35]. In the carrier-less or baseband UWB systems information is transmitted with the assistance of trains of time-shifted pulses through PPM. In the TH-PPM UWB systems multiple pulses are usually used to transmit a single symbol for the sake of enhancing the transmission performance. Recently, the direct-sequence spread-spectrum technique has also been proposed for implementation of UWB communications [78]. In DS-UWB systems a data bit is transmitted associated with multiple chips and the chip-duration is usually equal to the width of the basic time-domain pulse. Straight forwardly, in DS-UWB the conventional DS-CDMA related techniques may be applied for improving the multiple-access capability [78, 79]. As analysed in detail in Chapter 2 both the TH-UWB scheme and DS-UWB scheme have their advantages as well as disadvantages.

In this chapter we propose and investigate a novel UWB scheme, namely the hybrid (DS-TH) UWB system, which employs both DS spreading and TH. It can be shown that the hybrid DS-TH

UWB system is capable of inheriting the advantages of both the DS-UWB and TH-UWB, while simultaneously avoiding their disadvantages. Conventionally, hybrid DS and TH schemes have not been drawn much attention, since, it is generally recognised that the combination of DS with TH increases the complexity of implementation and that the timing requirement may become more stringent [49, 145]. However, in the hybrid DS-TH systems the search space, which is usually very large in UWB systems due to long spreading sequences and fine timing resolution, can be significantly reduced [146, 147]. Hence, the code acquisition and timing tracking in hybrid DS-TH UWB systems may become relatively easy. Additionally, the hybrid DS-TH UWB systems are capable of providing more degrees-of-freedom for system design and reconfigurations than either the pure DS-UWB schemes or the pure TH-UWB schemes. Furthermore, it can be shown that both the TH-UWB and DS-UWB schemes constitute special examples of the hybrid DS-TH UWB.

In this chapter we investigate the performance of hybrid DS-TH UWB system, when communicating over UWB channels associated with various detection strategy. For simplicity, we assume that in this chapter the hybrid DS-TH UWB systems employs binary phase shift keying (BPSK) modulation. More specifically, in Section 3.2, the transmitted signal in the hybrid DS-TH UWB system is introduced along with the channel model and receiver structure. In Section 3.3, we consider the detection of the hybrid DS-TH UWB signal using MF. In Section 3.4 the performance of the hybrid DS-TH UWB system is compared with that of the pure DS-UWB and pure TH-UWB systems, when the conventional single-user correlation detector or conventional MMSE-MUD is employed. Section 3.5 analyses the complexity of the correlation and MMSE-MUD when considering UWB communications. Finally, in Section 3.6 the performance of the above-mentioned three types of UWB systems is investigated and compared, when communicating over typical UWB channels experiencing Nakagami-m fading. Our study and simulation results in this chapter show that there exists a trade off between the DS and TH spreading factors of the hybrid DS-TH UWB systems. Given the channel conditions, SNR value and the total spreading factor equalling to the product of the DS and TH spreading factors, there exists optimum DS and TH spreading factors which result in the lowest achievable BER.

3.2 System Description

3.2.1 Transmitted Signal

The transmitter schematic block diagram for the considered hybrid DS-TH UWB system is shown in Fig. 3.1. In our hybrid DS-TH UWB system BPSK baseband modulation is assumed for simplicity.

As shown in Fig. 3.1, a data bit of the kth user is first modulated by a N_c-length DS spreading sequence, yielding N_c chips. Then, the N_c chips are transmitted by invoking N_c time-domain pulses within one symbol-duration, where the locations of the N_c time-domain pulses are determined by the TH pattern assigned to the kth user. According to Fig. 3.1, it can be shown that the hybrid DS-TH UWB signal transmitted by the kth user can be written as [148]

$$s^{(k)}(t) = \sqrt{\frac{E_b}{N_c T_\psi}} \sum_{j=0}^{\infty} b^{(k)}_{\left\lfloor \frac{j}{N_c} \right\rfloor} d^{(k)}_j \psi \left[t - jT_c - c^{(k)}_j T_\psi \right] \tag{3.1}$$

where $\lfloor x \rfloor$ represents the floor function, which returns the largest integer less than or equal to x, $\psi(t)$ is the basic time-domain pulse of width T_ψ, which satisfies $\frac{1}{T_\psi} \int_0^{T_\psi} \psi^2(t) dt = 1$. The bandwidth of the hybrid DS-TH UWB system is determined by the basic time-domain pulse. For brevity, the parameters used in (3.1) and in our forthcoming discourse are listed as follows:

- E_b: Energy per bit;
- N_c: Number of chips per bit, which is defined as the DS spreading factor;
- N_ψ: Number of time slots in a chip, which is defined as the TH spreading factor;
- T_ψ: Duration of a time-hopping slot, which is equal to the duration of the basic UWB pulse;
- T_c: Chip-duration, which satisfies $T_c = N_\psi T_\psi$;
- T_b: Bit-duration, which satisfies $T_b = N_c T_c = N_c N_\psi T_\psi$;
- $b^{(k)}_i \in \{+1, -1\}$: The ith data bit transmitted by user k;
- $d^{(k)}_j \in \{+1, -1\}$: Binary DS spreading sequence assigned to the kth user;
- $c^{(k)}_j$: TH sequence assigned to the kth user, $c^{(k)}_j \in \{0, 1, \cdots, N_\psi - 1\}$ and takes any value with equal probability;
- $N_c N_\psi$: Total spreading factor of the hybrid DS-TH UWB system.

From the above description it can be observed that if $N_\psi = 1$, T_ψ and T_c are equal and in this case the hybrid DS-TH UWB scheme is reduced to the pure DS-UWB scheme. By contrast, the hybrid DS-TH UWB scheme with $N_c = 1$ is reduced to the pure TH-UWB scheme. As shown in (3.1), each chip transmits a pulse and the location of the pulse within a chip is determined by the TH sequence $\{c^{(k)}_j\}$, where $c^{(k)}_j$ takes a value in $\{0, 1, 2, \cdots, N_\psi - 1\}$ with equal probability. In the hybrid DS-TH

UWB system total processing gain is $N = N_c N_\psi$. Note that, the conventional TH-UWB system represents a STH system, where one pulse is transmitted within a bit-duration. By contrast, hybrid DS-TH UWB system is a FTH system, where N_c pulses are transmitted associated with one bit.

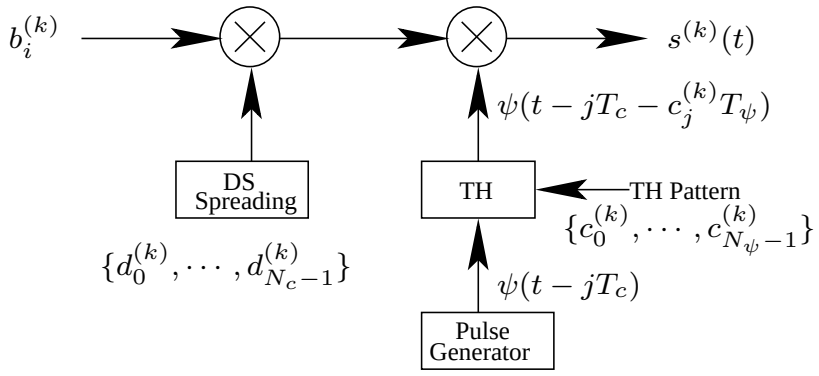

Figure 3.1: Transmitter schematic block diagram of hybrid direct-sequence time-hopping UWB System.

The principles of hybrid DS-TH UWB scheme can be further understood with the aid of Fig. 3.2. In this figure the $(V-2)$th bit of duration T_b is first divided into N_c chips having duration of T_c seconds. Each chip corresponds to an appropriate value determined by the DS-spreading code. Then, each chip-duration of T_c is further divided into N_ψ time-slots with duration T_ψ seconds. The time-slot activated for transmitting a pulse is determined by the respective TH pattern assigned. For example, in Fig. 3.2, the first time-slot of the second chip is activated to transmit a pulse. From the above analysis, we can see that the bit-duration obeys $T_b = N_c T_c = N_c N_\psi T_\psi$.

3.2.2 Channel Model

The CIR of the UWB channels considered in the chapter is given by [86]

$$h(t) = \sum_{l=0}^{L-1} h_l \delta(t - T_0 - lT_\psi) \tag{3.2}$$

where L represents the number of resolvable multipaths at the receiver, $h_l = |h_l|e^{j\phi}$ represents the channel gain of the lth resolvable multipath component, T_0 denotes the transmission delay of the line-of-sight (LOS) signal from the transmitter to the receiver, while lT_ψ represents the excess delay of the lth resolvable path.

In order to make the channel model sufficiently general so that it can be modified for modelling different communications environments, we assume that, firstly, the delay-spread of the UWB chan-

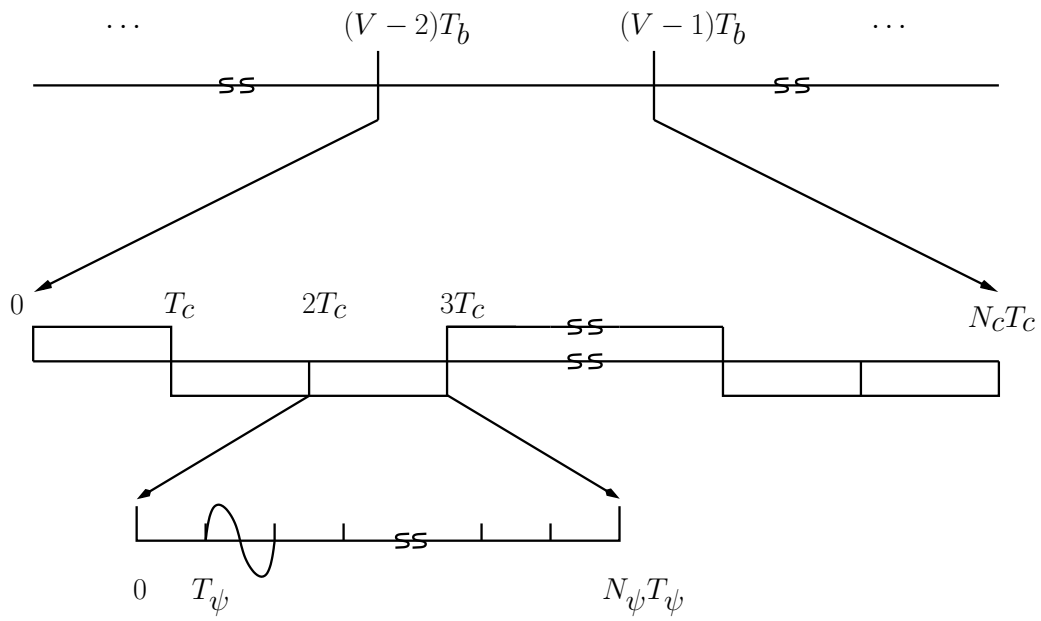

Figure 3.2: Structure of the time-domain hybrid DS-TH UWB signals.

nels spans g data bits, yielding $(g-1)N_cN_\psi < (L-1) \leq gN_cN_\psi$. Secondly, we assume that among the L number of resolvable multipath components there are L_s relatively strong multipath components, which convey the majority of the average power transmitted. Furthermore, we assume that the L_s number of significant multipath components are randomly distributed over the L number of resolvable multipaths, but retaining the same within each data block.

In UWB communications it has been found that the empirical distribution of the fading gains differs remarkably from the Rayleigh distribution. This is because that UWB signals are capable of providing a fine resolution in the time-domain, implying that usually only a small number of multipath components fall within an interval of the resolution. In this case, the Gaussian approximation for deriving the Rayleigh distribution is not satisfied. As shown in [29], the measured data shows that, in UWB communications, the fading amplitudes usually follow lognormal or Nakagami distribution, which has been validated with the aid of Kolmogorov-Smirnov testing associated with a significance level of 1%. Due to the above facts, in this chapter, the Nakagami distribution is introduced for modelling the fading of the UWB channels concerned. Specifically, we assume that the amplitude of the fading gain obeys the independent Nakagami-m distribution with a probability density function

(PDF) given by [49]

$$\begin{aligned} P_{|h_l|}(r) &= M\left(|h_l|, m_l, \Omega_l\right) \\ &= \frac{2m_l^{m_l} r^{2m_l-1}}{\Gamma(m_l)\Omega_l^{m_l}} \exp(-m_l/\Omega_l)r^2, \qquad r > 0 \end{aligned} \tag{3.3}$$

where $\Gamma(\cdot)$ is the gamma function, m_l is the Nakagami fading parameter corresponding to the lth resolvable multipath component and the parameter Ω_l is given by $\Omega_l = E[|h_l|^2]$ [49]. Furthermore, we assume that the phase rotation due to fading channel is uniformly distributed in $[0, 2\pi]$. Let us now consider the receiver structure.

3.2.3 Receiver Model

Let us assume that the hybrid DS-TH UWB system supports K users. Then, when the DS-TH UWB signal as shown in (3.1) is transmitted over the Nakagami-m fading channels with the CIR as shown in (3.2), the received signal can be expressed as

$$\begin{aligned} r(t) &= \sqrt{\frac{E_b}{N_c T_\psi}} \sum_{k=1}^{K} \sum_{l=0}^{L-1} \sum_{j=0}^{\infty} h_l^{(k)} b_{\left\lfloor \frac{j}{N_c} \right\rfloor}^{(k)} d_j^{(k)} \psi_{rec}\left[t - jT_c - c_j^{(k)} T_\psi - T_0 - lT_\psi - \tau_k\right] \\ &+ n(t) \end{aligned} \tag{3.4}$$

where $n(t)$ represents the additive white Gaussian noise (AWGN) with zero-mean and single-sided power spectrum density of N_0 per dimension, τ_k takes into account the lack of synchronisation among the users as well as transmission delay, while $\psi_{rec}(t)$ represents the time-domain pulse received, which is usually the second derivative [40] of the transmitted pulse $\psi(t)$, as seen in (3.1).

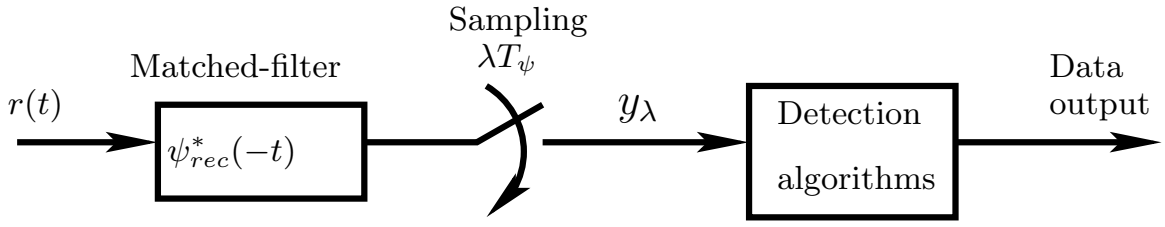

Figure 3.3: Receiver block diagram for detecting hybrid direct-sequence time-hopping UWB signals.

The receiver structure for detection of DS-TH UWB signal is shown in Fig. 3.3. The received signal is first passed through a MF having the impulse response $\psi^*_{rec}(-t)$. The output of the MF is then sampled at a rate of $1/T_\psi$. Hence, if M number of data bits are detected, the detector can collect

a total $(MN_cN_\psi + L - 1)$ number of samples for detection, where $(L-1)$ is due to the L number of resolvable multipaths. Specifically, the λth sample can be obtained by sampling MF's output at the time instant $t = T_0 + (\lambda+1)T_\psi$, which can be expressed as

$$y_\lambda = \left(\sqrt{\frac{E_b T_\psi}{N_c}}\right)^{-1} \int_{T_0+\lambda T_\psi}^{T_0+(\lambda+1)T_\psi} r(t)\psi^*_{rec}(t)dt, \qquad \lambda = 0, 1, \cdots, MN_cN_\psi + L - 2 \tag{3.5}$$

3.3 Representation of the Received Signal

Let us define

$$\boldsymbol{y} = [y_0, y_1, \cdots, y_{MN_cN_\psi+L-2}]^T \tag{3.6}$$

$$\boldsymbol{n} = [n_0, n_1, \cdots, n_{MN_cN_\psi+L-2}]^T \tag{3.7}$$

Then, according to (3.5), it can be shown that the element n_λ in $\boldsymbol{n}$ can be represented as

$$n_\lambda = \left(\sqrt{\frac{E_b T_\psi}{N_c}}\right)^{-1} \int_{T_0+\lambda T_\psi}^{T_0+(\lambda+1)T_\psi} n(t)\psi^*_{rec}(t)dt, \qquad \lambda = 0, 1, \cdots, MN_cN_\psi + L - 2 \tag{3.8}$$

which is a Gaussian random variable with mean zero and a variance $\sigma^2 = N_0/2E_b$ per dimension. Furthermore, upon subsituting the received signal in the form of (3.4) into (3.5), it can be shown that, after some simplifications, $\boldsymbol{y}$ can be expressed as

$$\boldsymbol{y} = \boldsymbol{CHb} + \boldsymbol{n} = \sum_{k=1}^{K} \boldsymbol{C}_k \boldsymbol{H}_k \boldsymbol{b}_k + \boldsymbol{n} \tag{3.9}$$

where $\boldsymbol{b}_k = [b_0^{(k)}, b_1^{(k)}, \cdots, b_{M-1}^{(k)}]^T$ contains the M number of data bits transmitted by the kth user, the channel matrix of the kth user, $\boldsymbol{H}_k$ is given by

$$\boldsymbol{H}_k = \text{diag}\,\{\boldsymbol{h}_k, \boldsymbol{h}_k, \ldots, \boldsymbol{h}_k\} \tag{3.10}$$

which is a $(ML \times M)$-dimensional matrix with $\boldsymbol{h}_k$ given by the CIR of user k as

$$\boldsymbol{h}_k = \left[h_0^{(k)}, h_1^{(k)}, \ldots, h_{L-1}^{(k)}\right]^T \tag{3.11}$$

The spreading matrix $\boldsymbol{C}_k$ of the kth user as shown in (3.9) is a $[(MN_cN_\psi + L - 1) \times (ML)]$ dimensional matrix, which can be expressed in a form as

$$\boldsymbol{C}_k = \begin{bmatrix} \boldsymbol{C}_0^{(k)} & \mathbf{0} & \mathbf{0} & \mathbf{0} & \mathbf{0} \\ \mathbf{0} & \boldsymbol{C}_1^{(k)} & \mathbf{0} & \vdots & \vdots \\ \vdots & \vdots & \ddots & \mathbf{0} & \mathbf{0} \\ \mathbf{0} & \mathbf{0} & \mathbf{0} & \boldsymbol{C}_{M-2}^{(k)} & \mathbf{0} \\ \mathbf{0} & \mathbf{0} & \mathbf{0} & \mathbf{0} & \boldsymbol{C}_{M-1}^{(k)} \end{bmatrix} \tag{3.12}$$

where each column has $(M-1)$ number of $\mathbf{0}$ matrices of $(N_cN_\psi \times L)$ dimension, $\boldsymbol{C}_i^{(k)}$ is the spreading matrix corresponding to the ith data bit of the kth user, which is a $((N_cN_\psi + L - 1) \times L)$ dimensional matrix and can be represented as

$$\boldsymbol{C}_i^{(k)} = \begin{bmatrix} e^{(k)}_{iN_cN_\psi} & 0 & \dots & 0 & 0 \\ e^{(k)}_{iN_cN_\psi+1} & e^{(k)}_{iN_cN_\psi} & \dots & 0 & 0 \\ \vdots & \vdots & \ddots & \vdots & \vdots \\ e^{(k)}_{iN_cN_\psi+L-2} & e^{(k)}_{iN_cN_\psi+L-3} & \dots & e^{(k)}_{iN_cN_\psi} & 0 \\ e^{(k)}_{iN_cN_\psi+L-1} & e^{(k)}_{iN_cN_\psi+L-2} & \dots & e^{(k)}_{iN_cN_\psi+1} & e^{(k)}_{iN_cN_\psi} \\ e^{(k)}_{iN_cN_\psi+L} & e^{(k)}_{iN_cN_\psi+L-1} & \dots & e^{(k)}_{iN_cN_\psi} & e^{(k)}_{iN_cN_\psi+1} \\ \vdots & \vdots & \ddots & \vdots & \vdots \\ e^{(k)}_{(i+1)N_cN_\psi-1} & e^{(k)}_{(i+1)N_cN_\psi-2} & \dots & e^{(k)}_{(i+1)N_cN_\psi-L+1} & e^{(k)}_{(i+1)N_cN_\psi-L} \\ 0 & e^{(k)}_{(i+1)N_cN_\psi-1} & \dots & e^{(k)}_{(i+1)N_cN_\psi-L+2} & e^{(k)}_{(i+1)N_cN_\psi-L+1} \\ \vdots & \vdots & \ddots & \vdots & \vdots \\ 0 & 0 & \dots & e^{(k)}_{(i+1)N_cN_\psi-1} & e^{(k)}_{(i+1)N_cN_\psi-2} \\ 0 & 0 & \dots & 0 & e^{(k)}_{(i+1)N_cN_\psi-1} \end{bmatrix} \tag{3.13}$$

where e_x will be the product of DS spreading factor and TH-pattern and will take a value of $\{+1, -1, 0\}$ depending upon the product of DS and TH-pattern. In more detail the spreading matrix $\boldsymbol{C}_i^{(k)}$ can be structured by Fig. 3.4. From Fig. 3.4, it can be observed that, if the N_ψ of the number of time-slots per chip is less than the number of resolvable multipaths, then strong inter-chip-interference ICI exists. By contrast, if the number of resolvable multipaths is less than the number of time-slots per chip, the ICI is then less severe. For example, let the ith bit of user k is spread over $N_c = 3$ chips, where each chip is divided into $N_\psi = 2$ time-slots. Let the number of resolvable

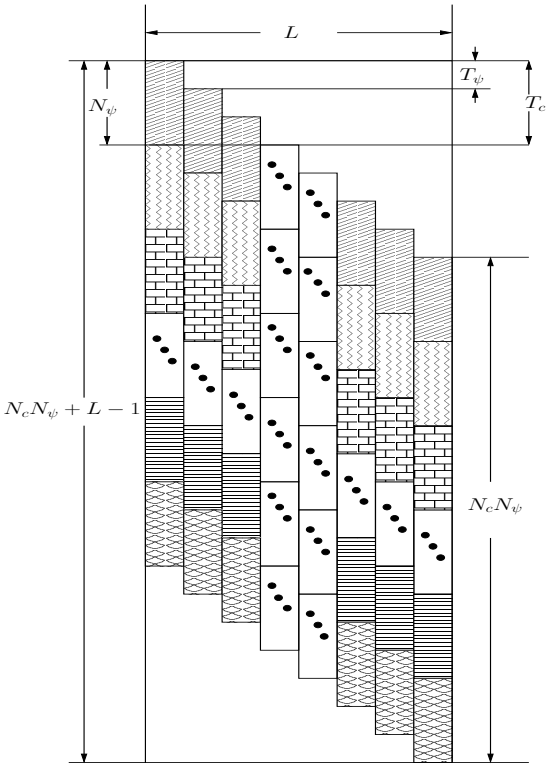

Figure 3.4: Structure of the spreading matrix $\boldsymbol{C}_i^{(k)}$ for the ith data bit of user k in hybrid direct-sequence time-hopping UWB systems communicating over the UWB channels having L number of resolvable multipaths.

multipaths be $L = 4$. Furthermore, let the TH pattern used for the ith bit be $(0, 1, 1)$ and the DS spreading code be $(d_0^{(k)}, d_1^{(k)}, d_2^{(k)})$. Then, it can be shown that the spreading matrix for the ith bit of user k can be expressed as

$$\boldsymbol{C}_i^{(k)} = \begin{bmatrix} d_0^{(k)} & 0 & 0 & 0 \\ 0 & d_0^{(k)} & 0 & 0 \\ 0 & 0 & d_0^{(k)} & 0 \\ d_1^{(k)} & 0 & 0 & d_0^{(k)} \\ 0 & d_1^{(k)} & 0 & 0 \\ d_2^{(k)} & 0 & d_1^{(k)} & 0 \\ 0 & d_2^{(k)} & 0 & d_1^{(k)} \\ 0 & 0 & d_2^{(k)} & 0 \\ 0 & 0 & 0 & d_2^{(k)} \end{bmatrix} \tag{3.14}$$

As the spreading matrix $\boldsymbol{C}_i^{(k)}$ of the kth user for the ith bit is known, the spreading matrix $\boldsymbol{C}_k$ as

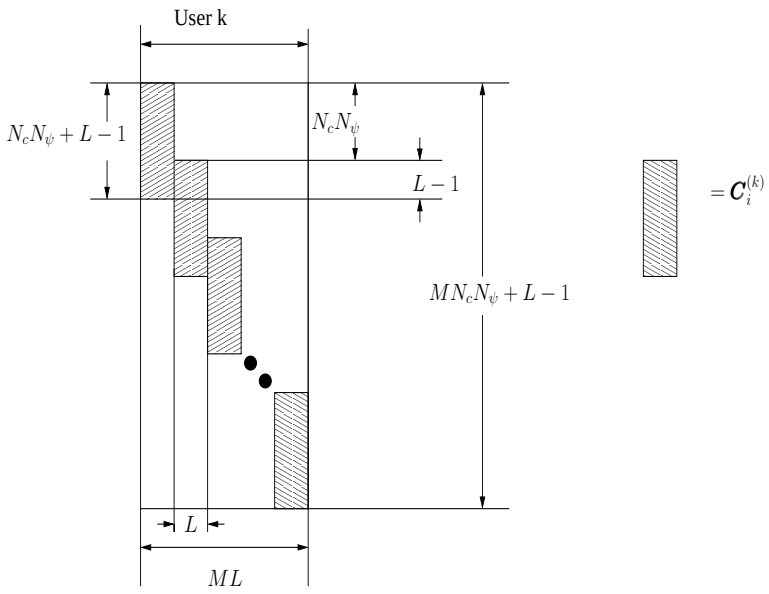

Figure 3.5: Spreading matrix $\boldsymbol{C}_k$ for the kth user in hybrid direct-sequence and time-hopping UWB systems.

seen in (3.9) for the kth user transmitting a block of M number of bits can be readily obtained, which has the structure as shown in Fig. 3.5. As shown in Fig. 3.5, the spreading matrix $\boldsymbol{C}_k$ is a $((MN_cN_\psi + L - 1) \times ML)$ dimensional matrix. In order to have a close look of the structure of $\boldsymbol{C}_k$, let us extend the previous example by assuming that the kth user transmits $M = 3$ data bits within a block. Let us assume that the TH pattern for the first bit be $(0, 1, 1)$, for the second bit be $(1, 0, 0)$ and for the last bit be $(0, 0, 1)$. The DS-spreading code for the first bit is $(d_0^{(k)}, d_1^{(k)}, d_2^{(k)})$ for the second bit is $(d_3^{(k)}, d_4^{(k)}, d_5^{(k)})$ and the for last bit is $(d_6^{(k)}, d_7^{(k)}, d_8^{(k)})$, respectively. Then, the DS-TH code for the first bit is $(d_0^{(k)}, 0, 0, d_1^{(k)}, 0, d_2^{(k)})$, for second bit is $(0, d_3^{(k)}, d_4^{(k)}, 0, d_5^{(k)}, 0)$ and for the last bit is $(d_6^{(k)}, 0, d_7^{(k)}, 0, 0, d_8^{(k)})$, respectively. In this case, it can be shown that the spreading matrix $\boldsymbol{C}_k$ for

user k can be expressed as

$$\boldsymbol{C}_k = \tag{3.15}$$

$$\left[\begin{array}{cccc|cccc|cccc}
d_0^{(k)} & 0 & 0 & 0 & 0 & 0 & 0 & 0 & 0 & 0 & 0 & 0 \\
0 & d_0^{(k)} & 0 & 0 & 0 & 0 & 0 & 0 & 0 & 0 & 0 & 0 \\
0 & 0 & d_0^{(k)} & 0 & 0 & 0 & 0 & 0 & 0 & 0 & 0 & 0 \\
d_1^{(k)} & 0 & 0 & d_0^{(k)} & 0 & 0 & 0 & 0 & 0 & 0 & 0 & 0 \\
0 & d_1^{(k)} & 0 & 0 & 0 & 0 & 0 & 0 & 0 & 0 & 0 & 0 \\
d_2^{(k)} & 0 & d_1^{(k)} & 0 & 0 & 0 & 0 & 0 & 0 & 0 & 0 & 0 \\
\hline
0 & d_2^{(k)} & 0 & d_1^{(k)} & 0 & 0 & 0 & 0 & 0 & 0 & 0 & 0 \\
0 & 0 & d_2^{(k)} & 0 & d_3^{(k)} & 0 & 0 & 0 & 0 & 0 & 0 & 0 \\
0 & 0 & 0 & d_2^{(k)} & d_4^{(k)} & d_3^{(k)} & 0 & 0 & 0 & 0 & 0 & 0 \\
\hline
0 & 0 & 0 & 0 & 0 & d_4^{(k)} & d_3^{(k)} & 0 & 0 & 0 & 0 & 0 \\
0 & 0 & 0 & 0 & d_5^{(k)} & 0 & d_4^{(k)} & d_3^{(k)} & 0 & 0 & 0 & 0 \\
0 & 0 & 0 & 0 & 0 & d_5^{(k)} & 0 & d_4^{(k)} & 0 & 0 & 0 & 0 \\
\hline
0 & 0 & 0 & 0 & 0 & 0 & d_5^{(k)} & 0 & d_6^{(k)} & 0 & 0 & 0 \\
0 & 0 & 0 & 0 & 0 & 0 & 0 & d_5^{(k)} & 0 & d_6^{(k)} & 0 & 0 \\
0 & 0 & 0 & 0 & 0 & 0 & 0 & 0 & d_7^{(k)} & 0 & d_6^{(k)} & 0 \\
\hline
0 & 0 & 0 & 0 & 0 & 0 & 0 & 0 & 0 & d_7^{(k)} & 0 & d_6^{(k)} \\
0 & 0 & 0 & 0 & 0 & 0 & 0 & 0 & 0 & 0 & d_7^{(k)} & 0 \\
0 & 0 & 0 & 0 & 0 & 0 & 0 & 0 & d_8^{(k)} & 0 & 0 & d_7^{(k)} \\
0 & 0 & 0 & 0 & 0 & 0 & 0 & 0 & 0 & d_8^{(k)} & 0 & 0 \\
0 & 0 & 0 & 0 & 0 & 0 & 0 & 0 & 0 & 0 & d_8^{(k)} & 0 \\
0 & 0 & 0 & 0 & 0 & 0 & 0 & 0 & 0 & 0 & 0 & d_8^{(k)}
\end{array}\right]$$

where the first four columns correspond to the first bit, the next four columns corresponds to the second bit and the last four columns correspond to the last bit. From (3.15) it can be easily observed that the ISI of the first and last bit is less than that of the middle bit. From (3.15) we can also be implied that the ISI increases as the number of multipaths increases. In order to mitigate the ISI, each bit may be assigned with a different spreading code, so that the cross-correlation between the current bit and the following bit is small. Otherwise, if the same spreading code is used for all bits, then the cross-correlation between the current and following bits is high, which will generate stronger ISI and make the detection difficult.

Finally, the spreading matrix $\boldsymbol{C}$ of the K users as mentioned associated with (3.9) can be shown as Fig. 3.6, where $\boldsymbol{C}_i^{(k)}$ is shown in Fig. 3.4. The dimensions of $\boldsymbol{C}$ are $((MN_cN_\psi + L - 1) \times (MLK))$. Let us now consider the detection of the hybrid DS-TH UWB signals in the next section.

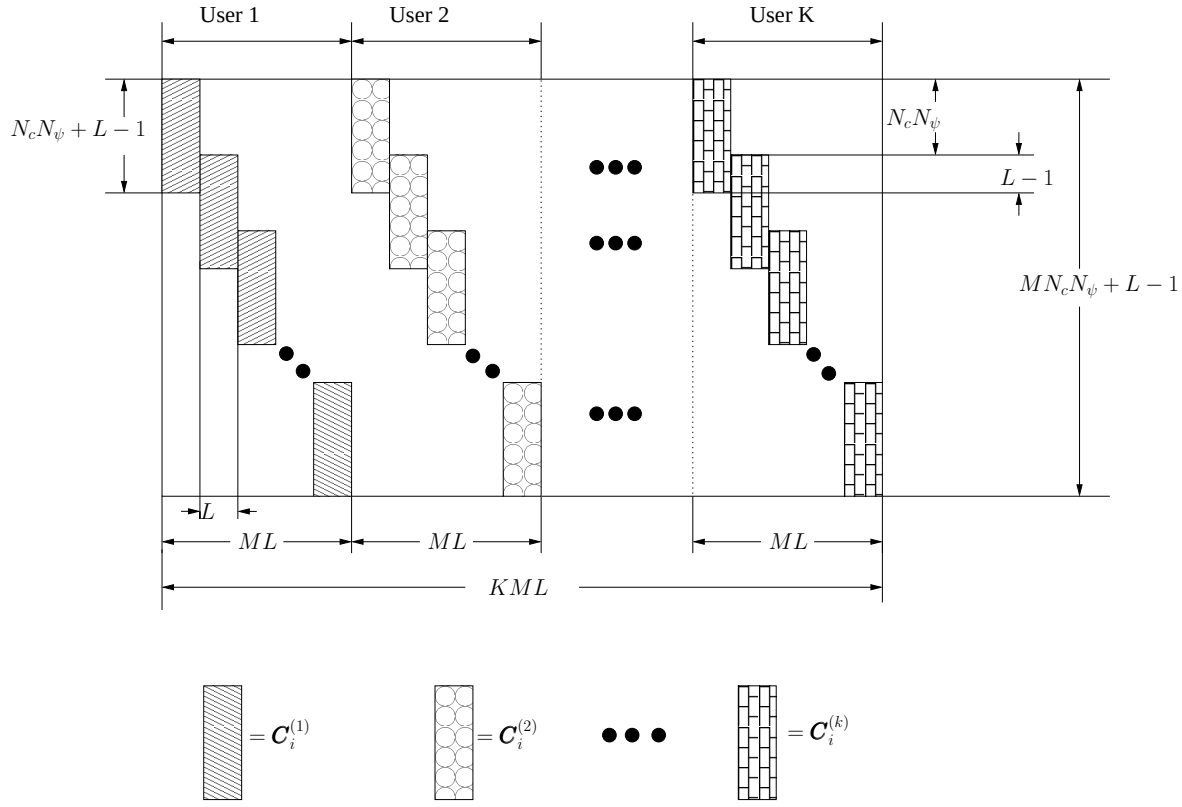

Figure 3.6: Spreading matrix $\boldsymbol{C}$ for the K users supported by the hybrid direct-sequence time-hopping UWB system.

3.4 Signal Detection

Despite achieving optimum error performance the optimal detectors [149] are impractical to be implemented due to their high complexity, which grows exponentially in the order of $O(2^{MK})$, where M denotes the number of bits per detection block and K denotes the number of users supported [150]. Additionally, in optimum detectors, stringent requirements, such as channel knowledge, code waveforms of all the users and strict synchronization, are hard to be satisfied, which also make the optimal detectors impractical to be implemented, especially, in real-time sense [151]. For this sake, in practice sub-optimal detectors having relatively low complexity is usually desirable [151, 152]. For example, linear detectors [151, 152] having a linear detection complexity are often the initial options to be con-

sidered for implementation. Therefore, in this chapter, we consider the linear detectors including the conventional correlation detector and minimum mean squared error (MMSE) detector.

Since the hybrid DS-TH UWB signals experience both MUI and ISI, ideally, the window selected for detection of the desired user should span all the bits transmitted by all the users [5]. However, due to real-time applications and avoiding yielding large delay, it is often desirable to consider a window of samples $\boldsymbol{y}_i$ for detecting only the ith data bit [153]. However, when choosing the window size we should realize that there is a trade-off between the achievable performance and the window size.

In this section we consider the bit-by-bit detection in the hybrid DS-TH UWB system. As the delay-spread of the considered UWB channel spans g data bits as mentioned in Sub-section 3.2.2, strong ISI may exist in the hybrid DS-TH UWB system. Specifically, according to our analysis in Section 3.2, it can be shown that there are $\min(i, g-1)$ data bits before the desired data bit and $\min(M-1-i, g-1)$ data bits after the desired data bit, which interfere with the desired ith bit. Hence, in our bit-by-bit detection, the observations for detecting the ith bit of the 1st user, can be formed by the $(N_c N_\psi + L - 1)$ samples as

$$\boldsymbol{y}_i = [y_{iN_cN_\psi}, y_{iN_cN_\psi+1}, \cdots, y_{(i+1)N_cN_\psi+L-2}]^T \tag{3.16}$$

Furthermore, it can be shown that $\boldsymbol{y}_i$ can be expressed as

$$\begin{aligned}\boldsymbol{y}_i = &\underbrace{\boldsymbol{C}_i^{(1)}\boldsymbol{h}_1 b_i^{(1)}}_{\text{Desired signal}} + \underbrace{\sum_{k=2}^{K}\boldsymbol{C}_i^{(k)}\boldsymbol{h}_k b_i^{(k)}}_{\text{MUI from the ith data bit}} + \boldsymbol{n}_i \\ &+ \underbrace{\sum_{k=1}^{K}\sum_{\substack{j=\max(0,i-g)\\ i\neq 0}}^{i-1}\underline{\mathbf{C}}_j^{(k)}\boldsymbol{h}_k b_j^{(k)}}_{\text{MUI+ISI from the bits before bit } i} + \underbrace{\sum_{k=1}^{K}\sum_{\substack{j=i+1\\ i\neq M-1}}^{\min(M-1,i+g)}\bar{\boldsymbol{C}}_j^{(k)}\boldsymbol{h}_k b_j^{(k)}}_{\text{MUI + ISI from the bits after bit } i}\end{aligned} \tag{3.17}$$

where $\boldsymbol{n}_i = [n_{iN_cN_\psi}, n_{iN_cN_\psi+1}, \cdots, n_{iN_cN_\psi+L-2}]^T$ is the noise vector. $\underline{\mathbf{C}}_j^{(k)}$ is the spreading matrix associated with the jth bit transmitted before bit i. Let $x = ((N_cN_\psi + L - 1) - (i-j)N_cN_\psi)$, then

it can be shown that $\underline{\mathbf{C}}_j^{(k)}$ can be represented as

$$\underline{\mathbf{C}}_j^{(k)} = \left[\begin{array}{c|ccccc} & & & & & \\ 0\cdots 0 & e^{(k)}_{(j+1)N_cN_\psi-1} & e^{(k)}_{(j+1)N_cN_\psi-2} & \cdots & e^{(k)}_{(j+1)N_cN_\psi-x} & \\ 0\cdots 0 & 0 & e^{(k)}_{(j+1)N_cN_\psi-1} & \cdots & e^{(k)}_{(j+1)N_cN_\psi-x+1} & \\ \vdots\ddots\vdots & \vdots & \vdots & \ddots & \vdots & x \\ 0\cdots 0 & 0 & 0 & \cdots & e^{(k)}_{(j+1)N_cN_\psi-1} & \\ \hline 0\cdots 0 & 0 & 0 & \ldots & 0 & \\ \vdots\ddots\vdots & \vdots & \vdots & \ddots & \vdots & \\ 0\ldots 0 & 0 & 0 & \ldots & 0 & \end{array}\right] \begin{array}{l} \\ \\ \\ \\ \\ \\ \\ \end{array} \begin{array}{l} \\ \\ \\ \\ \\ \\ N_cN_\psi+L-1-x \end{array} \tag{3.18}$$

$$\begin{array}{cc} L-x & x \end{array}$$

where x rows in (3.18) correspond to the last x rows of $\boldsymbol{C}_j^{(k)}$ as shown in (3.13). From (3.18) it can be observed that as x increases, more rows associated with the jth bit interfere with the desired ith bit, hence causing severe ISI. By contrast, as x decreases, fewer rows associated with the jth bit interfere with the desired ith bit, thus, yielding less ISI.

In (3.17) $\bar{\boldsymbol{C}}_j^{(k)}$ is the spreading matrix corresponding to the jth bit transmitted after bit i. Let $x = ((N_cN_\psi + L - 1) - (j-i)N_cN_\psi)$. Then, it can be shown that $\bar{\boldsymbol{C}}_j^{(k)}$ can be represented as

$$\bar{\boldsymbol{C}}_j^{(k)} = \left[\begin{array}{ccccc|c} 0 & 0 & \ldots & 0 & 0\ldots 0 & \\ \vdots & \vdots & \ddots & \vdots & \vdots\ddots\vdots & \\ 0 & 0 & \ldots & 0 & 0\cdots 0 & \\ \hline e^{(k)}_{jN_cN_\psi} & 0 & \ldots & 0 & 0\cdots 0 & \\ \vdots & \vdots & \ddots & \vdots & \vdots\ddots\vdots & \\ e^{(k)}_{jN_cN_\psi+x-2} & e^{(k)}_{jN_cN_\psi+x-3} & \cdots & 0 & 0\cdots 0 & \\ e^{(k)}_{jN_cN_\psi+x-1} & e^{(k)}_{jN_cN_\psi+x-2} & \cdots & e^{(k)}_{jN_cN_\psi} & 0\cdots 0 & \end{array}\right] \begin{array}{l} \\ \\ \\ \\ \\ \\ \end{array} \begin{array}{l} N_cN_\psi+L-1-x \\ \\ \\ x \\ \\ \\ \end{array} \tag{3.19}$$

$$\begin{array}{cc} x & L-x \end{array}$$

where x rows as shown in (3.19) correspond to the first x rows of $\boldsymbol{C}_j^{(k)}$ of (3.13). Again, when x increases, more rows from the jth bit interfere with the desired ith bit and cause severer ISI. By contrast, as x decreases, fewer rows from the jth bit interfere with the desired ith bit, which hence

generate lower ISI.

Let us now consider the detection of the ith data bit of the 1st user.

3.4.1 Correlation Detector

Correlation detector is also referred to as the conventional matched-filter (CMF) [152], which is a single-user detector without the ability to remove MUI, ICI and ISI. However, the correlation detector has the lowest complexity, which requires only the channel knowledge $\boldsymbol{h}_1$ and the knowledge about the spreading matrix $\boldsymbol{C}_i^{(k)}$, in order to detect the ith data bit of the 1st user. Specifically, for the correlation detector, the decision variable $z_i^{(1)}$ for $b_i^{(1)}$ of the ith data bit of the 1st user, can be expressed as

$$\begin{aligned} z_i^{(1)} &= \boldsymbol{h}_1^H(\boldsymbol{C}_i^{(1)})^T\boldsymbol{y}_i = \boldsymbol{h}_1^H(\boldsymbol{C}_i^{(1)})^T\Bigg\{\underbrace{\boldsymbol{C}_i^{(1)}\boldsymbol{h}_1 b_i^{(1)}}_{\text{Desired signal}} + \underbrace{\sum_{k=2}^{K}\boldsymbol{C}_i^{(k)}\boldsymbol{h}_k b_i^{(k)}}_{\text{MUI}} + \boldsymbol{n}_i \\ &+ \underbrace{\sum_{k=1}^{K}\sum_{\substack{j=\max(0,i-g)\\ i\neq 0}}^{i-1}\underline{\boldsymbol{C}}_j^{(k)}\boldsymbol{h}_k b_j^{(k)}}_{\text{MUI+ISI from the bits before bit } i} + \underbrace{\sum_{k=1}^{K}\sum_{\substack{j=i+1\\ i\neq M-1}}^{\min(M-1,i+g)}\bar{\boldsymbol{C}}_j^{(k)}\boldsymbol{h}_k b_j^{(k)}}_{\text{MUI+ISI from the bits after bit } i}\Bigg\} \end{aligned} \tag{3.20}$$

and the estimate to the ith data bit of the 1st user is given by

$$\hat{b}_i^{(1)} = \text{sgn}\left(z_i^{(1)}\right) \tag{3.21}$$

where $\text{sgn}(x)$ is the sign function. As shown in (3.20), the correlation detector experiences both MUI and ISI. Thus, the error performance of the hybrid DS-TH UWB system degrades as the number of users supported increases.

3.4.2 Minimum Mean-Square Error Detector

Multiuser detector can increase the spectral-efficiency of a multiuser system and make it support more users [83, 149]. The minimum mean-square error MMSE detector is a linear multiuser detector, which employs a range of advantages. The MMSE detector is capable of suppressing both the MUI and background noise. It outperforms the decorrelating detector in terms of the achievable BER performance. Additionally, the MMSE detector can be implemented with the aid of the adaptive techniques, as shown in the following chapters.

In the context of the MMSE detector the received signal vector $\boldsymbol{y}_i$ as shown in (3.17) is processed by a complex weight vector $\boldsymbol{w}_1$, in order to detect bit $b_i^{(1)}$ transmitted by the desired user 1. Correspondingly, the decision variable can be expressed as [16, 154]

$$z_i^{(1)} = \boldsymbol{w}_1^H \boldsymbol{y}_i \tag{3.22}$$

where the optimum weight vector $\boldsymbol{w}_1$ is chosen such that it minimises the mean-square error (MSE) between the transmitted bit $b_i^{(1)}$ and the decision variable $z_i^{(1)}$, yielding [16, 154]

$$\begin{aligned} J(\boldsymbol{w}_1) &= \arg\min_{w} E\left[\left|b_i^{(1)} - z_i^{(1)}\right|^2\right] \\ &= \arg\min_{w} E\left[\left|b_i^{(1)} - \boldsymbol{w}_1^H \boldsymbol{y}_i\right|^2\right] \end{aligned} \tag{3.23}$$

It can be shown that the optimum weight vector $\boldsymbol{w}_1$ in MMSE sense can be expressed as [16, 154]

$$\boldsymbol{w}_1 = \boldsymbol{R}_{y_i}^{-1} \boldsymbol{r}_{y_i b_i^{(1)}} \tag{3.24}$$

where $\boldsymbol{R}_{y_i}$ is the auto-correlation matrix of the received signal vector $\boldsymbol{y}_i$, which can be represented as

$$\begin{aligned} \boldsymbol{R}_{y_i} &= E\left[\boldsymbol{y}_i \boldsymbol{y}_i^H\right] \\ &= \boldsymbol{C}_i^{(1)} \boldsymbol{h}_1 \boldsymbol{h}_1^H \left(\boldsymbol{C}_i^{(1)}\right)^T + \sum_{k=2}^{K} \boldsymbol{C}_i^{(k)} \boldsymbol{h}_k \boldsymbol{h}_k^H \left(\boldsymbol{C}_i^{(k)}\right)^T + 2\sigma^2 \boldsymbol{I} \\ &+ \sum_{k=1}^{K} \sum_{\substack{j=\max(0,i-g) \\ i\neq 0}}^{i-1} \underline{\mathbf{C}}_j^{(k)} \boldsymbol{h}_k \boldsymbol{h}_k^H \left(\underline{\mathbf{C}}_j^{(k)}\right)^T + \sum_{k=1}^{K} \sum_{\substack{j=i+1 \\ i\neq M-1}}^{\min(M-1,i+g)} \bar{\boldsymbol{C}}_j^{(k)} \boldsymbol{h}_k \boldsymbol{h}_k^H \left(\bar{\boldsymbol{C}}_j^{(k)}\right)^T \\ &= \boldsymbol{C}_i^{(1)} \boldsymbol{h}_1 \boldsymbol{h}_1^H \left(\boldsymbol{C}_i^{(1)}\right)^T + \tilde{\boldsymbol{R}}_I \end{aligned} \tag{3.25}$$

where, by definition,

$$\begin{aligned} \tilde{\boldsymbol{R}}_I &= \sum_{k=2}^{K} \boldsymbol{C}_i^{(k)} \boldsymbol{h}_k \boldsymbol{h}_k^H \left(\boldsymbol{C}_i^{(k)}\right)^T + \sum_{k=1}^{K} \sum_{\substack{j=\max(0,i-g) \\ i\neq 0}}^{i-1} \underline{\mathbf{C}}_j^{(k)} \boldsymbol{h}_k \boldsymbol{h}_k^H \left(\underline{\mathbf{C}}_j^{(k)}\right)^T \\ &+ \sum_{k=1}^{K} \sum_{\substack{j=i+1 \\ i\neq M-1}}^{\min(M-1,i+g)} \bar{\boldsymbol{C}}_j^{(k)} \boldsymbol{h}_k \boldsymbol{h}_k^H \left(\bar{\boldsymbol{C}}_j^{(k)}\right)^T + 2\sigma^2 \boldsymbol{I} \end{aligned} \tag{3.26}$$

which denotes the autocorrelation matrix of interference plus noise. Note that, in practice $\boldsymbol{R}_{y_i}$ can

be estimated at the receiver without requiring the knowledge about the other users. In (3.24) $\boldsymbol{r}_{y_i b_i^{(1)}}$ is the cross-correlation vector between the transmitted bit $b_i^{(1)}$ of the desired user and the received observation vector $\boldsymbol{y}_i$. $\boldsymbol{r}_{y_i b_i^{(1)}}$ can be expressed as [155]

$$\boldsymbol{r}_{y_i b_i} = E\left[\boldsymbol{y}_i b_i^{*(1)}\right] = \boldsymbol{C}_i^{(1)} \boldsymbol{h}_1 \tag{3.27}$$

Hence, upon subsituting (3.25) and (3.27) into (3.24), the optimum weight $\boldsymbol{w}_1$ for the MMSE detector can be expressed as [155]

$$\boldsymbol{w}_1 = \left[\boldsymbol{C}_i^{(1)} \boldsymbol{h}_1 \boldsymbol{h}_1^H \left(\boldsymbol{C}_i^{(1)}\right)^T + \tilde{\boldsymbol{R}}_I\right]^{-1} \boldsymbol{C}_i^{(1)} \boldsymbol{h}_1 \tag{3.28}$$

When applying the *matrix inversion lemma*, we obtain [1]

$$\left[\boldsymbol{C}_i^{(1)} \boldsymbol{h}_1 \boldsymbol{h}_1^H \left(\boldsymbol{C}_i^{(1)}\right)^T + \tilde{\boldsymbol{R}}_I\right]^{-1} = \frac{\tilde{\boldsymbol{R}}_I^{-1}}{1 + \boldsymbol{h}_1^H \left(\boldsymbol{C}_i^{(1)}\right)^T \tilde{\boldsymbol{R}}_I^{-1} \boldsymbol{C}_i^{(1)} \boldsymbol{h}_1} \tag{3.29}$$

Substituting this result into (3.28) yields

$$\boldsymbol{w}_1 = \frac{\tilde{\boldsymbol{R}}_I^{-1} \boldsymbol{C}_i^{(1)} \boldsymbol{h}_1}{1 + \boldsymbol{h}_1^H \left(\boldsymbol{C}_i^{(1)}\right)^T \tilde{\boldsymbol{R}}_I^{-1} \boldsymbol{C}_i^{(1)} \boldsymbol{h}_1} \tag{3.30}$$

Finally, when substituting (3.30) into (3.22), the decision variable $z_i^{(1)}$ for $b_i^{(1)}$ can be expressed as

$$z_i^{(1)} = \frac{\boldsymbol{h}_1^H \left(\boldsymbol{C}_i^{(1)}\right)^T \tilde{\boldsymbol{R}}_I^{-1} \boldsymbol{y}_i}{1 + \boldsymbol{h}_1^H \left(\boldsymbol{C}_i^{(1)}\right)^T \tilde{\boldsymbol{R}}_I^{-1} \boldsymbol{C}_i^{(1)} \boldsymbol{h}_1} \tag{3.31}$$

When approximating $z_i^{(1)}$ as a Gaussian random variable, then the mean of $z_i^{(1)}$ can be expressed as

$$E\left[z_i^{(1)}\right] = \boldsymbol{w}_1^H \boldsymbol{C}_i^{(1)} \boldsymbol{h}_1 b_i^{(1)} \tag{3.32}$$

[1] *Matrix inverse Lemma*: if $\boldsymbol{A}$ is a $(N \times N)$ matrix and $\boldsymbol{b}$ is a N-dimensional vector, then [16] $\left(\boldsymbol{A} + \boldsymbol{b}\boldsymbol{b}^H\right)^{-1} = \frac{\boldsymbol{A}^{-1}}{1 + \boldsymbol{b}^H \boldsymbol{A}^{-1} \boldsymbol{b}}$.

While the second-order moment can be expressed as

$$\begin{aligned} E\left[\left[z_i^{(1)}\right]^2\right] &= E\left[z_i^{(1)}(z_i^{(1)})^H\right] = \boldsymbol{w}_1^H E[\boldsymbol{y}_i \boldsymbol{y}_i^H]\boldsymbol{w}_1 \\ &= \boldsymbol{w}_1^H\left[\boldsymbol{C}_i^{(1)}\boldsymbol{h}_1\boldsymbol{h}_1^H\left(\boldsymbol{C}_i^{(1)}\right)^T + \tilde{\boldsymbol{R}}_I\right]\boldsymbol{w}_1 \end{aligned} \tag{3.33}$$

and the variance of $z_i^{(1)}$ can be evaluated by

$$\begin{aligned} Var\left[z_i^{(1)}\right] &= E\left[\left[z_i^{(1)}\right]^2\right] - \left[E\left[z_i^{(1)}\right]\right]^2 \\ &= \boldsymbol{w}_1^H\left[\boldsymbol{C}_i^{(1)}\boldsymbol{h}_1\boldsymbol{h}_1^H\left(\boldsymbol{C}_i^{(1)}\right)^T + \tilde{\boldsymbol{R}}_I\right]\boldsymbol{w}_1 - \left[E\left[\boldsymbol{w}_1^H\boldsymbol{C}_i^{(1)}\boldsymbol{h}_1\right]\right]^2 \\ &= \boldsymbol{w}_1^H\boldsymbol{C}_i^{(1)}\boldsymbol{h}_1\boldsymbol{h}_1^H\left(\boldsymbol{C}_i^{(1)}\right)^T\boldsymbol{w}_1 + \boldsymbol{w}_1^H\tilde{\boldsymbol{R}}_I\boldsymbol{w}_1 - \boldsymbol{w}_1^H\boldsymbol{C}_i^{(1)}\boldsymbol{h}_1\boldsymbol{h}_1^H\left(\boldsymbol{C}_i^{(1)}\right)^T\boldsymbol{w}_1 \\ &= \boldsymbol{w}_1^H\tilde{\boldsymbol{R}}_I\boldsymbol{w}_1 \end{aligned} \tag{3.34}$$

Furthermore, when we apply (3.31) in (3.32) and (3.34), we obtain

$$\begin{aligned} E\left[z_i^{(1)}\right] &= \frac{\boldsymbol{h}_1^H\left(\boldsymbol{C}_i^{(1)}\right)^T\tilde{\boldsymbol{R}}_I^{-1}\boldsymbol{C}_i^{(1)}\boldsymbol{h}_1 b_i^{(1)}}{1+\boldsymbol{h}_1^H\left(\boldsymbol{C}_i^{(1)}\right)^T\tilde{\boldsymbol{R}}_I^{-1}\boldsymbol{C}_i^{(1)}\boldsymbol{h}_1} \\ Var\left[z_i^{(1)}\right] &= \frac{\boldsymbol{h}_1^H\left(\boldsymbol{C}_i^{(1)}\right)^T\tilde{\boldsymbol{R}}_I^{-1}\boldsymbol{C}_i^{(1)}\boldsymbol{h}_1}{\left(1+\boldsymbol{h}_1^H\left(\boldsymbol{C}_i^{(1)}\right)^T\tilde{\boldsymbol{R}}_I^{-1}\boldsymbol{C}_i^{(1)}\boldsymbol{h}_1\right)^2} \end{aligned} \tag{3.35}$$

Consequently, the signal-to-interference-plus-noise ratio (SINR) achieved by the MMSE detector can be expressed as

$$\begin{aligned} \gamma_i^{(1)} &= \frac{\left[E\left[z_i^{(1)}\right]\right]^2}{Var\left[z_i^{(1)}\right]} \\ &= \boldsymbol{h}_1^H\left(\boldsymbol{C}_i^{(1)}\right)^T\tilde{\boldsymbol{R}}_I^{-1}\boldsymbol{C}_i^{(1)}\boldsymbol{h}_1 \\ &= \text{MMSE}^{-1} - 1 \end{aligned} \tag{3.36}$$

where $E\left[[b_i^{(1)}]^2\right] = 1$ and MMSE denotes the minimum MSE achieved by the MMSE detector,

which it can be shown given by [156]

$$\begin{aligned} \text{MMSE} &= 1 - \boldsymbol{r}_{y_i b_i}^H \boldsymbol{w}_1 \\ &= \frac{1}{1 + \boldsymbol{h}_1^H \left(\boldsymbol{C}_i^{(1)}\right)^T \tilde{\boldsymbol{R}}_I^{-1} \boldsymbol{C}_i^{(1)} \boldsymbol{h}_1} \end{aligned} \tag{3.37}$$

According to the principles of the MMSE detector as above-derived the MMSE detector requires both the channel knowledge and the knowledge about the spreading sequences in the context of all the active users. Let us below analyse the complexity of the correlation and MMSE detectors.

3.5 Complexity Analysis

This section analyses the complexity of both the conventional correlation detector and the MMSE detector, when they are applied in the hybrid DS-TH UWB systems. The complexity is measured by the number of multiplications and additions that are required to detect a bit transmitted of by the desired user. Note that, the number of multiplications and additions needed to perform certain matrix operations are given as follows.

- According to [150], multiplication of a $(M \times N)$ matrix with a $(N \times L)$ matrix requires $M(N-1)L$ additions and MNL multiplications. When $N >> 1$, we also have $M(N-1)L \approx MNL$.
- Computing the inverse of a matrix of $(M \times M)$-dimensional, using cholesky decomposition requires $M^3/6$ additions and $M^3/6$ multiplications.

3.5.1 Correlation Detector

For the correlation detector, as shown in (3.20), the decision variable for detecting $b_i^{(1)}$ can be formed as

$$z_i^{(1)} = \boldsymbol{h}_1^H (\boldsymbol{C}_i^{(1)})^T \boldsymbol{y}_i \tag{3.38}$$

Let $\mathcal{T} = N_c N_\psi + L - 1$. Then, it can be readily shown that the number additions and multiplications for the operations involved in the correlation detector can be given as shown in Table 3.1. Therefore, in order to detect a bit using the correlation detector, the total number of additions and multiplications required is $2(L+1)\mathcal{T}$.

Operations	Number of additions	Number of multiplications
$\boldsymbol{h}_1^H \left(\boldsymbol{C}_i^{(1)}\right)^T$	$L\mathcal{T}$	$L\mathcal{T}$
$z_i^{(1)}$	$\mathcal{T}$	$\mathcal{T}$

Table 3.1: Number of operations required for the correlation detector.

3.5.2 MMSE Detector

When MMSE detector is employed, the decision variable for detecting $b_i^{(1)}$ is given in (3.22), which is

$$z_i^{(1)} = \boldsymbol{r}_{y_i b_i^{(1)}}^H \left(\boldsymbol{R}_{y_i}^{-1}\right)^H \boldsymbol{y}_i \tag{3.39}$$

The number of multiplications and additions required to perform the involved operations are summarised in Table 3.2.

Operations	Number of additions	Number of multiplications
$\boldsymbol{r}_{yb_i^{(1)}}^H = \boldsymbol{h}_1^H \left(\boldsymbol{C}_i^{(1)}\right)^T$	$L\mathcal{T}$	$L\mathcal{T}$
$\boldsymbol{C}_i^{(1)}\boldsymbol{h}_1\boldsymbol{h}_1^H\boldsymbol{C}_i^{(1)}$	$2L\mathcal{T}$	$2L\mathcal{T}$
$\sum_{k=2}^{K} \boldsymbol{C}_i^{(k)}\boldsymbol{h}_k\boldsymbol{h}_k^H\boldsymbol{C}_i^{(k)}$	$2(K-1)L\mathcal{T}$	$2(K-1)L\mathcal{T}$
$\sum_{k=1}^{K}\sum_{\substack{j=\max(0,i-g)\\ i\neq 0}}^{i-1} \underline{\boldsymbol{C}}_j^{(k)}\boldsymbol{h}_k\boldsymbol{h}_k^H \left(\underline{\boldsymbol{C}}_j^{(k)}\right)^T$	$2gLK\mathcal{T}$	$2gLK\mathcal{T}$
$\sum_{k=1}^{K}\sum_{\substack{j=i+1\\ i\neq M-1}}^{\min(M-1,i+g)} \bar{\boldsymbol{C}}_j^{(k)}\boldsymbol{h}_k\boldsymbol{h}_k^H \left(\bar{\boldsymbol{C}}_j^{(k)}\right)^T$	$2gLK\mathcal{T}$	$2gLK\mathcal{T}$
$\boldsymbol{R}_{y_i}$	$4\mathcal{T}^2$	$-$
$\boldsymbol{R}_{y_i}^{(-1)}$	$\mathcal{T}^3/6$	$\mathcal{T}^3/6$
$\boldsymbol{R}_{y_i}^{(-1)}\boldsymbol{r}_{yb_i^{(1)}}$	$\mathcal{T}^2$	$\mathcal{T}^2$
$z_i^{(1)}$	$\mathcal{T}$	$\mathcal{T}$

Table 3.2: Number of operations required for the MMSE detector.

Therefore, the total number of additions or multiplications required to detect one bit using MMSE

detection is $\mathcal{T}^3/6 + 5\mathcal{T}^2 + 2KL(1+2g)\mathcal{T} + (L+1)\mathcal{T}$ or $\mathcal{T}^3/6 + \mathcal{T}^2 + 2KL(1+2g)\mathcal{T} + (L+1)\mathcal{T}$ respectively, while the total number of operations for detection of one bit using MMSE detector is given by $\mathcal{T}^3/3 + 6\mathcal{T}^2 + 4KL(1+2g)\mathcal{T} + 2(L+1)\mathcal{T}$. Hence, when comparing the MMSE detector with the correlation detector, the MMSE detector requires $\mathcal{T}^3/3 + 6\mathcal{T}^2 + 4KL(1+2g)\mathcal{T}$ more operations than the correlation detector, in order to detect one bit.

Note that, the complexity considered above does not include that for channel estimation. When channel estimation is considered, the complexity of both the correlation detector and MMSE detector will be much higher. As shown in Tables 3.1 and 3.2, the complexity is mainly determined by the value of $\mathcal{T} = N_c N_\psi + L - 1$, which might be very big. In the following two chapters we are motivated to reduce the detection complexity in the hybrid DS-TH UWB systems.

3.6 Performance Results and Discussions

This section provides a range of simulation results to characterise the error rate performance of the pure TH-UWB, pure DS-UWB and different hybrid DS-TH systems, which employ either the single-user correlation detector or the MMSE-MUD. In order to compare these different systems, we use the following assumptions and system settings.

1) Coherent BPSK baseband modulation;

2) It is assumed that there are L number of resolvable multipaths and the total average received power over these multipaths are normalised to unity. Out of these L number of resolvable multipaths, there are L_s number of relatively strong paths, which carry 85% of the total average power transmitted, while the rest $(L - L_s)$ multipaths carry only 15% of total average power transmitted;

3) Each multipath channel is assumed to experience Nakagami-m fading with the fading severity determined by the value of m. The fading of the L multipath channel is assumed to be statistically independent.

4) In our simulations the Nakagami-m fading parameter was assumed to be $m = 1$, so that the upper bound BER can be found, since in this case the Nakagami-m distribution is reduced to Rayleigh distribution, and the fading becomes less severer as the value of m increases.

3.6.1 Correlation Detector

In this section the BER performance of hybrid DS-TH UWB system is provided and compared with that of the pure TH-UWB and pure DS-UWB systems, when a single-user correlation detector is employed. Fig. 3.7 shows the BER versus SNR per bit performance of the pure DS, pure TH and hybrid DS-TH UWB systems supporting $K = 1, 7$ or 15 users, when the UWB signals are transmitted over uncorrelated Rayleigh fading channels. In our simulations, the total spreading factor was retained to be $N_c N_\psi = 128$. As mentioned previously in this chapter, when the DS spreading factor $N_c = 1$ our hybrid DS-TH UWB system is reduced to the pure TH-UWB system. The hybrid DS-TH UWB system is reduced to the pure DS-UWB system when $N_\psi = 1$. In our simulations the number of resolvable multipaths was fixed to $L = 15$ out of which there are 5 strong resolvable paths conveying 85% of the total transmitted power. It can be easily observed from Fig. 3.7 that the hybrid DS-TH UWB system using $N_c = 8$, $N_\psi = 16$ outperforms the pure DS-UWB and TH-UWB systems. Since the correlation receiver does not have the capability to suppress MUI, as shown in Fig. 3.7, the BER performance of all the three systems becomes worse, when the number of users supported increases from $K = 1$, to 7 and 15.

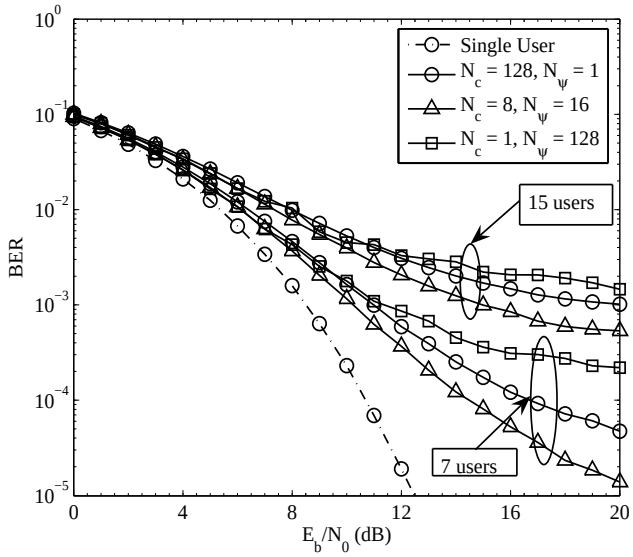

Figure 3.7: BER versus SNR per bit performance of the hybrid DS-TH, pure DS-UWB and pure TH-UWB systems using single-user correlation receiver when communicating over a Rayleigh fading channels. The product of time-hopping and direct-sequence spreading factors is a constant of $N_c N_\psi = 128$. There are a total $L = 15$ number of resolvable multipaths, out of which 5 multipaths have 85% of the total transmitted power.

Fig. 3.8 and Fig. 3.9, illustrate the BER versus SNR per bit performance of the hybrid DS-TH

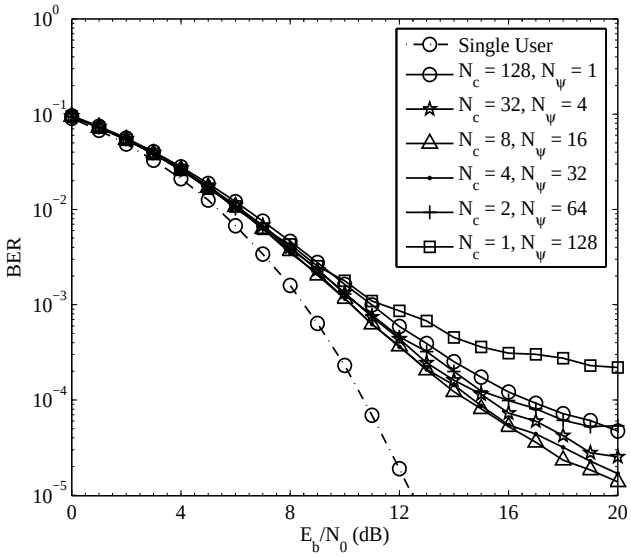

Figure 3.8: BER versus SNR per bit performance of different hybrid DS-TH, pure DS-UWB and pure TH-UWB systems using single-user correlation receiver when supporting $K = 7$ users and communicating over a Rayleigh fading channels. The product of time-hopping and direct-sequence spreading factors is a constant of $N_c N_\psi = 128$. There are a total $L = 15$ number of resolvable multipaths, out of which 5 multipaths have 85% of the total transmitted power.

UWB systems having different combinations of DS and TH spreading factors, when communicating over Rayleigh fading channels. In our simulations we assumed that the UWB systems supported $K = 7$ and $K = 15$ users. The number of resolvable multipaths are fixed to $L = 15$, where 5 of which conveyed 85% of the total transmitted power. Again the simulation results in Fig. 3.8 and Fig. 3.9 show that the hybrid DS-TH UWB system may outperform the pure DS-UWB and pure TH-UWB systems, when certain DS and TH spreading factors are used. However, from Fig. 3.8 and Fig. 3.9 it can be seen that a trade-off exists between the DS spreading factor N_c and the TH spreading factor N_ψ. Given the total spreading factor of $N_c N_\psi$, there is an optimum combination of (N_c, N_ψ), which yields the lowest achievable BER specifically, when the value of $N_c N_\psi = 128$, it can be observed from Fig. 3.8 and Fig. 3.9 that the best BER performance is achieved, when we choose $N_c = 8$ and $N_\psi = 16$.

Fig. 3.10 shows the effect of the number of users supported on the BER performance of the pure DS-UWB, pure TH-UWB and hybrid DS-TH UWB systems at a SNR per bit of $E_b/N_0 = 14$ dB, when communicating over uncorrelated Rayleigh fading channels. We assumed that the number of resolvable multipaths was $L = 15$, which contained $L_s = 5$ strongest paths conveying 85% of the transmitted power. From the results of the Fig. 3.10 we observe that the BER performance of the hybrid DS-TH systems using ($N_c = 8$, $N_\psi = 16$), ($N_c = 16$, $N_\psi = 8$) or ($N_c = 64$, $N_\psi = 2$) is better

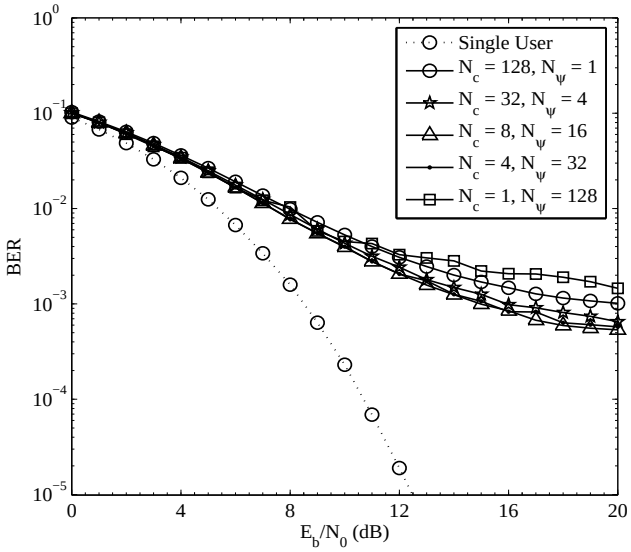

Figure 3.9: BER versus SNR per bit performance of different hybrid DS-TH, pure DS-UWB and pure TH-UWB systems using single-user correlation receiver when supporting $K = 15$ users and communicating over a Rayleigh fading channels. The product of time-hopping and direct-sequence spreading factors is a constant of $N_c N_\psi = 128$. There are a total $L = 15$ number of resolvable multipaths, out of which 5 multipaths have 85% of the total transmitted power.

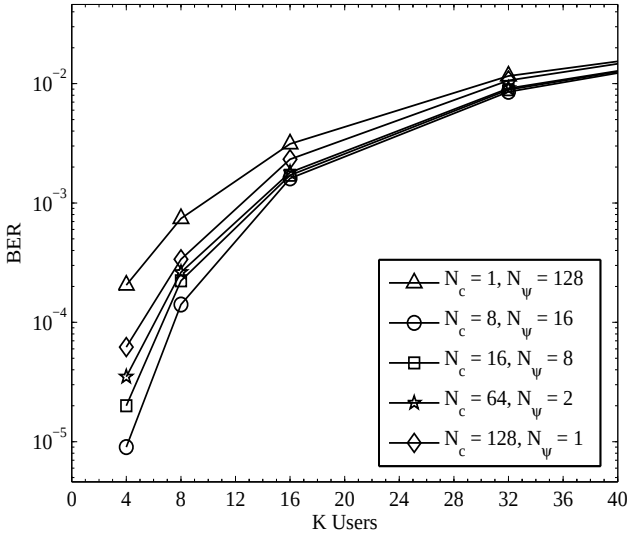

Figure 3.10: BER versus number of users K performance of pure DS-UWB, pure TH-UWB and hybrid DS-TH UWB systems using correlation receiver at $E_b/N_0 = 14$ dB when communicating over Rayleigh fading channels. The total spreading factor is $N_c N_\psi = 128$. The total number of resolvable multipaths are $L = 15$, where $L_s = 5$ strongest paths convey 85% of the transmitted power.

than that of the pure DS-UWB system or that of the pure TH-UWB system. As shown in Fig. 3.10, the hybrid DS-TH UWB system using $N_c = 8$ and $N_\psi = 16$ achieves the best BER performance. By

contrast, the pure TH-UWB system achieves the worst BER performance in comparison with all the other UWB schemes. Additionally, as shown in Fig. 3.10, as the number of users increases, the BER performance of all the UWB systems becomes worse, since the single-user correlation detector does not have the capability to suppress efficiently the MUI.

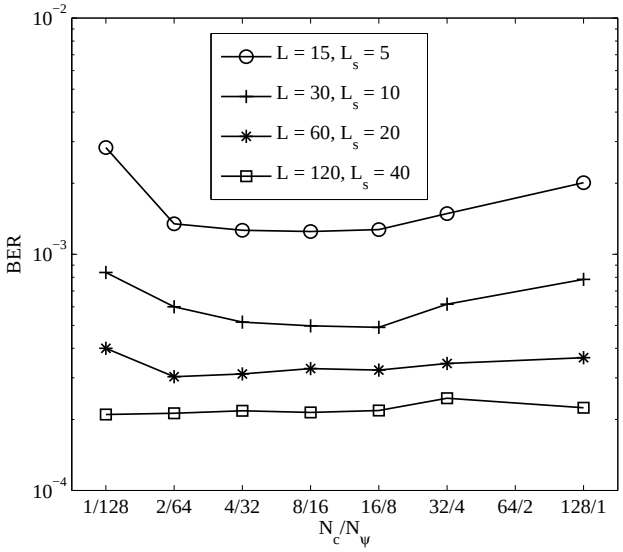

Figure 3.11: BER performance of hybrid DS-TH UWB systems using various DS and TH spreading factors while retaining the total spreading factor $N_c N_\psi = 128$, when communicating over multipath Rayleigh fading channels. The other parameters are $E_b/N_0 = 14$ dB, the total number of users supported are fixed to $K = 15$.

Fig. 3.11 shows the effect of the number of resolvable multipaths as well as the DS and TH spreading factors, on the BER performance of hybrid DS-TH UWB systems operated at a SNR of $E_b/N_0 = 14$ dB. In our simulations we assumed that the number of users supported was $K = 15$, the number of resolvable paths was L, where L_s out of L were the strongest paths that conveyed 85% of the transmitted power. From the results of Fig. 3.11, we observe that, given the total spreading factor, the total number of resolvable multipaths as well as the number of strongest resolvable multipaths, there exists an optimum hybrid DS-TH UWB scheme, which is capable of achieving the lowest BER. For example, when $L = 30$ and $L_s = 10$, the best BER performance is achieved by the hybrid DS-TH UWB system using $N_c = 8$ and $N_\psi = 16$, respectively. Furthermore, from the results of Fig. 3.11, it can be observed that the BER performance of all the UWB systems improves as the number of resolvable paths increases. Additionally, as the number of resolvable multipaths approaches the total spreading factor of $N_c N_\psi = 128$, as shown in Fig. 3.11, all the UWB systems considered approach a similar BER performance.

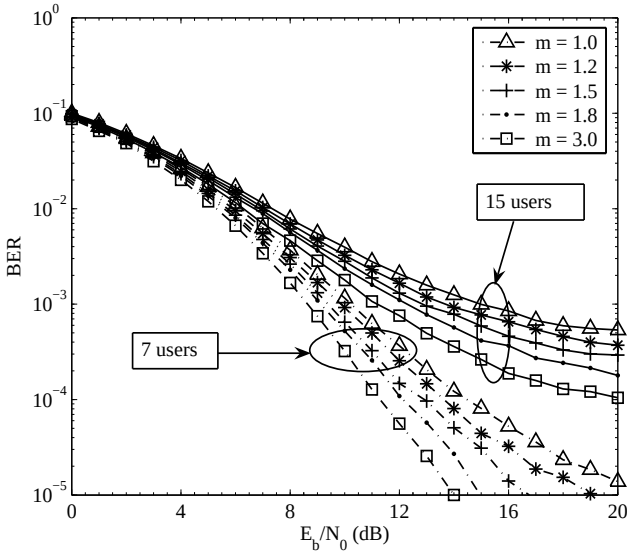

Figure 3.12: BER versus SNR per bit performance of the hybrid DS-TH UWB system using correlation receiver when communicating over Nakagami-m fading channels. In our simulations, the total spreading factor was $N_c N_\psi = 128$, the DS spreading factor was $N_c = 8$ and the TH spreading factor was $N_\psi = 16$. The total number of resolvable multipaths were 15, which contained 5 strongest multipath conveying 85% of the transmitted power.

Finally, Fig. 3.12 illustrates the BER performance of the hybrid DS-TH UWB system, when communicating over Nakagami-m fading channels associated with different m values. The other parameters used in our simulation were the DS spreading factor $N_c = 8$, the TH spreading factor $N_\psi = 16$, and $K = 7$ or $K = 15$. From Fig. 3.12, it can be readily observed that the BER performance improves, as the value of m increases. This is because increasing the value of m implies that the corresponding channel's quality improves, resulting in that the BER performance of the hybrid DS-TH UWB system improves. Let us now consider the error performance of various UWB systems when multiuser MMSE detector is employed.

3.6.2 MMSE Detector

In this section the BER performance of the hybrid DS-TH UWB system using MMSE detection is investigated and compared with that of the pure TH-UWB and pure DS-UWB systems. Fig. 3.13 shows the BER versus SNR performance of hybrid DS-TH UWB, pure DS-UWB and pure TH-UWB system, supporting $K = 7$ or 15 users, when communicating over uncorrelated Rayleigh fading channels. Since the MMSE detector is capable of efficiently mitigating the MUI, ICI and ISI as shown in Fig. 3.13 the BER performance achieved by the hybrid DS-TH UWB systems is close to the single-user BER performance bound for the scenarios considered. The hybrid DS-TH UWB using

various spreading factors, the pure DS-UWB and pure TH-UWB systems all achieve a similar BER performance. As shown in Fig. 3.13, when $K = 15$ users are supported, the BER performance of the hybrid DS-TH UWB system using $N_c = 8$ and $N_\psi = 16$ is slightly better than that of the pure DS- or pure TH-UWB schemes.

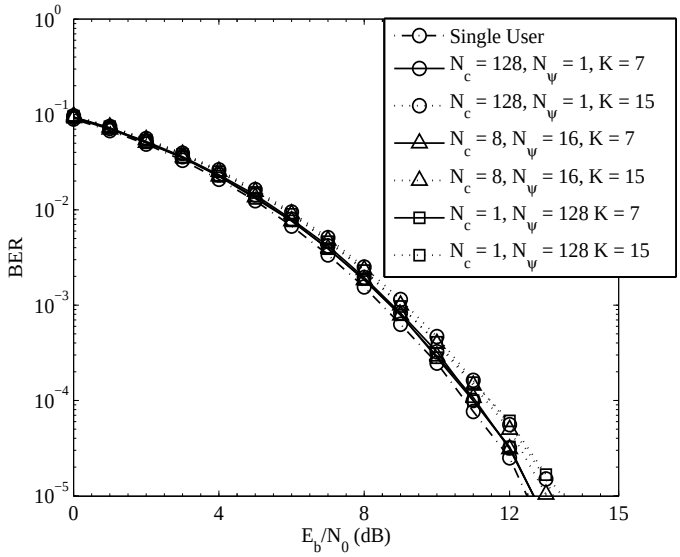

Figure 3.13: BER versus SNR per bit performance of hybrid DS-TH, pure DS-UWB and pure TH-UWB systems using MMSE detector, when communicating over Rayleigh fading channels. The parameters used in our simulations were the total spreading factor of $N_c N_\psi = 128$, the total number of resolvable multipaths of $L = 15$, and $L_s = 5$ strongest multipaths conveying 85% of the transmitted power.

Fig. 3.14 studies the effect of the number of users on the achievable BER performance of different UWB systems, when communicating over a Rayleigh fading channels. In our simulations the E_b/N_0 was fixed to 10 dB, the total spreading factor was fixed to $N_c N_\psi = 128$ and the number of resolvable multipaths was $L = 15$ out of which there were $L_s = 5$ strongest paths conveying 85% of the transmitted power. The results of Fig. 3.14 show that the BER performance of all the pulsed-based UWB systems considered is generally the same, which degrades slightly, when the number of users supported increases. When comparing Fig. 3.10 corresponding to the correlator detector with Fig. 3.14 corresponding to the MMSE detector, we can readily know that the MMSE detector outperforms the correlation detector in terms of their achievable BER performance, when supporting multiusers.

As Fig. 3.11 for the correlation detector, Fig. 3.15 studies the effect of the number of resolvable multipaths and the DS and TH spreading factors on the achievable BER performance of the hybrid DS-TH UWB systems. In our simulations, the SNR per bit was fixed to $E_b/N_0 = 10$dB and the number of users supported was $K = 15$. From the results of Fig. 3.15, it can be observed that, when

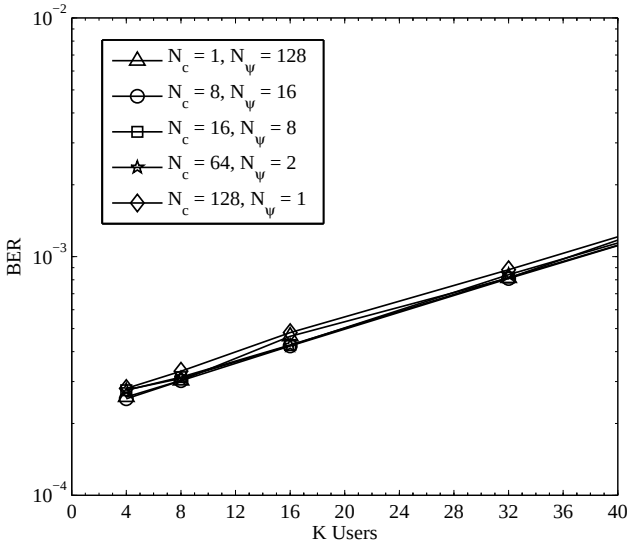

Figure 3.14: BER versus number of users K performance of pure DS-UWB, pure TH-UWB and hybrid DS-TH UWB systems using MMSE receiver at $E_b/N_0 = 10$ dB when communicating over Rayleigh fading channels. The total spreading factor is $N_cN_\psi = 128$. The total number of resolvable multipaths are $L = 15$, where $L_s = 5$ strongest paths convey 85% of the transmitted power.

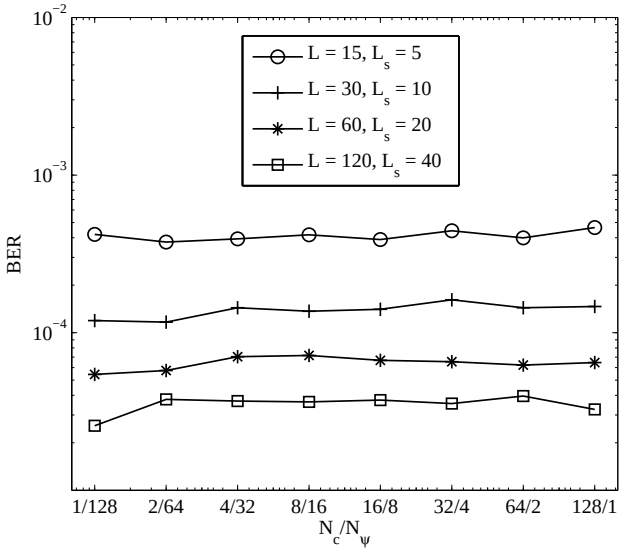

Figure 3.15: BER performance of hybrid DS-TH UWB systems using various DS and TH spreading factors while retaining the total spreading factor $N_cN_\psi = 128$, when communicating over multipath Rayleigh fading channels. The other parameters are $E_b/N_0 = 10$ dB, the total number of users supported are fixed to $K = 15$.

MMSE detector is employed, the hybrid DS-TH UWB systems using various DS and TH spreading factors are capable of achieving a similar BER performance, given the total spreading factor is same. Hence, in practice, the DS and TH spreading factors may be adjusted, in order to minimize the

complexity of the hybrid DS-TH UWB systems. Additionally, we can observe from the Fig. 3.15 that, as the number of multipaths increases, the BER performance of all the UWB systems improves due to multipath diversity provided by the UWB channels.

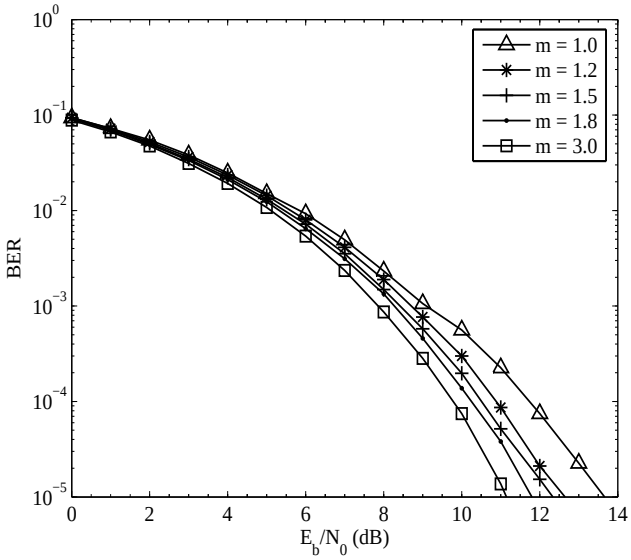

Figure 3.16: BER versus SNR per bit performance of the hybrid DS-TH UWB system using MMSE receiver when communicating over Nakagami-m fading channels. In our simulations, the total spreading factor was $N_c N_\psi = 128$, the DS spreading factor was $N_c = 8$ and the TH spreading factor was $N_\psi = 16$. The total number of resolvable multipaths were 15, which contained 5 strongest multipath conveying 85% of the transmitted power.

Finally, Fig. 3.16 shows the BER performance of the hybrid DS-TH UWB systems, when communicating over Nakagami-m fading channels associated with different m values. In our simulations we assumed that the hybrid DS-TH UWB system used a DS spreading factor of $N_c = 8$ and a TH spreading factor of $N_\psi = 16$, and that $K = 15$ users were supported. We assumed that the UWB channel had $L = 15$ number of resolvable multipaths and that there were $L_s = 5$ strongest multipaths, which conveyed 85% of the transmitted power. From the results of Fig. 3.16, we can see that, as the m value increases, the BER performance of the hybrid DS-TH UWB system improves, since the channel quality improves with the increase of the value of m.

Finally, when comparing the results of Figs. 3.7- 3.12 with that of Figs. 3.13- 3.16, we conclude that the MMSE detector significantly outperforms the correlation detector, when the UWB system supports multiple users.

3.6.3 Effect of Channel Characteristics

Above we have investigated the BER performance of the pure DS-, pure TH- as well as the hybrid DS-TH UWB systems, when communicating over the UWB channels, which we mainly assumed that there were L number of resolvable multipaths and that there $L_s < L$ number of strong resolvable multipath conveying 85% of the transmitted power. Below we provide the BER performance of the hybrid DS-TH UWB systems, when communicating over the UWB channels proposed in the standards, which were summarised in Table 2.3 and characterised in [29].

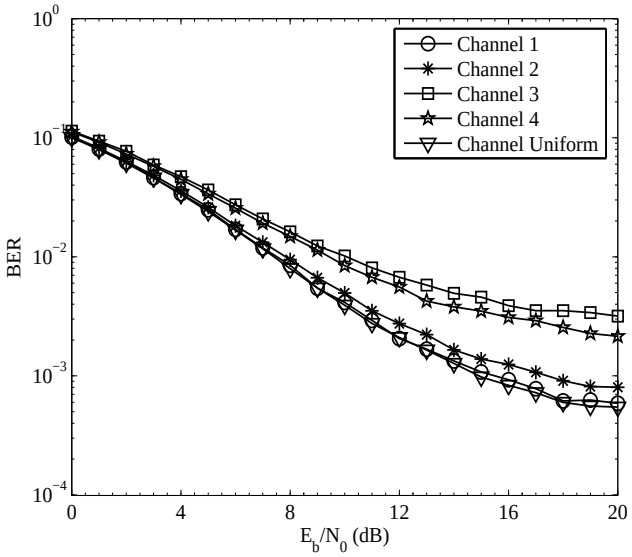

Figure 3.17: BER versus average SNR per bit performance of hybrid DS-TH UWB system using correlation detector when communicating over various types of UWB channels characterised in Table 2.3. In our simulations the UWB channels were assumed to experience Rayleigh fading, and the other parameters were $N_c = 16$, $N_\psi = 8$ and $K = 15$.

Figs. 3.17 and 3.18 show the BER versus SNR per bit performance of hybrid DS-TH UWB systems using correlation (Fig. 3.17) and MMSE (Fig. 3.18) detectors, when communicating over various types of UWB channels, as characterised in Table 2.3. In Table 2.3 the first four types of channels are the S-V type of UWB channels proposed in [29], which have been analysed in Section 2.5.2.2 of Chapter 2. For the uniform channel we assume that there are $L = 15$ resolvable multipaths, which include $L_s = 5$ strong paths containing 85% of the transmitted power. In addition to the above-mentioned, in our simulations we assumed that the DS spreading factor was $N_c = 16$, the TH spreading factor was $N_\psi = 8$ and that the hybrid DS-TH UWB system supported $K = 15$ users. From the results of Fig. 3.17 and Fig. 3.18 it can be observed that the best BER performance is achieved by the hybrid DS-TH UWB systems when communicating over the uniformly distributed

UWB channels, which have $L = 15$ resolvable multipaths and 5 of which posses 85% of the transmitted power. As seen in Figs. 3.17 and 3.18, the hybrid DS-TH UWB systems over the Channel model-1 UWB channels are capable of achieving a similar BER performance as the systems over the uniform UWB channels. The BER performance over Channel model-2 UWB channels is slightly worse than that achieved over the Channel model-1 and uniform UWB channels. Finally, the BER performance of the hybrid DS-TH UWB systems over the Channel model-3 and Channel model-4 UWB channels is worse than that of the hybrid DS-TH UWB systems over the other types of UWB channels. For both correlation and MMSE detectors, the hybrid DS-TH UWB systems achieve the worst BER performance when communicating over the Channel model-3 UWB channels.

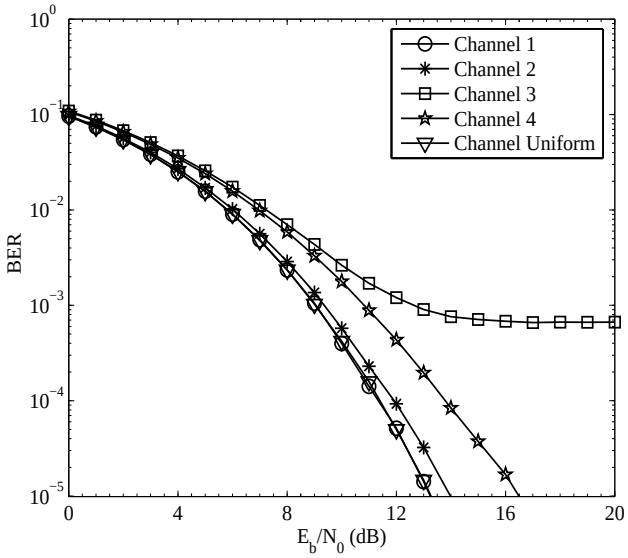

Figure 3.18: BER versus average SNR per bit performance of hybrid DS-TH UWB systems employing MMSE detector, when communicating over various types of UWB channels characterised in Table 2.3. In our simulations the UWB channels were assumed to experience multipath Rayleigh fading and the other parameters were $N_c = 16$, $N_\psi = 8$ and $K = 5$.

3.7 Summary and Conclusions

In this chapter hybrid DS-TH UWB system is proposed and investigated along with its two special cases, namely the pure DS-UWB system and pure TH-UWB system. It has been shown that the hybrid DS-TH UWB system is capable of providing more degrees of freedom for system design and reconfiguration than the pure DS-UWB system or pure TH-UWB system. The transmitted signal, followed by the UWB channel model as well as the receiver model for the hybrid DS-TH UWB have been presented. Furthermore, the BER versus SNR per bit performance of the hybrid DS-TH UWB

systems, pure DS-UWB systems and the pure TH-UWB systems have been investigated, when the user signals are transmitted over the UWB channels modelled by the Nakagami-m fading. Furthermore, in this chapter our study has been based on the assumptions that the delay-spread of the UWB channels may span several bit durations and that there exist a huge number of resolvable multipaths at the UWB receiver. In this chapter the BER performance and the implementation complexity of the UWB system have been investigated, when either the correlation detector or the multiuser MMSE detectors are employed. From our analysis and performance results, we may draw the following conclusions.

- **Single-User Correlation Receiver:** The correlation detector conflicts both MUI and ISI, when communicating over UWB channels. The BER performance of the UWB systems degrades significantly, as the number of users supported increases. In the hybrid DS-TH UWB systems using the single-user correlation detector, a trade-off exists between the DS and TH spreading factors. It can be shown that the best BER performance of the hybrid DS-TH UWB system may be achieved by appropriately choosing the DS and TH spreading factors. The hybrid DS-TH UWB systems using the optimum DS and TH spreading factors outperform the corresponding pure DS-UWB and pure TH-UWB systems. The complexity of the single-user correlation detector is proportional to $2(L+1)\mathcal{T}$, where $\mathcal{T}$ stands for $(N_c N_\psi + L - 1)$. Hence, in the pulse-based UWB systems, even the single-user correlation detector may demand a high complexity, due to the high number of resolvable multipaths of the UWB channels.

- **Multiuser MMSE Receiver:** It can be shown that the MMSE detector is capable of mitigating efficiently the MUI and ISI. When supporting multiple users, the multiuser MMSE detector significantly outperforms the single-user correlation detector in terms of their achievable BER performance. However, the complexity of the MMSE detector is significantly higher than the correlation detector. The complexity of the MMSE detector is proportional to $\mathcal{T}^3/3 + 6\mathcal{T}^2 + 4KL(1+2g)\mathcal{T}$, where, again, $\mathcal{T} = (N_c N_\psi + L - 1)$. It can be observed from the simulations results that the BER performance of the three types of UWB systems considered is in general similar, when the MMSE detector is employed. However, for some special cases as seen, for example in Fig. 3.13, the hybrid DS-TH UWB system may slightly outperform the pure DS-UWB or pure TH-UWB system. In contrast to the single-user correlation detector, which only requires the channel and spreading code's knowledge of the desired users, the MMSE detector considered in this chapter requires the complete knowledge about the spreading codes and the channels of all the active users, in order to detect the desired user.

Therefore, the MMSE detector considered in this chapter is extremely hard to be implemented, considering the characteristics of the UWB channels, which usually have a huge number of resolvable multipaths when each of the resolvable multipaths conveys very low power. For this sake, therefore, in Chapters 4 and 5, we will focus our attention on design of low complexity detectors for the hybrid DS-TH UWB systems.

Chapter 4

Adaptive Detection in Hybrid DS-TH UWB Systems

4.1 Introduction

In our previous chapter, it has been shown that in order to improve the BER performance of hybrid DS-TH UWB systems, especially, in multiuser scenarios, MMSE-MUD should be employed. As shown in Chapter 3, when employing the MMSE-MUD, the weighting vector $\boldsymbol{w}_1$ is required to be computed which needs to invert the auto-correlation matrix $\boldsymbol{R}_{y_i}$, which is $((N_cN_\psi+L-1)\times(N_cN_\psi+L-1))$ dimensional. However, the complexity of computing $\boldsymbol{R}_{y_i}^{-1}$ might be very high, since the values of N_cN_ψ and L are usually high. Furthermore, in order to implement the MMSE-MUD, signature waveforms, delays as well as complete channel knowledge, which includes both the amplitudes and phases of all the channels, of all the active users are required by the MMSE-MUD [157–161]. However, in practical UWB communications environment, it is usually extremely hard to obtain this information [16, 162–164]. For example, when using channel estimation techniques to estimate the UWB channels, it has been found that there are as large as 400 parameters required to be estimated in a typical UWB indoor channel [14]. Without any doubt, estimating such a large number of parameters will further increase significantly the system complexity, which is already too high even when detection is only considered [165]. Additionally, it is well-known that channel estimation has a critical impact on the attainable performance of the wireless systems. This becomes even severe when UWB communications are considered, since in the UWB systems the power conveyed by each resolvable multipath is usually very low, making its estimation even harder [68, 166–171]. Therefore, in this

chapter adaptive detection that is free from channel estimation is proposed for detection of the hybrid DS-TH UWB signals.

To be more specific, in this chapter we propose and investigate a range of training based adaptive detectors operated based on the principles of MMSE [152] for the hybrid DS-TH UWB systems. We focus our attention on the three types of low-complexity adaptive detectors, which are implemented based on the principles of least mean-square (LMS), normalized least mean-square (NLMS) and recursive least square (RLS), respectively [16]. As our forthcoming discourse shown, these adaptive detectors are free from channel estimation and are capable of achieving the approximate MMSE solutions with the aid of training sequences of certain length. In this chapter we investigate the achievable BER performance of the adaptive detectors and compare it with that of the ideal MMSE-MUD [172], which demands ideal knowledge about the UWB channels and the signature sequences of all active users [152, 157], as shown in the last chapter. The BER performance of the hybrid DS-TH UWB, pure DS-UWB and pure TH-UWB systems, which employ the above-mentioned adaptive/ideal detectors, is investigated, when communicating over indoor UWB channels modelled by the S-V channel model [13, 117]. The advantages and disadvantages of the considered adaptive detectors are analyzed in the context of UWB communications. Furthermore, the complexity of the adaptive detectors is analyzed and compared with that of the single-user correlation receiver and also with that of the ideal MMSE-MUD considered in Chapter 3.

Our study in this chapter shows that the three types of adaptive detectors are highly efficient detection schemes for pulse-based UWB systems. They are free from channel estimation and can effectively capture the transmitted energy dispersed over UWB channels. They are capable of achieving a BER performance close to that achieved by the ideal MMSE-MUD. Furthermore, as our forthcoming complexity analysis shown, the detection complexity of an adaptive detectors may be significantly lower than that of the correlation receiver, even without taking account of the complexity required by the correlation receiver for channel estimation.

The remainder of the chapter is organised as follows. In the next section, the general description for the training-based adaptive detectors is described. In Section 4.2 the training and decision-directed detection modes are described in detail. Specifically, the LMS, NLMS and RLS adaptive detectors are studied in Sections 4.2.1, 4.2.2 and 4.2.3, respectively. In Section 4.3 the complexity of the LMS, NLMS and RLS adaptive detectors are analysed. Simulation results are provided in Section 4.4 and finally, in Section 4.5 the summary and conclusions of the chapter are presented. Let us first consider the training based adaptive detectors.

4.2 Description of Training-Based Adaptive Detectors

The training-based adaptive detectors are usually operated in two modes. The first mode is the training mode, during which the weights of the adaptive filters are adjusted with the aid of training symbols. In the context of the hybrid DS-TH UWB communications, the training symbols are first spread based on the principles of that described in Chapter 3 by invoking a DS spreading sequence of length N_c and a TH pattern of length N_ψ. Then, when the training sequence is transmitted over UWB channels, the receiver can obtain the observation samples, as shown in (3.5) in Chapter 3. After the receiver obtains $(N_cN_\psi + L - 1)$ number of observation samples in the context of one training symbol, the $(N_cN_\psi + L - 1)$ observation samples are processed multiplying it with a $(N_cN_\psi + L - 1)$ length weight vector $\boldsymbol{w}_1$ in order to provide an estimate for the training symbol considered. As the training symbol is known to the receiver, it is then subtracted from the estimated symbol to yield an estimation error, which is utilised to update the weight vector $\boldsymbol{w}_1$. The above process is repeated associated with each of the training symbols. Finally, after the training, an approximate solution for the weight vector $\boldsymbol{w}_1$ is obtained.

After obtaining a sub-optimal weight vector $\boldsymbol{w}_1$ with the aid of training, the adaptive detector can now be switched to the signal detection mode. During the signal detection stage the adaptive detector is operated under decision-directed (DD) mode. Under the DD mode, the received signal is multiplied by the sub-optimal weight vector $\boldsymbol{w}_1$ to provide estimates to the transmitted symbols. Then, the detected symbols are fed-back to the adaptive detector, which makes use of the detected symbols to further improve the weight vector $\boldsymbol{w}_1$ [173].

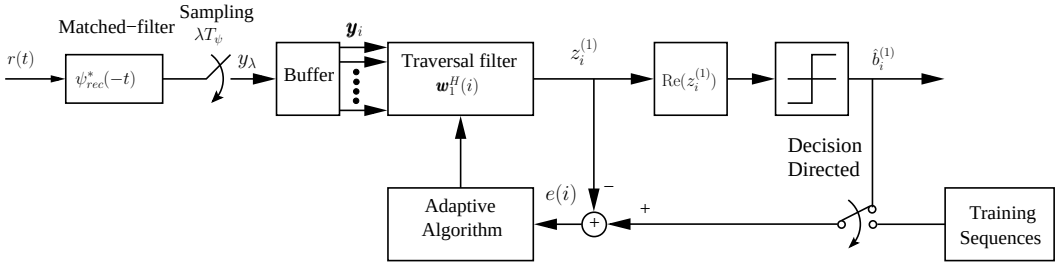

Figure 4.1: Illustration of the training based adaptive detector for the hybrid DS-TH UWB system.

The concept of the adaptive detector for the hybrid DS-TH UWB systems can be further augmented by Fig. 4.1, where the traversal filter is shown in principle in Fig. 4.2. During the training stage, the data known to the receiver is first transmitted over the UWB channel. At the receiver as shown in Fig. 4.1, this received signal is first passed through a matched-filter having the impulse

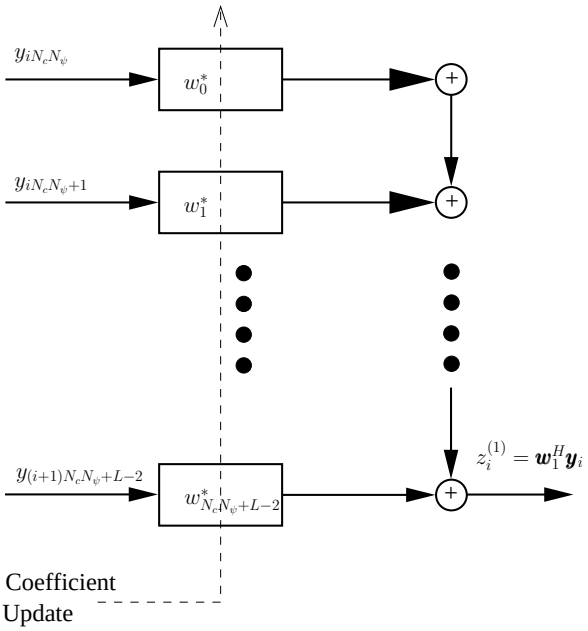

Figure 4.2: Schematic for traversal filter implementation.

response $\psi^*_{rec}(-t)$ and is sampled to obtain observation samples. For each data bit the receiver can obtain $(N_cN_\psi + L - 1)$ samples, which are stored in the buffer as shown in Fig. 4.1. Then, the observation samples are input to the traversal filter, in order to yield the estimate $z_i^{(1)}$ to the transmitted data bit $b_i^{(1)}$. As the training sequence is known to the receiver, so is $b_i^{(1)}$, hence, an estimation error can be calculated, which is the desired training bit subtracted from the estimation $z_i^{(1)}$. As shown in Fig. 4.1 this error signal is utilised to update the weights $\boldsymbol{w}_1^H$ of the traversal filters so that the weight vector converges to the optimum weight vector.

After the training mode is completed and a sub-optimal $\boldsymbol{w}_1$ is achieved, the receiver is then switched to the DD mode. During the DD mode, the adaptive detector is operated in the same way as it is during the training mode, except that now the weight vector is updated with the aid of the detected data bits, which might be unreliable.

Note that, when designing adaptive detectors for UWB systems, the following factors are required to be considered.

- Convergence speed;
- Tracking ability;
- Robustness of the algorithm;

- Computational Complexity.

First, when designing adaptive detectors for UWB systems, fast converging algorithms are required. With fast converging algorithms the overhead incurred during the training mode can be reduced, thus increasing the data-rate of the UWB systems [174–176]. However, in UWB systems the number of taps of the traversal filter may be very large due to possible high spreading factor and large number of resolvable multipaths. It has been shown in [177, 178], that the convergence of an adaptive algorithm depends on the filter length. The convergence speed usually decreases with the increase of the filter length. Secondly, in most adaptive algorithms there is a tradeoff between the convergence speed and the ensemble-average squared error (EASE), higher EASE is achieved in most cases with a faster convergence. This higher EASE also leads to a worst BER performance. The convergence speed of an adaptive algorithm also determines the tracking ability of the adaptive algorithm. The tracking ability of an adaptive algorithm represents the capability to track the statistical variation in a nonstationary environment [16]. Therefore, when the adaptive algorithm has accomplished its training mode, a robust tracking algorithm is required to track the time-variant environment. In UWB communications, due to a huge bandwidth employed, there may be a huge number of resolvable multipaths present at the receiver [14]. In this case, a fast tracking algorithm must be employed by the adaptive detectors for UWB systems, so that the multipath signals can be reliably tracked. Thirdly, robust algorithms are required for detection in UWB environments. This requirement is further necessitated by the fact that the UWB systems are usually required to co-exist with other narrowband and wideband systems, which typically transmit with higher power as compared to the UWB systems. For example, in cellular communications environment, cellular phones transmit up to $+30$ dBm, which is 10^7 times higher than the PSD of the UWB signals [62]. Hence, in such high interference environments, the desired adaptive algorithms should be robust to combat the interference caused by the narrowband and wideband communication systems. Additionally, strong ISI exists due to a large number of multipaths, hence, the adaptive algorithms should be robust to the ISI. Finally, in practical UWB systems, the computational complexity of the receivers should be very low. In this chapter, we will show that the adaptive detectors are capable of providing better BER performance as compared to the matched filter receiver. However, the better BER performance is achieved at the expense of a slightly increased detection complexity [179, 180]. Let us now discuss the adaptive algorithms by first considering the LMS detector.

4.2.1 Least Mean Square Adaptive Detector

The LMS algorithm was first proposed by Widrow and Hoff, while in [16] Haykin derived the LMS algorithm by using the steepest descent method. The basic idea of the LMS algorithm is to find a sub-optimal weight vector $\boldsymbol{w}_1$ through stochastic gradient techniques, in order to achieve MMSE between the transmitted symbol $b_i^{(1)}$ and the decision variable $z_i^{(1)}$ as shown in (4.1). Hence, the cost-function $J(\boldsymbol{w}_1(i))$ in the context of the desired user 1 at the ith transmission can be represented as [16]

$$\begin{aligned} J(\boldsymbol{w}_1(i)) &= E[||b_i^{(1)} - z_i^{(1)}||^2] = E[||b_i^{(1)} - \boldsymbol{w}_1^H(i)\boldsymbol{y}_i||^2] \\ &= \sigma^2_{b_i^{(1)}} - \boldsymbol{r}^H_{y_i b_i^{(1)}}\boldsymbol{w}_1(i) - \boldsymbol{w}_1^H(i)\boldsymbol{r}_{y_i b_i^{(1)}} + \boldsymbol{w}_1^H(i)\boldsymbol{R}_{y_i}\boldsymbol{w}_1(i) \end{aligned} \tag{4.1}$$

where $\sigma^2_{b_i^{(1)}} = 1$ is the variance of the desired symbol vector and $\boldsymbol{w}_1(i)$ denotes the weight vector at the ith transmission symbol duration. With the aid of the steepest-descent algorithm, the weight vector $\boldsymbol{w}_1(i)$ is successively adjusted in the direction of the steepest descent, which is opposite to that of the gradient vector of the cost function. Therefore, the updated equation for the weight vector can be expressed as [16]

$$\boldsymbol{w}_1(i+1) = \boldsymbol{w}_1(i) - \frac{1}{2}\mu\boldsymbol{g}(i) \tag{4.2}$$

where $\boldsymbol{w}_1(i)$ and $\boldsymbol{w}_1(i+1)$ are the weight vectors at time instant i and $(i+1)$, respectively, μ is the step-size and $\boldsymbol{g}(i)$ denotes the gradient vector of the cost function $J(\boldsymbol{w}_1(i))$, which can be expressed as [16]

$$\boldsymbol{g}(i) = \nabla J(\boldsymbol{w}_1(i)) = \frac{\partial J(\boldsymbol{w}_1(i))}{\partial(\boldsymbol{w}_1(i))} \tag{4.3}$$

Upon substituting (4.1) into (4.3), we obtain [16]

$$\boldsymbol{g}(i) = -2\boldsymbol{r}_{y_i b_i^{(1)}} + 2\boldsymbol{R}_{y_i}\boldsymbol{w}_1(i) \tag{4.4}$$

Furthermore, upon substituting (4.4) into (4.2), we have the weight update equation

$$\boldsymbol{w}_1(i+1) = \boldsymbol{w}_1(i) + \mu[\boldsymbol{r}_{y_i b_i^{(1)}} - \boldsymbol{R}_{y_i}\boldsymbol{w}_1(i)], \quad i = 0, 1, 2, \cdots \tag{4.5}$$

According to the above analysis, we know that the LMS algorithm determines the MMSE solution recursively. In practice the exact measurement of the gradient vector of (4.4) are not available, as the a-prior knowledge about the auto-correlation matrix $\boldsymbol{R}_{y_i}$ and the cross-correlation vector $\boldsymbol{r}_{y_i b_i^{(1)}}$ are not known at the receiver. Therefore when operated in an unknown environment, the gradient vector

has to be estimated with the aid of the received data. Specifically, the one-step estimations to the auto-correlation matrix $\boldsymbol{R}_{y_i}$ and the cross-correlation $\boldsymbol{r}_{y_i b_i^{(1)}}$ can be expressed as [16]

$$\begin{aligned} \boldsymbol{R}_{y_i} &= \boldsymbol{y}_i \boldsymbol{y}_i^H \\ \boldsymbol{r}_{y_i b_i^{(1)}} &= \boldsymbol{y}_i b_i^{*(1)} \end{aligned} \tag{4.6}$$

where $b_i^{(1)}$ is known to the receiver, when using the adaptive receiver in the training mode, while it can be estimated when using the adaptive receiver in the DD mode. However, the detected bit might be unreliable.

Upon substituting the estimates of the auto-correlation matrix $\boldsymbol{R}_{y_i}$ and the cross-correlation $\boldsymbol{r}_{y_i b_i^{(1)}}$ as shown in (4.6) into (4.3), the one-step estimate to the gradient of $J(\boldsymbol{w}_1(i))$ can be expressed as [16]

$$\boldsymbol{g}(i) = \nabla J(\boldsymbol{w}_1(i)) = -2\boldsymbol{y}_i b_i^{(1)} + 2\boldsymbol{y}_i \boldsymbol{y}_i^H \boldsymbol{w}_1(i) \tag{4.7}$$

Moreover, when substituting (4.7) into (4.2), the recursive equation for updating the weight vector can be expressed as

$$\begin{aligned} \boldsymbol{w}_1(i+1) &= \boldsymbol{w}_1(i) + \mu \boldsymbol{y}_i [b_i^{*(1)} - \boldsymbol{y}_i^H \boldsymbol{w}_1(i)] \\ &= \boldsymbol{w}_1(i) + \mu \boldsymbol{y}_i [b_i^{(1)} - \boldsymbol{w}_1^H(i) \boldsymbol{y}_i]^* \\ &= \boldsymbol{w}_1(i) + \mu \boldsymbol{y}_i e^*(i) \end{aligned} \tag{4.8}$$

where, by definition, $e(i) = b_i^{(1)} - \boldsymbol{w}_1^H(i)\boldsymbol{y}_i$, which denotes the estimation error at the ith updating step.

It has been shown that the convergence rate of the LMS algorithm as above-described depends on the step-size employed and the statistics of the input-vector $\boldsymbol{y}_i$ [181–185]. In order to attain an optimum convergence speed, an appropriate step-size value of μ needs to be determined, which is usually very difficult to find in a non-stationary communication environment [16]. In the non-stationary communication environment, an appropriate step-size performing well in a given environment might not be suitable for another environment. In the LMS adaptive algorithm, the step-size is directly proportional to the misadjustment of the algorithm, which is defined as the ratio between the excess MSE and the MMSE [154]. It can be observed that when using a larger step-size, faster convergence is achieved, which reduces the length of the training sequence and improves the spectral-efficiency of the UWB system. However, a large step-size leads to a higher misadjustment, resulting in a higher

MSE value or divergence of the algorithm. For this sake, a small step-size is required which however, reduces the convergence speed and the spectral-efficiency of the UWB system [186]. Concerning the effect of the input vector $\boldsymbol{y}_i$, when the input vector $\boldsymbol{y}_i$ becomes longer, the LMS algorithm easily suffers from the gradient-noise amplification problem [16]. Finally, although its implementation complexity is low, the LMS algorithm however, has a relatively low convergence speed, which implies relatively long training overhead and hence relatively low throughput [179]. However, the complexity of the LMS algorithm is low [16], which will be discussed in detail in Section 4.3.

The LMS adaptive detector can be summarised as follows.

❏ *Parameters*:

$\mu =$ a suitable step-size, $0 < \mu < \dfrac{2}{E[||\boldsymbol{y}_i||^2]}$.

❏ *Initialisation*:

$\boldsymbol{w}_1(0)$; $\boldsymbol{w}_1(0) = \mathbf{0}$, when without *a-prior* knowledge.

❏ *Weight vector update*:

For $i = 0, 1, 2, \ldots$, compute

estimation error: $e(i) = b_i^{(1)} - \boldsymbol{w}_1^H(i)\boldsymbol{y}_i$, and

weight vector: $\boldsymbol{w}_1(i+1) = \boldsymbol{w}_1(i) + \mu \boldsymbol{y}_i e^*(i)$.

Let us now describe the NLMS adaptive detector.

4.2.2 Normalised Least Mean Square Adaptive Detector

The normalised least-mean square (NLMS) also belongs to the category of stochastic gradient algorithm, and like LMS adaptive algorithm the associated optimisation criteria is the MMSE [178]. The NLMS algorithm was proposed independently by Nagumo and Noda [16] and Albert and Gardner [16] in 1967. Originally, the NLMS adaptive algorithm was proposed in order to mitigate the gradient noise amplification problem, which the LMS algorithm suffers from, when the input vector $\boldsymbol{y}_i$ is long [16]. It has been shown that the NLMS algorithm is more robust than the LMS adaptive algorithm, since the gradient noise amplification problem can be mitigated in the NLMS adaptive algorithm [16, 179]. Consequently, the NLMS adaptive algorithm is capable of achieving a relatively high convergence speed, no matter whether the input data is correlated or uncorrelated [16].

Furthermore, the NLMS adaptive algorithm is independent of the varying communications environment [186, 187]. Additionally, the NLMS adaptive algorithm is capable of achieving a lower excess MSE than the LMS adaptive algorithm, when they have an equivalent convergence rate [187–189].

In NLMS adaptive detector, the step-size is time-varying which is given by [16]

$$\mu(i) = \frac{\mu}{\delta + ||\boldsymbol{y}_i||^2} \tag{4.9}$$

where δ is a small positive constant that is introduced to avoid numerical overflow, when the magnitude of the input vector $\boldsymbol{y}_i$ is small [188, 190], $||\boldsymbol{y}_i||^2$ is the Euclidean norm of the input vector which is time-varying and μ is the adaptation constant, which satisfies $0 < \mu < 2$. Correspondingly, the weight update equation in the NLMS adaptive detection can be described as [16]

$$\begin{aligned} \boldsymbol{w}_1(i+1) &= \boldsymbol{w}_1(i) + \mu(i)\boldsymbol{y}_i e^*(i) \\ &= \boldsymbol{w}_1(i) + \frac{\mu}{\delta + ||\boldsymbol{y}_i||^2}\boldsymbol{y}_i e^*(i) \\ &= \boldsymbol{w}_1(i) + \frac{\mu}{\delta + ||\boldsymbol{y}_i||^2}\boldsymbol{y}_i [b_i^{(1)} - \boldsymbol{w}_1^H(i)\boldsymbol{y}_i]^* \end{aligned} \tag{4.10}$$

Provided that the step-size μ and δ are properly set, the overhead incurred by training mode can be reduced by using the NLMS adaptive detector due to its faster convergence rate in comparison with the LMS adaptive detector, but at the cost of a negligible increase of complexity [16, 191]. The complexity of the NLMS adaptive detector will be discussed in Section 4.3.

Finally, the NLMS adaptive detector can be summarised as:

❑ *Parameters*:

μ = a suitable step-size, $0 < \mu < 2$.

❑ *Initialisation*:

$\boldsymbol{w}_1(0)$; $\boldsymbol{w}_1(0) = \mathbf{0}$, when without *a-prior* knowledge.

❑ *Weight vector update*:

For $i = 0, 1, 2, \ldots$, compute

estimation error: $e(i) = b_i^{(1)} - \boldsymbol{w}_1^H(i)\boldsymbol{y}_i$,

weight vector: $\boldsymbol{w}_1(i+1) = \boldsymbol{w}_1(i) + \frac{\mu}{\delta + ||\boldsymbol{y}_i||^2}\boldsymbol{y}_i e^*(i)$.

According to [192], the main problem with the stochastic gradient algorithms, such as the LMS and NLMS adaptive algorithms, is their heavily dependence on the eigenvalue distribution of the autocorrelation matrix $\boldsymbol{R}_{y_i}$ of the input signals. It has been shown [178] that the larger is the ratio between the highest and smallest eigen-values, the slower is the convergence speed. Hence, the LMS and NLMS adaptive algorithms might converge very slowly, when the input signals are coloured noise [192]. Furthermore, as shown in (4.8) and (4.10), the LMS and NLMS adaptive algorithms have only single adjustable parameter which is μ, for controlling the convergence rate [193]. In order to achieve higher convergence rate, more complex algorithms might be required, which have additional parameters in addition to the step-size to control the convergence speed. Let us below consider the RLS adaptive algorithm, which is capable of providing higher convergence rate than the LMS and NLMS adaptive algorithms [193].

4.2.3 Recursive Least Square Adaptive Detector

In this section the RLS adaptive detector [16] is introduced for detection of UWB signals. The RLS adaptive algorithm is class of adaptive algorithm derived based on minimisation of the sum of the weighted squared error. This adaptive algorithm can exploit all the information contained in the received data that is invoked in the RLS adaptive algorithm. Hence, the RLS adaptive algorithm may have a substantially higher computational complexity than the LMS or NLMS algorithm. However, the RLS algorithm is capable of achieving a significantly higher convergence rate than the LMS or NLMS algorithm [16, 193]. Let us below develop the RLS adaptive algorithm.

According to the MMSE detection, the optimum weight vector $\boldsymbol{w}_1(i)$ at time i can be expressed as [16]

$$\boldsymbol{w}_1(i) = \boldsymbol{R}_{y_i}^{-1} \boldsymbol{r}_{y_i b_i^{(1)}} \tag{4.11}$$

where $\boldsymbol{R}_{y_i} = \sum_{j=1}^{i} \lambda^{i-j} \boldsymbol{y}_i \boldsymbol{y}_i^H$ is the estimate to the autocorrelation matrix, λ is the forgetting factor accounting for the contribution of data. In (4.11) the estimate to the cross-correlation vector is given by $\boldsymbol{r}_{y_i b_i^{(1)}} = \sum_{j=1}^{i} \lambda^{i-j} \boldsymbol{y}_j b_j^{(1)}$. Explicitly, the autocorrelation matrix and cross-correlation vector can be written as

$$\begin{aligned} \boldsymbol{R}_{y_i} &= \lambda \boldsymbol{R}_{y_{(i-1)}} + \boldsymbol{y}_i \boldsymbol{y}_i^H \\ \boldsymbol{r}_{y_i b_i^{(1)}} &= \lambda \boldsymbol{r}_{y_{(i-1)} b_{(i-1)}^{(1)}} + \boldsymbol{y}_i b_i^{*(1)} \end{aligned} \tag{4.12}$$

respectively. Using matrix-inverse Lemma, the inverse of the auto-correlation matrix can be repre-

sented as [16]

$$\boldsymbol{R}_{y_i}^{-1} = \lambda^{-1}\boldsymbol{R}_{y_{(i-1)}}^{-1} - \frac{\lambda^{-2}\boldsymbol{R}_{y_{(i-1)}}^{-1}\boldsymbol{y}_i\boldsymbol{y}_i^H\boldsymbol{R}_{y_{(i-1)}}^{-1}}{1+\lambda^{-1}\boldsymbol{y}_i^H\boldsymbol{R}_{y_{(i-1)}}^{-1}\boldsymbol{y}_i} \tag{4.13}$$

For convenience of notation, let us define the inverse autocorrelation matrix as [16]

$$\boldsymbol{P}(i) = \boldsymbol{R}_{y_i}^{-1} \tag{4.14}$$

Furthermore, let us define [16]

$$\boldsymbol{k}(i) = \frac{\lambda^{-1}\boldsymbol{P}(i-1)\boldsymbol{y}_i}{1+\lambda^{-1}\boldsymbol{y}_i^H\boldsymbol{P}(i-1)\boldsymbol{y}_i} \tag{4.15}$$

as the RLS gain vector [16]. By rearranging the above equation

$$\begin{aligned}\boldsymbol{k}(i) =& \lambda^{-1}\boldsymbol{P}(i-1)\boldsymbol{y}_i - \lambda^{-1}\boldsymbol{k}(i)\boldsymbol{y}_i^H\boldsymbol{P}(i-1)\boldsymbol{y}_i \\ =& \left[\lambda^{-1}\boldsymbol{P}(i-1) - \lambda^{-1}\boldsymbol{k}(i)\boldsymbol{y}_i^H\boldsymbol{P}(i-1)\right]\boldsymbol{y}_i\end{aligned} \tag{4.16}$$

Then, upon applying (4.14) and (4.15) into (4.13), the inverse of the autocorrelation matrix can be expressed as [16]

$$\boldsymbol{P}(i) = \lambda^{-1}\boldsymbol{P}(i-1) - \lambda^{-1}\boldsymbol{k}(i)\boldsymbol{y}_i^H\boldsymbol{P}(i-1) \tag{4.17}$$

With the aid of (4.12), it can be shown that the weight vector $\boldsymbol{w}_1(i)$ of (4.11) can be written as

$$\begin{aligned}\boldsymbol{w}_1(i) &= \boldsymbol{P}(i)\boldsymbol{r}_{y_i b_i^{(1)}} \\ &= \lambda\boldsymbol{P}(i)\boldsymbol{r}_{y_{(i-1)}b_{(i-1)}^{(1)}} + \boldsymbol{P}(i)\boldsymbol{y}_i b_i^{*(1)}\end{aligned} \tag{4.18}$$

Then, substituting (4.17) in (4.18) yields

$$\begin{aligned}\boldsymbol{w}_1(i) &= \boldsymbol{P}(i-1)\boldsymbol{r}_{y_{(i-1)}b_{(i-1)}^{(1)}} - \boldsymbol{k}(i)\boldsymbol{y}_i^H\boldsymbol{P}(i-1)\boldsymbol{r}_{y_{(i-1)}b_{(i-1)}^{(1)}} + \boldsymbol{P}(i)\boldsymbol{y}_i b_i^{*(1)} \\ &= \boldsymbol{R}_{y_{(i-1)}}^{-1}\boldsymbol{r}_{y_{(i-1)}b_{(i-1)}^{(1)}} - \boldsymbol{k}(i)\boldsymbol{y}_i^H\boldsymbol{R}_{y_{(i-1)}}^{-1}\boldsymbol{r}_{y_{(i-1)}b_{(i-1)}^{(1)}} + \boldsymbol{P}(i)\boldsymbol{y}_i b_i^{*(1)} \\ &= \boldsymbol{w}_1(i-1) - \boldsymbol{k}(i)\boldsymbol{y}_i^H\boldsymbol{w}_1(i-1) + \boldsymbol{P}(i)\boldsymbol{y}_i b_i^{*(1)}\end{aligned} \tag{4.19}$$

Finally, using the fact that $\boldsymbol{P}(i)\boldsymbol{y}_i$ equals the gain vector $\boldsymbol{k}(i)$, (4.19) can be represented as

$$\begin{aligned} \boldsymbol{w}_1(i) &= \boldsymbol{w}_1(i-1) + \boldsymbol{k}(i)[b_i^{*(1)} - \boldsymbol{y}_i^H \boldsymbol{w}_1(i-1)] \\ &= \boldsymbol{w}_1(i-1) + \boldsymbol{k}(i)\xi^*(i) \end{aligned} \tag{4.20}$$

where the estimation error $\xi(i)$ is defined as [16]

$$\xi(i) = b_i^{(1)} - \boldsymbol{w}_1^H(i-1)\boldsymbol{y}_i \tag{4.21}$$

In order to carry out the RLS-assisted adaptive detection, the weight vector is required to be initialized. As in [16], a soft-contrained initialisation can be employed, which sets

$$\boldsymbol{P}(0) = \delta^{-1}\boldsymbol{I} \tag{4.22}$$

where δ is referred as the regularization factor, which is usually a small positive constant for a high SNR, but a relatively large positive constant for a low SNR [16, 194]. Furthermore, when no a-prior knowledge is available, the initial weight vector $\boldsymbol{w}(0)$ is typically set to be a null vector.

The stability of the RLS adaptive algorithm is dependent on the following factors [178]

- The initialisation of the inverse autocorrelation matrix, $\boldsymbol{P}(0) = \delta^{-1}\boldsymbol{I}$;
- The value of the forgetting factor, λ.

It has been shown that the choice of δ is critical for nonstationary communications environments [178]. It turns out that in the nonstationary communications environment the convergence properties of the RLS adaptive algorithm differ significantly, when different values of δ is applied [194]. A small value of δ leads to instability of the algorithm(overshoot phenomenon). However, when the value of δ increases, the convergence speed of the RLS adaptive algorithm reduces especially, at the start of the adaptation [178]. The choice of the forgetting factor λ also affects the stability, the convergence speed and the tracking behaviour of the RLS Adaptive algorithm [178]. It has been found that for achieving a stable algorithm a value of λ should be chosen between $\left(1 - \frac{1}{(N_c N_\psi + L - 1)}\right)$ and $\left(1 - \frac{1}{10(N_c N_\psi + L - 1)}\right)$ [178]. It has been shown that the RLS adaptive algorithm has the higher computational complexity than the LMS and NLMS adaptive algorithms [178, 192]. However, the RLS adaptive algorithm is more suitable for rapidly time-varying environments than the LMS and NLMS adaptive algorithms [195]. The computational complexity of the RLS adaptive algorithm will be discussed in Section 4.3 along with the LMS and NLMS adaptive algorithms.

Finally, the procedure of the RLS adaptive detector is summarised as follows.

❏ *Parameters*:

λ = a suitable forgetting factor is chosen in the range

$$\left(1 - \frac{1}{(N_c N_\psi + L - 1)}\right) \leq \lambda \leq \left(1 - \frac{1}{10(N_c N_\psi + L - 1)}\right)$$

❏ *Initialisation*:

$\boldsymbol{w}_1(0)$; $\boldsymbol{w}_1(0) = \mathbf{0}$, when without *a-prior* knowledge.

$\boldsymbol{P}(0) = \delta^{-1}\boldsymbol{I}$, where δ is set as a relatively small positive constant for higher SNR,

and as a relatively large positive constant for lower SNR.

❏ *Computation*: For $i = 1, 2, \ldots$, compute

gain vector: $\boldsymbol{k}(i) = \dfrac{\lambda^{-1}\boldsymbol{P}(i-1)\boldsymbol{y}_i}{1 + \lambda^{-1}\boldsymbol{y}_i^H \boldsymbol{P}(i-1)\boldsymbol{y}_i}$,

a-priori estimation error: $\xi(i) = b_i^{(1)} - \boldsymbol{w}_1^H(i-1)\boldsymbol{y}_i$,

weight vector: $\boldsymbol{w}_1(i) = \boldsymbol{w}_1(i-1) + \boldsymbol{k}(i)\xi^*(i)$,

inverse of autocorrelation matrix: $\boldsymbol{P}(i) = \lambda^{-1}\boldsymbol{P}(i-1) - \lambda^{-1}\boldsymbol{k}(i)\boldsymbol{y}_i^H\boldsymbol{P}(i-1)$.

Let us now analyze the computation complexity of the adaptive algorithms considered in this section.

4.3 Complexity of Adaptive Detectors

In this section, we analyze the complexity of the LMS, NLMS and the RLS adaptive detectors. The complexity is measured with the help of the number of multiplications and additions required to detect a symbol of the desired user. As in the last chapter we set $\mathcal{T} = N_c N_\psi + L - 1$.

4.3.1 Complexity of Least Mean Square Adaptive Detector

In adaptive detection, the LMS algorithm, is the most simple to implement. The estimate of the ith bit of the 1st user can be given as

$$z_i^{(1)} = \boldsymbol{w}_1^H(i)\boldsymbol{y}_i \tag{4.23}$$

The update equation for the weight vector $\boldsymbol{w}_1(i+1)$ is given in (4.8), which is

$$\boldsymbol{w}_1(i+1) = \boldsymbol{w}_1(i) + \mu \boldsymbol{y}_i e^*(i) \tag{4.24}$$

According to (4.23) and (4.24), it can be shown that the complexity for the LMS adaptive algorithm can be summarised as shown in is calculated as shown in Table 4.1.

Operations	Number of additions	Number of multiplications
$z_i^{(1)}$	$\mathcal{T}$	$\mathcal{T}$
$e(i)$	1	$-$
$\mu \boldsymbol{y}_i e^*(i)$	$-$	$2\mathcal{T}$
$\boldsymbol{w}_1(i+1)$	$\mathcal{T}$	$-$

Table 4.1: Complexity of Least Mean Square (LMS) adaptive detector.

Therefore, in order to detect a symbol of the desired user, the total number of operations required by the LMS adaptive detector is $(5\mathcal{T}+1)$. Explicitly, if $\mathcal{T}$ is very large, we can ignore 1, and the complexity of the LMS adaptive detector is hence $5\mathcal{T}$.

4.3.2 Complexity of Normalised Least Mean Square Adaptive Detector

As shown in Section 4.2.2, in the NLMS adaptive detection the estimate of the ith bit of the 1st user can be expressed as

$$z_i^{(1)} = \boldsymbol{w}_1^H(i)\boldsymbol{y}_i \tag{4.25}$$

Correspondingly, the updated equation for the weight vector $\boldsymbol{w}_1(i+1)$ is given by (4.10), which is

$$\boldsymbol{w}_1(i+1) = \boldsymbol{w}_1(i) + \frac{\mu}{\delta + ||\boldsymbol{y}_i||^2}\boldsymbol{y}_i e^*(i) \tag{4.26}$$

Therefore, the number of operations required by the NLMS adaptive algorithm can be summarised in Table 4.2.

Hence, in order to detect a symbol of the desired user, the total number of operations required is $7\mathcal{T}+2$, which can be approximately expressed as $7\mathcal{T}$, if $\mathcal{T}$ is very large.

Operations	Number of additions	Number of multiplications
$z_i^{(1)}$	$\mathcal{T}$	$\mathcal{T}$
$e(i)$	1	$-$
$\|\|\boldsymbol{y}_i\|\|^2$	$\mathcal{T}-1$	$\mathcal{T}$
$\frac{\mu}{\delta+\|\|\boldsymbol{y}_i\|\|^2}\boldsymbol{y}_i e^*(i)$	1	$2\mathcal{T}+1$
$\boldsymbol{w}_1(i+1)$	$\mathcal{T}$	$-$

Table 4.2: Complexity of Normalised Least Mean Square (NLMS) adaptive detector.

4.3.3 Complexity of Recursive Least Square Adaptive Detector

For the RLS adaptive detection, the ith bit of the 1st user can be expressed as

$$z_i^{(1)} = \boldsymbol{w}_1^H(i)\boldsymbol{y}_i \tag{4.27}$$

where the weight vector is obtained through the update equation

$$\begin{aligned} \boldsymbol{w}_1(i) &= \boldsymbol{w}_1(i-1) + \boldsymbol{k}(i)\xi^*(i) \\ &= \boldsymbol{w}_1(i-1) + \frac{\lambda^{-1}P(i-1)\boldsymbol{y}_i}{1+\lambda^{-1}\boldsymbol{y}_i^H\boldsymbol{P}(i-1)\boldsymbol{y}_i}\xi^*(i) \end{aligned} \tag{4.28}$$

as shown in Section 4.2.3 of this chapter. The number of operations invoked in the RLS adaptive detector are summarized in Table 4.3. Hence, in order to detect a symbol of the desired user, the total number of operations by the RLS adaptive detector is $11\mathcal{T}^2+8\mathcal{T}+3$, which is approximately $11\mathcal{T}^2$, if the value of $\mathcal{T}$ is high.

Let us now provide and discuss the achievable error performance of the adaptive detectors.

4.4 Performance Results and Discussion

This section provides a range of simulation results characterising the error rate performance of the hybrid DS-TH systems employing the various adaptive detectors as shown in Section 4.2. Furthermore, since both the pure DS-UWB and pure TH-UWB schemes constitute special examples of the hybrid

Operations	Number of additions	Number of multiplications
$z_i^{(1)}$	$\mathcal{T}$	$\mathcal{T}$
$\xi(i)$	1	$-$
$\lambda^{-1}P(i-1)\boldsymbol{y}_i$	$\mathcal{T}^2$	$\mathcal{T}^2+\mathcal{T}$
$\boldsymbol{y}_i^H\boldsymbol{P}(i-1)\boldsymbol{y}_i$	$\mathcal{T}^2+\mathcal{T}$	$\mathcal{T}^2+\mathcal{T}$
$1+\lambda^{-1}\boldsymbol{y}_i^H\boldsymbol{P}(i-1)\boldsymbol{y}_i$	1	1
$\boldsymbol{k}(i)$	$-$	$\mathcal{T}$
$\boldsymbol{k}(i)\xi^*(i)$	$-$	$\mathcal{T}$
$\boldsymbol{w}_1(i)$	$\mathcal{T}$	$-$
$\lambda^{-1}\boldsymbol{k}(i)\boldsymbol{y}_i^H\boldsymbol{P}(i-1)$	$2\mathcal{T}^2$	$3\mathcal{T}^2$
$\lambda^{-1}\boldsymbol{P}(i-1)$	$-$	$\mathcal{T}^2$
$P(i)$	$\mathcal{T}^2$	$-$

Table 4.3: Complexity of Recursive Least Square (RLS) adaptive detector.

DS-TH UWB scheme, their BER performance is also investigated in this section. In our simulations, the following assumptions were employed:

1) Coherent BPSK baseband modulation without channel coding;

2) The energy per symbol was kept constant. The total spreading factor was constant and was $N_cN_\psi = 64$. It is worth mentioning again that in this case, the hybrid DS-TH UWB system is reduced to the pure DS-UWB system when $N_c = 64$ and $N_\psi = 1$, while it is reduced to the pure TH-UWB system when $N_c = 1$ and $N_\psi = 64$. Furthermore, in our simulations for the hybrid DS-TH UWB system, the DS spreading factor was fixed to $N_c = 16$, while the TH spreading factor was fixed to $N_\psi = 4$;

3) For the UWB channels, the number of resolvable multipaths was assumed to be $L = 15$ and the normalised doppler frequency was set to $f_dT_b = 0.0001$. Furthermore, in our simulations the S-V channel model was employed, where the channel gains were assumed to obey the Rayleigh distribution. The parameters of the S-V channel model used in our simulations are summarised in Table 4.4, where 'LoS' means that the channel model contains line-of-sight (LoS) propagation paths [117].

	$1/\Lambda$	Γ	γ
LoS	14.11ns	2.63ns	4.58ns

Table 4.4: Fitted Saleh Valenzuela Channel Model Parameter

Let us now provide and discuss the performance of the LMS-, NLMS- and RLS-aided adaptive detectors in the following relevant subsections.

4.4.1 Performance Results Using Least Mean Square Adaptive Detector

In this section the performance results of the hybrid DS-TH UWB systems using LMS-aided adaptive detector are presented. Initially, learning curves for the hybrid DS-TH UWB system supporting single or multiple users are depicted, when different step-sizes are chosen. Then, BER performance for the hybrid DS-TH UWB systems are presented, when the LMS adaptive detector is employed. In this subsection, all the simulations were carried out in the LoS communications environment.

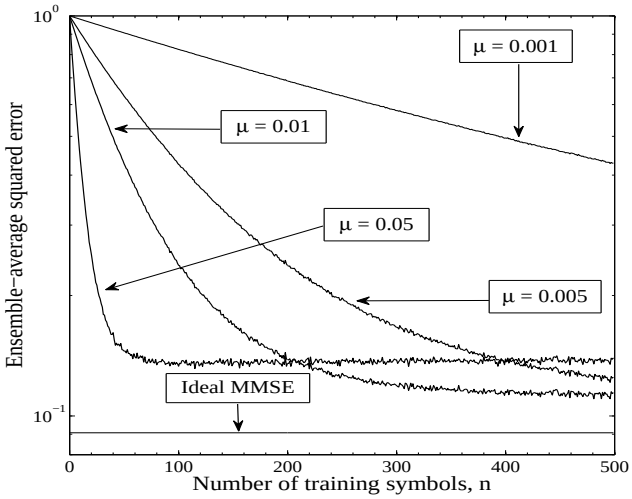

Figure 4.3: Learning curves of the LMS adaptive detector with different step-size μ for the hybrid DS-TH UWB system supporting single user, when communicating over the S-V UWB Rayleigh fading channels having $L = 15$ resolvable multipaths and a doppler frequency $f_d T_b = 0.0001$. The DS spreading factor is $N_c = 16$, the TH-spreading factor is $N_\psi = 4$ and the SNR per bit is $E_b/N_0 = 10$ dB.

Fig. 4.3 shows the learning curves of the LMS adaptive detector for the hybrid DS-TH UWB system supporting single user when communicating over the S-V UWB channels having $L = 15$ number of resolvable multipaths and a doppler frequency $f_d T_b = 0.0001$. In our simulations, the

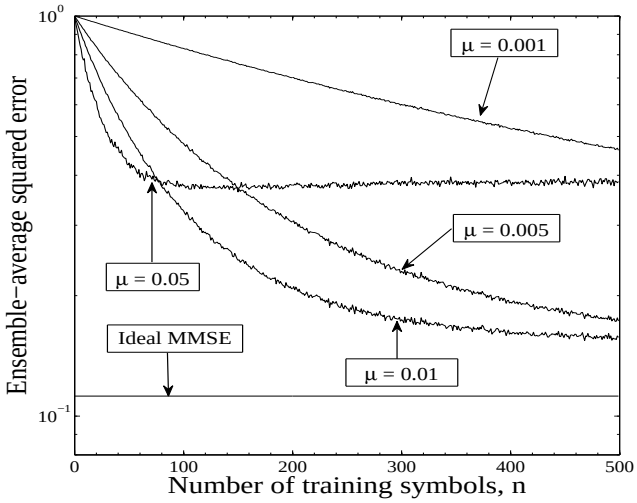

Figure 4.4: Learning curves of the LMS adaptive detector with different step-size μ for the hybrid DS-TH UWB system supporting $K = 15$ users, when communicating over the S-V UWB Rayleigh fading channels having $L = 15$ resolvable multipaths and a doppler frequency $f_d T_b = 0.0001$. The DS spreading factor is $N_c = 16$, the TH-spreading factor is $N_\psi = 4$ and the SNR per bit is $E_b/N_0 = 10$ dB.

DS-spreading factor was assumed to be $N_c = 16$ while the TH-spreading factor was fixed to $N_\psi = 4$. Furthermore, the SNR per bit was set as $E_b/N_0 = 10$ dB. The ensemble average was obtained from $10,000$ independent realizations. From the results of Fig. 4.3, we observe that the convergence speed of the LMS adaptive detector depends heavily on the step-size μ. For a large step-size value of $\mu = 0.05$, the adaptive detector converges to its steady-state value after about 100 iterations. By contrast, when a smaller step-size value, such as $\mu = 0.001$ and $\mu = 0.005$ is employed, the convergence speed may be very slow. As seen in Fig. 4.3, when $\mu = 0.001$, the LMS adaptive detector does not converge even after 500 iterations.

Fig. 4.4 shows the learning curves of the LMS adaptive detector for the hybrid DS-TH UWB system when communicating over the S-V UWB channels having $L = 15$ resolvable paths and a doppler frequency $f_d T_b = 0.0001$. In our simulations the DS-spreading factor was $N_c = 16$, the TH-spreading factor was $N_\psi = 4$ and $E_b/N_0 = 10$ dB. The ensemble average was obtained through $10,000$ independent realizations. As shown in Fig. 4.4, the learning curve for $\mu = 0.05$ converges much faster than the learning curves with the other step-size values. In comparison with the results shown in Fig. 4.3, the corresponding MSE is increased because of MUI. Furthermore, it can be observed from Fig. 4.3 and Fig. 4.4, that a relatively higher step-size usually results in higher convergence speed, which hence leads to less number of iterations, and higher spectral-efficiency of

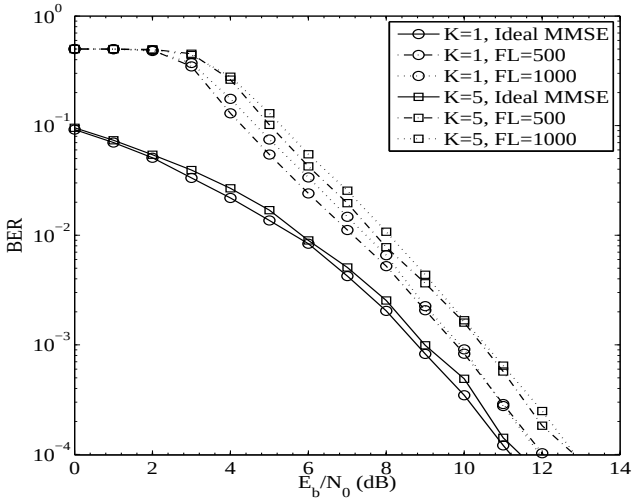

Figure 4.5: BER versus SNR performance of the hybrid DS-TH UWB system supporting single or $K = 5$ users, when communicating over Rayleigh fading channels modelled by the S-V model having $L = 15$ number of resolvable multipaths. The other parameters used in our simulations were $f_d T_b = 0.0001$, $N_c = 16$, $N_\psi = 4$, $\mu = 0.05$ and $\mu_{DD} = 0.01$. The frame length (FL) was set to 500 or 1000, while the length of the training sequence was 160 bits.

the hybrid DS-TH UWB system. However, as the step-size is directly related to misadjustment of the algorithm, increasing the step-size also increases the misadjustment of the algorithm which results in higher MSE values as shown in Fig. 4.3 and Fig. 4.4. Based on this observation, in our following simulations, a bigger step-size is usually employed during the training mode so that the adaptive detector can converge with a high speed. By contrast, during the DD mode, a smaller step-size is utilised in order to reduce the misadjustment and consequently to reduce the MSE. Additionally, from the results of Fig. 4.3 and Fig. 4.4 we are implied that misadjustment becomes more prominent when multiple users are supported. Consequently, the decrease of spectral-efficiency due to using small step-size might be used for trade off an improved MSE performace.

Fig. 4.5 shows the BER performance of the hybrid DS-TH UWB system supporting single or $K = 5$ users when communicating over Rayleigh faded UWB channels having $L = 15$ number of resolvable paths. The step-size used during the training mode was $\mu = 0.05$, while during the DD mode was $\mu_{DD} = 0.01$. The DS-spreading factor was $N_c = 16$ and the TH-spreading factor was $N_\psi = 4$. It can be observed that the BER performance of the LMS-assisted adaptive detector becomes closer to that of the ideal MMSE detector, as the SNR increases. As shown in Fig. 4.5, in our simulations two types of frame length were considered, which were 500 and 1000. It can be observed from Fig. 4.5 that, if an appropriate step-size is employed the BER performance of the

hybrid DS-TH UWB systems using a frame length of 1000 approaches to that of the hybrid DS-TH UWB systems using a frame length 500. Note that, since for both cases the number of training bits was 160, hence, the spectral-efficiency of systems using the frame-length of 1000 is 84% while that using a frame-length of 500 is only 68%. Furthermore, from the results of Fig. 4.5 it can be observed that the LMS-aided detector is much worse than the ideal MMSE at the low SNR region. The BER performance of the hybrid DS-TH UWB systems at low SNR region may be improved by using longer training sequences associated with smaller step-size. However, in this case the spectral-efficiency of the hybrid DS-TH UWB systems will be decreased. Additionally, from the water-fall BER curves as shown in Fig. 4.5, we are implied that LMS adaptive detector is capable of efficiently mitigating both the ISI and MUI.

Fig. 4.6, shows the effect of the step-size used during the DD-mode on the BER performance of the hybrid DS-TH UWB systems, when communicating over the UWB channels modelled by the S-V Rayleigh faded model. In Fig. 4.6, $\mu_{DD} = 0$ corresponds to without using the DD-mode. It can be observed from the results of Fig. 4.6 that, for the low-complexity LMS adaptive detector, it is necessary to choose an appropriate step-size in order to achieve a BER performance that is close to that achieved by the ideal MMSE detector with perfect channel knowledge. When the LMS adaptive detector does not update its weights after the training mode, which corresponds to the case of $\mu_{DD} = 0$ there is a significant loss in BER performance in comparison with the cases using an appropriate step-size such as $\mu_{DD} = 0.01$, for weight updating. For a given step-size of $\mu_{DD} = 0$ or 0.01, the BER corresponding to a frame-length $FL = 500$ is slightly lower than that corresponding to $FL = 1000$. However, as discussed previously, this better BER performance is obtained at the expense of a lower spectral-efficiency, as higher percentage of training symbols were transmitted in the former case than in the latter case. Furthermore, the results of Fig. 4.6 explicitly show that the DD approach can be employed in order to improve the BER performance as well as the spectral-efficiency of the hybrid DS-TH UWB systems. However, if an inappropriate step-size is used, as shown Fig. 4.6 the BER performance may become even worse than that of the LMS adaptive detector without the DD operations. The reason behind this BER performance loss is that the inappropriate step-size causes a high misadjustment, as mentioned previously, which further leads to a high MSE. Consequently, the error probability becomes higher and the receiver may update its weights according to the erroneously detected bits with the assumption that they are correct. As no reliable information is fed back, the erroneously detected bits may make the adaptive detector even worse due to error propagation. This is the case especially at low SNR when the BER is higher than 10^{-2}. As shown in Fig. 4.6 the BER performance becomes better as the SNR increases. Therefore, it might be appropriate to utilise DD-

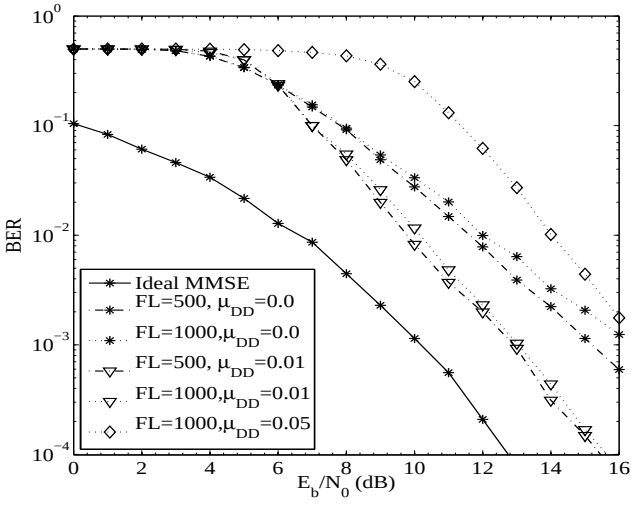

Figure 4.6: BER versus SNR performance of the hybrid DS-TH UWB system supporting $K = 15$ users, when communicating over the UWB channels modelled by the S-V Rayleigh fading model. The other parameters used in our simulations were $L = 15$, $f_d T_b = 0.0001$, $N_c = 16$, $N_\psi = 4$ and $\mu = 0.05$. The frame length (FL) 500 or 1000, while the length of the training sequence was 160 bits.

mode, if the SNR is sufficiently high, yielding that the BER is lower than 10^{-2}. Another possible solution to this problem is to use soft decisions instead of hard decisions to upgrade the weights of the adaptive detector. However, using soft decisions may increase the complexity of the UWB systems. Additionally, in order to make the adaptive detector updated toward converging, a smaller step-size than that used in the training mode may be employed. From the results of Fig. 4.6, we can see that the BER performance difference for the systems using $FL = 1000$ and 500 is about 1dB when using no DD-mode. By contrast, when the DD-mode associated with $\mu_{DD} = 0.01$ is employed, this BER performance difference is significantly reduced.

Finally, Figs. 4.7 and 4.8 show the BER versus SNR performance of various UWB systems using LMS adaptive detection and supporting single, $K = 5$ or $K = 15$ users. From the results of Fig. 4.7, it can be observed that the BER performance of the pure DS-, pure TH- and hybrid DS-TH UWB systems is approximately the same, when step-size and all other parameters are the same. From the results of Fig. 4.8, it can be observed that the BER performance of the pure DS-, pure TH- and hybrid DS-TH UWB systems is also approximately the same, when the adaptive detectors use no DD-mode operations. However, when the DD-mode is applied with an appropriate step-size, then, for given other parameters, the BER performance of the hybrid DS-TH UWB system is slightly better than that of the pure TH- or pure DS-UWB system. Furthermore, from the results shown in Figs. 4.7 and 4.8,

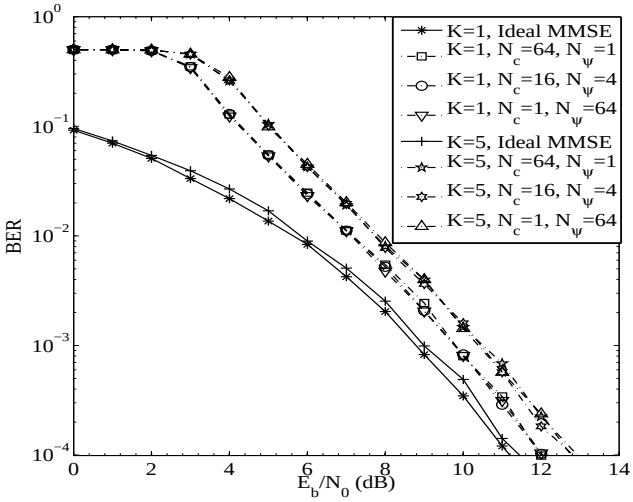

Figure 4.7: BER versus SNR performance of the DS-,TH- and hybrid DS-TH UWB systems supporting single and $K = 5$ users, when communicating over the UWB channels modelled by the S-V Rayleigh fading model. The other parameters used in our simulations were $l = 15$, $f_d T_b = 0.0001$, $\mu = 0.05$ and $\mu_{DD} = 0.01$. The frame length (FL) was 1000 and there were 160 training symbols per frame.

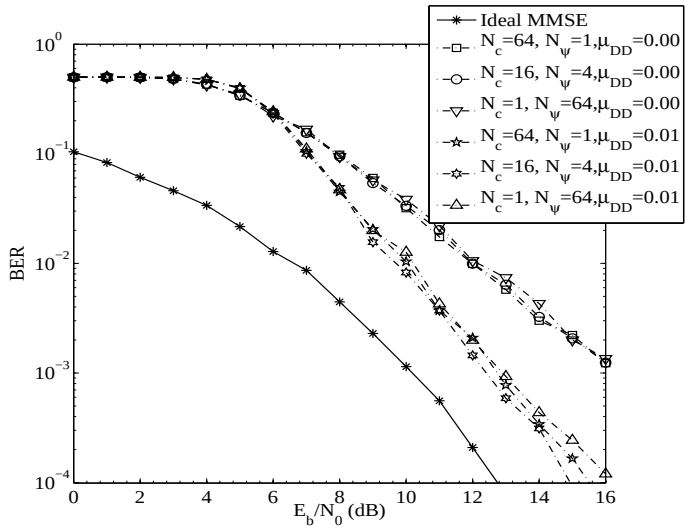

Figure 4.8: BER versus SNR performance of the DS-,TH- and hybrid DS-TH UWB systems supporting $K = 15$ users, when communicating over the UWB channels modelled by the S-V channel Rayleigh fading model. The other parameters used in our simulations were $f_d T_b = 0.0001$, $\mu = 0.05$, and $L = 15$. The frame length (FL) was 1000 and there were 160 training symbols per frame.

we can conclude that the LMS adaptive detection is efficient for all UWB systems.

4.4.2 Performance Results Using Normalised Least Mean Square Adaptive Detector

In this section, we present the performance results of the hybrid DS-TH UWB systems employing the NLMS adaptive detection. All our simulations were carried out in the context of the UWB channels with LoS propagation. Furthermore, the BER performance results of the pure DS- and pure TH-UWB are provided as special examples of hybrid DS-TH UWB systems.

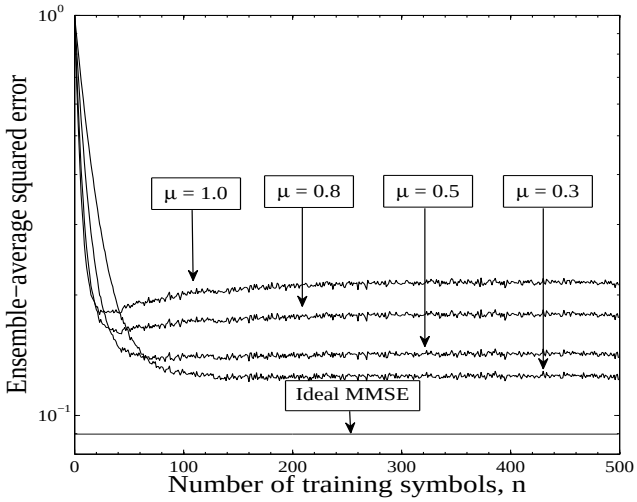

Figure 4.9: Learning curves of the NLMS adaptive detector with different adaptation step-sizes μ, when the hybrid DS-TH UWB systems supports single user and communicates over the UWB channels modelled by the S-V Rayleigh fading model. The other parameters were $E_b/N_0 = 10$dB, Doppler frequency-shift $f_dT_b = 0.0001$, $N_c = 16$, $N_\psi = 4$ and $L = 15$. The ensemble-averaged results were taken over $10,000$ independent realizations of the channel.

Fig. 4.9 and Fig. 4.10 shows the ensemble MSE learning curve of the NLMS adaptive detector using different adaptation step-sizes of μ at $E_b/N_0 = 10$dB, when the hybrid DS-TH UWB supports $K = 1$ (Fig. 4.9) and $K = 15$ users (Fig. 4.10). The ensemble average was taken over $10,000$ independent realizations. From the results of Fig. 4.9 and Fig. 4.10, it can be observed that, as the value of the adaptation step-size μ increases, the rate of convergence increases. Hence, as the value of μ increases, less number of training bits is required for the NLMS adaptive detector to reach its steady state value, and consequently, the spectral-efficiency of the hybrid DS-TH UWB systems can be improved. However, as shown in Figs. 4.9 and 4.10, a higher value of μ results in faster convergence, but also leads to a higher MSE value. Based on the above observations, it can be implied that variable step-sizes may be utilised by the NLMS adaptive detector, so that it can converge to a low MSE value,

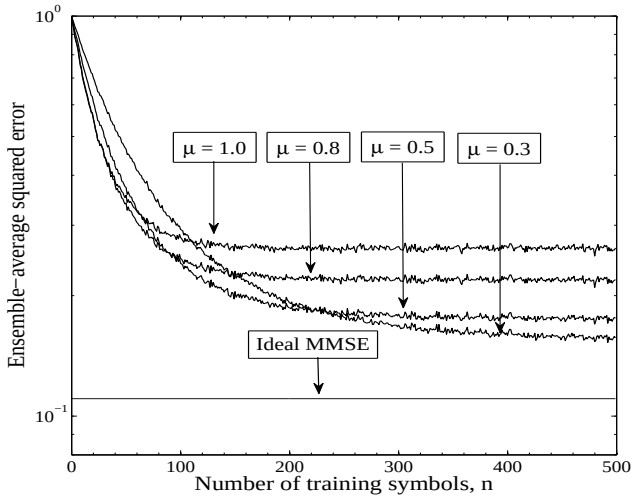

Figure 4.10: Learning curves of the NLMS adaptive detector with different adaptation step-size μ, when the hybrid DS-TH UWB system supports $K = 15$ users and communicates over the UWB channels modelled by the S-V Rayleigh fading model. The other parameters were $E_b/N_0 = 10$dB, Doppler frequency-shift $f_dT_b = 0.0001$, $N_c = 16$, $N_\psi = 4$ and $L = 15$. The ensemble-averaged results were taken over $10,000$ independent realizations of the channel.

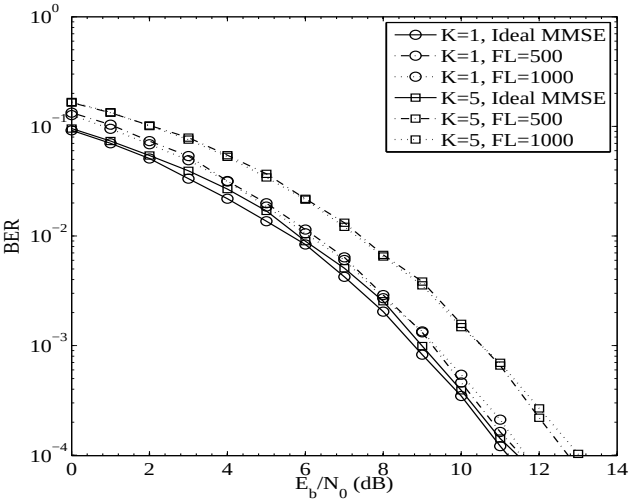

Figure 4.11: BER versus SNR performance of the hybrid DS-TH UWB system supporting single or $K = 5$ users, when communicating over the UWB channels modelled by S-V Rayleigh fading channel model. The other parameters used in our simulations were $f_dT_b = 0.0001$, $\mu = 0.5$, $\mu_{DD} = 0.05$, $N_c = 16$, $N_\psi = 4$ and $L = 15$. The frame length (FL) was set to 500 and 1000, respectively, where the training length (TL) was 160 symbols.

but with the aid of short training sequences.

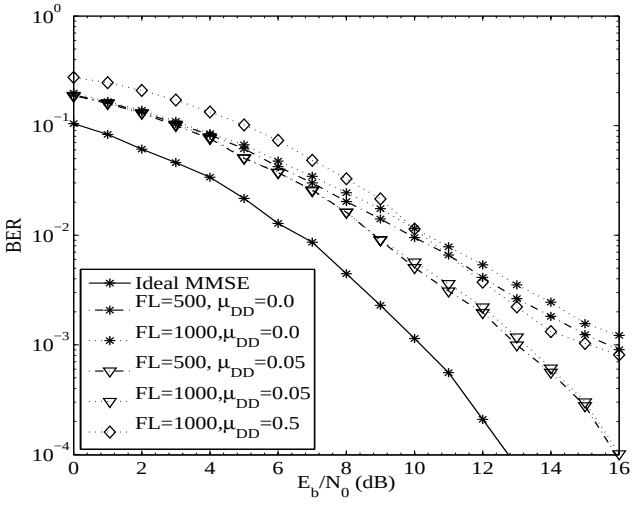

Figure 4.12: BER versus SNR performance of the hybrid DS-TH UWB system supporting $K = 15$ users, when communicating over the UWB channels modelled by the S-V Rayleigh fading model. The other parameters used in our simulations were $f_dT_b = 0.0001$, $\mu = 0.5$, $N_c = 16$, $N_\psi = 4$ and $L = 15$. The frame length (FL) was set to 500 or 1000, where the training length (TL) was 160 symbols.

Fig. 4.11 shows the BER performance of the hybrid DS-TH UWB system supporting single or $K = 5$ users, when communicating over the UWB channels modelled by the S-V Rayleigh fading model. It can be observed from the Fig. 4.11 that the NLMS-aided adaptive detector performs nearly as well as an ideal MMSE detector requiring perfect channel knowledge when the systems support single user. However, a BER performance loss of about 1dB occurs, as the results of possibly using inappropriate step-size, when $K = 5$ users are supported. As shown in Fig. 4.11, the BER curves are in the presence of water fall, implying that the hybrid DS-TH UWB system with the aid of the NLMS adaptive detector is capable of efficiently suppressing the MUI and ISI. Furthermore, it can be observed that the BER performance corresponding to the frame length of $FL = 500$ is slightly better than that corresponds to $FL = 1000$. However, this improved BER performance is obtained at the expense of a lower spectral-efficiency as analysed previously in this section. Hence, it can be concluded that the spectral-efficiency of the hybrid DS-TH UWB system might sometimes be used to trade for the BER performance of the system, a lower spectral-efficiency for a better BER performance.

Fig. 4.12 shows the BER performance of the hybrid DS-TH UWB system supporting $K = 15$ number of users when communicating over the UWB channels modelled by the S-V Rayleigh fading model. From the results of Fig. 4.12, it can be observed that the BER performance of the NLMS-

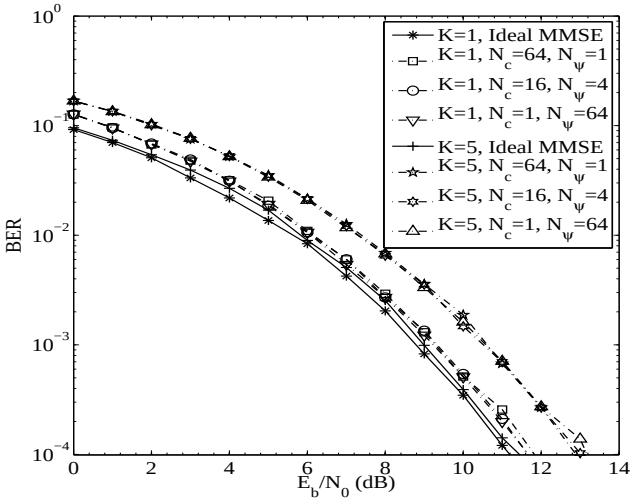

Figure 4.13: BER versus SNR performance of the DS-,TH- and hybrid DS-TH UWB systems supporting single and $K = 5$ users, when communicating over the UWB channels modelled by S-V Rayleigh fading model. The other parameters used in our simulations were $f_d T_b = 0.0001$, $\mu = 1.0$, $\mu_{DD} = 0.05$ and $L = 15$, respectively. The frame length (FL) was set to 1000 where the training length was 160 symbols.

aided adaptive detector is dependend on the step-size chosen for the DD-mode. From Fig. 4.12 it can be inferred that using the DD-mode may enhance the BER performance. If no DD is applied, a considerable loss in BER performance occurs, when the SNR is high. However, it can also be observed that the BER performance of the hybrid DS-TH UWB system degrades, when the an inappropriate step-size for the DD-mode is applied, which results in high misadjustment, or high error probability, as discussed associated with Fig. 4.6. As shown in Fig. 4.12, when an appropriate step-size is applied by the DD-mode, the BER performance difference corresponding to FL$= 500$ and to FL$= 1000$ is very small.

The BER performance of the pure DS-UWB, pure TH-UWB and hybrid DS-TH UWB systems using NLMS adaptive detection is plotted in Fig. 4.13 when both the training and DD mode are employed. From the results of Fig. 4.13 it can be observed that the BER performance of all the UWB system are the same when single and $K = 5$ users are supported. Finally, the BER performance of pure DS-UWB, pure TH-UWB and hybrid DS-TH UWB systems supporting $K = 15$ users is depicted in Fig. 4.14, when using no DD-mode ($\mu_{DD} = 0$) or using the DD-mode associated with a step-size ($\mu_{DD} = 0.05$). It can be observed that the BER performance of the hybrid DS-TH UWB system is slightly better than that of the pure DS-UWB or pure TH-UWB system for both $\mu_{DD} = 0$ and $\mu_{DD} = 0.05$. Furthermore, from the results of Figs. 4.13 and 4.14, it can be implied that all the

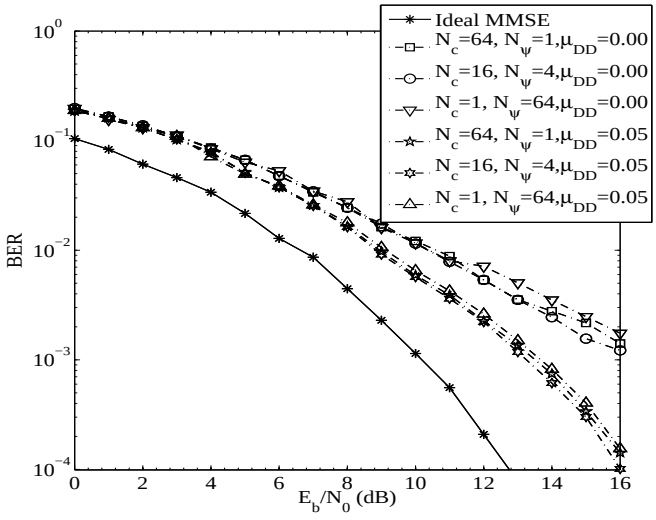

Figure 4.14: BER versus SNR performance of the DS-,TH- and hybrid DS-TH UWB systems supporting $K = 15$ users, when communicating over the UWB channels modelled by the S-V Rayleigh fading model. The other parameters used in our simulations were $f_d T_b = 0.0001$, $\mu = 0.5$, $\mu_{DD} = 0.05$ and $L = 15$. The frame length (FL) was set to 1000 and the training length (TL) was 160 symbols respectively.

UWB systems are capable of efficiently mitigating both the MUI and ISI. Moreover, from the shown results in Figs. 4.11- 4.14 it can be concluded that the NLMS adaptive detector can be employed in the context of all the UWB systems considered, in order to enhance their BER performance with relatively low complexity.

4.4.3 Performance Results Using Recursive Least Square Adaptive Detector

In this section, the convergence behaviour and BER performance of the hybrid DS-TH UWB systems using the RLS adaptive detector are investigated. As in the RLS adaptive detector the convergence rate is depended on both the regularization factor δ and the forgetting factor λ, the learning behaviour is hence studied by keeping one of them constant while varying the other. Besides the learning behaviour, the BER performance of hybrid DS-TH UWB system, pure DS and pure TH-UWB is investigated, when the forgetting factor is fixed to $\lambda = 0.998$ and the regularisation factor is fixed to $\delta = 0.05$. As in the previous two subsections, for the LMS and NLMS adaptive detectors, in this section all our simulations were carried out in LoS UWB communication environments. Let us first show the learning curves of the RLS adaptive detection.

Figs. 4.15 and 4.16 show the ensemble mean-square error learning curves of the RLS adaptive detector for the hybrid DS-TH UWB system supporting single or $K = 15$ users, when using different

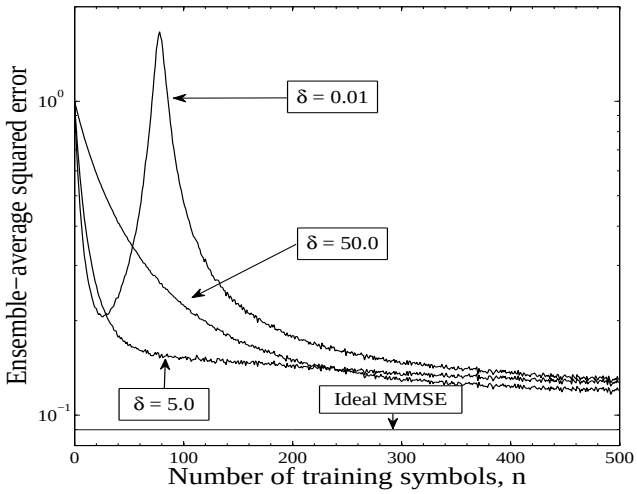

Figure 4.15: Learning curves of the RLS adaptive detector using different regularisation factor δ, for the hybrid DS-TH UWB system supported single user, when communicating over the S-V Rayleigh fading channels. The other parameters were $E_b/N_0 = 10$dB, Doppler frequency-shift $f_dT_b = 0.0001$, $\lambda = 0.998$, $N_c = 16$, $N_\psi = 4$ and $L = 15$.

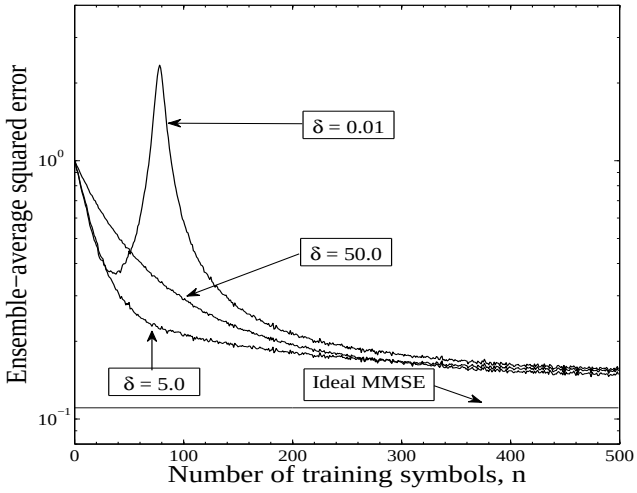

Figure 4.16: Learning curves of the RLS adaptive detector using different regularisation factor δ, for the hybrid DS-TH UWB system supporting $K = 15$ users, when communicating over the S-V Rayleigh fading channels. The other parameters were $E_b/N_0 = 10$dB, Doppler frequency-shift $f_dT_b = 0.0001$, $\lambda = 0.998$, $N_c = 16$, $N_\psi = 4$ and $L = 15$.

regularisation factors δ but keeping the forgetting factor fixed to $\lambda = 0.998$. The ensemble average was obtained by taking the average over $10,000$ independent realizations of the UWB channel. It can be observed from Fig. 4.15 and Fig. 4.16, that when the forgetting factor λ is fixed, the regularisation factor δ plays an important role for the convergence of the RLS adaptive detector. According to [16, 194], the regularisation factor can be given as $\delta = \sigma_{y_i}^2(1-\lambda)^\alpha$, where the value of $\alpha \leq 0$ for low and medium SNR values. It can be observed that for $\delta = 0.01$, which corresponds to a value of $\alpha > 0$, in both the Fig. 4.15 and Fig. 4.16 an overshoot phenomena is observed, where the RLS adaptive detector produces a highly fluctuating estimates during the initialisation period.

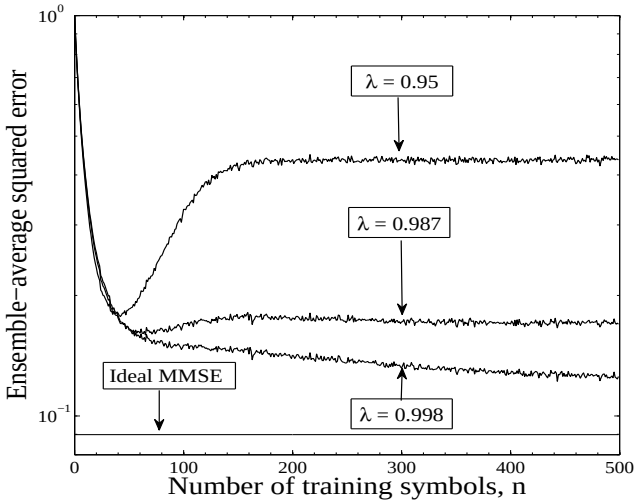

Figure 4.17: Learning curves of the RLS adaptive detector using different forgetting factor λ, for the hybrid DS-TH UWB system supporting single user, when communicating over the S-V Rayleigh fading channels. The other parameters were $E_b/N_0 = 10$dB, Doppler frequency-shift $f_d T_b = 0.0001$, regularisation factor $\delta = 5.0$, $N_c = 16$, $N_\psi = 4$ and $L = 15$.

Figs. 4.17 and 4.18 show the effect of forgetting factor λ on the ensemble mean-square error learning behaviour of the RLS adaptive detector for the hybrid DS-TH UWB system supporting single or $K = 15$ users, when the regularisation factor is fixed to $\delta = 5$. As mentioned in the previous section, in order for the RLS adaptive detector to be stable, the value of λ must satisfy $((1 - 1/(N_c N_\psi + L - 1)) \leq \lambda \leq (1 - 1/10(N_c N_\psi + L - 1)))$. Since for the hybrid DS-TH UWB system considered, we have $(N_c N_\psi + L - 1) = 78$, the optimum value of λ is hence in the range $0.987 \leq \lambda \leq 0.998$. From the results of Figs. 4.17 and 4.18 we can observe that as the value of λ increases in the constrained range, RLS adaptive detector converges to a lower MSE value. However, this improvement requires that the RLS adaptive detector has a higher memory, as the forgetting

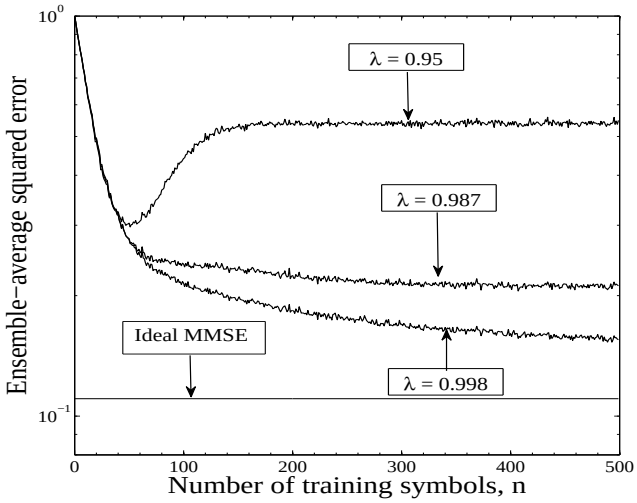

Figure 4.18: Learning curves of the RLS adaptive detector using different forgetting factor λ, for the hybrid DS-TH UWB system supporting $K = 15$ users, when communicating over the S-V Rayleigh fading channels. The other parameters were $E_b/N_0 = 10$dB, Doppler frequency-shift $f_dT_b = 0.0001$, regularisation factor $\delta = 5.0$, $N_c = 16$, $N_\psi = 4$ and $L = 15$.

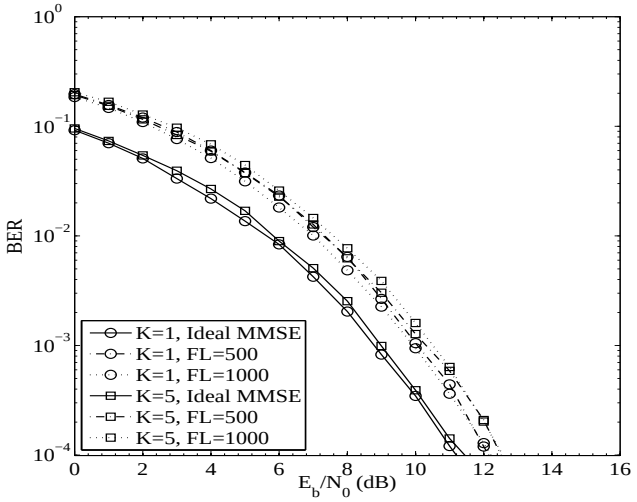

Figure 4.19: BER versus SNR performance of the hybrid DS-TH UWB system supporting single or $K = 5$ users, when communicating over the UWB channels modelled by the S-V Rayleigh fading model. The other parameters used in our simulations were $f_dT_b = 0.0001$, $\lambda = 0.998$, $\delta = 5.0$, $\lambda_{DD} = 0.998$, $N_c = 16$, $N_\psi = 4$ and $L = 15$. The frame length (FL) was set to 500 or 1000, respectively, of which 160 symbols were used for training.

factor λ becomes higher.

Fig. 4.19 shows the BER performance of the hybrid DS-TH UWB system supporting single user

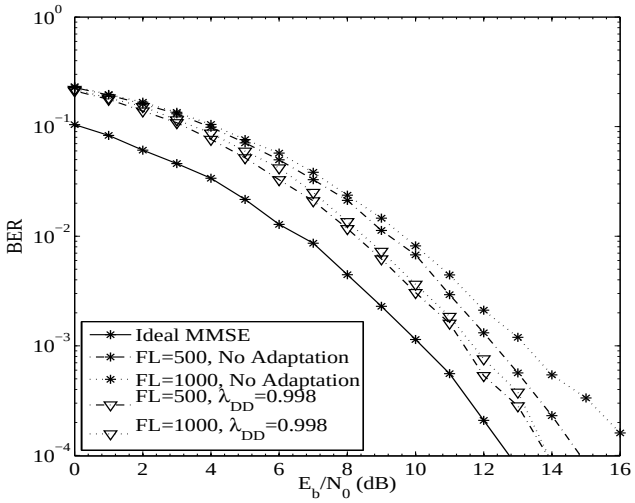

Figure 4.20: BER versus SNR performance of the hybrid DS-TH UWB system supporting $K = 15$ users, when communicating over the UWB channels modelled by the S-V Rayleigh fading model. The other parameters used in our simulations were $f_dT_b = 0.0001$, $\lambda = 0.998$, $\delta = 5.0$, $\lambda_{DD} = 0.998$, $N_c = 16$, $N_\psi = 4$ and $L = 15$. The frame length (FL) was set to 500 or 1000, respectively, of which 160 symbols were used for training.

or $K = 5$ users when communicating over the UWB channels modelled by the S-V Rayleigh fading model. It can be observed from Fig. 4.19 that the RLS adaptive detector is capable of achieving a BER performance that is close to (about 1dB of difference) that of the ideal MMSE detector with perfect channel knowledge when either single or five users are supported. The BER performance corresponding to both $FL = 500$ and $FL = 1000$ is approximately the same, despite the former case using relatively more training symbols, which is $160/500$ than the latter case, which is $160/1000$. Furthermore, the results of Fig. 4.19 show that the RLS adaptive detector is capable of efficiently mitigating both the ISI and MUI, when communicating over UWB channels.

Fig. 4.20 shows the BER performance of the hybrid DS-TH UWB system supporting $K = 15$ users and communicating over S-V channel modelled by Rayleigh fading. In the Fig. 4.20 the term "No Adaptation" means that the filters are not updated after training, therefore, DD approach is not applied. It can be observed that a gain of at least 2dB could be achieved when using the $FL = 500$ as compared to $FL = 1000$ when no adaptation is done. This improved performance is achieved at the expense of lower spectral efficiency as more training sequences are transmitted in the former as compared to the latter. However, it can be observed that if the same forgetting factor is used for the decision directed approach a considerable gain in performance is realised. Furthermore, it can be observed that the difference between the BER performance of $FL = 500$ and $FL = 1000$ becomes

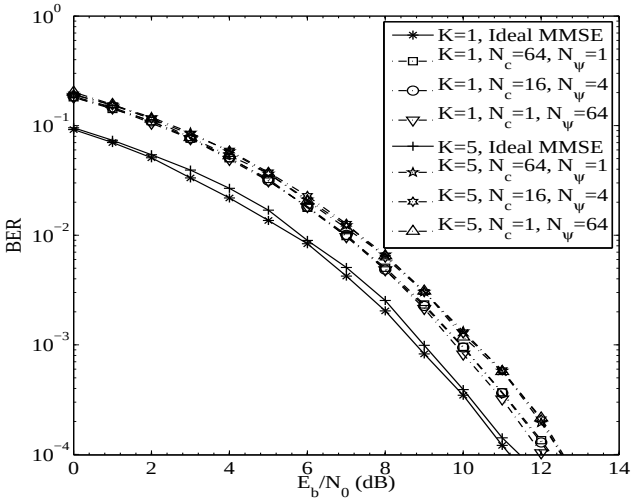

Figure 4.21: BER versus SNR performance of the pure DS-UWB, pure TH-UWB and hybrid DS-TH UWB system supporting single or $K = 5$ users, when communicating over the UWB channels modelled by the S-V Rayleigh fading model. The other parameters used in our simulations were $f_d T_b = 0.0001$, $\lambda = 0.998$, $\delta = 5.0$, $\lambda_{DD} = 0.998$ and $L = 15$. The frame length (FL) was set to 1000 of which 160 symbols were used for training.

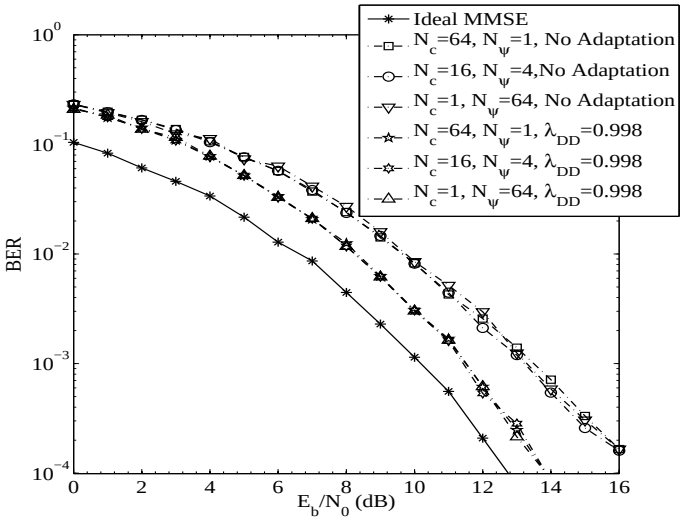

Figure 4.22: BER versus SNR performance of the pure DS-UWB, pure TH-UWB and hybrid DS-TH UWB system supporting $K = 15$ users, when communicating over the UWB channels modelled by the S-V Rayleigh fading model. The other parameters used in our simulations were $f_d T_b = 0.0001$, $\lambda = 0.998$, $\delta = 5.0$, $\lambda_{DD} = 0.998$ and $L = 15$. The frame length (FL) was set to 1000 of which 160 symbols were used for training.

negligible.

Finally, in Fig. 4.21 the BER performance of the hybrid DS-TH UWB system is compared with that of the pure TH-UWB and pure DS-UWB systems, when single or $K = 5$ users are supported. From the results of Fig. 4.21, it can be observed that, for the same set of values of K, N_c and N_ψ, the BER performance of all the UWB systems considered is approximately the same when the RLS adaptive detector is employed. Fig. 4.22 shows the BER performance of the pure DS-UWB, hybrid DS-TH UWB and pure TH-UWB systems, when using or without using the DD approach. As in Fig. 4.20, from the results of Fig. 4.22, it can be observed that a substaintial performance gain can be achieved when the DD approach is applied to improve the RLS adaptive detector after the training. As shown in Fig. 4.22, when the same scenario is considered, the BER performance of all the pulsed-based UWB systems is approximately the same, when the RLS adaptive detector is employed. Hence, we can conclude from Figs. 4.21 and 4.22 that the RLS adaptive detector may be employed for all the pulsed-based UWB systems in order to improve their BER performance. Let us now compare the BER performance of different adaptive detectors in the next section.

4.4.4 Performance Comparison of Different Adaptive Detectors

In this section, the BER performance results of the hybrid DS-TH UWB systems using the LMS, NLMS and RLS adaptive detectors are presented and compared. First, the learning curves of the adaptive detectors are depicted, when single or $K = 15$ users are supported by the hybrid DS-TH UWB system. Then, the BER performance of the hybrid DS-TH UWB systems is presented, when different adaptive detectors are employed associated with using the DD-mode. Note that, all our simulations were carried out in the LoS UWB communications environment.

Figs. 4.23 and 4.24 show the ensemble mean-square error learning curves of the LMS, NLMS and RLS adaptive detectors when the hybrid DS-TH UWB systems support single or $K = 15$ users at a SNR of $E_b/N_0 = 10$ dB. Specifically, the parameters used in our simulations were $\mu_{LMS} = 0.05$, $\mu_{NLMS} = 0.5$, $\lambda_{RLS} = 0.998$ and $\delta_{RLS} = 5.0$. The ensemble average was taken over $10,000$ independent realizations of the UWB channel. As the results of Fig. 4.23 shown for the single-user scenario, all the adaptive detectors considered converge to approximately the same MSE value. However, as the number of users is increased to $K = 15$, as Fig. 4.24 shown, the LMS adaptive detector performs the worst among the three adaptive detectors considered. From Fig. 4.24, it can be observed that the RLS adaptive detector is capable of converging to the lowest MSE value, when compared to the LMS and NLMS adaptive detectors. This is because the RLS adaptive detector has more degrees-of-freedom than the LMS and NLMS adaptive detectors, which make the convergence rate and MSE of the RLS scheme are not determined by only single parameter as in the LMS and

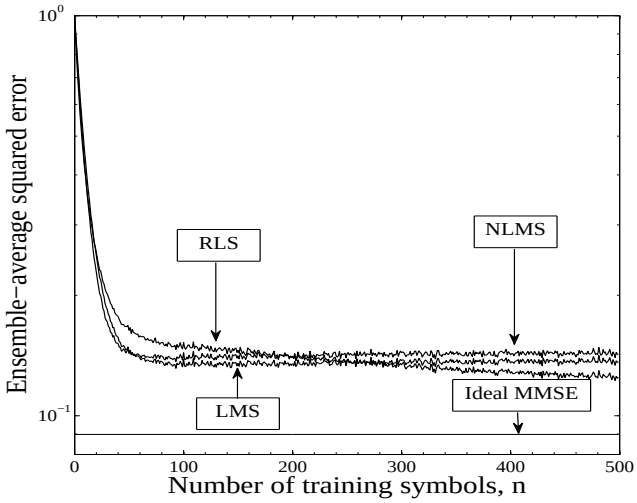

Figure 4.23: Learning curves of the adaptive detectors based on the LMS, NLMS and RLS principles for the hybrid DS-TH UWB systems supporting single user when communicating over the UWB channels modelled by the S-V Rayleigh fading model. The other parameters were $E_b/N_0 = 10$ dB, Doppler frequency-shift $f_dT_b = 0.0001$, $N_c = 16$, $N_\psi = 4$, $L = 15$, $\mu_{LMS} = 0.05$, $\mu_{NLMS} = 0.5$, $\lambda_{RLS} = 0.998$ and $\delta_{RLS} = 5.0$, respectively.

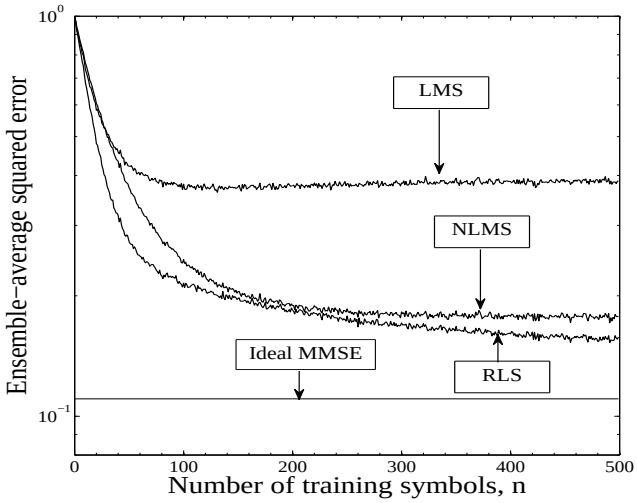

Figure 4.24: Learning curves of the adaptive detectors based on the LMS, NLMS and RLS principles for the hybrid DS-TH UWB systems supporting $K = 15$ users when communicating over the UWB channels modelled by the S-V Rayleigh fading model. The other parameters were $E_b/N_0 = 10$ dB, Doppler frequency-shift $f_dT_b = 0.0001$, $N_c = 16$, $N_\psi = 4$, $L = 15$, $\mu_{LMS} = 0.05$, $\mu_{NLMS} = 0.5$, $\lambda_{RLS} = 0.998$ and $\delta_{RLS} = 5.0$, respectively.

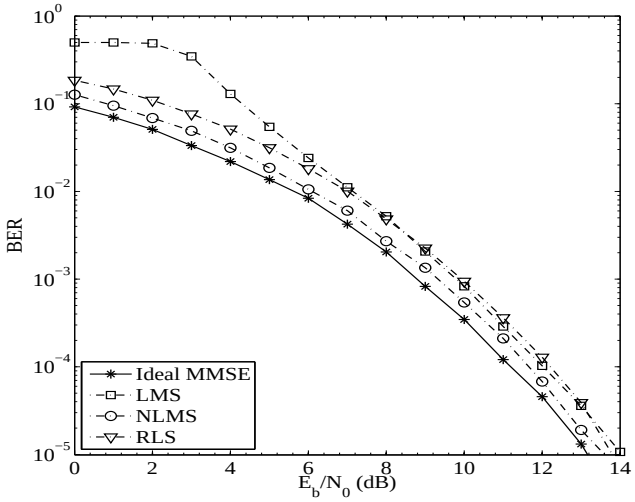

Figure 4.25: BER versus SNR performance of the hybrid DS-TH UWB systems when supporting single user, while communicating over the UWB channels modelled by the S-V Rayleigh fading model. The other parameters used in our simulations were $f_dT_b = 0.0001$, $\mu_{LMS} = 0.05$, $\mu_{DDLMS} = 0.01$, $\mu_{NLMS} = 0.05$, $\mu_{DDNLMS} = 0.05$, $\delta_{RLS} = 5.0$, $\lambda_{RLS} = 0.998$, $\lambda_{DDRLS} = 0.998$, $N_c = 16$, $N_\psi = 4$ and $L = 15$. The frame length (FL) was set to 1000, while the training length (TL) was 160 symbols.

NLMS adaptive detectors.

In Figs. 4.25, 4.26 and 4.27 we compare the BER performance of the hybrid DS-TH UWB systems employing the LMS, NLMS and RLS adaptive detectors, when the DD-mode is applied. The number of users supported was single (Fig. 4.25), $K = 5$(Fig. 4.26) or $K = 15$(Fig. 4.27), respectively. When the single user case is considered, as shown in Fig. 4.25, the NLMS adaptive detector achieves the best BER performance among the three adaptive detectors considered. When $K = 5$ users are supported, as shown in Fig. 4.26, the BER performance of all the three adaptive detectors is approximately the same when the SNR is sufficiently high. By contrast, when $K = 15$ users are supported, as shown in Fig. 4.27, the RLS adaptive detector performs the best among the three detectors.

Let us finally present the summary and conclusions of this chapter.

4.5 Summary and Conclusions

In this chapter we have investigated the adaptive detection in the pulse-based UWB systems, illustrating that the adaptive detection is highly efficient detection for employment in the pulse-based UWB

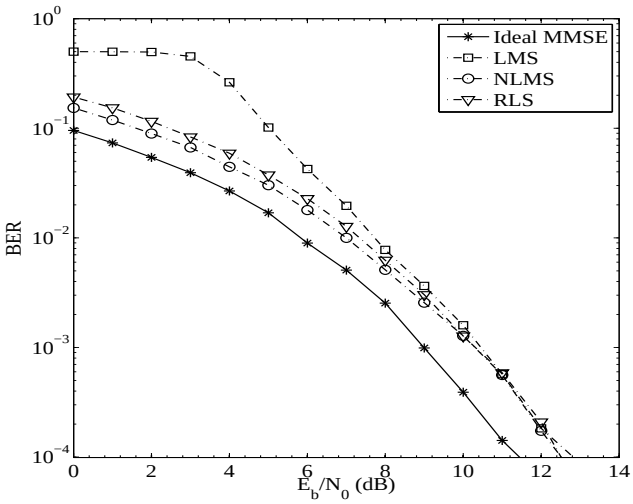

Figure 4.26: BER versus SNR performance of the hybrid DS-TH UWB systems when supporting $K = 5$ users, while communicating over the UWB channels modelled by the S-V Rayleigh fading model. The other parameters used in our simulations were $f_dT_b = 0.0001$, $\mu_{LMS} = 0.05$, $\mu_{DDLMS} = 0.01$, $\mu_{NLMS} = 0.3$, $\mu_{DDNLMS} = 0.1$, $\delta_{RLS} = 5.0$, $\lambda_{RLS} = 0.998$, $\lambda_{DDRLS} = 0.998$, $N_c = 16$, $N_\psi = 4$ and $L = 15$. The frame length (FL) was set to 1000, while the training length (TL) was 160 symbols.

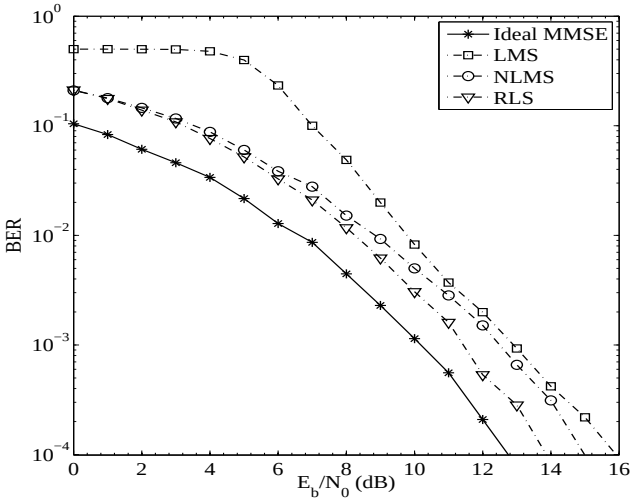

Figure 4.27: BER versus SNR performance of the hybrid DS-TH UWB systems when supporting $K = 15$ users, while communicating over the UWB channels modelled by the S-V Rayleigh fading model. The other parameters used in our simulations were $f_dT_b = 0.0001$, $\mu_{LMS} = 0.05$, $\mu_{DDLMS} = 0.01$, $\mu_{NLMS} = 0.8$, $\mu_{DDNLMS} = 0.1$, $\delta_{RLS} = 5.0$, $\lambda_{RLS} = 0.998$, $\lambda_{DDRLS} = 0.998$, $N_c = 16$, $N_\psi = 4$ and $L = 15$. The frame length (FL) was set to 1000, while the training length (TL) was 160 symbols.

systems. The adaptive detectors are free from channel estimation, can effectively capture the transmitted energy that is spread over many multipaths and are capable of achieving the BER performance that is close to that achieved by the ideal MMSE-MUD, which depends on the ideal CSI. Furthermore, the complexity of the adaptive detectors is analyzed, which shows that the detection complexity of an adaptive detector may be even lower than that of the single-user correlation detector, even without taking into account of the complexity required by the correlation detector for channel estimation. In more detail, our study in this chapter can be summarised as follows.

- The LMS adaptive detector is derived based on the stochastic gradient algorithms. The basic principles of the LMS adaptive detector are finding a sub-optimal weight vector $\boldsymbol{w}_1$ through stochastic gradient techniques in order to achieve the MMSE between the transmitted symbol $b_i^{(1)}$ and the decision variable $z_i^{(1)}$. The procedure of the LMS adaptive detector is summarised in Table 4.2.1. The complexity of the LMS adaptive detector has been calculated in Section 4.3.1, which is found to be $(5(N_c N_\psi + L - 1) + 2)$. Finally, the performance results of the hybrid DS-TH UWB systems using the LMS adaptive detector are presented in Section 4.4.1. Our study and performance results show that the LMS adaptive detector constitutes one of the efficient detection schemes that can be applied to the pure DS-, pure TH- or hybrid DS-TH UWB systems. However, the LMS adaptive detector may not perform well, if the SNR is relatively low.

- As the LMS adaptive detector, the NLMS adaptive detector is also derived based on the stochastic gradient principles. In comparison with the LMS adaptive detector, the NLMS adaptive detector can mitigate the gradient noise amplification problem, when the size of the adaptive filter increases. NLMS adaptive detector can also achieve a higher convergence speed than the LMS adaptive detector. The operation procedure of the NLMS adaptive detector is summarised in Table 4.2.2. The complexity of the NLMS adaptive detector is studied in Section 4.3.2, which has been found to be $(7(N_c N_\psi + L - 1) + 2)$. Finally, the learning and BER performance results of the NLMS adaptive detector has been investigated in Section 4.4.2. Our study and performance results show that the NLMS adaptive detector can also be applied to the pure DS-, pure TH- or hybrid DS-TH UWB systems. Generally, the BER performance of the NLMS adaptive detector is found to be better than that of the LMS adaptive detector.

- The RLS adaptive detector is derived based on the principles of least squares, where the weight vector $\boldsymbol{w}_1$ is chosen to minimize the cost function consisting of the sum of error squares. The operation procedure of the RLS adaptive detector is summarised in Table 4.2.3. Since the RLS

adaptive detector has more degrees-of-freedom that can be used for controlling the convergence speed than the LMS and NLMS adaptive detectors, the RLS adaptive detector has the highest convergence rate among the three detectors considered. The complexity of the RLS adaptive detector is considered in Section 4.3.3, which is $(11(N_cN_\psi + L - 1)^2 + 8(N_cN_\psi + L - 1) + 3)$. The learning and BER performance of the RLS adaptive detector has been studied in Section 4.4.3. Our study and simulation results shown that the RLS adaptive detector can be deployed in the pure DS-, pure TH- and hybrid DS-TH UWB systems. The RLS adaptive detector outperforms the LMS and NLMS adaptive detectors in terms of their achievable BER performance.

Finally, Table 4.5 illustrated the complexity required by the different detectors for the hybrid DS-TH UWB systems. From Table 4.5, we can observe that the complexity of both the LMS and NLMS adaptive detectors is significantly lower than the single-user correlation detector, even without considering the complexity required by the correlation detector for channel estimation. The complexity of the RLS adaptive detector is slightly higher than that of the correlation detector, however, it is significantly lower that that of the ideal MMSE detector, which also requires channel estimation. Therefore, we conclude that the adaptive detectors considered in this chapter may be beneficial to UWB communications. They are free from channel estimation, relatively low complexity and efficient for achieving a reasonable BER performance.

Detection Scheme	Spreading factor, $N_c N_\psi$	Number of resolvable multipaths, L	Selected rank, U	No. of operations for detecting one bit
Correlation detector	64	15	78	2496
		100	163	32926
	128	15	142	4544
		100	227	45854
Ideal MMSE detector	64	15	78	176670
		100	163	1523780
	128	15	142	1015350
		100	227	4054300
LMS adaptive detector	64	15	78	391
		100	163	816
	128	15	1423	711
		100	227	1136
NLMS adaptive detector	64	15	78	548
		100	163	1143
	128	15	142	996
		100	227	1591
RLS adaptive detector	64	15	78	67551
		100	163	293566
	128	15	142	222943
		100	227	568638

Table 4.5: Complexity comparison of different detectors for the hybrid DS-TH UWB system.

Chapter 5

Adaptive Reduced-Rank Detection for Hybrid DS-TH UWB System

5.1 Introduction

One of the major challenges in pulse-based UWB communications is to design the low-complexity receivers, which are capable of achieving a reasonable BER performance [1, 29, 32, 34]. However, as the MDP in UWB communications environment is generally sparse [29], there are usually a large number of resolvable multipaths that are required to be acquired by the receiver in order to achieve good BER performance. Hence, as shown in Chapter 3 even when the conventional single-user correlation detector is employed, the complexity might still be very high, since a huge number of multipath channels are required to be estimated and the detection complexity also increases linearly with the number of resolvable multipaths [90]. Furthermore, the BER performance of the single-user correlation detector deteriorates as the number of users increases as shown in Chapter 3 [148]. In order to improve the BER performance, MUDs, such as MMSE MUD, may be employed by the pulse-based UWB systems at the expense of higher complexity. The MMSE-MUD is capable of automatically combining all the multipaths presenting within the time-duration of an observation window [172], which retains a constant complexity for the MMSE-MUD. Furthermore, the MMSE-MUD is convenient to be implemented using low-complexity adaptive techniques [16, 196], yielding the adaptive detectors such as the adaptive LMS, NLMS and RLS detectors as studied in Chapter 4.

As shown in Chapter 4 adaptive detectors are free from channel estimation and are capable of achieving the approximate MMSE solutions with the aid of training sequences of certain length [197].

The efficiency of an adaptive detector can be characterised by its convergence speed, BER performance, robustness and implementation complexity [16]. According to the adaptive filter theory [16] and also our study in Chapter 4, the above-mentioned characteristics are dependent on the length of the traversal filter involved. In general, a longer traversal filter results in lower convergence speed, which in turn means that a longer sequence is required to train the filter. Consequently, the data-rate and spectral-efficiency of the corresponding communications system decreases. The robustness of an adaptive filter also degrades as the filter length increases, since it requires to estimate more channel-dependent variables [16, 157, 198, 199]. Furthermore, as shown in Chapter 4 when a longer adaptive filter is employed, the computational complexity is also higher, since more operations are required for the corresponding detection and estimation. Due to the reasons as above-mentioned, therefore, in this chapter reduced-rank techniques are proposed for the adaptive detection of the hybrid DS-TH UWB signals, in order to achieve low-complexity detection in hybrid DS-TH UWB systems.

To be more specific, in this chapter three types of reduced-rank techniques are investigated in the contexts of the RLS adaptive detection in the hybrid DS-TH UWB systems. The reduced-rank schemes are derived based on the principles of principal component analysis (PCA), of cross-spectral metric (CSM) and of Taylor polynomial approximation (TPA), respectively [151, 172, 196, 200, 200–204, 204–209]. The BER performance of the hybrid DS-TH UWB systems using the reduced-rank RLS adaptive detection is investigated, when communicating over UWB channels modelled by the S-V channel model [117]. Furthermore, the implementation complexity of the full-rank ideal MMSE-MUD studied in Chapter 3, the full-rank RLS adaptive detector of Chapter 4 and the various reduced-rank RLS adaptive detectors is analyzed and compared.

In comparison with the full-rank adaptive detectors studied in Chapter 4, the reduced-rank adaptive detectors have the following advantages when they are applied in the hybrid DS-TH UWB systems.

1) **Convergence Speed**: In UWB communications the adaptive detectors are usually required to converge fast, so that the overhead incurred for training is short. In the hybrid DS-TH UWB systems using a DS-spreading factor N_c and a TH-spreading factor N_ψ and communicating over an UWB channel having L resolvable paths when the full-rank adaptive detector is considered, the length of the traversal filter is $(N_c N_\psi + L - 1)$. Owing to possibly a high spreading factor of $N_c N_\psi$ and/or a huge number of resolvable multipaths L of the UWB channels, the length of the traversal filter may be extreme. Consequently, the convergence speed of the adaptive detectors might be very low, since the convergence speed of an adaptive is inversely proportional

to its length [16, 32, 157, 178, 198, 199, 210, 211]. By contrast, when the reduced-rank adaptive detector is employed the traversal filter may be significantly shorter than $(N_c N_\psi + L - 1)$ of the traversal filter's length for the full-rank adaptive detector [83, 157, 210, 212–216]. Therefore, the convergence speed of the reduced-rank adaptive detector may be significantly faster than that of the corresponding full-rank adaptive detector. Consequently, the reduced-rank adaptive detector may use relatively short training sequences, which in turn results in higher data-rate or spectral-efficiency than the corresponding full-rank adaptive detector.

2) **Achievable BER Performance**: Our study and simulation results in this chapter show that, for given system parameters, the hybrid DS-TH UWB systems using reduced-rank adaptive detectors are capable of achieving a similar BER performance as that of using full-rank adaptive detector, provided that the rank, say U, of the subspace used for detection, which is hence referred to as detection subspace, is sufficiently high. In Section 5.4 performance results and more detailed analysis will be provided in the context of the various reduced-rank techniques.

3) **Robustness:** According to the adaptive filter theory [16], the robustness of an adaptive algorithm usually becomes worse, when the length of its corresponding traversal filter increases. Our reduced-rank adaptive detectors for the hybrid DS-TH UWB system only require to find U estimates for the U-length traversal filter, instead of finding $(N_c N_\psi + L - 1)$ estimates in the full-rank adaptive detector. Furthermore, due to the characteristics of UWB channels, there are many resolvable multipaths conveying only very low power. The low-power resolvable multipaths are hard to be acquired by the full-rank adaptive detectors and are sensitive to the background noise. By contrast, the reduced-rank techniques considered in this chapter are capable of identifying automatically the relatively strong multipath signals and projecting them onto the reduced-rank detection subspace. Hence, the adaptive filter operated in this reduced-rank detection subspace becomes less sensitive to the background noise. Owing to the above considerations, therefore, we may argue that the reduced-rank adaptive detectors are more robust than the full-rank adaptive detectors, when they are applied for the hybrid DS-TH UWB systems.

4) **Computational Complexity**: In comparison with a full-rank adaptive detector, which is operated in a space of rank $(N_c N_\psi + L - 1)$, the corresponding reduced-rank adaptive detector is operated in the detection subspace having a rank of U, which can be significantly lower than $(N_c N_\psi + L - 1)$, as shown in our forthcoming discourse. Hence, as to be detailed in Section 5.3, the complexity of the reduced-rank adaptive detector can be much lower than that of

the corresponding full-rank adaptive detector.

Note that, in this chapter we investigate specifically the reduced-rank RLS adaptive detector, since it generally has a higher convergence speed than the LMS and NLMS adaptive detectors. However, our approaches are general, which can be readily extended to the hybrid DS-TH UWB systems using the LMS or NLMS adaptive detection. The remainder of this chapter is organised as follows. In the next section, the general procedure for reduced-rank detection is described. Furthermore, in this section the rank reduction techniques based on the PCA, CSM and TPA are investigated in conjunction with the hybrid DS-TH UWB systems using the RLS-adaptive detection. Section 5.3 addresses the computational complexity of the reduced-rank detection schemes associated with PCA, CSM and TPA, respectively. Simulation results regarding these schemes are provided in Section 5.4 and finally in Section 5.5 the summary and conclusions of the chapter are presented. Let us now discuss the reduced-rank schemes in the upcoming section.

5.2 Reduced-Rank RLS Adaptive Detection

5.2.1 General Theory

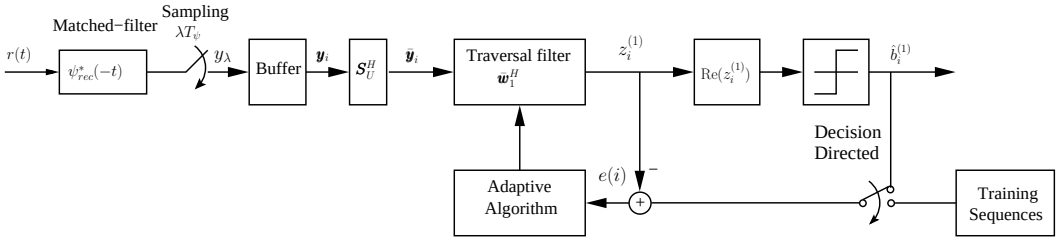

Figure 5.1: Schematic block diagram of reduced-rank adaptive detector for the hybrid DS-TH UWB systems.

With the subspace reduced-rank detection the number of coefficients to be determined is reduced by projecting the received signal in a higher dimensional observation space to a lower dimensional subspace [196]. The reduced-rank RLS adaptive detector considered in this chapter is operated in two modes as the full-rank adaptive detectors studied in Chapter 4. The detector starts with the training mode to find a detection subspace and train the adaptive filter, followed by the DD-mode in order to enhance the detection performance. Fig. 5.1 shows the block diagram of the reduced-rank adaptive detector for the hybrid DS-TH UWB system. As shown in the previous chapters the received signal $r(t)$ is first passed through the matched-filter, which is sampled at the rate of $1/\lambda T_\psi$

to produce the observations, as shown in Fig. 5.1. In order to detect the ith bit of the desired user, which is the first user in our case, $(N_c N_\psi + L - 1)$ observation samples can be collected and stored in the buffer, which is expressed as $\boldsymbol{y}_i$ as shown in Fig. 5.1. Then, the observation vector $\boldsymbol{y}_i$ is projected to a U-dimensional subspace by multiplying $\boldsymbol{y}_i$ with a reduced-rank matrix $\boldsymbol{S}_U$, which is a $((N_c N_\psi + L - 1) \times U)$ dimensional matrix and $U < (N_c N_\psi + L - 1)$. Specifically, for a bit-by-bit detector, the U-dimensional vector in the reduced-rank subspace can be expressed as

$$\bar{\boldsymbol{y}}_i = \boldsymbol{S}_U^H \boldsymbol{y}_i \tag{5.1}$$

where a bar over $\boldsymbol{y}_i$ is used to indicate that it is related to the reduced-rank subspace. Furthermore, $\boldsymbol{S}_U$ can be represented as

$$\boldsymbol{S}_U = \boldsymbol{P}_U (\boldsymbol{P}_U^H \boldsymbol{P}_U)^{-1} \tag{5.2}$$

where $\boldsymbol{P}_U$ can be viewed as a processing matrix of dimension $(U \times (N_c N_\psi + L - 1))$ with its row vectors forming an U-dimensional subspace, while $(\boldsymbol{P}_U^H \boldsymbol{P}_U)^{-1}$ is the normalisation factor. After projecting the received signal $\boldsymbol{y}_i$ to a lower dimensional detection subspace determined by $\boldsymbol{P}_U(\boldsymbol{S}_U)$, as shown in Fig. 5.1, the decision variable for detecting the ith bit $b_i^{(1)}$ of the first user can now be formed as

$$\boldsymbol{z}_i^{(1)} = \bar{\boldsymbol{w}}_1^H \bar{\boldsymbol{y}}_i \tag{5.3}$$

where the weight vector $\bar{\boldsymbol{w}}_1$ is an U-length vector, which can be determined with the aid of the RLS adaptive detection principles as shown in the previous chapter.

When comparing (3.22) and (5.3), we can find that the dimension of the observation vector is now reduced from $(N_c N_\psi + L - 1)$ of $\boldsymbol{y}_i$ to U of $\bar{\boldsymbol{y}}_i$, and the auto-correlation matrix of $\bar{\boldsymbol{y}}_i$ is hence only $(U \times U)$-dimensional. Therefore, the complexity of the reduced-rank detector may be significantly lower than that of the full-rank adaptive detectors, if the rank U can be significantly lower than $(N_c N_\psi + L - 1)$. Hence, in the reduced-rank detection it is important to determine a processing matrix $\boldsymbol{P}_U$ with its rank of U as low as possible, while the BER performance achieved by the hybrid DS-TH UWB system using reduced-rank detection can be close to that achieved by the full-rank adaptive detectors studied in Chapter 4. In this chapter three types of reduced-rank techniques are considered, which are now described as follows.

5.2.2 Eigenspace: Principal Components Analysis

The principal component analysis (PCA) is a well-studied rank reduction scheme [201, 203]. This reduced-rank scheme was based on the principal component analysis of the auto-correlation matrix $\boldsymbol{R}_{y_i}$, which was originally developed by Hotelling and Eckart [200]. Since the auto-correlation matrix $\boldsymbol{R}_{y_i}$ is Hermitian, eigen-analysis can be employed to represent the auto-correlation matrix $\boldsymbol{R}_{y_i}$ in terms of its eigen-values and associated eigen-vectors. In the PCA-assisted reduced-rank detection the eigenvectors corresponding to the relatively high eigenvalues are retained to form the processing matrix $\boldsymbol{P}_U$.

During the training mode, the auto-correlation matrix $\boldsymbol{R}_{y_i}$ can be estimated according to

$$\boldsymbol{R}_{y_i} \approx \frac{1}{M}\sum_{i=1}^{M} \boldsymbol{y}_i \boldsymbol{y}_i^H \tag{5.4}$$

where M represents the number of bits invoked in the estimation. Upon carrying the eigen-decomposition on $\boldsymbol{R}_{y_i}$, we obtain

$$\boldsymbol{R}_{y_i} = \boldsymbol{\Phi}\boldsymbol{\Lambda}\boldsymbol{\Phi}^H \tag{5.5}$$

where $\boldsymbol{\Phi}$ is an unitary matrix consisting of the eigenvectors of $\boldsymbol{R}_{y_i}$, which can be expressed as

$$\boldsymbol{\Phi} = \left[\boldsymbol{\phi}_1, \boldsymbol{\phi}_2, \cdots, \boldsymbol{\phi}_{N_c N_\psi + L - 1}\right] \tag{5.6}$$

while $\boldsymbol{\Lambda}$ is a diagonal matrix consisting of the eigenvalues of $\boldsymbol{R}_{y_i}$, i.e.,

$$\boldsymbol{\Lambda} = \text{diag}\{\lambda_1, \lambda_2, \cdots, \lambda_{N_c N_\psi + L - 1}\} \tag{5.7}$$

The eigenvector $\boldsymbol{\phi}_i$ in (5.6) corresponds to the eigenvalue λ_i in (5.7). If S represents the dimension of the signal subspace and the eigen-values are arranged in such a way that $\lambda_1 \geq \lambda_2 \geq \cdots \geq \lambda_{N_c N_\psi + L - 1}$. Correspondingly, the eigen-vectors are expressed as $\boldsymbol{\phi}_1, \boldsymbol{\phi}_2, \cdots, \boldsymbol{\phi}_{N_c N_\psi + L - 1}$. Then, there are S number of eigenvalues of $\lambda_1, \lambda_2, \cdots, \lambda_S$ corresponding to the signal subspace, while the other $V = (N_c N_\psi + L - 1 - S)$ eigenvalues of $\lambda_{S+1}, \lambda_{S+2}, \cdots, \lambda_{N_c N_\psi + L - 1}$ corresponds to the noise subspace. Therefore, the auto-correlation matrix $\boldsymbol{R}_{y_i}$ can be expressed as

$$\boldsymbol{R}_{y_i} = \left[\boldsymbol{\Phi}_S | \boldsymbol{\Phi}_V\right] \left[\begin{array}{c|c} \boldsymbol{\Lambda}_S & \boldsymbol{0} \\ \hline \boldsymbol{0} & \boldsymbol{\Lambda}_V \end{array}\right] \left[\begin{array}{c} \boldsymbol{\Phi}_S^H \\ \hline \boldsymbol{\Phi}_V^H \end{array}\right] \tag{5.8}$$

where $\mathbf{\Lambda}_S$ contains the eigenvalues associated with the signal subspace determined by $\mathbf{\Phi}_S$ and $\mathbf{\Lambda}_V$ contains the eigenvalues of noise subspace which is determined by $\mathbf{\Phi}_V$. Furthermore, we have $\mathbf{\Phi}_S = [\boldsymbol{\phi}_1, \boldsymbol{\phi}_2, \cdots, \boldsymbol{\phi}_S]$ and $\mathbf{\Phi}_V = [\boldsymbol{\phi}_{S+1}, \boldsymbol{\phi}_{S+2}, \cdots, \boldsymbol{\phi}_{N_c N_\psi + L - 1}]$.

Based on the above analysis, in the context of the PCA-assisted reduced-rank adaptive detection, the processing matrix $\boldsymbol{P}_U$ is constructed by the first U columns of $\mathbf{\Phi}$, i.e., we have

$$\boldsymbol{P}_U = [\boldsymbol{\phi}_1, \boldsymbol{\phi}_2, \cdots, \boldsymbol{\phi}_U] \tag{5.9}$$

In the context of the PCA-assisted reduced-rank detection, it has been shown that, if the rank U of the detection subspace $\boldsymbol{P}_U$ is higher than the rank S of the signal subspace $\mathbf{\Phi}_S$, then the PCA-assisted reduced-rank MMSE detection is capable of attaining the same error performance as the full-rank MMSE detection [172]. Otherwise, the error performance of the PCA-assisted reduced-rank detection will deteriorate if the rank U is less than the rank S of the signal subspace. Therefore, the PCA-based reduced-rank method is very effective only if the dimension S is known and significantly lower than $(N_c N_\psi + L - 1)$. Otherwise, if the rank S of the signal subspace is high and a rank $U < S$ is used, then the PCA-based reduced-rank detection may experience severe MUI. Let us now consider another eigen-decomposition assisted reduced-rank scheme, which is known as the cross-spectral metric (CSM).

5.2.3 Eigenspace: Cross-Spectral Metric

The CSM-assisted reduced-rank method was proposed by Goldstein and Reed in 1997 [202]. Similar to the PCA-assisted reduced-rank scheme, the CSM-assisted reduced-rank technique derives the detection subspace $\boldsymbol{P}_U$ also through eigen-decomposition of the auto-correlation matrix $\boldsymbol{R}_{y_i}$ of (5.4) [202]. This rank reduction scheme has been proposed, e.g., in [204], because the detection subspace formed in the PCA-based scheme by the eigenvectors corresponding to the U largest eigenvalues does not necessarily represent the best set of U eigenvectors resulting in the lowest MSE. Therefore, in the context of the CSM-assisted reduced-rank detection, the processing matrix $\boldsymbol{P}_U$ is formed by a set of U eigenvectors, which are chosen from $\mathbf{\Phi}$ and result in a minimum MSE [172, 200, 202, 217, 218].

Specifically, for our CSM-assisted reduced-rank adaptive detection, the processing matrix $\boldsymbol{P}_U$ can be formed as follows. First, it can be shown that (5.5) of the auto-correlation matrix can be

represented as

$$\boldsymbol{R}_{y_i} = \boldsymbol{\Phi}\boldsymbol{\Lambda}\boldsymbol{\Phi}^H = \sum_{i=1}^{N_c N_\psi + L - 1} \lambda_i \boldsymbol{\phi}_i \boldsymbol{\phi}_i^H \tag{5.10}$$

The inverse of $\boldsymbol{R}_{y_i}$ can hence be expressed as

$$\boldsymbol{R}_{y_i}^{-1} = \sum_{i=1}^{N_c N_\psi + L - 1} \frac{\boldsymbol{\phi}_i \boldsymbol{\phi}_i^H}{\lambda_i} \tag{5.11}$$

According to [172], the minimum MSE of the hybrid DS-TH UWB system after the MMSE-MUD is given by

$$\text{MMSE} = 1 - \frac{1}{2}(\boldsymbol{C}_i^{(1)}\boldsymbol{h}_1)^H \boldsymbol{R}_{y_i}^{-1}(\boldsymbol{C}_i^{(1)}\boldsymbol{h}_1) \tag{5.12}$$

Upon substituting (5.11) into (5.12), we obtain

$$\text{MMSE} = 1 - \frac{1}{2}\left(\sum_{i=1}^{N_c N_\psi + L - 1} \frac{||\boldsymbol{h}_1^H (\boldsymbol{C}_i^{(1)})^T \boldsymbol{\phi}_i||^2}{\lambda_i}\right) \tag{5.13}$$

Let the CSMs be defined as [200]

$$\text{CSM}(i) = ||\boldsymbol{h}_1^H (\boldsymbol{C}_i^{(1)})^T \boldsymbol{\phi}_i||^2 / \lambda_i, \quad i = 1, 2, \cdots, N_c N_\psi + L - 1 \tag{5.14}$$

Then, as shown in (5.13), in order to achieve the minimum MSE after the reduced-rank MMSE detection in the U-rank detection subspace, the U number of largest CSMs in the bracket of (5.13) should be maintained in the detection subspace. Hence, in the context of the CSM-assisted reduced-rank detection, the processing matrix $\boldsymbol{P}_U$ can be formed by the eigen-vectors in $\boldsymbol{\Phi}$, which yield the U number of largest CSMs in the form of (5.14).

(5.13) shows that the CSM-assisted reduced-rank technique requires the knowledge about the spreading sequence and also the CSI associated with the desired user. By contrast, the PCA-assisted reduced-rank technique does not require this knowledge. Note that, in our simulations in Section 5.4.2, the knowledge required for finding the detection subspace in the CSM-assisted reduced-rank adaptive detection during the training mode is obtained from (5.4) with the aid of the training sequences. Specifically, during the training mode, $\boldsymbol{C}_i^{(1)}\boldsymbol{h}_1$ seen in (5.14) is estimated according to

$$\hat{E}\{\boldsymbol{C}_i^{(1)}\boldsymbol{h}_1\} = \frac{1}{M}\sum_{j=1}^{M} \boldsymbol{y}_j b_j^{*(1)} \tag{5.15}$$

where M denotes the length of the training sequence and a 'hat' above E implies estimation. By contrast, during the data transmission, if the decision-directed approach is applied, the detected data-bit may be fed back to enhance the estimation. In this case, the estimate to $\boldsymbol{C}_i^{(1)}\boldsymbol{h}_1$ can be denoted as

$$\hat{E}\{\boldsymbol{C}_i^{(1)}\boldsymbol{h}_1\} = \frac{1}{M+D}\sum_{j=1}^{M+D} E\{\boldsymbol{y}_j b_j^{(1)}\} \tag{5.16}$$

where D represents the number of detected data bits involved in the estimation. From (5.14) and (5.16) it is implied that, if a detected data bit is fed-back, the CSM in (5.14) needs to be computed again, which increases the complexity of detection. Let us now, describe the TPA-assisted reduced-rank technique, which does not require eigen-decomposition.

5.2.4 Taylor Polynomial Approximation

The major problem with the reduced-rank techniques based on the eigen-decomposition is the computational complexity. It has been found that the complexity for determining the eigenvectors and eigenvalues of a Hermitian matrix is similar as that for finding the inverse of the same matrix [205]. Furthermore, in a heavily loaded system, where the rank S approaches $(N_c N_\psi + L - 1)$, the size of the adaptive filter may not be reduced when using the PCA- or CSM-based techniques. In these scenarios, the reduced-rank detection based on the PCA or CSM may not provide any particular advantages over the conventional full-rank detection, when the detection alone is considered. Alternatively, the TPA-assisted rank-reduction technique may be employed for finding the detection subspace $\boldsymbol{P}_U$. The TPA-assisted reduced-rank technique has some advantages over both the PCA- and CSM-assisted reduced-rank techniques [172, 200]. First, it does not depend on the eigen-decomposition of the auto-correlation matrix $\boldsymbol{R}_{y_i}$. Second, the detection subspace's rank in the TPA-assisted reduced-rank scheme does not scale with the system size, including the number of users supported, the total spreading factor $N_c N_\psi$ as well as the number of resolvable multipaths. Hence, this reduced-rank technique may be very promising for detection in the hybrid DS-TH UWB communications, since it is usually associated with a big spreading factor $N_c N_\psi$ and the UWB channels usually have a high number of resolvable paths. Furthermore, the BER performance of the TPA-assisted reduced-rank detector is capable of converging to that of the full-rank detector with a detection subspace of very low rank, as shown in [153, 172, 200, 219–225] and also in Section 5.4.3 of this chapter.

Let $\lambda_{\max}$ be the maximum eigenvalue of $\boldsymbol{R}_{y_i}$. Let ρ be a constant satisfying $0 < \rho < 1/\lambda_{\max}$.

Then, the Taylor expansion of the auto-correlation matrix $\boldsymbol{R}_{y_i}^{-1}$ can be expressed as

$$\begin{aligned}\boldsymbol{R}_{y_i}^{-1} = \rho(\rho\boldsymbol{R}_{y_i})^{-1} &= \rho[\boldsymbol{I} - (\boldsymbol{I} - \rho\boldsymbol{R}_{y_i})]^{-1} \\ &= \rho\sum_{j=0}^{\infty}(\boldsymbol{I} - \rho\boldsymbol{R}_{y_i})^j \end{aligned} \tag{5.17}$$

The first U terms in (5.17) can be adopted to approximated $\boldsymbol{R}_{y_i}^{-1}$, i.e.,

$$\begin{aligned}\boldsymbol{R}_{y_i}^{-1} &\approx \rho\sum_{j=0}^{U-1}(\boldsymbol{I} - \rho\boldsymbol{R}_{y_i})^j \\ &= a_0\boldsymbol{I} + a_1\boldsymbol{R}_{y_i} + \cdots + a_{U-1}\boldsymbol{R}_{y_i}^{U-1} \end{aligned} \tag{5.18}$$

However, determining the coefficients $\{a_i\}$ in (5.18) is complicated. Furthermore, the finite order approximation that results from tail-cutting of infinite order approximation generally does not lead to the best fit among all approximations of the same order [201]. Specifically, in the context of the TPA-assisted reduced-rank adaptive detector, a processing matrix $\boldsymbol{P}_U$ can be constructed as [172]

$$\boldsymbol{P}_U = [\boldsymbol{C}_i^{(1)}\boldsymbol{h}_1, \boldsymbol{R}_{y_i}\boldsymbol{C}_i^{(1)}\boldsymbol{h}_1, \cdots, \boldsymbol{R}_{y_i}^{U-1}\boldsymbol{C}_i^{(1)}\boldsymbol{h}_1] \tag{5.19}$$

where $\boldsymbol{R}_{y_i}$ and $\boldsymbol{C}_i^{(1)}\boldsymbol{h}_1$ are estimated based on (5.4) and (5.15) with the aid of training sequences. Let us now proceed to consider the computational complexity of the reduced-rank adaptive detectors associated with these rank-reduction schemes.

5.3 Complexity of Reduced-Rank Adaptive Detectors

In this section, the computational complexity of the PCA-, CSM- and TPA-assisted reduced-rank adaptive detectors is investigated in the context of the hybrid DS-TH UWB system. The complexity of the detectors is measured by the number of multiplications and additions required to detect one bit of a user. We assume that the RLS-aided adaptive detection is employed, whose computational complexity has been studied in the previous chapter, which is equivalent to $11\mathcal{T}^2 + 8\mathcal{T} + 3$, where $\mathcal{T} = N_c N_\psi + L - 1$. Let us first consider the computational complexity of the PCA-assisted reduced-rank RLS adaptive detector.

5.3.1 Complexity of PCA-Assisted Reduced-Rank RLS Adaptive Detector

In the context of the PCA-assisted reduced-rank scheme, the processing matrix is $\boldsymbol{P}_U = [\boldsymbol{\phi}_1, \boldsymbol{\phi}_2, \cdots, \boldsymbol{\phi}_U]$, which consists of the U eigenvectors corresponding to the U largest eigenvalues as shown in Section 5.2.2. Note that it takes about $\mathcal{T}$ multiplications to calculate the eigenvalue from an autocorrelation matrix [226]. Furthermore, when the eigenvectors are calculated, it takes $\mathcal{T}^3$ number of additions and $\mathcal{T}^3$ number of multiplications to determine the required eigenvectors [226].

However, with the aid of efficient computing approaches, this complexity could be reduced to $\mathcal{T}^3/6$ number of additions and multiplications [227]. Furthermore, as shown in [227], if the bubble sort algorithm is replaced by the comb sort algorithm for determining the maximum eigenvalue of a matrix, the complexity can be reduced to $\log_2(\mathcal{T})$ from $\mathcal{T}$.

Operations	Number of additions	Number of multiplications
$\boldsymbol{R}_{y_i}$	$2\mathcal{T}F_L$	$\mathcal{T}^2F_L$
$\boldsymbol{R}_{y_i} = \boldsymbol{\Phi}\boldsymbol{\Lambda}\boldsymbol{\Phi}^H$	$\mathcal{T}^3/6$	$\mathcal{T}^3/6$
$\max\{\lambda_i\}, i = 1, \cdots, U$	$U\log_2\mathcal{T}$	-
$\bar{\boldsymbol{y}}_i = \boldsymbol{S}_U^H\boldsymbol{y}$	$U(\mathcal{T}-1)F_L$	$U\mathcal{T}F_L$
RLS adaptive detector	$(5U^2+3U+2)F_L$	$(6U^2+5U+1)F_L$

Table 5.1: Summary of the number of operations required by the PCA-assisted reduced-rank RLS adaptive detector.

Table 5.1 summarises the number of operations required by the PCA-assisted reduced-rank RLS adaptive detector. In the Table 5.1, F_L denotes the length of the frame. From Table 5.1 it can be observed that the number of additions required is $(F_L(U\mathcal{T}+5U^2+2\mathcal{T}+2U+2)+\mathcal{T}^3/6+U\log_2\mathcal{T})$, while number of multiplications required is $(F_L(\mathcal{T}^2+U\mathcal{T}+6U^2+5U+1)+\mathcal{T}^3/6)$, respectively. Therefore, the total number of operations required for the detection of a frame is

$$N_F = F_L(\mathcal{T}^2+2U\mathcal{T}+2\mathcal{T}+11U^2+7U+3)+\mathcal{T}^3/3+U\log_2\mathcal{T} \tag{5.20}$$

Finally, the total number of operations required to detect one bit is given by

$$N_b = \mathcal{T}^2+2U\mathcal{T}+2\mathcal{T}+11U^2+7U+3+\frac{\mathcal{T}^3/3+U\log_2\mathcal{T}}{F_L} \tag{5.21}$$

5.3.2 Complexity of CSM-Assisted Reduced-Rank RLS Adaptive Detector

In the CSM-assisted reduced-rank RLS adaptive detection, the processing matrix $\boldsymbol{P}_U = [\boldsymbol{\phi}_1, \boldsymbol{\phi}_2, \cdots, \boldsymbol{\phi}_U]$, where the eigenvectors correspond to the U largest CSM values defined as $\text{CSM}(i) = ||\boldsymbol{h}_1^H(\boldsymbol{C}_i^{(1)})^T\phi_i||^2/\lambda_i, \quad i = 1, 2, \cdots, U$, as shown in Section 5.2.3. Table 5.2 shows the number of additions and multiplications required by the component processing in the CSM-assisted reduced-rank RLS adaptive detector for the hybrid DS-TH UWB system.

Operations	Number of additions	Number of multiplications
$\boldsymbol{R}_{y_i}$	$2\mathcal{T}F_L$	$\mathcal{T}^2F_L$
$\boldsymbol{R}_{y_i} = \boldsymbol{\Phi}\boldsymbol{\Lambda}\boldsymbol{\Phi}^H$	$\mathcal{T}^3/6$	$\mathcal{T}^3/6$
$\boldsymbol{R}_{y_i}^{-1}$	-	$\mathcal{T}$
$\boldsymbol{h}_i^H(\boldsymbol{C}_i^{(1)})^T$	T_L	$\mathcal{T}T_L$
$\boldsymbol{h}_i^H(\boldsymbol{C}_i^{(1)})^T\boldsymbol{\phi}_i$	$\mathcal{T}^2 - \mathcal{T}$	$\mathcal{T}^2$
$\frac{\|\|\boldsymbol{h}_i^H(\boldsymbol{C}_i^{(1)})^T\boldsymbol{\phi}_i\|\|^2}{\lambda_i}$	$\mathcal{T}$	$\mathcal{T}$
$\max\left\{\frac{\boldsymbol{h}_i^H(\boldsymbol{C}_i^{(1)})^T\boldsymbol{\phi}_i}{\lambda_i}\right\}, i = 1, \cdots, U$	$U\log_2\mathcal{T}$	-
$\bar{\boldsymbol{y}}_i = \boldsymbol{S}_U^H\boldsymbol{y}$	$U(\mathcal{T}-1)F_L$	$U\mathcal{T}F_L$
RLS adaptive detector	$(5U^2+3U+2)F_L$	$(6U^2+5U+1)F_L$

Table 5.2: Summary of the number of operations required by the CSM-assisted reduced-rank RLS adaptive detector.

In Table 5.2, F_L and T_L represents respectively the frame length and the length of training sequence. From Table 5.2, it can be known that the total number of additions is $((2\mathcal{T} + U\mathcal{T} + 5U^2 + 2U + 2)F_L) + T_L + \mathcal{T}^3/6 + \mathcal{T}^2 + U\log_2\mathcal{T})$ additions while the total number of multiplications is $(F_L(\mathcal{T}^2 + U\mathcal{T} + 6U^2 + 5U + 1) + \mathcal{T}T_L + \mathcal{T}^3/6 + \mathcal{T}^2 + 2\mathcal{T})$ respectively. Hence, the total number of operations required for detection of a frame is

$$\begin{aligned} N_F &= F_L(\mathcal{T}^2 + 2\mathcal{T} + 2U\mathcal{T} + 11U^2 + 7U + 3) \\ &+ T_L(\mathcal{T}+1) + \mathcal{T}^3/3 + 2\mathcal{T}^2 + 2\mathcal{T} + U\log_2\mathcal{T} \end{aligned} \tag{5.22}$$

Furthermore, the number of operations required to detect a bit can be expressed as

$$\begin{aligned} N_b &= \mathcal{T}^2 + 2\mathcal{T} + 2U\mathcal{T} + 11U^2 + 7U + 3 \\ &+ \frac{(\mathcal{T}+1)T_L + \mathcal{T}^3/3 + 2\mathcal{T}^2 + 2\mathcal{T} + U\log_2\mathcal{T}}{F_L} \end{aligned} \tag{5.23}$$

Note that, as shown in Table 5.2, the quantities, such as CSI and the desired user's signature, required by the CSM-assisted reduced-rank RLS adaptive detector are obtained through the training process. Let us now discuss the complexity of the TPA-assisted reduced-rank RLS adaptive detection.

5.3.3 Complexity of TPA-Assisted Reduced-Rank RLS Adaptive Detector

In the context of the TPA-assisted reduced-rank RLS adaptive detection, the processing matrix is formed as $\boldsymbol{P}_U = [\boldsymbol{C}_i^{(1)}\boldsymbol{h}_1, \boldsymbol{R}_{y_i}\boldsymbol{C}_i^{(1)}\boldsymbol{h}_1, \cdots, \boldsymbol{R}_{y_i}^{U-1}\boldsymbol{C}_i^{(1)}\boldsymbol{h}_1]$. Once $\boldsymbol{R}_{y_i}$, which is $(\mathcal{T}\times\mathcal{T})$, and $\boldsymbol{C}_i^{(1)}\boldsymbol{h}_1$, which is $(\mathcal{T}\times 1)$, are given, it can be readily known that computing $\boldsymbol{R}_{y_i}\boldsymbol{C}_i^{(1)}\boldsymbol{h}_1$ requires $\mathcal{T}^2$ additions and $\mathcal{T}^2$ multiplications. Furthermore, given $\boldsymbol{R}_{y_i}^{i}\boldsymbol{C}_i^{(1)}\boldsymbol{h}_1$, computing $\boldsymbol{R}_{y_i}^{i+1}\boldsymbol{C}_i^{(1)}\boldsymbol{h}_1 = \boldsymbol{R}_{y_i}\boldsymbol{R}_{y_i}^{i}\boldsymbol{C}_i^{(1)}\boldsymbol{h}_1$ also requires $\mathcal{T}^2$ additions and $\mathcal{T}^2$ multiplications. Hence, we can known that the number of operations for forming $\boldsymbol{P}_U$ is $(U-1)\mathcal{T}^2$ additions and $(U-1)\mathcal{T}^2$ multiplications. The number of operations required by the components of the TPA-assisted reduced-rank RLS adaptive detector is summarized in Table 5.3. As shown in Table 5.3, only the training mode is employed to derive the required information for the TPA-assisted reduced-rank RLS adaptive detector.

Operations	Number of additions	Number of multiplications
$\boldsymbol{R}_{y_i}$	$2\mathcal{T}F_L$	$\mathcal{T}^2F_L$
$\boldsymbol{C}_i^{(1)}\boldsymbol{h}_i$	T_L	$\mathcal{T}T_L$
Forming $\boldsymbol{P}_U$	$(U-1)\mathcal{T}^2$	$(U-1)\mathcal{T}^2$
$\bar{\boldsymbol{y}}_i = \boldsymbol{S}_U^H\boldsymbol{y}$	$U(\mathcal{T}-1)F_L$	$U\mathcal{T}F_L$
RLS adaptive detector	$(5U^2+3U+2)F_L$	$(6U^2+5U+1)F_L$

Table 5.3: Summary of the number of operations required by the TPA-assisted reduced-rank RLS adaptive detector.

From Table 5.3, we can know that the total number of operations required for detection of a frame

is

$$N_F = \begin{cases} (2\mathcal{T}+21)F_L + (\mathcal{T}+1)T_L, & U=1 \\ (\mathcal{T}^2+2\mathcal{T}+2U\mathcal{T}+11U^2+7U+3)F_L & \\ +(\mathcal{T}+1)T_L + 2(U-1)\mathcal{T}^2, & U=2,3\cdots,8 \end{cases} \tag{5.24}$$

Furthermore, the total number of operations required to detect a bit can be expressed as

$$N_b = \begin{cases} 2\mathcal{T}+21+\frac{(\mathcal{T}+1)T_L}{F_L}, & U=1 \\ \mathcal{T}^2+2\mathcal{T}+2U\mathcal{T}+11U^2+7U+3+\frac{(\mathcal{T}+1)T_L+2(U-1)\mathcal{T}^2}{F_L}, & U=2,3\cdots,8 \end{cases} \tag{5.25}$$

From (5.24) and (5.25), we are implied that, if $\mathcal{T} >> U$, the complexity of the TPA-assisted reduced-rank RLS adaptive detector is $O(\mathcal{T}^2)$.

5.4 Performance Results and Discussion

This section provides a range of simulation results for characterising the learning and BER performance of the hybrid DS-TH UWB systems using various reduced-rank RLS adaptive detectors. In our simulations we adopt the following assumptions.

1) Coherent binary phase-shift keying (BPSK) baseband modulation;

2) The total spreading factor is constant of $N_c N_\psi = 64$. Hence, for the pure DS-UWB systems the DS spreading factor is $N_c = 64$, while for the pure TH-UWB systems the TH spreading factor is $N_\psi = 64$. For the hybrid DS-TH UWB systems, the DS spreading factor is fixed to $N_c = 16$ and the TH spreading factor is fixed to $N_\psi = 4$;

3) Two types of UWB channels are considered. In the context of the first type UWB channels, the number of resolvable multipaths is $L = 15$. Correspondingly, the factor $g = 1$. By contrast, the second type of UWB channels is highly frequency-selective, the number of resolvable multipaths is $L = 150$, implying that the factor $g = 3$. For both cases, the normalised Doppler frequency shift is given by $f_d T_b = 0.0001$. Furthermore, in our simulations the UWB channels are modelled by the S-V channel model with the channel gains obeying the Rayleigh distribution. The parameters of the S-V channel model used in our simulations are summarised in Table 5.4, where 'LoS' means that the UWB channel considered contains a line-of-sight (LoS) propagation path [117];

	$1/\Lambda$	Γ	γ
LoS	14.11ns	2.63ns	4.58ns

Table 5.4: Parameters characterzing the S-V channel model used in simulations.

4) Each frame is constituted by $F_L = 1000$ bits (symbols), where $T_L = 160$ bits (symbols) are the training bits (symbols). Hence, the spectral-efficiency of the hybrid DS-TH UWB systems is $(1000 - 160)/1000 = 84\%$.

Note that, for the hybrid DS-TH UWB scheme and UWB channels considered, the rank of the observation space is $N_c N_\psi + L - 1 = 78$ for the case $L = 15$ and $N_c N_\psi + L - 1 = 213$ for the case $L = 150$, respectively.

Furthermore, during our discussion the rank of signal subspace is often used in comparison with the rank U of the detection subspace invoked in the reduced-rank adaptive detection. Note that, for a hybrid DS-TH UWB system supporting K users and communicating over the UWB channels associated with a factor of g, the rank of the signal subspace is about $K(g + 1)$, where the factor of $(g + 1)$ is due to that of a desired bit conflicts interference from $(g + 1)$ bits of an interfering user.

Let us first show and discuss the performance results of hybrid DS-TH UWB systems using the PCA-assisted reduced-rank adaptive detection.

5.4.1 Performance of PCA-Assisted Reduced-Rank RLS Adaptive Detector

In this section the performance results of the hybrid DS-TH UWB systems using the PCA-assisted reduced-rank RLS adaptive detector is presented. First, the learning performance of the PCA-assisted reduced-rank RLS adaptive detector is discussed in the context of the hybrid DS-TH UWB systems supporting single or multiple users, when the detection subspace having different rank of U is considered. Then, the BER versus SNR per bit performance of the hybrid DS-TH UWB systems supporting single or multiple users is illustrated, when the PCA-assisted reduced-rank RLS adaptive detector employs different ranks of U for the detection subspace.

Fig. 5.2 shows the ensemble-average squared error learning curve of the PCA-assisted reduced-rank adaptive detector with the detection subspace using a rank $U = 1,\ 10$ or 78, when the hybrid DS-TH UWB system supports single user. In our simulations the ensemble average was taken over 2000 independent realizations of the UWB channel characterized by Table 5.4. From the results of Fig. 5.2 it can be observed that the convergence speed of the PCA-assisted reduced-rank adaptive detector depends on the rank U of the detection subspace, i.e., the length of the adaptive filter. When

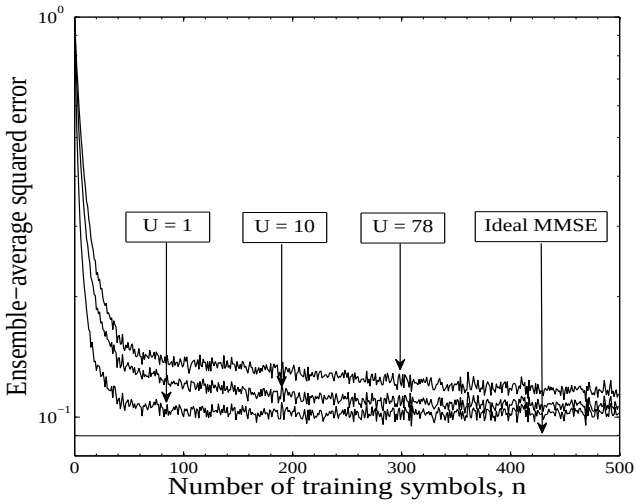

Figure 5.2: Learning curves of the PCA-based reduced-rank RLS adaptive detector for the hybrid DS-TH UWB system supporting single user, when communicating over correlated Rayleigh fading channels modelled by the S-V channel model associated with a normalised Doppler frequency-shift $f_dT_b = 0.0001$. The other parameters were $E_b/N_0 = 10$dB, $\lambda_{RLS} = 0.9987$, $\delta = 5.0$, $g = 1$, $N_c = 16$, $N_\psi = 4$ and $L = 15$, respectively.

$U = 1$, the adaptive detector attains the highest convergence speed and also reaches the lowest MSE. The reason for this observation is that the asynchronous hybrid DS-TH UWB system supports only single user, which results in that the rank of the signal subspace is about $K(g + 1) = 3$. In this case, when the length of the adaptive filter is significantly longer than two, the adaptive filter collects not only the useful signal, but also the noise, which reduces the convergence speed and generates increased MSE. Furthermore, when comparing Fig. 5.2 with Fig. 4.15 in Section 4.4.3 of Chapter 4, we can find that the PCA-assisted reduced-rank adaptive detector is capable of converging faster than the full-rank RLS adaptive detector, which has a filter length of 78, when the hybrid DS-TH UWB system supports single user.

Figs. 5.3 and 5.4 show the ensemble-average squared error learning curve of the PCA-assisted reduced-rank RLS adaptive detector associated with the detection subspaces with different ranks of U, when the hybrid DS-TH UWB system supports $K = 5$ (Fig. 5.3) or $K = 15$ (Fig. 5.4) users. In our simulations the ensemble average was taken over 2000 independent realizations of the UWB channel characterized by Table 5.4. From the results of Figs. 5.3 and 5.4 we can observe that, similar as Fig. 5.2, the convergence speed of the PCA-assisted reduced-rank RLS adaptive detector is depended on the rank U of the detection subspace. When the rank U of the detection subspace is lower than the rank of the signal subspace, which is about 10 for $K = 5$ and 30 for $K = 15$, the adaptive

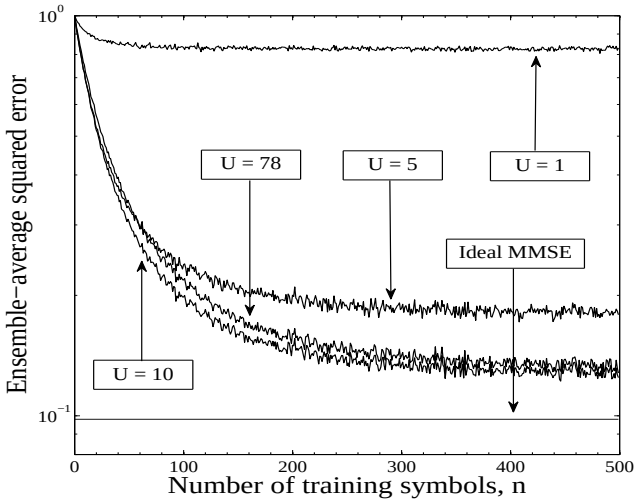

Figure 5.3: Learning curves of the PCA-based reduced-rank RLS adaptive detector for the hybrid DS-TH UWB system supporting $K = 5$ users, when communicating over correlated Rayleigh fading channels modelled by the S-V channel model associated with a normalised Doppler frequency-shift $f_d T_b = 0.0001$. The other parameters were $E_b/N_0 = 10$dB, $\lambda_{RLS} = 0.9987$, $\delta = 5.0$, $g = 1$, $N_c = 16$, $N_\psi = 4$ and $L = 15$, respectively.

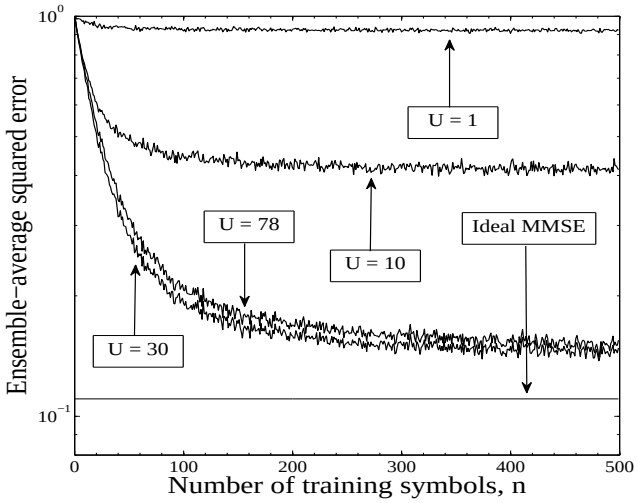

Figure 5.4: Learning curves of the PCA-based reduced-rank RLS adaptive detector for the hybrid DS-TH UWB system supporting $K = 15$ users, when communicating over correlated Rayleigh fading channels modelled by the S-V channel model associated with a normalised Doppler frequency-shift $f_d T_b = 0.0001$. The other parameters were $E_b/N_0 = 10$dB, $\lambda_{RLS} = 0.9987$, $\delta = 5.0$, $g = 1$, $N_c = 16$, $N_\psi = 4$ and $L = 15$, respectively.

detector converges to a relatively lower MSE value, as the rank U of the detection subspace increases. However, after the rank U of the detection subspace reaches the signal subspace's rank, further increasing the rank U of the detection subspace results in an increased MSE, as shown in Figs. 5.3 and 5.4. Therefore, in the hybrid DS-TH UWB systems using the PCA-assisted reduced-rank RLS adaptive detection, it is important to have the *a-priori* knowledge about the signal subspace's rank.

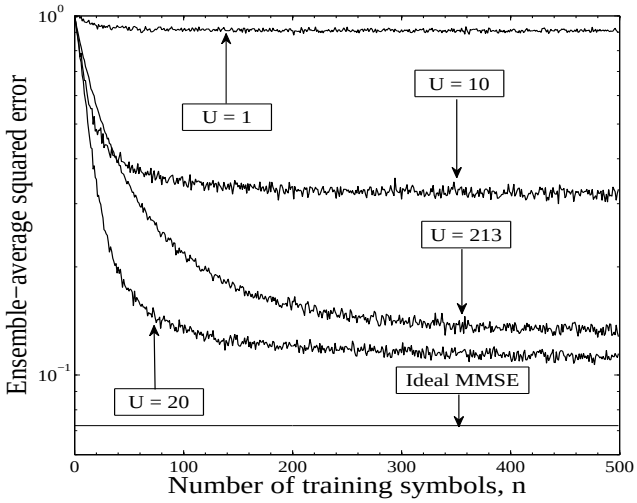

Figure 5.5: Learning curves of the PCA-based reduced-rank RLS adaptive detector for the hybrid DS-TH UWB system supporting $K = 5$ users, when communicating over correlated Rayleigh fading channels modelled by the S-V channel model associated with a normalized Doppler frequency-shift $f_d T_b = 0.0001$. The other parameters were $E_b/N_0 = 10$dB, $\lambda_{RLS} = 0.9995$, $\delta = 0.005$, $g = 3$, $N_c = 16$, $N_\psi = 4$ and $L = 150$, respectively.

In the above three figures, we assumed that the delay-spread of the UWB channels is lower than the bit duration resulting in $g = 1$. By contrast, Fig. 5.5 shows the ensemble-average squared-error learning curve of the PCA-based reduced-rank RLS adaptive detector, when the UWB channels experience severe ISI resulting in $g = 3$. Again, in our simulations the ensemble-average squared-error was calculated from 2000 independent realizations of the UWB channel, when the hybrid DS-TH UWB system supported $K = 5$ users at a given SNR value of $E_b/N_0 = 10$ dB. Again, from the results of Fig. 5.5, we observe that the convergence speed and converged MSE of the PCA-based reduced-rank RLS adaptive detector are depended on rank U of the detection subspace. When the rank U is lower than the rank of the signal subspace, which is about $K(g+1) = 20$, the ensemble-average squared-error converges to a relatively lower MSE value, when the rank U of detection subspace increases. Furthermore, as shown in Fig. 5.5, when the rank U equals the signal subspace's, i.e., when $U = 20$, the PCA-based reduced-rank RLS adaptive detector converges faster than the full-rank

RLS adaptive detector corresponding to the curve identified by $U = 213$. Additionally, the results in Fig. 5.5 show that the PCA-based reduced-rank RLS adaptive detector using $U = 20$ is capable of achieving an MSE that is lower than that achieved by the full-rank RLS adaptive detector studied in Chapter 4. The achieved MSE by the PCA-based reduced-rank RLS adaptive detector using $U = 20$ is close to the minimum MSE achieved by the ideal MMSE detector, if a sufficient number of training symbols is provided.

In summary, from the results of Figs. 5.2 - 5.5, we can conclude that the convergence speed and converged MSE of the PCA-assisted reduced-rank RLS adaptive detector are depended on the rank U of the detection subspace. The best convergence and MSE performance can be achieved, when the detection subspace has a rank U equalling to the signal subspace's rank. Since in hybrid DS-TH UWB systems the signal subspace's rank is in general significantly lower than the rank of the observation space, which is about $(N_c N_\psi + L - 1)$, the length of the adaptive filter used by the PCA-assisted reduced-rank RLS adaptive detector may hence be significantly shorter than that of the full-rank RLS adaptive detector. Furthermore, due to the relatively higher convergence speed in comparison with the full-rank RLS adaptive detector, the PCA-assisted reduced-rank RLS adaptive detector may require less number of training symbols and hence provide higher transmission data rate or higher spectral-efficiency for the hybrid DS-TH UWB systems, than the full-rank RLS adaptive detector studied in Chapter 4.

Fig. 5.6 shows the BER versus SNR per bit performance for the hybrid DS-TH UWB system using the PCA-assisted reduced-rank RLS adaptive detector to support single user, when communicating over the UWB channels modelled by the correlated Rayleigh fading. The other parameters used in our simulations are specified in the caption of the figure. From the results of Fig. 5.6 one can observe that the BER performance of the hybrid DS-TH UWB system is very close to that achieved by the ideal MMSE detection, when the rank of the detection subspace is $U = 1, 2$ or 78. Since the rank of the signal subspace in this case is two, as seen in Fig. 5.6, the BER performance becomes slightly better, as the detection subspace's rank increases from $U = 1$ to $U = 2$, when the SNR of E_b/N_0 is high. In Fig. 5.6 the BER curve corresponding to $U = 78$ represents the BER achieved by the full-rank RLS adaptive detector considered in the last chapter. Explicitly, the BER performance achieved by the PCA-assisted reduced-rank RLS adaptive detector associated with $U = 2$ is the same as that achieved by the full-rank RLS adaptive detector.

In Figs. 5.7 and 5.8 the BER versus SNR per bit performance of the hybrid DS-TH UWB systems using the PCA-assisted reduced-rank RLS adaptive detection is depicted. In our simulations we assumed that the hybrid DS-TH UWB systems supported $K = 5$ users for Fig. 5.7, while supported

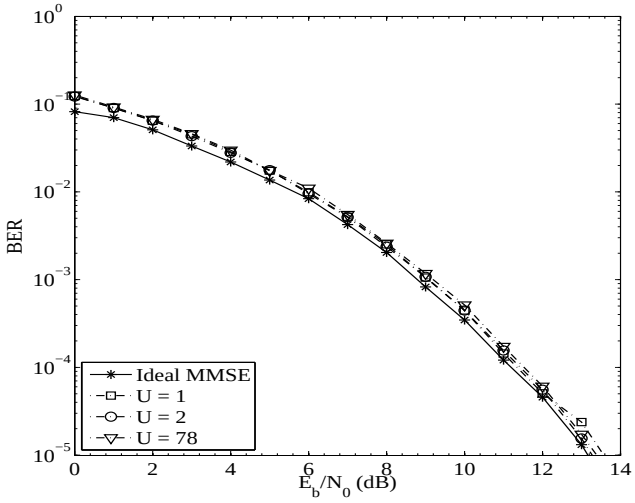

Figure 5.6: BER versus SNR per bit performance of the hybrid DS-TH UWB system using PCA-based reduced-rank RLS adaptive detection, when communicating over correlated Rayleigh fading channels modelled by the S-V channel model. The other parameters employed for the simulations were $K = 1$, $f_dT_b = 0.0001$, $\lambda_{RLS} = 0.9987$, $\delta = 0.05$, $g = 1$, $N_c = 16$, $N_\psi = 4$ and $L = 15$, respectively.

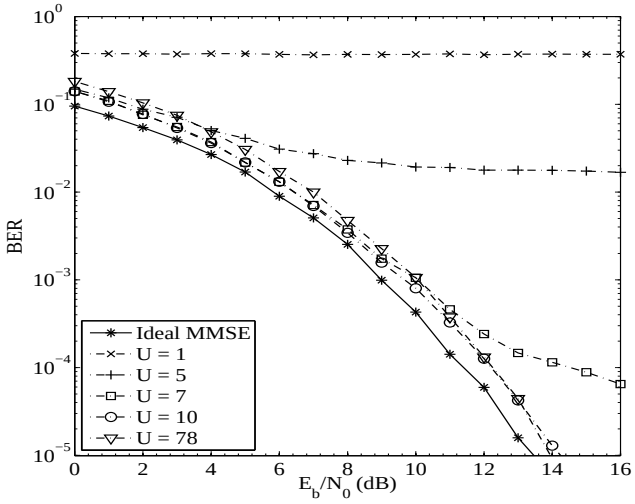

Figure 5.7: BER versus SNR per bit performance of the hybrid DS-TH UWB system using PCA-based reduced-rank RLS adaptive detection, when communicating over correlated Rayleigh fading channels modelled by the S-V channel model. The other parameters employed for the simulations were $K = 5$, $f_dT_b = 0.0001$, $\lambda_{RLS} = 0.9987$, $\delta = 0.05$, $N_c = 16$, $N_\psi = 4$ and $L = 15$, respectively.

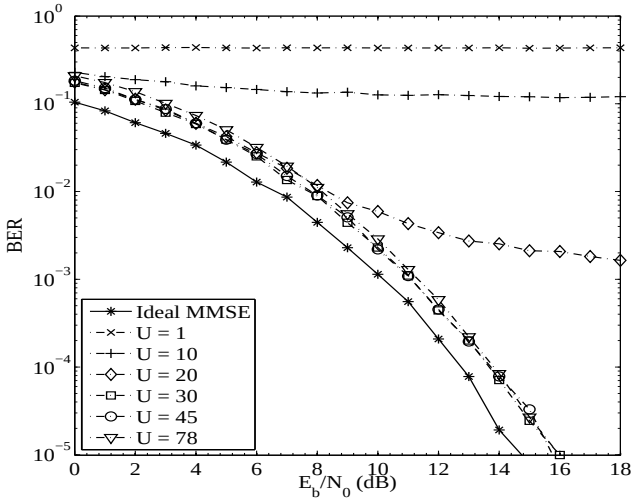

Figure 5.8: BER versus SNR per bit performance of the hybrid DS-TH UWB system using PCA-based reduced-rank RLS adaptive detection, when communicating over correlated Rayleigh fading channels modelled by the S-V channel model. The other parameters employed for the simulations were $K = 15$, $f_d T_b = 0.0001$, $\lambda_{RLS} = 0.9987$, $\delta = 0.05$, $N_c = 16$, $N_\psi = 4$ and $L = 15$, respectively.

$K = 15$ users for Fig. 5.8. The other parameters used for generating both figures were the same, as seen associated with the figures. From the results of Figs. 5.7 and 5.8, one can observe that the BER performance improves as the rank U of the detection subspace increases. When the rank U of the detection subspace reaches the signal subspace's rank, which is about 10 for Fig. 5.7 corresponding to $K = 5$ and about 30 for Fig. 5.8 corresponding to $K = 15$, the BER performance achieved by the PCA-assisted reduced-rank RLS adaptive detector reaches to that achieved by the full-rank RLS adaptive detector. However, when the detection subspace's rank U is lower than the rank of the signal subspace, error floors are likely to occur. As seen in Figs. 5.7 and 5.8, a lower rank U corresponds to a higher BER floor. Furthermore, as shown in Fig. 5.8, when the rank U of the detection subspace, e.g., $U = 45,\ 78$, is higher than the signal subspace's rank of 30, no performance gain is attainable except for incurring higher detection complexity. Therefore, in order to avoid this problem, in the PCA-assisted reduced-rank detection, it is important to have the *a-priori* knowledge of the actual rank of the signal subspace.

Fig. 5.9 shows the BER versus SNR per bit (E_b/N_0) performance of the hybrid DS-TH UWB system employing the PCA-based reduced-rank RLS adaptive detector to support $K = 5$ users, when communicating over UWB channels having $L = 150$ resolvable multipaths. Correspondingly, we have $g = 3$, implying that the rank of the signal subspace is about 20. From the results of Fig. 5.9,

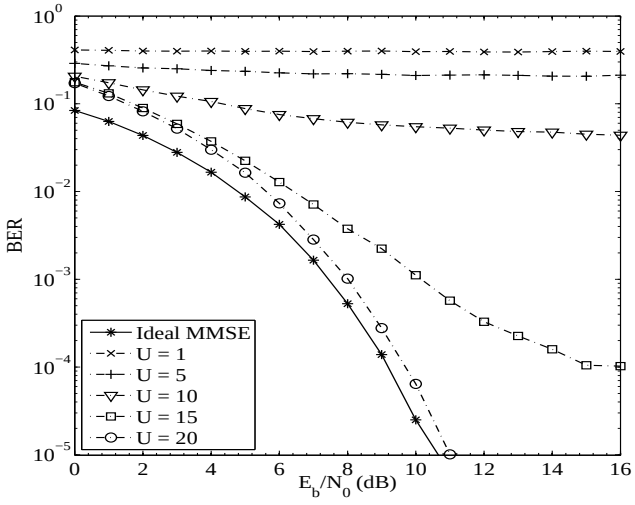

Figure 5.9: BER versus SNR per bit performance of the hybrid DS-TH UWB system using PCA-based reduced-rank RLS adaptive detection, when communicating over correlated Rayleigh fading channels modelled by the S-V channel model. The other parameters employed for the simulations were $K = 5$, $f_d T_b = 0.0001$, $\lambda_{RLS} = 0.9995$, $\delta = 0.005$, $g = 3$, $N_c = 16$, $N_\psi = 4$ and $L = 150$, respectively.

again, we can observe that the BER performance improves when the rank U of the detection subspace increases. However, when the rank U of the detection subspace reaches the rank $U = 20$ of the signal subspace, further increasing the rank U of the detection subspace does not result in further performance improvement. When the rank U of the detection subspace is lower than the rank of the signal subspace, error-floor is observed, implying that the multiuser interference cannot be efficiently suppressed by the PCA-assisted reduced-rank RLS adaptive detector. Furthermore, from the results of Fig. 5.9, we can observe that the PCA-based reduced-rank RLS adaptive detector results in certain performance loss in comparison with the ideal MMSE multiuser detector, even when the detection subspace has the same rank of $U = 20$ as the signal subspace. Specifically, the performance loss at the BER of 10^{-4} is about 0.7 dB.

When comparing the results in Fig. 5.7 with that in Fig. 5.9, both of which used the same parameters except $L = 15$ for Fig. 5.7 and $L = 150$ for Fig. 5.9, we can find that the BER performance shown in Fig. 5.9 is better than that shown in Fig. 5.7, when the PCA-assisted reduced-rank RLS adaptive detector is operated in the detection subspace having a rank U equalling to the rank of the corresponding signal subspace, which is 10 for Fig. 5.7 and 20 for Fig. 5.9. The reason for Fig. 5.9 to attain a better BER performance than Fig. 5.7 is that the UWB channels considered in the context of Fig. 5.9 has more resolvable multipaths than that considered in Fig. 5.7, hence, resulting in higher

diversity gain.

In summary, in the hybrid DS-TH UWB systems, if the signal subspace's rank is significantly lower than the rank of the observation space, which is $(N_c N_\psi + L - 1)$, then, the detection complexity may be significantly reduced without performance penalty by employing the PCA-assisted reduced-rank RLS adaptive detector, instead of using the full-rank RLS adaptive detector, as studied in the last chapter. However, as the number of users supported increases, resulting in that the rank of the signal subspace is close to the rank of the observation space, then, the benefit from using the PCA-assisted reduced-rank RLS adaptive detector is limited. Considering that in the PCA-assisted detection complexity is required for finding the detection subspace $\boldsymbol{P}_U$, therefore, in a heavily loaded hybrid DS-TH UWB system, the PCA-assisted reduced-rank detection might not be a promising option.

5.4.2 Performance of CSM-Assisted Reduced-Rank RLS Adaptive Detector

In this section we illustrate a range of performance results in order to show the characteristics and achievable BER performance of the hybrid DS-TH UWB systems using the CSM-assisted reduced-rank RLS adaptive detection. As in Section 5.4.1, the learning performance of the CSM-assisted reduced-rank RLS adaptive detector is first illustrated for the hybrid DS-TH UWB systems supporting single or multiple users, when the detection subspace employs different ranks of U. Then, the BER versus SNR per bit performance of the hybrid DS-TH UWB systems using the CSM-assisted reduced-rank RLS adaptive detection is investigated, when different communications and detection scenarios are considered.

Fig. 5.10 shows the ensemble-average squared error learning performance of the CSM-assisted reduced-rank RLS adaptive detector for the hybrid DS-TH UWB system supporting single user at an SNR per bit $E_b/N_0 = 10$dB. The average squared error was taken over 2000 independent realizations of the UWB channel. The other parameters used in our simulations were specified associated with the figure. Similar to the learning behaviour of the PCA-assisted reduced-rank RLS adaptive detector as shown in Fig. 5.2, it can be observed from Fig. 5.10 that the convergence speed of the CSM-assisted reduced-rank RLS adaptive detector is depended on the rank U of the detection subspace. Furthermore, it can be observed that the CSM-assisted reduced-rank adaptive detector is capable of converging faster than the full-rank adaptive detector corresponding to the learning curve of $U = 78$ in Fig. 5.10.

Figs. 5.11 and 5.12 show the learning performance of the CSM-assisted reduced-rank RLS adaptive detector, when the hybrid DS-TH UWB system supports $K = 5$ (Fig. 5.11) and $K = 15$

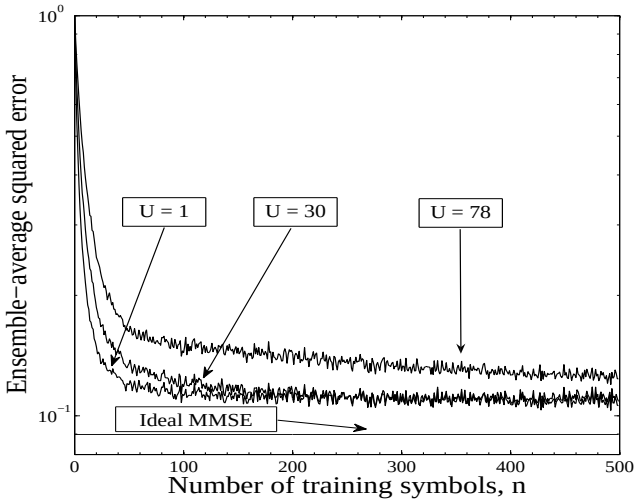

Figure 5.10: Learning curves of the CSM-based reduced-rank RLS adaptive detector for the hybrid DS-TH UWB system supporting single user, when communicating over correlated Rayleigh fading channels modelled by the S-V channel model associated with a normalized Doppler frequency-shift $f_dT_b = 0.0001$. The other parameters were $E_b/N_0 = 10$dB, $\lambda_{RLS} = 0.9987$, $\delta = 5.0$, $g = 1$, $N_c = 16$, $N_\psi = 4$ and $L = 15$, respectively.

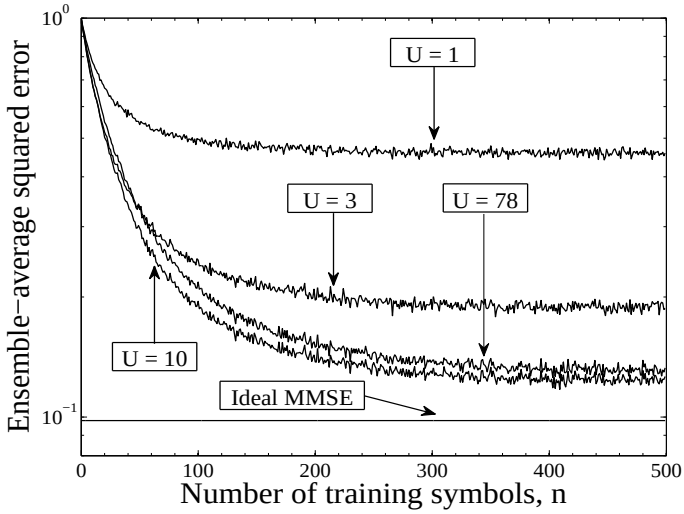

Figure 5.11: Learning curves of the CSM-based reduced-rank RLS adaptive detector for the hybrid DS-TH UWB system supporting $K = 5$ users, when communicating over correlated Rayleigh fading channels modelled by the S-V channel model associated with a normalized Doppler frequency-shift $f_dT_b = 0.0001$. The other parameters were $E_b/N_0 = 10$dB, $\lambda_{RLS} = 0.9987$, $\delta = 5.0$, $g = 1$, $N_c = 16$, $N_\psi = 4$ and $L = 15$, respectively.

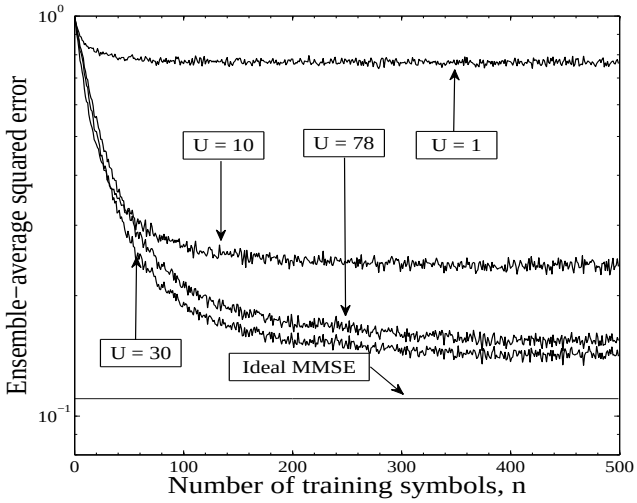

Figure 5.12: Learning curves of the CSM-based reduced-rank RLS adaptive detector for the hybrid DS-TH UWB system supporting $K = 15$ users, when communicating over correlated Rayleigh fading channels modelled by the S-V channel model associated with a normalized Doppler frequency-shift $f_d T_b = 0.0001$. The other parameters were $E_b/N_0 = 10$dB, $\lambda_{RLS} = 0.9987$, $\delta = 5.0$, $g = 1$, $N_c = 16$, $N_\psi = 4$ and $L = 15$, respectively.

(Fig. 5.12) users, respectively. Again, the ensemble-average squared error as shown in the figures was obtained by taking average over 2000 independent realizations of the UWB channel. From the results of Figs. 5.11 and 5.12 one can see that the CSM-assisted reduced-rank RLS adaptive detector is capable of attaining the highest convergence speed and also reaching the lowest MSE, if the rank U used by the detection subspace is equivalent to that of the signal subspace, which is about 10 in Fig. 5.11 and 30 in Fig. 5.12. Similar to the PCA-based reduced-rank RLS adaptive detector as shown in Figs. 5.3 and 5.4, the CSM-assisted reduced-rank RLS adaptive detector converges to the lower MSE, when increasing the rank U of the detection subspace, as shown in Figs. 5.11 and 5.12. However, if the rank U of the detection subspace is higher than that of the signal subspace, the CSM-assisted reduced-rank RLS adaptive detector may converge to a MSE, which is even higher than that achieved by the CSM-assisted reduced-rank RLS adaptive detector with a detection subspace having the same rank as the signal subspace.

Fig. 5.13 shows the BER versus SNR per bit performance of the hybrid DS-TH UWB system employing the CSM-assisted reduced-rank RLS adaptive detection to support $K = 1$ user, when the detection subspace has a reduced rank of $U = 1, 2$ or full rank of $U = 78$. Explicitly, the BER performance achieved in the context of the different detection scenarios is similar and it is close to that of the ideal MMSE detector, even there exists certain ISI.

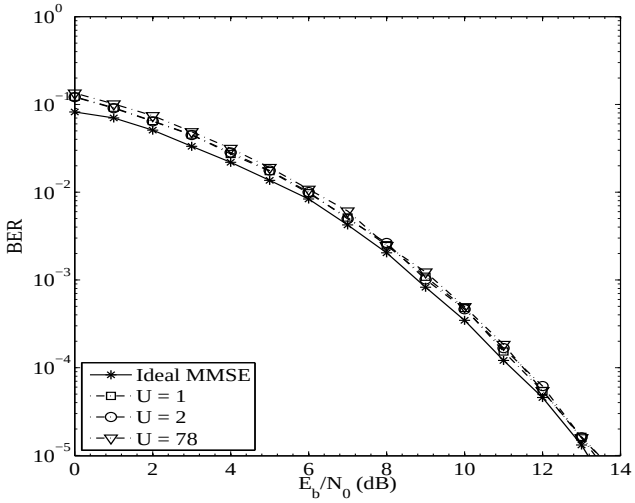

Figure 5.13: BER versus SNR per bit performance of the hybrid DS-TH UWB system using CSM-based reduced-rank RLS adaptive detection, when communicating over correlated Rayleigh fading channels modelled by the S-V channel model. The other parameters employed for the simulations were $K = 1$, $f_dT_b = 0.0001$, $\lambda_{RLS} = 0.9987$, $\delta = 5.0$, $g = 1$, $N_c = 16$, $N_\psi = 4$ and $L = 15$, respectively.

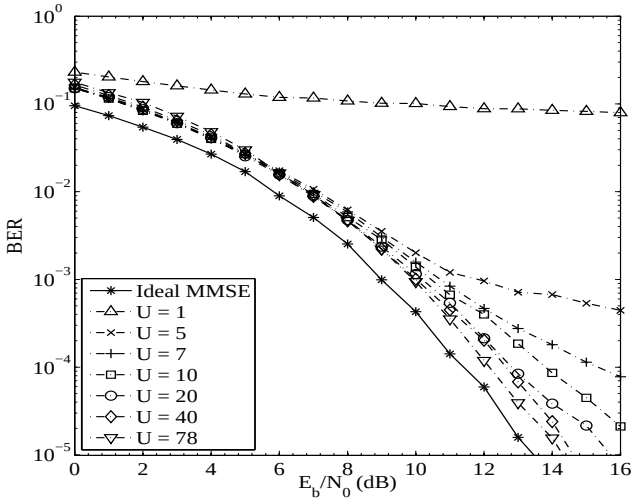

Figure 5.14: BER versus SNR per bit performance of the hybrid DS-TH UWB system using CSM-based reduced-rank RLS adaptive detection, when communicating over correlated Rayleigh fading channels modelled by the S-V channel model. The other parameters employed for the simulations were $K = 5$, $f_dT_b = 0.0001$, $\lambda_{RLS} = 0.9987$, $\delta = 5.0$, $g = 1$, $N_c = 16$, $N_\psi = 4$ and $L = 15$, respectively.

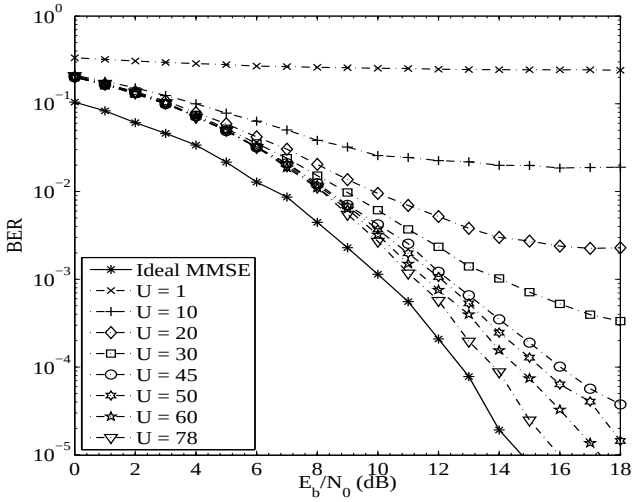

Figure 5.15: BER versus SNR per bit performance of the hybrid DS-TH UWB system using CSM-based reduced-rank RLS adaptive detection, when communicating over correlated Rayleigh fading channels modelled by the S-V channel model. The other parameters employed for the simulations were $K = 15$, $f_d T_b = 0.0001$, $\lambda_{RLS} = 0.9987$, $\delta = 5.0$, $g = 1$, $N_c = 16$, $N_\psi = 4$ and $L = 15$, respectively.

Figs. 5.14 and 5.15 show the BER versus SNR per bit performance of the hybrid DS-TH UWB system using the CSM-assisted reduced-rank RLS adaptive detection, when the detection subspace invokes different rank of U. Specifically, the hybrid DS-TH UWB system considered in Fig. 5.14 supported $K = 5$ users, while that considered in Fig. 5.15 supported $K = 15$ users. The other parameters used in our simulations were specified in the captions associated with the figures. From the results of Figs. 5.14 and 5.15 we can observe that the achievable BER performance of the hybrid DS-TH UWB system is depended on the rank U of the detection subspace. In general, the BER performance improves as the rank U of the detection subspace increases, but depended on the SNR per bit. Specifically, when the SNR per bit is low, the CSM-assisted reduced-rank RLS adaptive detector is capable of reaching a stable BER performance, when the rank U of the detection subspace is relatively low, such as $U = 5$ in Fig. 5.14. However, when the SNR per bit is relatively high, further increasing the rank U of the detection subspace may further improve the BER performance of the hybrid DS-TH UWB system. As shown in Figs. 5.14 and 5.15, if the rank U of the detection subspace is too lower, the CSM-assisted reduced-rank RLS adaptive detector may not efficiently mitigate the MUI and, in these cases, error-floors are observed.

Finally, in contrast to Fig. 5.14 associated with $L = 15$ and $g = 1$, Fig. 5.16 shows the BER versus SNR per bit performance of the hybrid DS-TH UWB systems employing the CSM-based reduced-

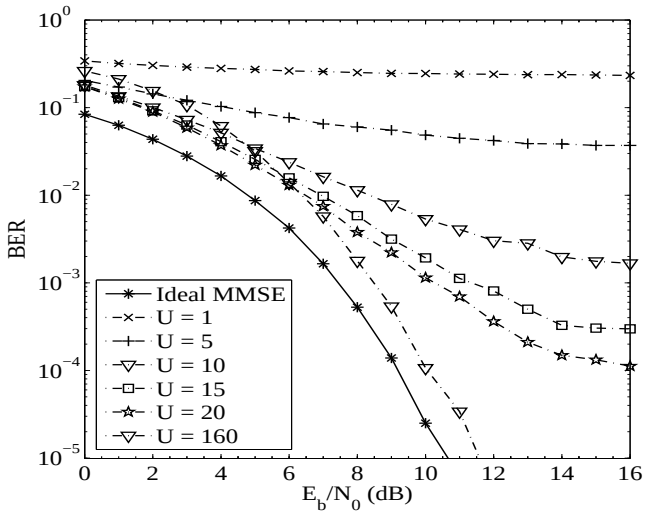

Figure 5.16: BER versus SNR per bit performance of the hybrid DS-TH UWB system using CSM-based reduced-rank RLS adaptive detection, when communicating over correlated Rayleigh fading channels modelled by the S-V channel model. The other parameters employed for the simulations were $K = 5$, $f_d T_b = 0.0001$, $\lambda_{RLS} = 0.9995$, $\delta = 0.005$, $g = 3$, $N_c = 16$, $N_\psi = 4$ and $L = 150$, respectively.

rank RLS adaptive detection to support $K = 5$ users, when $L = 150$ and $g = 3$. As observed in Fig. 5.14, the BER performance of the hybrid DS-TH UWB system improves, as the rank U of the detection subspace increases. Error-floors are observed, when the rank U of the detection subspace is not sufficiently high. As shown in Fig. 5.16, when the SNR value is lower than 7 dB, the CSM-based reduced-rank RLS adaptive detector using $U = 20$ is capable of achieving a better BER performance than the reduced-rank RLS adaptive MMSE-MUD based on a detection subspace having a rank of $U = 160$.

From Figs. 5.14 - 5.16, we find that, unlike Fig. 5.7 - 5.9 corresponding to the PCA-based reduced-rank RLS adaptive detection, the CSM-based reduced-rank RLS adaptive detector cannot reach the BER performance of the full-rank RLS adaptive detector, when the detection subspace reaches a rank equivalent to the signal subspace's rank. The reason for the above observation is that the fading channel is time-varying possibly with every data bit. However, the processing matrix $\boldsymbol{P}_U$ used in our simulations was fixed after the training mode and was not updated correspondingly to match each transmitted data bit.

In summary, as the PCA-assisted scheme, the CSM-assisted reduced-rank RLS adaptive detection is efficient if the signal subspace's rank is significantly lower than the rank $(N_c N_\psi + L - 1)$ of the observation space. However, if a hybrid DS-TH UWB system is heavily loaded, yielding that the

rank of the signal subspace is very high, then the CSM-assisted reduced-rank RLS adaptive detection might not be desirable.

5.4.3 Performance of TPA-Assisted Reduced-Rank RLS Adaptive Detector

In this section we illustrate the performance results of the hybrid DS-TH UWB systems using the TPA-assisted reduced-rank RLS adaptive detection, when communicating over UWB channels. The performance considered includes both the learning and BER performance. As our results in the previous two subsections shows, the PCA- or CSM-assisted reduced-rank RLS adaptive detector achieves the full-rank RLS adaptive detector's performance only when the detection subspace's rank U reaches the rank of the signal subspace. By contrast, our performance results in this subsection will show that the TPA-assisted reduced-rank RLS adaptive detector is capable of achieving the full-rank RLS adaptive detector's performance with a rank that can be significantly lower than the rank of the signal subspace. Furthermore, the detection subspace's rank achieving the full-rank adaptive detector's performance is generally independent of the signal subspace's rank, provided that the signal subspace's rank is sufficiently high.

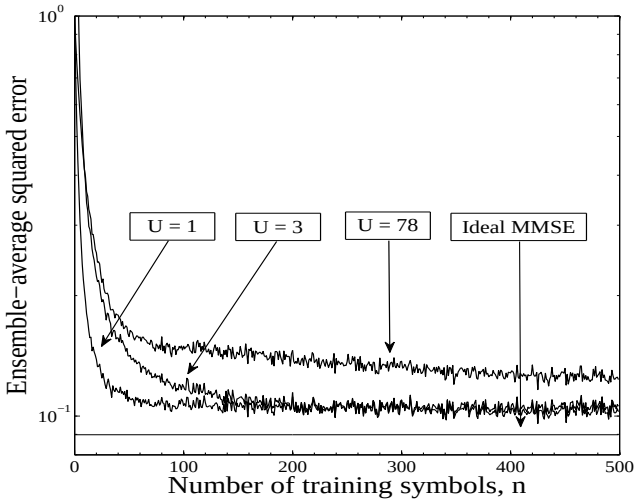

Figure 5.17: Learning curves of the TPA-based reduced-rank RLS adaptive detector for the hybrid DS-TH UWB system supporting single user, when communicating over correlated Rayleigh fading channels modelled by the S-V channel model associated with a normalized Doppler frequency-shift $f_d T_b = 0.0001$. The other parameters used simulations were $E_b/N_0 = 10$dB, $\lambda_{RLS} = 0.9987$, $\delta = 5.0$, $g = 1$, $N_c = 16$, $N_\psi = 4$ and $L = 15$, respectively.

Fig. 5.17 shows the learning performance of the TPA-assisted reduced-rank RLS adaptive detector for the hybrid DS-TH UWB system supporting single ($K = 1$) user. The ensemble-average squared-

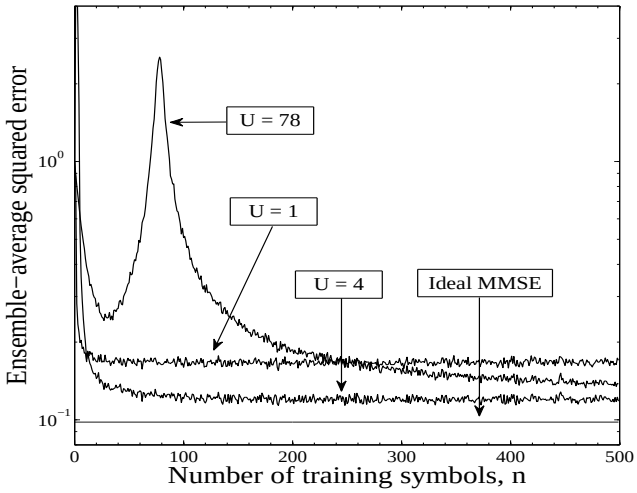

Figure 5.18: Learning curves of the TPA-based reduced-rank RLS adaptive detector for the hybrid DS-TH UWB system supporting $K = 5$ users, when communicating over correlated Rayleigh fading channels modelled by the S-V channel model associated with a normalized Doppler frequency-shift $f_d T_b = 0.0001$. The other parameters were $E_b/N_0 = 10$dB, $\lambda_{RLS} = 0.9987$, $\delta = 5.0$, $g = 1$, $N_c = 16$, $N_\psi = 4$ and $L = 15$, respectively.

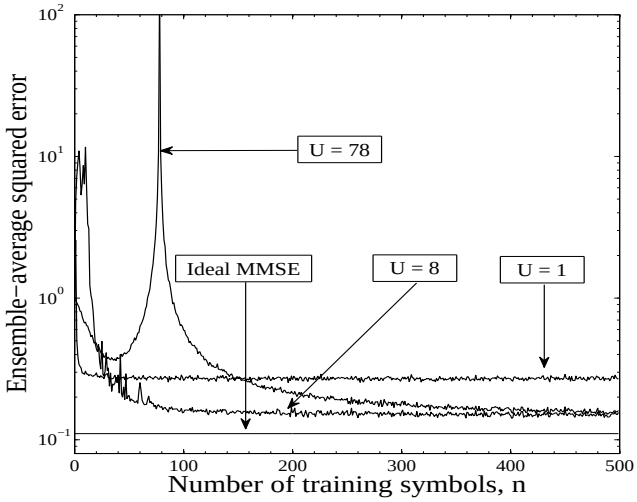

Figure 5.19: Learning curves of the TPA-based reduced-rank RLS adaptive detector for the hybrid DS-TH UWB system supporting $K = 15$ users, when communicating over correlated Rayleigh fading channels modelled by the S-V channel model associated with a normalized Doppler frequency-shift $f_d T_b = 0.0001$. The other parameters were $E_b/N_0 = 10$dB, $\lambda_{RLS} = 0.9987$, $\delta = 5.0$, $g = 1$, $N_c = 16$, $N_\psi = 4$ and $L = 15$, respectively.

error was obtained from averaging over 2000 independent realizations of the UWB channel. From the results of Fig. 5.17, it can be observed that the TPA-assisted reduced-rank RLS detector using $U = 1$ converges much faster than the full-rank RLS adaptive detector corresponding to $U = 78$. The TPA-assisted reduced-rank RLS detector using $U = 1$ also converges faster than that using $U = 3$. However, both of them converge to a similar MSE, which is lower than that converged by the full-rank RLS adaptive detector.

Figs. 5.18 and 5.19 demonstrate the learning performance of the TPA-based reduced-rank RLS adaptive detector for the hybrid DS-TH UWB systems supporting $K = 5$ (Fig. 5.18) and $K = 15$ (Fig. 5.19) users, respectively. Again, the MSE was obtained by the average over 2000 independent realizations of the UWB channel considered. The results of Figs. 5.18 and 5.19 show that the TPA-assisted reduced-rank RLS adaptive detector using the rank $U = 1$ converges the fastest among the cases considered. However, it converges to a relatively high MSE, in comparison with the other cases. As the rank U of the detection subspace increases, the TPA-assisted reduced-rank RLS adaptive detector converges slower, but usually can reach a lower MSE. Furthermore, when the rank $U = 78$ is applied, it can be observed that overshoot phenomena [194] is observed. The overshoot phenomena occurs because an inappropriate regularisation factor δ was used for the initialisation. This problem may be resolved by decreasing the value of δ, as mentioned in the previous chapter.

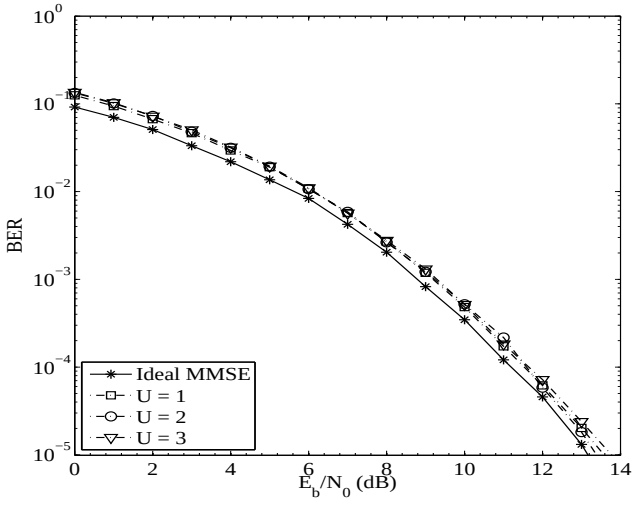

Figure 5.20: BER versus SNR per bit performance of the hybrid DS-TH UWB system using TPA-based reduced-rank RLS adaptive detection, when communicating over correlated Rayleigh fading channels modelled by the S-V channel model. The other parameters employed for the simulations were $K = 1$, $f_d T_b = 0.0001$, $\lambda_{RLS} = 0.9987$, $\delta = 5.0$, $g = 1$, $N_c = 16$, $N_\psi = 4$ and $L = 15$, respectively.

Fig. 5.20 shows the BER versus SNR per bit performance of the hybrid DS-TH UWB system employing the TPA-based reduced-rank RLS adaptive detector. The hybrid DS-TH UWB system supports single user. The results of Fig. 5.20 show that the TPA-assisted reduced-rank RLS adaptive detectors using a rank of $U = 1, 2$ and 3, respectively, are capable of achieving a similar BER performance, which is within 0.5dB of that achieved by the ideal MMSE detector, when the SNR per bit is sufficiently high. Furthermore, when comparing Fig. 5.20 with Fig. 4.19 in the last chapter, we can see that the TPA-assisted reduced-rank RLS adaptive detector using a rank of $U = 1, 2$ or 3 is capable achieving the same BER performance as the full-rank RLS adaptive detector. However, the complexity of the TPA-assisted reduced-rank RLS adaptive detector is significantly lower than that of the full-rank RLS adaptive detector.

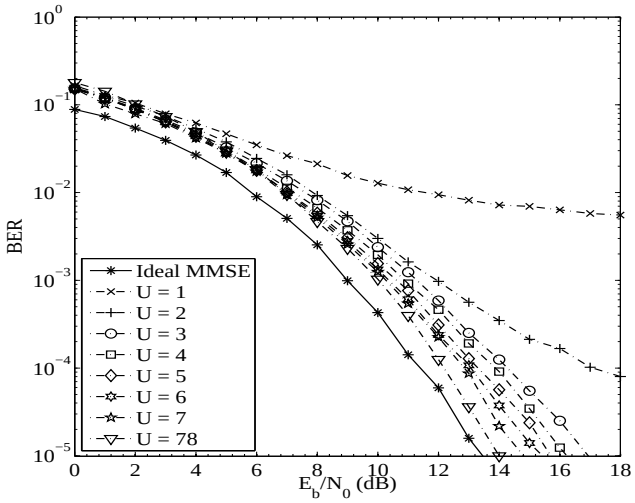

Figure 5.21: BER versus SNR per bit performance of the hybrid DS-TH UWB system using TPA-based reduced-rank RLS adaptive detection, when communicating over correlated Rayleigh fading channels modelled by the S-V channel model. The other parameters employed for the simulations were $K = 5$, $f_dT_b = 0.0001$, $\lambda_{RLS} = 0.9987$, $\delta = 5.0$, $g = 1$, $N_c = 16$, $N_\psi = 4$ and $L = 15$, respectively.

In Figs. 5.21 and 5.22 we investigate the BER versus SNR per bit performance of the hybrid DS-TH UWB systems using the TPA-assisted reduced-rank adaptive detection. In contrast to Fig. 5.20 corresponding to the system supporting single user, in Figs. 5.21 and 5.22 the number of users supported is $K = 5$ and $K = 15$, respectively. From the results of Figs. 5.21 and 5.22, it can be observed that the BER performance of the hybrid DS-TH UWB systems improves, as the rank U of the detection subspace is increased. When the SNR is low, for example lower than 7dB in Fig.5.21 and lower than 9dB in Fig. 5.22, the BER performance is close to each other when $U > 4$. By contrast, when

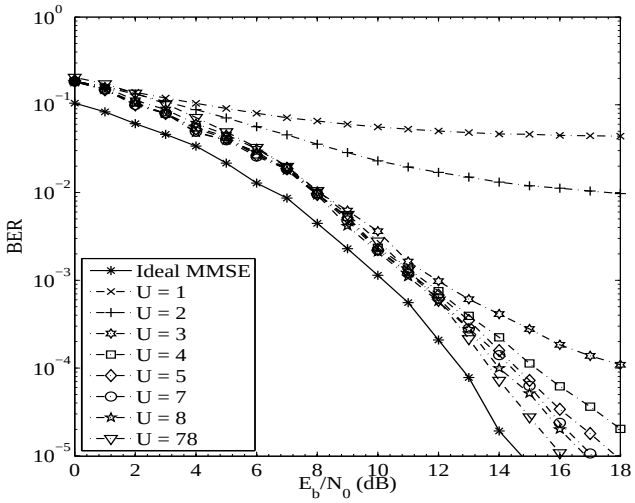

Figure 5.22: BER versus SNR per bit performance of the hybrid DS-TH UWB system using TPA-based reduced-rank RLS adaptive detection, when communicating over correlated Rayleigh fading channels modelled by the S-V channel model. The other parameters employed for the simulations were $K = 15$, $f_dT_b = 0.0001$, $\lambda_{RLS} = 0.9987$, $\delta = 5.0$, $g = 1$, $N_c = 16$, $N_\psi = 4$ and $L = 15$, respectively.

the SNR is high, as seen in Figs.5.21 and 5.22, the BER performance slightly improves as the rank U of the detection subspace is further increased beyond $U = 4$. However, as shown in Figs.5.21 and 5.22, the full-rank RLS adaptive detector's BER performance can be approximately achieved, when the detection subspace's rank is about $U = 7$ or 8. It is worth mentioning that, when the detection subspace's rank is $U = 1$, the TPA-assisted reduced-rank adaptive detector is actually reduced to a correlation adaptive detector.

Finally, in Fig. 5.23 we illustrate the BER versus SNR per bit performance of the hybrid DS-TH UWB system using the TPA-based reduced-rank RLS adaptive detector to support $K = 5$ user, when the UWB channel experiences $L = 150$ resolvable multipaths. Again, the BER performance improves, as the rank U of the detection subspace increases from $U = 1$ to $U = 7$. When comparing the results of Fig. 5.23 with that in Fig. 5.9, we can know that the TPA-based reduced-rank RLS adaptive detector using $U = 7$ is capable of achieving a similar BER performance as the PCA-assisted reduced-rank RLS adaptive detector using a rank of $U = 20$, which equals to the signal subspace's rank. Furthermore, when comparing the results of Fig. 5.23 corresponding to $L = 150$ with that in Fig. 5.21 corresponding to $L = 15$, we can find that, for the case of $U = 7$, the BER performance shown in Fig. 5.23 is better than that shown in Fig. 5.21.

In summary, from the results of Figs. 5.21 - 5.23, we can see that, in general, the TPA-assisted

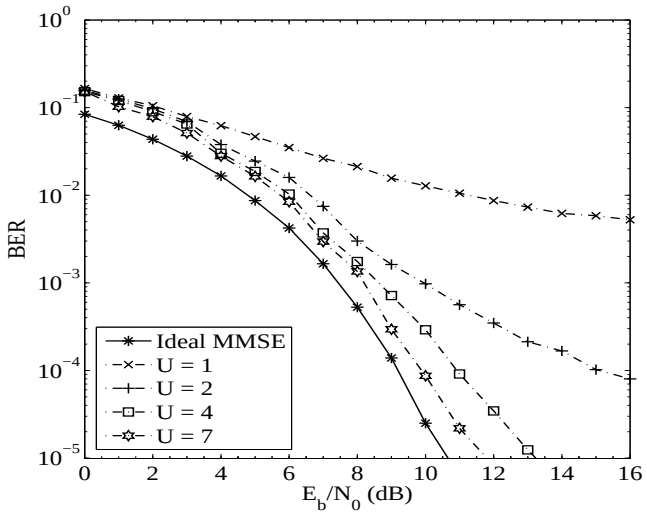

Figure 5.23: BER versus SNR per bit performance of the hybrid DS-TH UWB system using TPA-based reduced-rank RLS adaptive MMSE-MUD, when communicating over correlated Rayleigh fading channels modelled by the S-V channel model. The other parameters employed for the simulations were $K = 5$, $f_d T_b = 0.0001$, $\lambda_{RLS} = 0.9995$, $\delta = 0.005$, $g = 3$, $N_c = 16$, $N_\psi = 4$ and $L = 150$, respectively.

reduced-rank RLS adaptive detector using a detection subspace having a rank of about $U = 7$ or 8 is capable of achieving the BER performance, which is quite close to that achieved by the full-rank RLS adaptive detector. This full-rank RLS adaptive detector's BER performance is achieved regardless of the size of the hybrid DS-TH UWB systems as well as the number of resolvable multipaths of the UWB channels. Furthermore, from Figs. 5.17 - 5.19 we can see that the TPA-assisted reduced-rank RLS adaptive detector converges very fast, when the rank U of the detection subspace is relatively low. Explicitly, the above properties of the TPA-assisted reduced-rank RLS adaptive detection are very desirable for the pulse-based UWB systems, which might support a big number of users communicating over UWB channels having a huge number of low-power resolvable multipaths.

5.4.4 Performance Comparison of Reduced-Rank RLS Adaptive Detectors

So far, we have shown the learning and BER performance of the reduced-rank RLS adaptive detectors, which derive the detection subspaces based on the PCA-, CSM- and TPA-assisted rank reduction techniques, respectively. In this subsection the learning and BER performance of the reduced-rank RLS adaptive detectors using the above-mentioned three types of rank reduction techniques are compared in the context of the hybrid DS-TH UWB systems.

Figs. 5.24 and 5.25 show the learning performance of the reduced-rank RLS adaptive detectors,

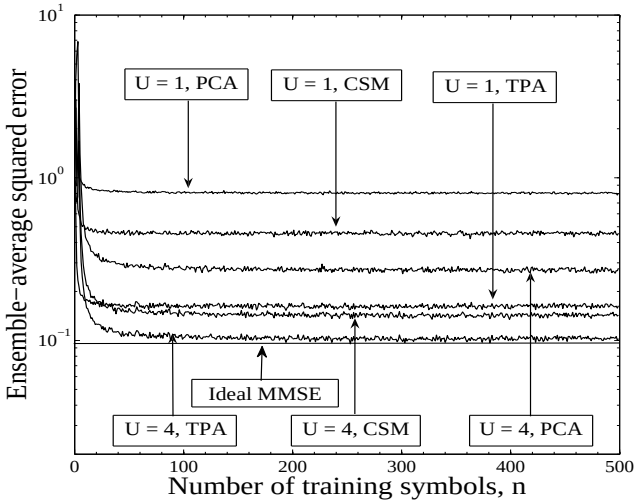

Figure 5.24: Learning curves of the PCA-, CSM- and TPA-based reduced-rank RLS adaptive detectors for the hybrid DS-TH UWB system supporting $K = 5$ users, when communicating over correlated Rayleigh fading channels modelled by the S-V channel model associated with a normalized Doppler frequency-shift $f_d T_b = 0.0001$. The other parameters were $E_b/N_0 = 10$dB, $\lambda_{RLS} = 0.9987$, $\delta = 5.0$, $g = 1$, $N_c = 16$, $N_\psi = 4$ and $L = 15$, respectively.

which derive their detection subspaces based on the principles of the PCA-, CSM- and TPA-based rank reduction techniques, as described in Section 5.2. In our simulations we assumed that the hybrid DS-TH UWB systems supported $K = 5$ users and that the average SNR per bit was $E_b/N_0 = 10$dB. In the context of Fig. 5.24 we assumed that the UWB channel had $L = 15$ resolvable multipaths corresponding to $g = 1$, while in the context of Fig. 5.25 we assumed that the UWB channel had $L = 150$ resolvable multipaths corresponding to $g = 3$. Additionally, the ensemble-average squared error shown in the figures was obtained from 2000 independent realizations. The other parameters were detailed associated with the figures. As the results of Figs. 5.24 and 5.25 shown, for a given rank U considered in the figures, the TPA-based scheme achieves the lowest MSE among the three rank reduction techniques. After the converging, the MSE achieved by the TPA-based scheme is significantly lower than the MSE achieved by the PCA- or CSM-based scheme. For a given rank U of the detection subspace, as shown in Figs. 5.24 and 5.25, the CSM-based reduced-rank scheme converges to a (slightly) lower MSE than the PCA-based rank reduction scheme.

Fig. 5.26 shows the ensemble-average squared error learning performance of the reduced-rank RLS adaptive detectors using the PCA-, CSM-, and TPA-assisted rank reduction techniques for the hybrid DS-TH UWB systems supporting $K = 15$ users. In our simulations we assumed that the average SNR per bit was $E_b/N_0 = 10$dB, the UWB channel resulted in $L = 15$ resolvable multipaths

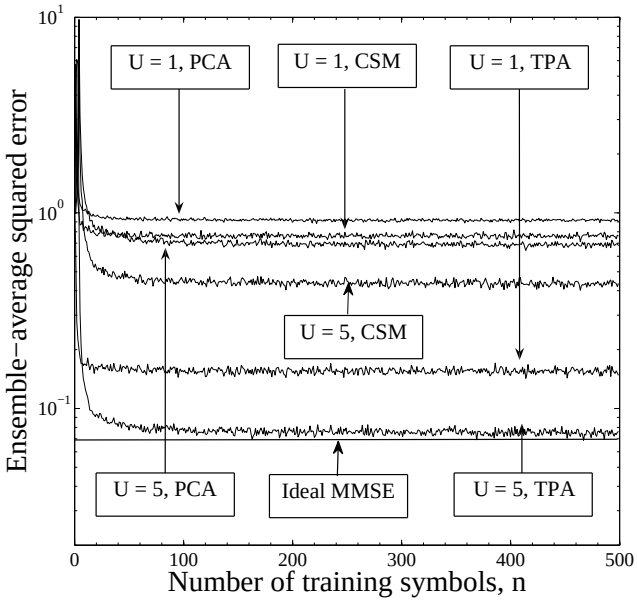

Figure 5.25: Learning curves of the PCA-, CSM- and TPA-based reduced-rank RLS adaptive detectors for the hybrid DS-TH UWB system supporting $K = 5$ users, when communicating over correlated Rayleigh fading channels modelled by the S-V channel model associated with a normalized Doppler frequency-shift $f_d T_b = 0.0001$. The other parameters were $E_b/N_0 = 10$dB, $\lambda_{RLS} = 0.9995$, $\delta = 0.005$, $g = 3$, $N_c = 16$, $N_\psi = 4$ and $L = 150$, respectively.

and the ensemble average was taken over 2000 independent realizations of the UWB channel. The other parameters used in our simulation were summarized associated with figure. Again, for a given considered rank U, the TPA-assisted rank reduction scheme is capable of achieving much lower MSE than the PCA- or CSM-based rank reduction scheme. The PCA-based rank reduction scheme achieves the worst MSE performance among the three rank reduction schemes for a given rank U of the detection subspace.

Additionally, from Fig. 5.24 to Fig. 5.26, we can observe that, when the rank U of the detection subpace increases, i.e., when the transceiver filter's length increases, the reduced-rank RLS adaptive detector using the PCA-, CSM- or TPA-based rank reduction scheme converges slower. This means that, once a higher rank U of the detection subspace is applied, the number of training symbols is also required to be increased, in order for the adaptive filter to converge.

Fig. 5.27 compares the BER versus SNR per bit performance of the hybrid DS-TH UWB systems supporting single user, when the PCA-, CSM- or TPA-assisted reduced-rank RLS adaptive detectors is employed. Since only single user is supported and the ISI is not severe, as shown in Fig. 5.27, all the reduced-rank RLS adaptive detector achieve a similar BER performance, which is quite close

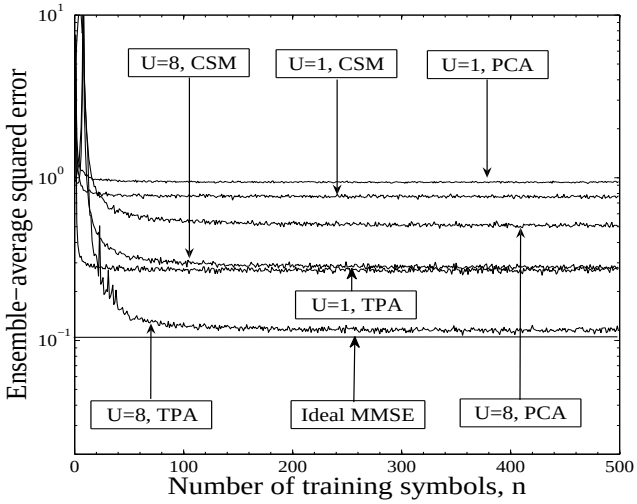

Figure 5.26: Learning curves of the PCA-, CSM- and TPA-based reduced-rank RLS adaptive detectors for the hybrid DS-TH UWB system supporting $K = 15$ users, when communicating over correlated Rayleigh fading channels modelled by the S-V channel model associated with a normalized Doppler frequency-shift $f_d T_b = 0.0001$. The other parameters were $E_b/N_0 = 10$dB, $\lambda_{RLS} = 0.9987$, $\delta = 5.0$, $g = 1$, $N_c = 16$, $N_\psi = 4$ and $L = 15$, respectively.

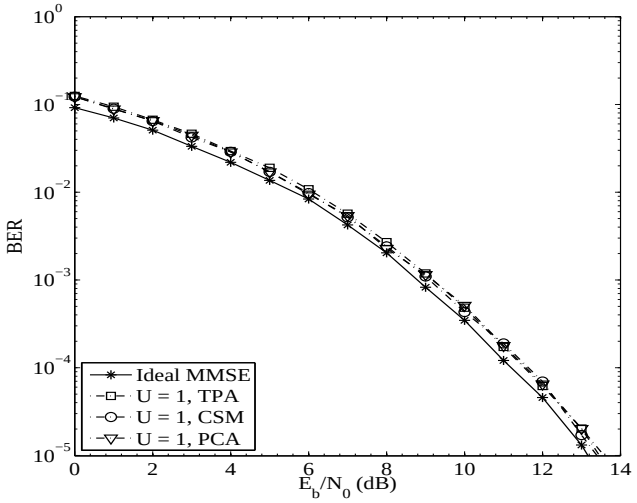

Figure 5.27: BER performance comparison of the hybrid DS-TH UWB system using PCA-, CSM- and TPA-based reduced-rank RLS adaptive detection, when communicating over correlated Rayleigh fading channels modelled by the S-V channel model. The parameters employed for the simulations were $K = 1$, $f_d T_b = 0.0001$, $\lambda_{RLS} = 0.9987$, $\delta = 0.5$, $g = 1$, $N_c = 16$, $N_\psi = 4$ and $L = 15$, respectively.

(less than 0.4dB at reasonably high SNR) to that achieved by the ideal MMSE detector considered in Chapter 3. Note that, when considering the computational complexity in this case, we find that the number of operations required for detecting one bit using the TPA-assisted reduced-rank technique is 189, while that using the PCA- and CSM-assisted reduced-rank techniques are 6575 and 6600, respectively. Hence, we are implied that the TPA-assisted scheme has the lowest computational complexity among the three rank reduction schemes considered.

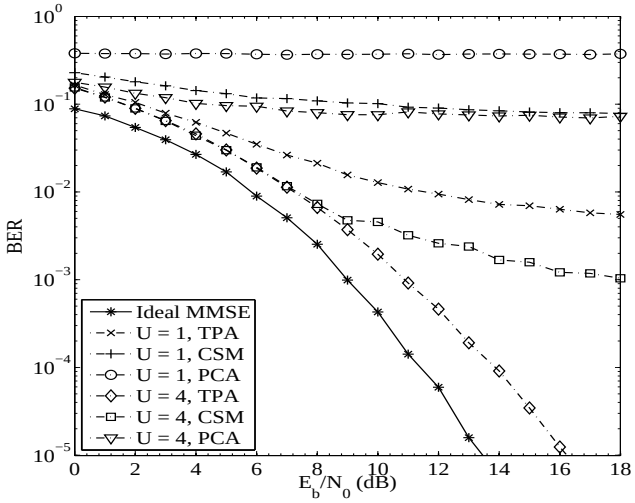

Figure 5.28: BER performance comparison of the hybrid DS-TH UWB system using PCA-, CSM- and TPA-based reduced-rank RLS adaptive detection, when communicating over correlated Rayleigh fading channels modelled by the S-V channel model. The parameters employed for the simulations were $K = 5$, $f_d T_b = 0.0001$, $\lambda_{RLS} = 0.9987$, $\delta = 0.005$, $g = 1$, $N_c = 16$, $N_\psi = 4$ and $L = 15$, respectively.

Finally, in Figs. 5.28, 5.29 and 5.30 we compare the BER versus SNR per bit performance of the hybrid DS-TH UWB systems using the three types of reduced-rank RLS adaptive detectors to support multiple users. Specifically, in the context of Figs. 5.28 and 5.29 the number of users supported by the hybrid DS-TH UWB systems was $K = 5$, while in Fig. 5.30 the number of users supported was $K = 15$. Furthermore, in our simulations the number of resolvable multipaths for Figs. 5.28 and 5.30 was $L = 15$ implying relatively low ISI. By contrast, the number of resolvable multipaths assumed for Fig. 5.29 was $L = 150$, which resulted in severe ISI, in addition to multiuser interference. From the results of Figs. 5.28, 5.29 and 5.30, we can observe that, for a given rank U of the detection subspace, the TPA-based reduced-rank RLS adaptive detector significantly outperforms the PCA- and CSM-based reduced-rank RLS adaptive detectors. Note that, the detection subspace's ranks considered in these figures are all lower than the corresponding signal subspace's ranks. As shown

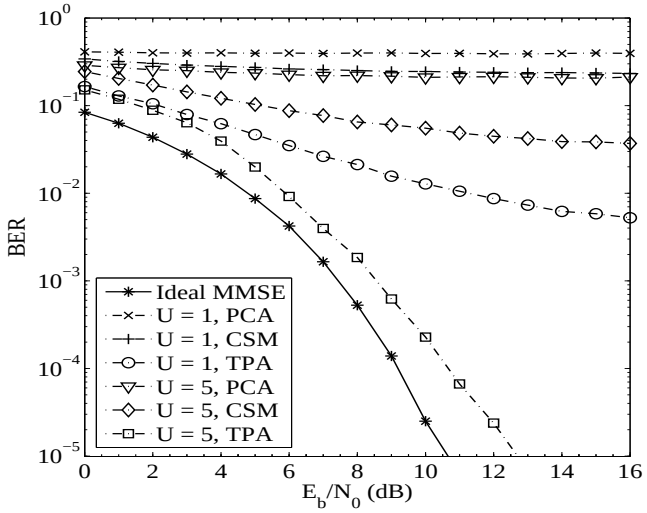

Figure 5.29: BER performance comparison of the hybrid DS-TH UWB system using PCA-, CSM- and TPA-based reduced-rank RLS adaptive detection, when communicating over correlated Rayleigh fading channels modelled by the S-V channel model. The parameters employed for the simulations were $K = 5$, $f_dT_b = 0.0001$, $\lambda_{RLS} = 0.9995$, $\delta = 0.005$, $g = 3$, $N_c = 16$, $N_\psi = 4$ and $L = 150$, respectively.

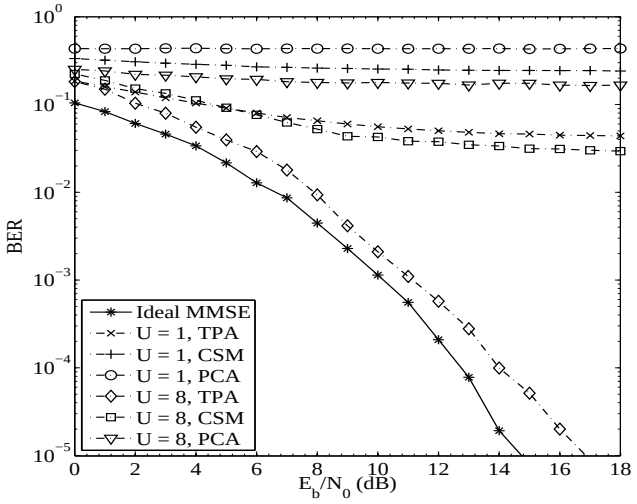

Figure 5.30: BER performance comparison of the hybrid DS-TH UWB system using PCA-, CSM- and TPA-based reduced-rank RLS adaptive detection, when communicating over correlated Rayleigh fading channels modelled by the S-V channel model. The parameters employed for the simulations were $K = 15$, $f_dT_b = 0.0001$, $\lambda_{RLS} = 0.9987$, $\delta = 0.005$, $g = 1$, $N_c = 16$, $N_\psi = 4$ and $L = 15$, respectively.

in Figs. 5.28, 5.29 and 5.30, in these cases, the PCA-based reduced-rank RLS adaptive detector is the worst among the three reduced-rank RLS detection schemes in terms of the achievable BER performance for $U = 1,\ 4,\ 5$ or 8.

5.5 Summary and Conclusions

In this chapter we have investigated the learning and BER performance of the hybrid DS-TH UWB systems using various reduced-rank RLS adaptive detectors, in order to illustrate the design trade-off between the affordable detection complexity and the achievable BER performance, when reduced-rank adaptive detection is employed. Three types of rank reduction techniques have been investigated in conjunction with the hybrid DS-TH UWB systems using the RLS-aided adaptive detection. The three types of reduced-rank detection schemes have been derived based on the principles of principal component analysis (PCA), cross-spectral metric (CSM) and Taylor polynomial approximation (TPA), respectively. Throughout the study provided in this chapter, the following observations may be derived.

- **Principal Component Analysis**: The PCA-assisted reduced-rank RLS adaptive detector is depended on the eigen-decomposition of the auto-correlation matrix $\boldsymbol{R}_{y_i}$ of the observation vector $\boldsymbol{y}_i$. In this reduced-rank scheme the U number of eigenvectors corresponding to the U largest eigenvalues of $\boldsymbol{R}_{y_i}$ are used to form the detection subspace (or processing matrix) $\boldsymbol{P}_U$. As shown in Section 5.2.2, the PCA-based scheme forms the detection subspace $\boldsymbol{P}_U$ without requiring the knowledge about the user to be detected. The complexity of the PCA-based reduced-rank RLS adaptive detector has been considered in Section 5.3.1, and the number of operations for detecting one bit has been found to be $((\mathcal{T}^2 + 2\mathcal{T} + 2U\mathcal{T} + 11U^2 + 7U + 3 + (\mathcal{T}^3/3 + U\log_2\mathcal{T})/F_L)$, where $\mathcal{T} = (N_cN_\psi + L - 1)$ and F_L denotes the frame-length. Finally, the learning and BER performance of the PCA-based reduced-rank RLS adaptive detector have been studied in Section 5.4.1. Our analysis and performance results show that the PCA-assisted reduced-rank RLS adaptive detector is capable of achieving the BER performance of the full-rank RLS adaptive detector, if the rank U of the detection subspace is not lower than the signal subspace's rank. Hence, the PCA-based scheme may allow a significant reduction of the detection subspace's rank, provided that the dimension of the signal subspace is significantly lower than the rank of the observation space spanned by the received signal $\boldsymbol{y}_i$, which is $(N_cN_\psi + L - 1)$ and may be very big if the total spreading factor and/or the number of resolvable multipaths are high. When this is not the case, for ex-

ample, when the hybrid DS-TH UWB system supports a high number of users resulting in that the signal subspace's rank exceeds the rank U of the detection subspace, then, mapping the received signal vectors to the detection subspace of rank U is likely to reduce the desired signal components. Consequently, the corresponding PCA-based reduced-rank RLS adaptive detector might conflict severe multiuser interference and the BER performance appears error-floors.

- **Cross-Spectral Metric**: The CSM-based reduced-rank RLS adaptive detector is also depended on the eigen-decomposition of the auto-correlation matrix $\boldsymbol{R}_{y_i}$ of the observation vector $\boldsymbol{y}_i$. As shown in Section 5.2.3, from $(N_c N_\psi + L - 1)$ eigenvectors of $\boldsymbol{R}_{y_i}$, the CSM-based scheme chooses the U eigenvectors having the U largest CSM values as defined in (5.14) to form the detection subspace $\boldsymbol{P}_U$. The detection subspace obtained in this way is the optimum selection of the $\binom{N_c N_\psi + L - 1}{U}$ eigenvectors in MMSE sense for reduction in rank. Hence, the CSM-based rank-reduction technique may be more efficient than the PCA-based rank-reduction technique, since the CSM-based scheme takes into account the energy in the subspace contributed by the desired user. However, as shown in (5.14), the CSM-based reduced-rank scheme requires to invoke the knowledge of $\boldsymbol{h}_1$ and $\boldsymbol{C}_i^{(1)}$ of the desired user, in order to form the detection subspace $\boldsymbol{P}_U$. The complexity of the CSM-assisted reduced-rank RLS adaptive detector has been considered in Section 5.3.2. It has been found that the number of operations for detecting one bit is $(\mathcal{T}^2 + 2\mathcal{T} + 2U\mathcal{T} + 11U^2 + 7U + 3 + ((\mathcal{T}+1)T_L + \mathcal{T}^3/3 + 2\mathcal{T}^2 + U\log_2\mathcal{T})/F_L)$, where T_L represents the number of symbols per frame used for training, in addition to the parameters mentioned previously. Finally, the learning behaviour of the CSM-based reduced-rank RLS adaptive detector and the BER performance of the hybrid DS-TH UWB systems using the CSM-based reduced-rank RLS adaptive detection have been depicted and discussed in Section 5.4.2. From our study and performance results, it can be found that the CSM-assisted reduced-rank RLS adaptive detector may converge faster than the full-rank RLS adaptive detector. Hence, the hybrid DS-TH UWB systems using the CSM-assisted reduced-rank RLS adaptive detection may result in a higher spectral-efficiency than that using the full-rank RLS adaptive detection. The CSM-assisted reduced-rank RLS adaptive detector is capable of achieving the BER performance of the full-rank RLS adaptive detector, when the rank U of the detection subspace reaches a value equivalent to the signal subspace's rank. Hence, like the PCA-based scheme, the CSM-based scheme may also reduce significantly the detection complexity, if the dimension of the signal subspace is significantly lower than that of the observation space spanned by the received signal $\boldsymbol{y}_i$.

- **Taylor Polynomial Approximation**: In contrast to the above two rank reduction schemes that are depended on the eigen-decomposion, the TPA-assisted reduced-rank adaptive detector forms its detection subspace $\boldsymbol{P}_U$ without depending on the eigen-decomposition of the auto-correlation matrix $\boldsymbol{R}_{y_i}$. Instead, it forms the detection subspace $\boldsymbol{P}_U$ based on the Taylor polynomial expansion of the inverse auto-correlation matrix $\boldsymbol{R}_{y_i}$, as shown in (5.19). Based on (5.19), we can know that the TPA-based reduced-rank scheme requires the knowledge of $\boldsymbol{h}_1$ and $\boldsymbol{C}_i^{(1)}$ of the desired user, in order to form the detection subspace $\boldsymbol{P}_U$. The complexity of the TPA-based reduced-rank RLS adaptive detector has been analysed in Section 5.3.3. It has been found that, if the detection subspace's rank is $U = 1$, the number of operations required to detect one bit is $(2\mathcal{T} + 21 + ((\mathcal{T}+1)T_L/F_L))$. However, if the detection subspace's rank is $U > 1$, then the number of operations required to detect one bit is $((\mathcal{T}^2 + 2\mathcal{T} + 2U\mathcal{T} + 11U^2 + 7U + 3) + ((\mathcal{T}+1)T_L + 2(U-1)\mathcal{T}^2/F_L))$. Finally, in Section 5.4.3 the learning and BER performance of the TPA-assisted reduced-rank RLS adaptive detector have been provided and analysed. The learning and BER performance results show that the TPA-assisted reduced-rank RLS adaptive detector is a highly efficient detection scheme. It usually does not require a high rank U (in comparison to the signal subspace's rank) to converge to a low MSE and it usually converges very fast. The TPA-assisted reduced-rank RLS adaptive detector is capable of converging to the full-rank RLS adaptive detector's performance with a rank U significantly lower than that of the signal subspace, especially when the signal subspace's rank is high. Furthermore, the detection subspace's rank U needed to achieve the full-rank RLS adaptive detector's performance does not scale with the system size determined by the observation space's dimension, which is $(N_c N_\psi + L - 1)$, and the number of users, K. Additionally, as shown in Tables 5.5 and 5.6, the TPA-based reduced-rank RLS adaptive detector usually has a lower complexity than the PCA- or CSM-based reduced-rank RLS adaptive detector. Owing to its above-mentioned properties, the TPA-assisted reduced-rank RLS adaptive detector may constitute a promising detection scheme for the hybrid DS-TH UWB systems, which may support a big number of users communicating over the UWB channels having a huge number of low-power resolvable multipaths.

Finally, the complexity of various detection schemes for the hybrid DS-TH UWB systems to detect one bit is summarized in Table 5.5. In Table 5.6 the number of operations required by the different detectors to detect one bit is provided in the context of a range of specific cases. For generating Table 5.6, we assumed that the frame-length was $F_L = 1000$ bits, which included $T_L = 160$ training bits. Hence, the spectral-efficiency of the hybrid DS-TH UWB systems is 84%. Additionally, the

Detection scheme	Number of operations for detecting one bit
Correlation detector	$2(L-1)\mathcal{T}$
Ideal MMSE detector	$\mathcal{T}^3/3+6\mathcal{T}^2+2(L+1)\mathcal{T}+4KL(1+4g)\mathcal{T}$
Full-rank RLS adaptive detector	$11\mathcal{T}^2+8\mathcal{T}+3$
PCA-based reduced-rank RLS adaptive detector	$\mathcal{T}^2+2\mathcal{T}+2U\mathcal{T}+11U^2+7U+3+\frac{\mathcal{T}^3/3+U\log_2\mathcal{T}}{F_L}$
CSM-based reduced-rank RLS adaptive detector	$\mathcal{T}^2+2\mathcal{T}+2U\mathcal{T}+11U^2+7U+3+\frac{1}{F_L}\left[(\mathcal{T}+1)T_L+\mathcal{T}^3/3+2\mathcal{T}^2+2\mathcal{T}+U\log_2\mathcal{T}\right]$
TPA-based reduced-rank RLS adaptive detector	$2\mathcal{T}+21+\frac{1}{F_L}\left[(\mathcal{T}+1)T_L\right],\ U=1$ $\mathcal{T}^2+2\mathcal{T}+2U\mathcal{T}+11U^2+7U+3+\frac{1}{F_L}\left[(\mathcal{T}+1)T_L+2(U-1)\mathcal{T}^2\right],\ U=2,3,\cdots$

Table 5.5: Complexity comparison of various detection schemes for the hybrid DS-TH UWB systems.

total spreading factor was assumed to be 64, where the DS spreading factor was $N_c = 16$ and the TH-spreading factor was $N_\psi = 4$, respectively. From the data shown in Table 5.6, it can be observed that the number of operations required for detecting one bit is reduced significantly for the reduced-rank RLS adaptive detection schemes in comparison with that required by the full-rank RLS adaptive detector. All the three reduced-rank RLS adaptive detectors considered in this chapter have a similar complexity, but, however, the number of operations required by the TPA-based reduced-rank scheme is usually slightly lower than that required by the PCA- or CSM-based reduced-rank scheme, for any given U and L. Furthermore, the data in Table 5.6 shows that the complexity of the reduced-rank RLS adaptive detectors is at a similar level as that of the single-user correlation detector studied in Chapter 3, which achieves much worse BER performance than the reduced-rank RLS adaptive detectors considered in this chapter.

Detection scheme	Number of resolvable multipaths, L	Rank of detection subspace, U	Number of operations for detecting one bit
Correlation detector	15	78	2496
	100	163	32926
Ideal MMSE detector	15	78	176670
	100	163	1523780
Full-rank RLS adaptive detector	15	78	67551
	100	163	293566
PCA-based reduced-rank RLS adaptive detector	15	1	6575
		8	8428
		15	11391
		45	36670
	100	1	28686
		8	31750
		15	35957
		45	66945
CSM-based reduced-rank RLS adaptive detector	15	1	6600
		8	8453
		15	11416
		45	36695
	100	1	28765
		8	31829
		15	36036
		45	67024
TPA-based reduced-rank RLS adaptive detector	15	1	189
		5	7125
		8	8023
	100	1	373
		5	28601
		8	30144

Table 5.6: Number of operations required for detecting one bit in the hybrid DS-TH UWB systems using various detection schemes.

Chapter 6

Conclusions and Future Work

In this final concluding chapter, we first provide a summary of the thesis in Section 6.1. Then, a range of topics concerning future research are presented in Section 6.2.

6.1 Summary and Conclusions

In this thesis we have proposed and investigated a novel pulse-based UWB system known as the hybrid DS-TH UWB system. This pulse-based UWB system provides more degrees-of-freedom as compared to the pure DS- and pure TH-UWB systems. Furthermore, it can be shown that both the TH-UWB and DS-UWB systems constitute special examples of the hybrid DS-TH UWB system. The main motivation of this thesis is to design low-complexity high-efficiency pulse-based UWB receivers, which are capable of achieving reasonable BER performance.

We have commenced in Chapter 2 with a detailed review of related work on UWB communications. According to the literature, UWB systems can be implemented by pulse-based or multi-carrier-based approached. Since our focus in this thesis is on the pulse-based UWB systems, in Chapter 2 a detailed review of pulse-based UWB systems is, hence presented. Short duration pulses designed for the pulse-based UWB systems have been analyzed in detail. Since FCC has imposed no restriction on the pulse shape, data modulation and MA schemes, different kinds of pulse shapes in Section 2.2.2, modulation techniques in Section 2.2.4 and different MA techniques in Section 2.2.5 can hence be employed in the pulse-based UWB systems, although each of them has its advantages and disadvantages in comparison with its counterparts. In this chapter, we have also provided a brief overview for the multi-carrier based UWB systems which are implemented by dividing the frequency band into several smaller bands with each band having at least 500 MHz of bandwidth. Furthermore, a

comparison between the pulse-based UWB schemes and multicarrier UWB schemes is carried out. Then, in Section 2.5 the main differences among the narrowband, wideband and UWB channels have been characterized, and statistics for modelling both the large-scale fading and small-scale fading of the UWB channels have been provided, with our emphasis on the small-scale fading, since UWB has been mainly considered for indoor and other short-distance communications. The S-V channel model, which was initially proposed for indoor wireless communications in [133], has been introduced as a typical UWB channel model for our study in the following chapters. Furthermore, the S-V channel model for UWB indoor wireless communications is discussed in detail. It is shown that the MDP in UWB communications environments is generally sparse, resulting in possibly a huge number of resolvable multipaths present at the UWB receiver. Hence, in UWB systems a large number of resolvable multipaths are usually required to be processed by the UWB receiver in order to achieve a good BER performance, which makes the design of low-complexity UWB receivers critical.

In Chapter 3 the hybrid DS-TH UWB system has been proposed and investigated. The transmitted signal, channel model and the receiver model for the hybrid DS-TH UWB have been presented. The performance of the hybrid DS-TH UWB systems have been investigated under the assumptions that the delay-spread of the channel may span several bit durations, resulting in a huge number of resolvable multipaths. In our investigation, both the single-user correlation detector and multiuser MMSE detector have been considered. From our studies we can draw the following observations.

- **Single-User Correlation Detector:** It is near optimum when the hybrid DS-TH UWB system supports single-user communicating over Nakagami-m Fading channels, if the delay-spread is not high, resulting in ignorable ISI. A tradeoff exists between the DS and TH spreading factors, when the single-user correlation detector is employed in a hybrid DS-TH UWB system. It can be shown that the best BER performance of the hybrid DS-TH UWB system may be obtained by appropriately choosing the DS and TH spreading factors. In this case, the hybrid DS-TH UWB system outperforms the pure DS-UWB or pure TH-UWB system. The complexity of the single-user correlation detector has been found to be $2(L+1)\mathcal{T}$, where $\mathcal{T} = N_c N_\psi + L - 1$. Furthermore, it has been shown that the BER performance of the single-user correlation detector deteriorates, when the number of users supported by the hybrid DS-TH UWB system increases.

- **Multiuser MMSE Detector:** In the context of the multiuser MMSE detector, it has been observed from the simulations results that the BER performance of the hybrid DS-TH UWB system, that of the pure DS-UWB system and that of the pure TH-UWB system are all similar,

when given the total spreading factor. However, for some specific DS and TH spreading factors, the BER performance of the hybrid DS-TH UWB system may be slightly better than the pure DS-UWB and pure TH-UWB systems. The complexity of the multiuser MMSE detector is very high and has been found to be $\mathcal{T}^3/3 + 6\mathcal{T}^2 + 4KL(1+2g)\mathcal{T} + 2(L+1)\mathcal{T}$, where again $\mathcal{T} = N_c N_\psi + L - 1$. In addition to the complexity for detection, the MMSE detector also requires the complete knowledge of the spreading codes of all the active users. Furthermore, the MMSE detector requires ideal channel knowledge associated with the active users, which is usually not available in UWB systems, since the received UWB signals are usually constituted by a huge number of low-power resolvable multipaths that are extremely hard to estimate.

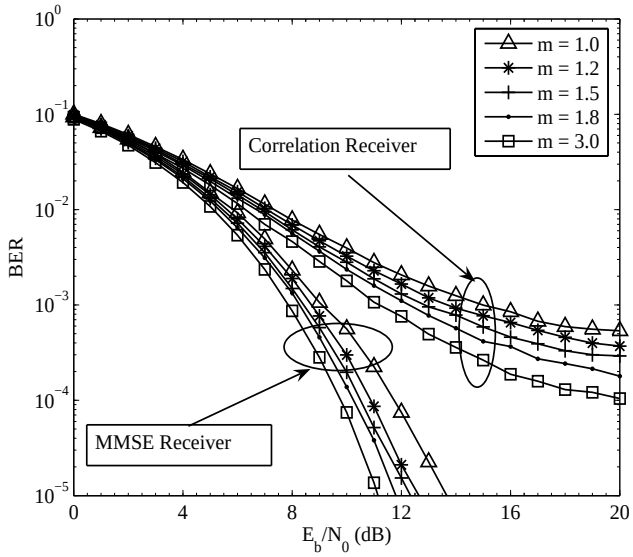

Figure 6.1: Comparison of BER versus SNR per bit performance of the hybrid DS-TH UWB systems using correlation and MMSE receivers to support $K = 15$ users, when communication over Nakagami-m fading channels. The total spreading factor is $N_c N_\psi = 128$, where the DS spreading factor is $N_c = 8$ while the TH spreading factor is $N_\psi = 16$. There are 15 number of resolvable multipaths, five of which convey 85% of the transmitted power.

As an example, Fig. 6.1 compares the BER versus SNR performance of the hybrid DS-TH UWB system employing the single-user correlation and multiuser MMSE detectors, when communicating over Nakagami-m fading channels associated with different fading parameters. In our simulations we assumed that the hybrid DS-TH UWB system supported $K = 15$ users. The number of resolvable multipaths were fixed to $L = 15$, where five of which conveyed 85% of the total transmitted power. From the results of Fig. 6.1 we can observe that as the channel quality improves, i.e., as the value of m increases, the BER performance of the hybrid DS-TH UWB improves. It is also observed from Fig. 6.1 that the BER performance of the MMSE receiver is significantly better than that of the

correlation receiver. However, we should note that the MMSE detector has much more complexity than the correlation detector.

In order to take the advantages of the multiuser MMSE detector but reduce the detection complexity in Chapter 4 we have proposed and investigated a range of training-based adaptive detectors for the hybrid DS-TH UWB systems. These adaptive detectors have lower complexity than the ideal MMSE detector considered in Chapter 3. Furthermore, these adaptive detectors are free from channel estimation and are capable of achieving the approximate MMSE solutions with the aid of some training sequences of certain length. In this chapter three types of low-complexity adaptive detectors have been considered, which are operated based on the principles of least mean-square (LMS), normalized least mean-square (NLMS) and recursive least square (RLS), respectively. From our analysis and performance results, we can draw the following observations.

- **LMS Adaptive Detector:** The LMS adaptive detector belongs to the category of stochastic gradient algorithms. The basic principle of the LMS detector is to find a sub-optimal weight vector $\boldsymbol{w}_1$ through stochastic gradient techniques, in order to approach the minimum mean-square error between the transmitted symbol $b_i^{(1)}$ and its corresponding decision variable $z_i^{(1)}$. The procedure of the LMS adaptive detector has been summarised in Table 4.2.1. The complexity of the LMS adaptive detector has been considered in Section 4.3.1 and is found to be $(5(N_c N_\psi + L - 1) + 2)$. Finally, the BER performance results for the hybrid DS-TH UWB systems employing the LMS adaptive detector have been presented in Section 4.4.1. It can be found that the LMS-aided adaptive detector constitutes one of the efficient detection schemes that can be applied to the pure DS-, pure TH- and hybrid DS-TH UWB systems. However, the LMS adaptive detector does not perform very well in the low SNR region.

- **NLMS Adaptive Detector:** The NLMS adaptive detector also works in the principles of stochastic gradient. The NLMS adaptive detector is capable of attaining faster convergence than the LMS adaptive detector. The algorithm of the NLMS adaptive detector is summarised in Table 4.2.2. The complexity of the NLMS has been analyzed in Section 4.3.2, which is $(7(N_c N_\psi + L - 1) + 2)$. Finally, the BER performance results of the hybrid DS-TH UWB systems employing the NLMS adaptive detector have been presented in Section 4.4.2. Our studies show that the NLMS adaptive detector is efficient for applying to the pure DS-, pure TH- and hybrid DS-TH UWB system. The BER performance of the NLMS adaptive detector is close to that of the ideal MMSE detector and slightly better than that of the LMS adaptive detector.

- **RLS Adaptive Detector:** The RLS adaptive detector is operated in the principle of least square,

which chooses a weight vector, say $\boldsymbol{w}_1$ to minimize the cost function that consists of the sum of error squares. The algorithm of the RLS adaptive detector is summarised in Table 4.2.3. It can be shown that the RLS adaptive detector employs more controllable parameters, or degrees-of-freedom than the LMS and NLMS adaptive detector. Therefore, when appropriate parameters are applied, the RLS adaptive detector is capable of attaining a higher convergence rate than the LMS or NLMS adaptive detector. The complexity of the RLS adaptive detector has been analyzed in Section 4.3.3, which is found to be $(11(N_cN_\psi + L - 1)^2 + 8(N_cN_\psi + L - 1) + 3)$. Hence, the complexity of the RLS adaptive detector might be very high for the hybrid DS-TH UWB system. Finally, the BER performance results of the hybrid DS-TH UWB systems employing the RLS adaptive detector have been illustrated and analyzed in Section 4.4.3. It can be shown that the RLS adaptive detector is capable of converging to the ideal MMSE detector. The BER performance of the hybrid DS-TH UWB systems using the RLS adaptive detection is very close to that of the hybrid DS-TH UWB systems using ideal MMSE detection. Furthermore, it is shown that the BER performance of the RLS adaptive detector is better than that of the LMS and NLMS adaptive detector.

It has been illustrated [16] that the efficiency of an adaptive detector can be characterised by its convergence speed, BER performance, robustness and implementation complexity. According to the adaptive filter theory [16] and also our study in Chapter 4, the above-mentioned characteristics of adaptive detection are dependent on the length of the traversal filter employed. In general, a longer traversal filter results in lower convergence speed, which, in turn, means that a longer training sequence is required to train the adaptive filter. Consequently, the data-rate and spectral-efficiency of the corresponding communications system decreases. The robustness of an adaptive filter also degrades as the filter length increases, since, in this case the adaptive filter requires to estimate more channel-dependent parameters [16,157,198,199]. Furthermore, as shown in Chapter 4, when a longer adaptive filter is employed, the computational complexity also becomes higher, since more operations are required for the corresponding detection and estimation. Due to the reason as above-mentioned, hence in Chapter 5 reduced-rank techniques are proposed for the adaptive detection of the hybrid DS-TH UWB signals, in order to achieve low-complexity detection in hybrid DS-TH UWB systems. With the reduced-rank detection the number of coefficients to be determined is reduced by projecting the received signal in a higher dimensional observation space to a lower dimensional subspace for detection. In this chapter, three classes of reduced-rank detectors have been investigated in conjuction with the proposed RLS-adaptive detector. The three classes of reduced-rank detectors have been derived based on the principles of PCA, CSM and TPA, respectively. Note that, although reduced-

rank detection has been studied only associated with the RLS adaptive detection scheme, however, these techniques are general and they can be similarly employed associated with LMS and NLMS adaptive detectors. From our analysis and simulation results, the main findings of Chapter 5 can be summarised as below.

- **Principal Component Analysis (PCA):** The PCA-assisted reduced-rank RLS adaptive detector is depended on the eigen-decomposition of the auto-correlation matrix $\boldsymbol{R}_{y_i}$ of the observation vector $\boldsymbol{y}_i$. In this reduced-rank scheme the U number of eigenvectors corresponding to the U largest eigenvalues of $\boldsymbol{R}_{y_i}$ are used to form the detection subspace (or processing matrix) $\boldsymbol{P}_U$. As shown in Section 5.2.2, the PCA-based scheme forms the detection subspace $\boldsymbol{P}_U$ without requiring the knowledge about the user to be detected. The complexity of the PCA-based reduced-rank RLS adaptive detector has been considered in Section 5.3.1, and the number of operations for detecting one bit has been found to be $((\mathcal{T}^2 + 2\mathcal{T} + 2U\mathcal{T} + 11U^2 + 7U + 3 + (\mathcal{T}^3/3 + U\log_2\mathcal{T})/F_L)$, where $\mathcal{T} = (N_cN_\psi + L - 1)$ and F_L denotes the frame-length. Finally, the learning and BER performance of the PCA-based reduced-rank RLS adaptive detector have been studied in Section 5.4.1. Our analysis and performance results show that the PCA-assisted reduced-rank RLS adaptive detector is capable of achieving the BER performance of the full-rank RLS adaptive detector, if the rank U of the detection subspace is not lower than the signal subspace's rank. Hence, the PCA-based scheme may allow a significant reduction of the detection subspace's rank, provided that the dimension of the signal subspace is significantly lower than the rank of the observation space spanned by the received signal $\boldsymbol{y}_i$, which is $(N_cN_\psi + L - 1)$ and may be very big if the total spreading factor and/or the number of resolvable multipaths are high. When this is not the case, for example, when the hybrid DS-TH UWB system supports a high number of users resulting in that the signal subspace's rank exceeds the rank U of the detection subspace, then, mapping the received signal vectors to the detection subspace of rank U is likely to reduce the desired signal components. Consequently, the corresponding PCA-based reduced-rank RLS adaptive detector might conflict severe multiuser interference and the BER performance appears error-floors.

- **Cross Spectral Metric (CSM):** The CSM-based reduced-rank RLS adaptive detector is also depended on the eigen-decomposition of the auto-correlation matrix $\boldsymbol{R}_{y_i}$ of the observation vector $\boldsymbol{y}_i$. As shown in Section 5.2.3, from $(N_cN_\psi + L - 1)$ eigenvectors of $\boldsymbol{R}_{y_i}$, the CSM-based scheme chooses the U eigenvectors having the U largest CSM values as defined in (5.14) to form the detection subspace $\boldsymbol{P}_U$. The detection subspace ob-

tained in this way is the optimum selection of the $\binom{N_c N_\psi + L - 1}{U}$ eigenvectors in MMSE sense for reduction in rank. Hence, the CSM-based rank-reduction technique may be more efficient than the PCA-based rank-reduction technique, since the CSM-based scheme takes into account the energy in the subspace contributed by the desired user. However, as shown in (5.14), the CSM-based reduced-rank scheme requires to invoke the knowledge of $\boldsymbol{h}_1$ and $\boldsymbol{C}_i^{(1)}$ of the desired user, in order to form the detection subspace $\boldsymbol{P}_U$. The complexity of the CSM-assisted reduced-rank RLS adaptive detector has been considered in Section 5.3.2. It has been found that the number of operations for detecting one bit is $(\mathcal{T}^2 + 2\mathcal{T} + 2U\mathcal{T} + 11U^2 + 7U + 3 + ((\mathcal{T}+1)T_L + \mathcal{T}^3/3 + 2\mathcal{T}^2 + U\log_2\mathcal{T})/F_L)$, where T_L represents the number of symbols per frame used for training, in addition to the parameters mentioned previously. Finally, the learning behaviour of the CSM-based reduced-rank RLS adaptive detector and the BER performance of the hybrid DS-TH UWB systems using the CSM-based reduced-rank RLS adaptive detection have been depicted and discussed in Section 5.4.2. From our study and performance results, it can be found that the CSM-assisted reduced-rank RLS adaptive detector may converge faster than the full-rank RLS adaptive detector. Hence, the hybrid DS-TH UWB systems using the CSM-assisted reduced-rank RLS adaptive detection may result in a higher spectral-efficiency than that using the full-rank RLS adaptive detection. The CSM-assisted reduced-rank RLS adaptive detector is capable of achieving the BER performance of the full-rank RLS adaptive detector, when the rank U of the detection subspace reaches a value equivalent to the signal subspace's rank. Hence, like the PCA-based scheme, the CSM-based scheme may also reduce significantly the detection complexity, if the dimension of the signal subspace is significantly lower than that of the observation space spanned by the received signal $\boldsymbol{y}_i$.

- **Taylor Polynomial Approximation (TPA):** In contrast to the above two rank reduction schemes that are depended on the eigen-decomposion, the TPA-assisted reduced-rank adaptive detector forms its detection subspace $\boldsymbol{P}_U$ without depending on the eigen-decomposition of the auto-correlation matrix $\boldsymbol{R}_{y_i}$. Instead, it forms the detection subspace $\boldsymbol{P}_U$ based on the Taylor polynomial expansion of the inverse auto-correlation matrix $\boldsymbol{R}_{y_i}$, as shown in (5.19). Based on (5.19), we can know that the TPA-based reduced-rank scheme requires the knowledge of $\boldsymbol{h}_1$ and $\boldsymbol{C}_i^{(1)}$ of the desired user, in order to form the detection subspace $\boldsymbol{P}_U$. The complexity of the TPA-based reduced-rank RLS adaptive detector has been analysed in Section 5.3.3. It has been found that, if the detection subspace's rank is $U = 1$, the number of

operations required to detect one bit is $(2\mathcal{T} + 21 + ((\mathcal{T} + 1)T_L/F_L))$. However, if the detection subspace's rank is $U > 1$, then the number of operations required to detect one bit is $((\mathcal{T}^2 + 2\mathcal{T} + 2U\mathcal{T} + 11U^2 + 7U + 3) + ((\mathcal{T} + 1)T_L + 2(U - 1)\mathcal{T}^2/F_L))$. Finally, in Section 5.4.3 the learning and BER performance of the TPA-assisted reduced-rank RLS adaptive detector have been provided and analysed. The learning and BER performance results show that the TPA-assisted reduced-rank RLS adaptive detector is a highly efficient detection scheme. It usually does not require a high rank U (in comparison to the signal subspace's rank) to converge to a low MSE and it usually converges very fast. The TPA-assisted reduced-rank RLS adaptive detector is capable of converging to the full-rank RLS adaptive detector's performance with a rank U significantly lower than that of the signal subspace, especially when the signal subspace's rank is high. Furthermore, the detection subspace's rank U needed to achieve the full-rank RLS adaptive detector's performance does not scale with the system size determined by the observation space's dimension, which is $(N_c N_\psi + L - 1)$, and K of the number of users. Additionally, as shown in Tables 5.5 and 5.6, the TPA-based reduced-rank RLS adaptive detector usually has a lower complexity than the PCA- or CSM-based reduced-rank RLS adaptive detector. Owing to its above-mentioned properties, the TPA-assisted reduced-rank RLS adaptive detector may constitute a promising detection scheme for the hybrid DS-TH UWB systems, which may support a big number of users communicating over the UWB channels having a huge number of low-power resolvable multipaths.

Finally, the number of operations required by the various detection schemes for the hybrid DS-TH UWB systems to detect one bit is summarised in Table 6.1. In Table 6.1 the number of operations required by the different detectors to detect one bit is provided in the context of a range of specific cases. For generating Table 6.1, we assumed that the frame-length was $F_L = 1000$ bits, which include $T_L = 160$ training bits. Hence, the spectral efficiency of the hybrid DS-TH UWB systems is 84%, when the full-rank or reduced-rank adaptive detectors are considered. Additionally, in our evaluations the total spreading factor was assumed to be 64, where the DS spreading factor was $N_c = 16$ and the TH-spreading factor was $N_\psi = 4$, respectively. From the data shown in Table 6.1, it can be observed that the number of operations required for detecting one bit is reduced significantly for the LMS and NLMS adaptive detectors as compared to the correlation detector. However, the complexity of the RLS adaptive detector is still very high as compared to the correlation detector but lower than that of the ideal MMSE detector. From the data shown in Table 6.1, it can be observed that the number of operations required for detecting one bit is reduced significantly for the reduced-rank RLS adaptive detection schemes in comparison with that required by the full-rank RLS adaptive detector.

Detection scheme	Number of resolvable multipaths, L	Rank of detection subspace, U	Number of operations for detecting one bit
Correlation detector	15	78	2496
	100	163	32926
Ideal MMSE detector	15	78	176670
	100	163	1523780
LMS adaptive detector	15	78	391
	100	163	816
NLMS adaptive detector	15	78	548
	100	163	1143
RLS adaptive detector	15	78	67551
	100	163	293566
PCA-based reduced-rank RLS adaptive detector	15	1	6575
		8	8428
		15	11391
	100	1	28686
		8	31750
		15	35957
CSM-based reduced-rank RLS adaptive detector	15	1	6600
		8	8453
		15	11416
	100	1	28765
		8	31829
		15	36036
TPA-based reduced-rank RLS adaptive detector	15	1	189
		5	7125
		8	8023
	100	1	373
		5	28601
		8	30144

Table 6.1: Number of operations required for detecting one bit in the hybrid DS-TH UWB systems using various detection schemes to support $K = 5$ users.

All the three reduced-rank RLS adaptive detectors considered have a similar complexity, but, however, the number of operations required by the TPA-based reduced-rank scheme is usually slightly lower than that required by the PCA- or CSM-based reduced-rank scheme, for any given values of U and L. Furthermore, the data in Table 6.1 shows that the complexity of the reduced-rank RLS adaptive detectors is at a similar level as that of the single-user correlation detector, which achieves much worse BER performance than the reduced-rank RLS adaptive detectors considered.

6.2 Future Work

In this section we provide some suggestions for potential future research.

1) In this thesis, the adaptive detectors considered are operated in the principles of MMSE. However, the MMSE detector is optimum only when the conditional probability density function (CDF) of the detector's output when given the transmitted symbol is Gaussian [228]. In pulse-based UWB systems, the CDF of the detector's output given the transmitted symbol is not Gaussian whenever there are multiple users present [25]. Furthermore, when designing a communication system, the ultimate requirement is the BER but not the MMSE. Therefore, adaptive minimum bit error rate (MBER) algorithms may be introduced to the hybrid DS-TH UWB systems in order to enhance the BER performance [228]. Furthermore, the reduced-rank techniques may be proposed for the MBER adaptive detector, in order to reduce its implementation complexity, as shown in Appendix A.

2) In this thesis, since our major emphasis is on the design of low-complexity UWB receivers, hence, when reduced-rank techniques are employed, the detection subspace determined by $\boldsymbol{S}_U$ is estimated during the training stage without updating during the data transmission. However, the detection subspace can be updated after the detection of one or several data bits during the data transmission stage. This joint update of the processing matrix $\boldsymbol{S}_U$ and the weight vector $\boldsymbol{w}$ will help to improve further the spectral-efficiency and the BER performance of the UWB system, but certainly, at the expense of higher complexity.

3) It has been well-recognized that the channel estimation in the pulse-based UWB systems is extremely difficult. Noncoherent techniques do not require channel estimation and allow to capture the majority of the transmitted energy by using simple correlators, even when there exist distortions and multipath propagation. Hence, efficient noncoherent detection techniques may be introduced to the hybrid DS-TH UWB systems, in order to achieve low-complexity detection.

4) In our study in this thesis, no error-control coding has been considered. However, error control coding is genrally employed by any wireless communications systems. Hence, it is important to investigate the achievable BER performance of the hybrid DS-TH UWB systems when certain error-control coding is employed. Furthermore, error-control coding may help to improve the convergence of the adaptive detectors. However, these issues need further research.

5) Multiple antenna and multiple-input and multiple-output (MIMO) as well as space-time processing have found a lot of application in recent years. Multiple antenna and MIMO principles may be applied to the UWB systems in order to boost their capacity. However, introducing multiple antennas to UWB systems will make the system operation even more complex. Hence, it is highly important to investigate the high-efficiency transmission and detection schemes for the multi-antenna UWB systems.

6) Finally, the mathematical performance analysis of the hybrid DS-TH UWB system communicating over various UWB channels is also interesting and highly challenging.

Appendix A

Adaptive Reduced-Rank Minimum Bit Error-Rate Detection for Hybrid Direct-Sequence Time-Hopping Ultrawide Bandwidth System

Pulse-based UWB communications schemes constitute a range of promising alternatives that may be deployed for home, personal-area, sensor network, etc. applications, where the communication devices are required to be low-complexity, high-reliability and minimum power consumption [1]. However, in pulse-based UWB systems the spreading factor is usually very high. The UWB channels are usually very sparse [29], resulting in that a huge number of low-power resolvable multipaths need to be processed at the receiver. As demonstrated in [1, 29], in pulse-based UWB communications the huge number of resolvable multipaths generally consist of a few relatively strong paths and many other weak paths. Unlike in the conventional wideband communications where strong paths usually arrive at the receiver before weak paths, in UWB communications the time-of-arrivals (ToAs) of the strong multipaths are random variables and are not necessary the multipaths arriving at the receiver at the earliest. Due to the above-described issues, therefore, in pulse-based UWB systems it is normally impractical to carry out directly the coherent detection, which depends on accurate channel estimation demanding extreme complexity. In fact, it has been recognized that the complexity might still be extreme, even when the conventional single-user matched-filter (MF) detector [149] is employed. This is because there are a huge number of multipath channels need to be estimated and the detection

complexity is at least proportional to the sum of the spreading factor and the number of resolvable multipaths [90].

In this appendix we consider the low-complexity detection in hybrid DS-TH UWB systems [148, 155], since the hybrid DS-TH UWB scheme is a generalized pulse-based UWB communication scheme, which includes both the pure DS-UWB and the pure TH-UWB as special cases [1, 148, 155]. The detector proposed is an adaptive detector operated in a reduced-rank detection subspace based on the least bit error-rate (LBER) principles [225, 228], which is hence referred to as the reduced-rank adaptive LBER detector. As our forthcoming discourse shown, the reduced-rank adaptive LBER detector does not depend on channel estimation. It achieves its near-optimum detection with the aid of a training sequence at the start of communication and then maintains its near-optimum detection based on the decision-directed (DD) principles during the communication [173]. The reduced-rank adaptive LBER detector does not require the knowledge about the number of resolvable multipaths as well as that about the locations of the strong resolvable multipaths; It only requires the knowledge (which is still not necessary accurate) about the maximum delay-spread of the UWB channels. Furthermore, the reduced-rank adaptive LBER detector is operated in a reduced-rank detection subspace obtained based on the principal component analysis (PCA) [196]. The detection subspace usually has a rank that is significantly lower than that of the original observation space. Owing to the above-mentioned properties of the reduced-rank adaptive LBER detector, we can argue that it is a low-complexity detection scheme, which is feasible for practical implementation.

Note that, in this appendix the LBER algorithm is preferred instead of the conventional least mean-square (LMS) algorithm [16], since, first, the LBER algorithm works under the minimum BER (MBER) principles, which may outperform the LMS algorithm that is operated in minimum mean-square error (MMSE) sense [228]. Second, the LBER algorithm has similar complexity as the LMS algorithm [228]. Furthermore, it has been observed [228] that the LBER algorithm may provide a higher flexibility for system design in comparison with the LMS algorithm.

A.1 Description of Hybrid DS-TH UWB System

The hybrid DS-TH UWB scheme considered in this appendix is the same as that considered in [229], where non-adaptive reduced-rank detection has been investigated.

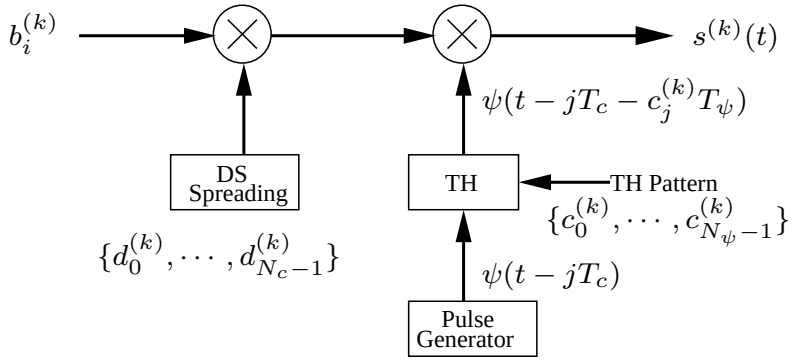

Figure A.1: Transmitter schematic block diagram of hybrid DS-TH UWB system.

A.1.1 Transmitted Signal

The transmitter schematic block diagram for the considered hybrid DS-TH UWB system is shown in Fig. A.1. We assume for simplicity that the hybrid DS-TH UWB system employs the binary phase-shift keying (BPSK) baseband modulation. As shown in Fig. A.1, a data bit of the kth user is first modulated by a N_c-length DS spreading sequence, which generates N_c chips. The N_c chips are then transmitted by N_c time-domain pulses within one symbol-duration, where the positions of the N_c time-domain pulses are determined by the TH pattern assigned to the kth user. Finally, as shown in Fig. A.1, the hybrid DS-TH UWB baseband signal transmitted by the kth user can be written as [148]

$$s^{(k)}(t) = \sqrt{\frac{E_b}{N_c T_\psi}} \sum_{j=0}^{\infty} b_{\left\lfloor \frac{j}{N_c} \right\rfloor}^{(k)} d_j^{(k)} \psi \left[t - jT_c - c_j^{(k)} T_\psi \right] \tag{A.1}$$

where $\lfloor x \rfloor$ represents the largest integer less than or equal to x, $\psi(t)$ is the basic time-domain pulse of width T_ψ, which satisfies $\int_0^{T_\psi} \psi^2(t)dt = T_\psi$. Note that, the bandwidth of the hybrid DS-TH UWB system is approximately equal to the reciprocal of T_ψ of the basic time-domain pulse's width. The other parameters in (A.1) as well as the other parameters used in this appendix are listed as follows:

- E_b: Energy per bit;
- N_c: Number of chips per bit and DS spreading factor;
- N_ψ: Number of time-slots in a chip and TH spreading factor;
- T_b and T_c: Bit-duration and chip-duration, which satisfies $T_b = N_c T_c$;
- T_ψ: Time-domain pulse width or width of a time-slot, which satisfies $T_c = N_\psi T_\psi$;

- $b_i^{(k)} \in \{+1, -1\}$: The ith data bit transmitted by user k;
- $\{d_j^{(k)}\}$: Random binary DS spreading sequence assigned to the kth user;
- $\{c_j^{(k)} \in \{0, 1, \cdots, N_\psi - 1\}\}$: Random TH sequence assigned to the kth user;
- $N_c N_\psi$: Total spreading factor of hybrid DS-TH UWB system.

Note that, both the pure DS-UWB and pure TH-UWB schemes constitute special cases of the hybrid DS-TH UWB scheme. Specifically, if $N_c > 1$ and $N_\psi = 1$, T_ψ and T_c are then equal and in this case the hybrid DS-TH UWB system is reduced to the pure DS-UWB system. By contrast, when $N_c = 1$ and $N_\psi > 1$, the hybrid DS-TH UWB scheme is then reduced to the pure TH-UWB scheme.

A.1.2 Channel Model

In this appendix the Saleh-Valenzuela (S-V) channel model is considered, which has the channel impulse response (CIR) [117]

$$h(t) = \sum_{v=0}^{V-1} \sum_{u=0}^{U-1} h_{u,v} \delta(t - T_v - T_{u,v}) \tag{A.2}$$

where V represents the number of clusters and U denotes the number of resolvable multipaths in a cluster. Hence, the total number of resolvable multipath components can be as high as $L = UV$. In (A.2) $h_{u,v} = |h_{u,v}| e^{j\theta_{u,v}}$ represents the fading gain of the uth multipath in the vth cluster, where $|h_{u,v}|$ and $\theta_{u,v}$ are assumed to obey the Rayleigh distribution [117] and uniform distribution in $[0, 2\pi)$, respectively. In (A.2) T_v denotes the arrival time of the vth cluster and $T_{u,v}$ the arrival time of the uth multipath in the vth cluster. In the considered UWB channel, the average power of a multipath component at a given delay, say at $T_v + T_{u,v}$, is related to the power of the first resolvable multipath of the first cluster through the relation of [117]

$$\Omega_{u,v} = \Omega_{0,0} \exp\left(-\frac{T_v}{\Gamma}\right) \exp\left(-\frac{T_{u,v}}{\gamma}\right) \tag{A.3}$$

where $\Omega_{u,v} = E\left[|h_{u,v}|^2\right]$ represents the power of the u resolvable multipath of the vth cluster, Γ and γ are the respective cluster and ray power decay constants.

According to (A.2), we can know that the maximum delay-spread of the UWB channels considered is $(T_V + T_{U,V})$ and the total number of resolvable multipaths is $L = \lfloor (T_V + T_{U,V})/T_\psi \rfloor + 1$. In

order to make the channel model sufficiently general, in this appendix we assume that the maximum delay spread $(T_V + T_{U,V})$ spans $g \geq 1$ data bits, implying that $(g-1)N_cN_\psi \leq (L-1) < gN_cN_\psi$.

A.1.3 Receiver Structure

Let us assume that the hybrid DS-TH UWB system supports K uplink users. When the K number of DS-TH UWB signals in the form of (A.1) are transmitted over UWB channels having the CIR as shown in (A.2), the received signal at the base-station (BS) can be expressed as

$$r(t) = \sqrt{\frac{E_b}{N_c T_\psi}} \sum_{k=1}^{K} \sum_{v=0}^{V-1} \sum_{u=0}^{U-1} \sum_{j=0}^{MN_c} h_{u,v}^{(k)} b_{\left\lfloor \frac{j}{N_c} \right\rfloor}^{(k)} d_j^{(k)} \times \psi_{rec}\left[t - jT_c - c_j^{(k)} T_\psi - T_v^{(k)} - T_{u,v}^{(k)} - \tau_k\right] + n(t) \quad \text{(A.4)}$$

where $n(t)$ represents an additive white Gaussian noise (AWGN) process, which has zero-mean and a single-sided power spectral density of N_0 per dimension, τ_k takes into account the lack of synchronisation among the user signals as well as the transmission delay, while $\psi_{rec}(t)$ is the received time-domain pulse, which is usually the second derivative of the transmitted pulse $\psi(t)$ [40].

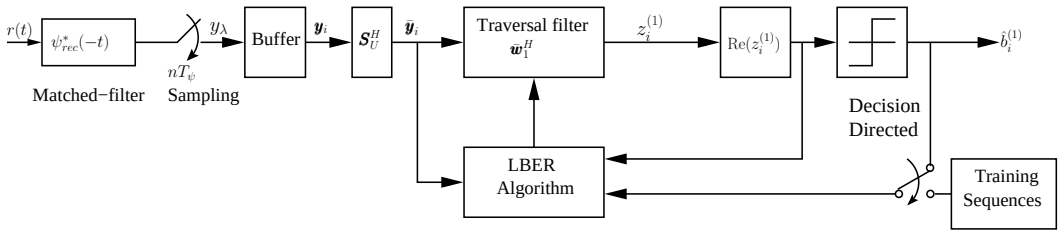

Figure A.2: Receiver schematic block diagram for the hybrid DS-TH UWB systems using reduced-rank adaptive LBER detection.

The receiver schematic block diagram for the hybrid DS-TH UWB using the considered reduced-rank adaptive LBER detection is shown in Fig. A.2. At the receiver, the received signal is first filtered by a MF having an impulse response of $\psi_{rec}^*(-t)$. The output of the MF is then sampled at a rate of $1/T_\psi$. Then, the observation samples are stored in a buffer, which are projected to a reduced-rank detection subspace, once a reduced-rank detection subspace $\boldsymbol{S}_U$ is obtained. Finally, the observations in the detection subspace are input to a traversal filter, which is controlled by the LBER algorithm, in order to generate estimates to the transmitted data bits.

Let us assume that a block of M data bits per user is transmitted. Then, according to Fig. A.2, the detector can collect a total of $(MN_cN_\psi + L - 1)$ number of samples, where $(L-1)$ is due to the

L number of resolvable multipaths. In more details, the λth sample can be obtained by sampling the MF's output at the time instant of $t = T_0 + (\lambda + 1)T_\psi$, which can be expressed as

$$y_\lambda = \left(\sqrt{\frac{E_b T_\psi}{N_c}}\right)^{-1} \int_{T_0+\lambda T_\psi}^{T_0+(\lambda+1)T_\psi} r(t)\psi_{rec}^*(t)dt \tag{A.5}$$

where T_0 denotes the ToA of the first multipath in the first cluster.

In order to reduce the detection complexity of the hybrid DS-TH UWB system, in this appendix we consider only the bit-by-bit based detection. Let the observation vector $\boldsymbol{y}_i$ and the noise vector $\boldsymbol{n}_i$ related to the ith data bit of the first user (reference user) be represented by

$$\boldsymbol{y}_i = [y_{iN_cN_\psi}, y_{iN_cN_\psi+1}, \cdots, y_{(i+1)N_cN_\psi+L-2}]^T \tag{A.6}$$

$$\boldsymbol{n}_i = [n_{iN_cN_\psi}, n_{iN_cN_\psi+1}, \cdots, n_{(i+1)N_cN_\psi+L-2}]^T \tag{A.7}$$

where the elements of $\boldsymbol{n}_i$ are Gaussian random variables distributed with zero-mean and a variance of $\sigma^2 = N_0/2E_b$ per dimension. Then, as shown in [148, 229], $\boldsymbol{y}_i$ can be expressed as

$$\begin{aligned}\boldsymbol{y}_i = &\underbrace{\sum_{k=1}^{K}\sum_{\substack{j=\max(0,i-g)\\ i\neq 0}}^{i-1} \underline{\boldsymbol{C}}_j^{(k)}\boldsymbol{h}_k\boldsymbol{b}_j^{(k)}}_{\text{ISI from the previous bits of } K \text{ users}} + \underbrace{\boldsymbol{C}_i^{(1)}\boldsymbol{h}_1 b_i^{(1)}}_{\text{Desired signal}} + \boldsymbol{n}_i \\ &+ \underbrace{\sum_{k=2}^{K}\boldsymbol{C}_i^{(k)}\boldsymbol{h}_k b_i^{(k)}}_{\text{Multiuser interference}} + \underbrace{\sum_{k=1}^{K}\sum_{\substack{j=i+1\\ i\neq M-1}}^{\min(M-1,i+g)} \bar{\boldsymbol{C}}_j^{(k)}\boldsymbol{h}_k\boldsymbol{b}_j^{(k)}}_{\text{ISI from the latter bits of } K \text{ users}}\end{aligned} \tag{A.8}$$

where the matrices and vectors have been defined in detail in [148, 229]. From (A.8), we observe that the ith data bit conflicts both severe inter-symbol interference (ISI) and multiuser interference (MUI), in addition to the Gaussian background noise.

When the conventional linear detectors without invoking reduced-rank techniques are considered, the decision variable for $b_i^{(1)}$ of the reference user can be expressed as

$$z_i^{(1)} = \boldsymbol{w}_1^H \boldsymbol{y}_i,\ i = 0, 1, \ldots, M-1 \tag{A.9}$$

where $\boldsymbol{w}_1$ is a $(N_cN_\psi + L - 1)$-length weight vector. Since in UWB communications the spreading factor N_cN_ψ might be very high and since the number of resolvable multipath L is usually huge in UWB channels, the vector $\boldsymbol{w}_1$, i.e., the filter length might be very large. Therefore, the com-

plexity of the corresponding detectors might be extreme, even when low-complexity linear detection schemes are considered. Furthermore, using very long filter for detection in UWB systems may significantly degrade the performance of the UWB systems. For example, using a longer traversal filter results in lower convergence speed and, hence, a longer sequence is required for training the filter [16]. Consequently, the data-rate and spectral efficiency of the corresponding communications system decreases. The robustness of an adaptive filter degrades as the filter length increases, since more channel-dependent variables are required to be estimated [172]. Furthermore, when a longer adaptive filter is employed, the computational complexity is also higher, since more operations are required for the corresponding detection and estimation. Therefore, in this appendix the reduced-rank adaptive LBER detector is proposed, in order to achieve low-complexity detection in hybrid DS-TH UWB systems.

A.2 Reduced-Rank Adaptive Least Bit-Error-Rate Detector

In reduced-rank detection the number of coefficients to be determined is reduced through projecting the received signals to a lower dimensional detection subspace [196]. Specifically, let $\boldsymbol{P}_U$ be an $((N_c N_\psi + L - 1) \times U)$ processing matrix with its U columns forming a U-dimensional subspace, where $U < (N_c N_\psi + L - 1)$. Then, for a given received vector $\boldsymbol{y}_i$, the U-length vector in the detection subspace can be expressed as

$$\bar{\boldsymbol{y}}_i = \underbrace{(\boldsymbol{P}_U^H \boldsymbol{P}_U)^{-1} \boldsymbol{P}_U^H}_{\boldsymbol{S}_U^H} \boldsymbol{y}_i \tag{A.10}$$

where an over-bar is used to indicate that the argument is in the reduced-rank detection subspace.

In this appendix, the PCA-assisted reduced-rank technique [196, 230] is employed for obtaining the processing matrix: Given the rank U of the detection subspace, the U number of eigenvectors corresponding to the U largest eigenvalues of the autocorrelation matrix of $\boldsymbol{y}_i$ are utilised to form the processing matrix $\boldsymbol{P}_U$ [230]. In more detail, the auto-correlation matrix of $\boldsymbol{y}_i$ can be represented using eigen-analysis as

$$\boldsymbol{R}_{y_i} = E[\boldsymbol{y}_i \boldsymbol{y}_i^H] = \boldsymbol{\Phi} \boldsymbol{\Lambda} \boldsymbol{\Phi}^H \tag{A.11}$$

where $\mathbf{\Lambda}$ is a diagonal matrix given by

$$\mathbf{\Lambda} = \text{diag}\{\lambda_1, \lambda_2, \cdots, \lambda_{N_c N_\psi + L - 1}\} \tag{A.12}$$

which contains the eigenvalues of $\boldsymbol{R}_{y_i}$, while $\mathbf{\Phi}$ is an unitary matrix consisting of the eigenvectors of $\boldsymbol{R}_{y_i}$, which can be written as

$$\mathbf{\Phi} = [\boldsymbol{\phi}_1, \boldsymbol{\phi}_2, \cdots, \boldsymbol{\phi}_{N_c N_\psi + L - 1}] \tag{A.13}$$

where $\boldsymbol{\phi}_i$ is the eigenvector corresponding to the eigenvalue λ_i.

Let assume that the eigenvalues are arranged in descent order obeying $\lambda_1 \geq \lambda_2 \geq \cdots \geq \lambda_{N_c N_\psi + L - 1}$. Then, the processing matrix $\boldsymbol{P}_U$ in the context of PCA-assisted reduced-rank technique is constructed by the first U columns of $\mathbf{\Phi}$, ie., we have $\boldsymbol{P}_U = [\boldsymbol{\phi}_1, \boldsymbol{\phi}_2, \cdots, \boldsymbol{\phi}_U]$.

Given the observations in the detection subspace as shown in (A.10), the linear detection of $b_i^{(1)}$ can be carried out by forming the decision variable

$$z_i^{(1)} = \bar{\boldsymbol{w}}_1^H \bar{\boldsymbol{y}}_i \tag{A.14}$$

where $\bar{\boldsymbol{w}}_1$ is now an U-length weight vector. According to the theory of the PCA-based reduced-rank detection [196], the full-rank BER performance can be achieved, provided that the rank U of the detection subspace is not lower than the rank of the signal subspace, which for our hybrid DS-TH UWB system is $K(g+1)$. However, if the rank of the detection subspace is lower than the signal subspace's rank, the reduced-rank detection then conflicts MUI. Consequently, the BER performance of the hybrid DS-TH UWB system using the PCA-based reduced-rank detection deteriorate, in comparison with the full-rank BER performance. Therefore, in the PCA-based reduced-rank detection it is important to have the knowledge about the signal subspace's rank. Note that, in our simulations considered in Section A.3, the signal subspace's rank was estimated through eigen-analysis of the autocorrelation matrix $\boldsymbol{R}_{y_i}$, which was estimated with the aid of a block of data bits.

In (A.14) the weight vector $\bar{\boldsymbol{w}}_1$ can be obtained with the aid of the sample-by-sample adaptive LBER algorithm proposed in [225]. In our reduced-rank adaptive LBER detector for the hybrid DS-TH UWB systems, the reduced-rank adaptive LBER is operated in two modes, namely, the training mode and the decision-directed (DD) mode, respectively. When operated in the training mode, the weight vector $\bar{\boldsymbol{w}}_1$ is adjusted with the aid of a training sequence, which is known to the receiver.

Correspondingly, the update equation in the LBER principle can be expressed as [228]

$$\bar{\boldsymbol{w}}_1(n+1) = \bar{\boldsymbol{w}}_1(n) + \mu \frac{\text{sgn}(b_i^{(1)}(n))}{2\sqrt{2\pi}\rho_n} \times \exp\left(-\frac{|\Re(z_i^{(1)}(n))|^2}{2\rho_n^2}\right) \bar{\boldsymbol{y}}_i(n),\ n = 1, 2, \ldots \tag{A.15}$$

where $\text{sgn}(x)$ is a sign-function, μ is the step-size and ρ_n is the so-called kernel width [228]. In the adaptive LBER algorithm, the step-size μ and the kernel width ρ_n are required to be set appropriately, in order to obtain a high convergence rate as well as a small and steady BER misadjustment. Furthermore, it has been observed [228] that the above-mentioned two parameters can provide a higher flexibility for system design in comparison with the adaptive LMS algorithm, which employs only single adjustable parameter of the step-size [16].

When the training stage is completed and the normal data transmission is started, the reduced-rank adaptive LBER detector is then switched to the DD mode. Under the DD mode, the estimated data bits by the receiver are fed back to the adaptive LBER filter, which is then updated in the LBER principle. Specifically, during the DD mode the update equation can be expressed as

$$\bar{\boldsymbol{w}}_1(n+1) = \bar{\boldsymbol{w}}_1(n) + \mu \frac{\text{sgn}(\hat{b}_i^{(1)}(n))}{2\sqrt{2\pi}\rho_n} \times \exp\left(-\frac{|\Re(z_i^{(1)}(n))|^2}{2\rho_n^2}\right) \bar{\boldsymbol{y}}_i(n),\ n = 1, 2, \ldots \tag{A.16}$$

where the estimate $\hat{b}_i^{(1)}$ is given by

$$\hat{b}_i^{(1)} = \text{sgn}(\Re\{z_i^{(1)}\}),\ i = 0, 1, \ldots, M-1 \tag{A.17}$$

Let us now provide our simulation results in the next section.

A.3 Simulation Results and Discussion

In this section the learning and BER performance of the reduced-rank adaptive LBER detector is investigated by simulations. In our simulations the total spreading factor was assumed to be a constant of $N_c N_\psi = 64$, where the DS-spreading factor was set to $N_c = 16$ and the TH-spreading factor was hence $N_\psi = 4$. The normalised Doppler frequency-shift of the UWB channels was fixed to $f_d T_b = 0.0001$. In our simulations the S-V channel model used in [117] was considered and the

channel gains were assumed to obey the Rayleigh distribution. In more detail, the parameters of the S-V channel model used in our simulations are summarized in the following Table.

$1/\Lambda$	Γ	γ
14.11 ns	2.63 ns	4.58 ns

Table A.1: Parameters for the S-V channel model used in simulations.

Fig. A.3 shows the ensemble-average squared error-rate (SER) learning curve of the reduced-rank adaptive LBER detector for the hybrid DS-TH UWB system supporting $K = 5$ users, when different step-size values are considered. Note that, the SER drawn in Fig. A.3 is defined as

$$\text{SER} = \left| \frac{\text{sgn}(b_i^{(1)}(n))}{2\sqrt{2\pi}\rho_n} \exp\left(-\frac{|\Re(z_i^{(1)}(n))|^2}{2\rho_n^2} \right) \right|^2 \tag{A.18}$$

which is proportional to the BER achieved by the reduced-rank adaptive LBER detector. In our simulations the signal-to-noise ratio (SNR) per bit was set to $E_b/N_0 = 10$dB, the ensemble-average SER was obtained from the average over 2000 independent realizations, the weight vector was initialized to $\bar{\boldsymbol{w}}(0) = \mathbf{1}$ of an all-one vector, and the rank of the detection subspace was chosen as $U = 20$. It can be observed from Fig. A.3 that the convergence speed of the reduced-rank adaptive LBER detector is depended on the step-size μ. Explicitly, there exists an optimum step-size value, which results in that the reduced-rank adaptive LBER detector converges to the lowest BER. As shown in Fig. A.3, when an inappropriate step-size is used, the convergence speed may become lower and the reduced-rank adaptive LBER detector may converge to a relatively higher SER.

Fig. A.4 shows the BER versus SNR per bit performance of the hybrid DS-TH UWB system using reduced-rank adaptive LBER detection, when communicating over the UWB channels experiencing correlated Rayleigh fading. The hybrid DS-TH UWB system considered supported $K = 5$ users and the normalised Dopper frequency-shift was assumed to be $f_d T_b = 0.0001$. Furthermore, we assumed that $g = 1$, implying that the desired bit conflicts ISI from one bit transmitted before the desired bit and also from one bit transmitted after the desired bit. Note that, given the parameters as shown in the caption of the figure, it can be shown that the rank of the signal subspace is $K(g+1) = 10$. From the results of Fig. A.4, we observe that, when the rank of the detection subspace is lower than that of the signal subspace, i.e., when $U \leq 10$, the BER performance of the hybrid DS-TH UWB system improves, as the rank of the detection subspace increases. The best BER performance is attained, when the rank of the detection subspace reaches the rank of the signal subspace. When the rank of

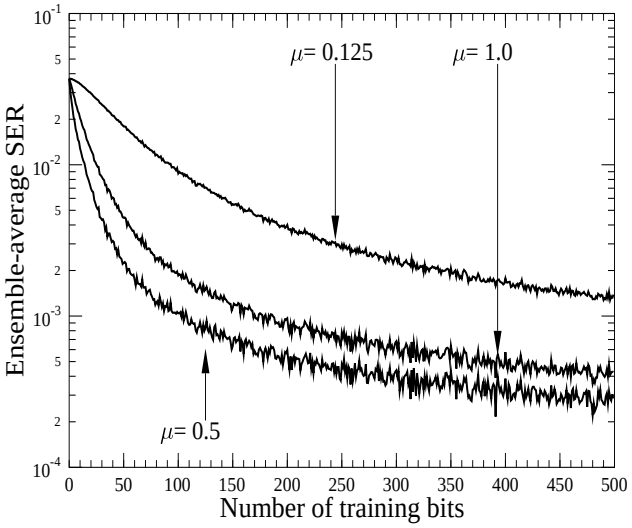

Figure A.3: Learning curves of the reduced-rank adaptive LBER detector for the hybrid DS-TH UWB system supporting $K = 5$ users, when the detection subspace has a rank of $U = 20$. The parameters used in the simulations were $E_b/N_0 = 10$dB, Doppler frequency-shift of $f_d T_b = 0.0001$, $\rho_n = \sqrt{10}\sigma_n$, $g = 1$, $N_c = 16$, $N_\psi = 4$ and $L = 15$.

the detection subspace is higher than that of the signal subspace, no further SNR gain is achievable. Furthermore, when the rank of the detection subspace is lower than that of the signal subspace, error-floor is observed, explaining that the MUI cannot be fully suppressed by the reduced-rank adaptive LBER detector.

Fig. A.5 shows the BER versus SNR per bit performance of the hybrid DS-TH UWB system using reduced-rank adaptive LBER detection, when communicating over the UWB channels experiencing correlated Rayleigh fading, which results in severe ISI. In contrast to Fig. A.4, where we assumed that $g = 1$ and the number of resolvable multipaths was $L = 15$, in the context of Fig. A.5 we assumed that $g = 3$ and $L = 150$. The other parameters used for Fig. A.5 were the same as those used for Fig. A.4. Note that, for the parameters considered in Fig. A.5, the rank of the signal subspace is $K(g + 1) = 20$. Again, as the results of Fig. A.5 shown, the BER performance improves as the rank of the detection subspace increases, until it reaches the rank of the signal subspace. In comparison with Fig. A.4, we can see that, for a given E_b/N_0 value, the full-rank BER shown in Fig. A.5 is lower than the corresponding full-rank BER shown in Fig. A.4. This is because the UWB channel considered associated with Fig. A.5 has $L = 150$ number of resolvable multipaths, which results in a higher diversity gain than the UWB channel considered associated with Fig. A.4, which has $L = 15$

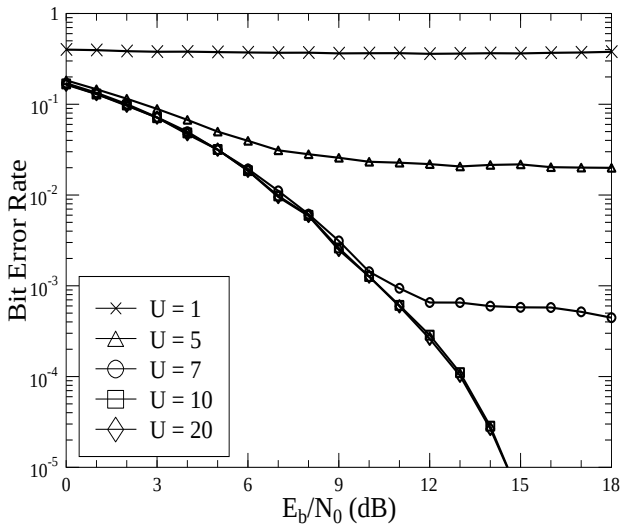

Figure A.4: BER performance of the hybrid DS-TH UWB systems using reduced-rank adaptive LBER detection, when communicating over the UWB channels modelled by the S-V channel model associated with correlated Rayleigh fading. The parameters used in the simulations were $K = 5$, $f_d T_b = 0.0001$, $\mu = 0.5$, $\rho_n = \sqrt{10}\sigma_n$, $g = 1$, $N_c = 16$, $N_\psi = 4$ and $L = 15$. The frame length was fixed to 1000 bits, where the first 160 bits were used for training.

number of resolvable multipaths.

A.4 Summary and Conclusions

In conclusions, our study and simulation results show that the reduced-rank adaptive LBER detector constitutes one of the efficient detectors for the hybrid DS-TH UWB systems. The reduced-rank technique can be employed for achieving low-complexity detection in the DS-TH UWB systems and for improving their efficiency. The reduced-rank adaptive LBER detector is capable of achieving the full-rank BER performance with the detection subspace having a rank that is significantly lower than $(N_c N_\psi + L - 1)$ of the original observation space.

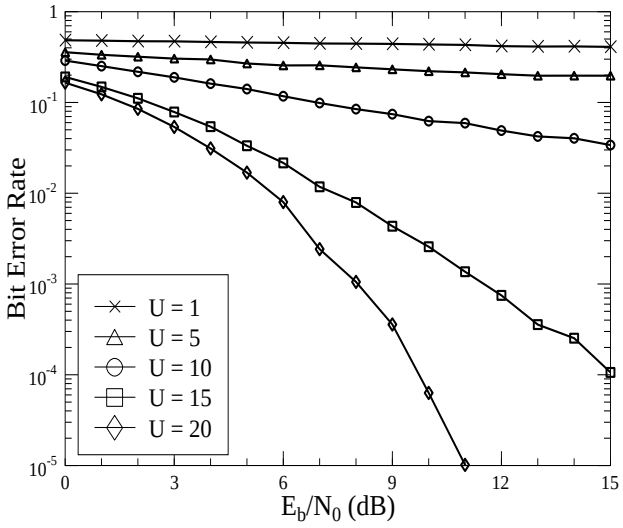

Figure A.5: BER performance of the hybrid DS-TH UWB systems using reduced-rank adaptive LBER detection, when communicating over the UWB channels modelled by the S-V channel model associated with correlated Rayleigh fading. The parameters used in the simulations were $K = 5$, $f_d T_b = 0.0001$, $\mu = 0.5$, $\rho_n = \sqrt{10}\sigma_n$, $g = 3$, $N_c = 16$, $N_\psi = 4$ and $L = 150$. The frame length was fixed to 1000 bits, where the first 160 bits were used for training.

Glossary

ADC	Analog-to-Digital Converter
AWGN	Additive White Gaussian Noise
BER	Bit Error Rate
BPSK	Binary Phase Shift Keying
CDMA	Code Division Multiplexing Access
CIR	Channel Impulse Response
CMF	Conventional Matched Filter
CP	Cyclic Prefix
CSI	Channel State Information
CSM	Cross-Spectral Metric
DD	Decision-Directed
DS	Direct Sequences
DS-TH	Direct-Sequence Time-Hopping
EASE	Ensemble-Average Squared Error
FCC	Federal Communications Commission
FFT	Fast Fourier transform

FH	Frequency Hopping
FTH	Fast Time Hopping
GHz	GigaHertz
GMSP	Gaussian Modified Sinusoidal Pulses
GP	Gaussian Pulses
GPS	Global Positioning System
GSM	Global System for Mobiles
HF	High Frequency
HP	Hermite Polynomial
IPI	Inter Pulse Interference
ISI	Inter Symbol Interference
LANL	Los Alamos National Laboratories
LF	Low Frequency
LLNL	Lawrence Livermore National Laboratories
LMS	Least Mean Square
LOS	Line Of Sight
LR-WPAN	Low-Rate Wireless Personal Area Network
LTI	Linear Time Invariant
MA	Multiple Access
MAI	Multiple Access Interference
MBOK	M-ary Bi-Orthogonal Keying
MDP	Multipath Delay Profile
MF	Matched-Filtering

MHz	MegaHertz
MMSE-MUD	Minimum Mean Square Error Multi-User Detector
MPPM	M-ary Pulse Position Modulation
MSE	Mean Square Error
MUI	Multi-User Interference
NBI	Narrow Band Interference
NLMS	Normalised Least Mean Square
ns	nanoseconds
OFDM	Orthogonal Frequency Divison Multiplexing
OOK	On-Off Keying
PAM	Pulse Amplitude Modulation
PAN	Personal Area Networks
PAPR	Peak-to-Average Power Ratio
PCA	Principal Components Analysis
PCTH	Pseudo-Chaotic Time-Hopping
PDF	Probability Density Function
PN	Pseudo-Noise
PPM	Pulse Position Modulation
PS	Prolate Spheroidal
PSD	Power Spectral Density
PSM	Pulse Shape Modulation
QoS	Quality-of-Services
QPSK	Quadrature Phase-Shift Keying

RLS	Recursive Least Square
S-V	Saleh-Valenzuela
SINR	Signal-to-Interference-plus-Noise Ratio
SNR	Signal-to-Noise Ratio
STDL	Statistical Tapped Delay Line
STH	Slow Time Hopping
TESM	Triangular enveloped sinusoidal monocycle
TH	Time Hopping
THMA	Time Hopping Multiple Access
TPA	Taylor Polynomial Approximation
UMTS	Universal Mobile Telecommunications System
USAF	United States Air Force
UWB	UltraWide Bandwidth
WSN	Wireless Sensor Networks
ZP	Zero Padding

Bibliography

[1] J. H. Reed, *An Introduction to Ultra Wideband Communication Systems*. Prentice Hall, 2005.

[2] F. Nekooger, *Ultra-Wideband Communications: Fundamentals and Applications*. Prentice Hall, 2005.

[3] W. P. Siriwongpairat and K. J. R. Liu, *Ultra-wideband Communications Systems Multiband OFDM approach*. John Wiley and Sons, 2008.

[4] M. Ghavami, L. B. Michael, and R. Kohno, *Ultra Wideband signals and systems in communication engineering*. John Wiley and Sons, Ltd, 2 ed., 2007.

[5] S. Wood and R. Aiello, *Essentials of UWB*. Cambridge University Press, 2008.

[6] M. Z. Win, D. Dardari, A. F. Molisch, W. Wiesbeck, and J. Zhang, "History and applications of UWB," *Proceedings of the IEEE*, vol. 97, pp. 198–204, February 2009.

[7] M. G. D. Benedetto, T. Kaiser, A. F. Molisch, I. Oppermann, C. Politano, and D. Porcino, *UWB Communication Systems A Comprehensive Overview*. Hindawi Publishing Corporation, 2006.

[8] X. Shen, M. Guizani, R. C. Qiu, and T. Le-Ngoc, *Ultra-wideband wireless communications and networks*. Wiley, 2006.

[9] J. A. Gutierrez, M. Naeve, E. Callaway, M. Bourgeois, V. Mitter, and B. Heile, "IEEE 802.15.4: a developing standard for low-power low-cost wireless personal area networks," *IEEE Network*, vol. 15, pp. 12–19, September–October 2001.

[10] S. Gezici, T. Zhi, G. B. Giannakis, H. Kobayashi, A. F. Molisch, H. V. Poor, and Z. Sahinoglu, "Localization via ultra-wideband radios: a look at positioning aspects for future sensor networks," *IEEE Signal Processing Magazine*, vol. 22, pp. 70–84, July 2005.

[11] J. Zhang, P. V. Orlik, Z. Sahinoglu, A. F. Molisch, and P. Kinney, "UWB systems for wireless sensor networks," *Proceedings of the IEEE*, vol. 97, pp. 313–331, February 2009.

[12] J. D. Taylor, *Ultra-wideband Radar Technology*. CRC Press, 2001.

[13] A. F. Molisch, "Ultrawideband propagation channels-theory measurement and modeling," *IEEE Transactions on Vehicular Technology*, vol. 54, pp. 1528–1545, September 2005.

[14] L. Yang and G. B. Giannakis, "Ultra-wideband communications: an idea whose time has come," *IEEE Signal Processing Magazine*, vol. 21, pp. 26–54, November 2004.

[15] M. Chiani and A. Giorgetti, "Coexistence between UWB and narrow-band wireless communication systems," *Proceedings of the IEEE*, vol. 97, pp. 231–254, February 2009.

[16] S. Haykin, *Adaptive Filter Theory*. Prentice Hall, 4 ed., 2002.

[17] B. Sklar, *Digital Communications Fundamentals and Applications*. Prentice Hall, 1988.

[18] T. M. Cover and J. A. Thomas, *Elements of Information Theory*. Wiley Series in Telecommunications and Signal Processing, 2nd ed., 2006.

[19] C.-C. Chong, F. Watanabe, and H. Inamura, "Potential of UWB technology for the next generation wireless communications," in *IEEE Ninth International Symposium on Spread Spectrum Techniques and Applications*, (Manaus-Amazon), pp. 422–429, August 2006.

[20] J. C. Adams, W. Gregorwich, L. Capots, and D. Liccardo, "Ultra-wideband for navigation and communications," in *IEEE Proceedings Aerospace Conference,*, vol. 2, (Big Sky, MT), pp. 785–2, March 2001.

[21] R. Giuliano and F. Mazzenga, "On the coexistence of power-controlled ultrawide-band systems with UMTS, GPS, DCS1800 and fixed wireless systems," *IEEE Transactions on Vehicular Technology*, vol. 54, pp. 62–81, January 2005.

[22] L. Fullerton, "UWB waveforms and coding for communications and radar," in *National Telesystems Conference, NTC*, (Atlanta, GA), pp. 139–141, March 1991.

[23] G. M. Maggio, N. Rulkov, and L. Reggiani, "Pseudo-chaotic time hopping for UWB impulse radio," *IEEE Transactions on Circuits and Systems I: Fundamental Theory and Applications*, vol. 48, pp. 1424–1435, December 2001.

[24] M. Z. Win and R. Scholtz, "Impulse radio: how it works," *IEEE Communications Letters*, vol. 2, pp. 36–38, February 1998.

[25] M. Z. Win and R. Scholtz, "Ultra-wide bandwidth time-hopping spread-spectrum impulse radio for wireless multiple-access communications," *IEEE Transactions on Communications*, vol. 48, pp. 679–689, April 2000.

[26] X. Huang and Y. Li, "Performances of impulse train modulated ultra-wideband systems," in *IEEE International Conference on Communications, ICC*, vol. 2, (St.-Petersburg, Russia), pp. 758–762, April–May 2002.

[27] M. Mahfouz, A. Fathy, Y. Yang, E. E. Ali, and A. Badawi, "See-through-wall imaging using ultra wideband pulse systems," in *34th Proceedings of Applied Imagery and Pattern Recognition Workshop*, (Washington, DC), October 2005.

[28] L. Ma, Z. Zhang, and X. Tan, "A Novel Through-Wall Imaging Method Using Ultra WideBand Pulse System," in *International Conference on Intelligent Information Hiding and Multimedia Signal Processing, IIH-MSP*, (Pasadena,CA), pp. 147–150, December 2006.

[29] A. F. Molisch, J. R. Foerster, and M. Pendergrass, "Channel models for ultrawideband personal area networks," *IEEE Wireless Communications*, vol. 10, pp. 14–21, December 2003.

[30] W. Hirt, "Ultra-wideband radio technology: overview and future research," *Elsevier Journal in Computer Cummunications*, vol. 26, pp. 46–52, 2003.

[31] R. J. Fontana, "Recent system applications of short-pulse ultra-wideband (UWB) technology," *IEEE Transactions on Microwave Theory and Techniques*, vol. 52, pp. 2087–2104, September 2004.

[32] R. A. Scholtz, D. M. Pozar, and W. Namgoong, "Ultra-Wideband Radio," *Eurasip Journal on Applied Signal Processing*, vol. 3, pp. 252–272, 2005.

[33] T. W. Barrett, "History of Ultrawideband (UWB) Radar and Communicatons:Pioneers and Innovators," *Progress In Electromagnetics Symposium (PIERS2000), Cambridge, MA*, July 2000.

[34] R. A. Scholtz, "Multiple access with time-hopping impulse modulation," in *IEEE Military Communications Conference, MILCOM*, vol. 2, (Boston, MA), pp. 447–450, October 1993.

[35] E. Fishler and H. V. Poor, "Low Complexity Multiuser Detectors for Time-Hopping Impulse Radio Systems," *IEEE Transactions on Signal Processing*, vol. 52, pp. 2561–2571, September 2004.

[36] M. Hamalainen, V. Hovinen, R. Tesi, J. H. J. Iinatti, and M. Latva-aho, "On the UWB system coexistence with GSM900, UMTS/WCDMA and GPS," *IEEE Journal on Selected Areas in Communications*, vol. 20, no. 9, pp. 1712–1721, 2002.

[37] B. Hu and N. C. Beaulieu, "Pulse shaping in UWB communication systems," in *IEEE 60th Vehicular Technology Conference, VTC-Fall*, vol. 7, (Los Angeles, CA), pp. 5175–5179, September 2004.

[38] B. Hu and N. C. Beaulieu, "Pulse shapes for ultrawideband communication systems," *IEEE Transactions on Wireless Communications*, vol. 4, pp. 1789–1797, July 2005.

[39] N. C. Beaulieu and B. Hu, "On Determining a Best Pulse Shape for Multiple Access Ultra-Wideband Communication Systems," *IEEE Transactions on Wireless Communications*, vol. 7, pp. 3589–3596, September 2008.

[40] J. Zhang, T. D. Abhayapala, and R. A. Kennedy, "Role of pulses in ultra wideband systems," in *IEEE International Conference on Ultra-Wideband, ICU*, (Zurich, Switzerland), pp. 565–570, September 2005.

[41] L. E. Miller, "Models for UWB pulses and their effects on narrowband direct conversion receivers," in *IEEE Conference on Ultra Wideband Systems and Technologies, UWBST*, (Reston, VA), pp. 101–105, November 2003.

[42] N. C. Beaulieu and B. Hu, "A Novel pulse design algorithm for ultra-wideband communications," in *IEEE Global Telecommunications Conference, GLOBECOMM*, vol. 5, (Dallas, Texas), pp. 3220–3224, November–December 2004.

[43] T. S. Rappaport, *Wireless Communications Principles and Practice*. Prentice Hall, 1999.

[44] K. P. Wallace, A. B. Parr, B. L. Cho, and Z. Ding, "Performance analysis of a spectrally compliant ultra-wideband pulse design," *IEEE Transactions on Wireless Communications*, vol. 4, pp. 2172–2181, September 2005.

[45] R. C. Qiu, H. Liu, and X. Shen, "Ultra-wideband for multiple access communications," *IEEE Communications Magazine*, vol. 43, pp. 80–87, February 2005.

[46] B. Godara, G. Blamon, and A. Fabre, "UWB: A New Efficient Pulse Shape and its Corresponding Simple Transceiver," in *2nd International Symposium on Wireless Communication Systems, ISWCS*, (Siena, Italy), pp. 365–369, September 2005.

[47] B. Parr, B. Cho, K. Wallace, and Z. Ding, "A Novel ultra-wideband pulse design algorithm," *IEEE Communications Letters*, vol. 7, pp. 219–221, May 2003.

[48] H. Sheng, P. Orlik, A. M. Haimovich, L. J. Cimini, and JinyunZhang, "On the spectral and power requirements for ultra-wideband transmission," in *IEEE International Conference on Communications, ICC*, vol. 1, (Anchorage, Alaska), pp. 738–742, May 2003.

[49] J. G. Proakis, *Digital Communications*. Mcgraw Hill, 4 ed., 2000.

[50] N. Krishnapura, S. Pavan, C. Mathiazhagan, and B. Ramamurthi, "A baseband pulse shaping filter for Gaussian minimum shift keying," in *IEEE International Symposium on Circuits and Systems, ISCAS*, vol. 1, (Monterey, CA), pp. 249–252, May-June 1998.

[51] H. Kim and Y. Joo, "Fifth-derivative Gaussian pulse generator for UWB system," in *IEEE Radio Frequency integrated Circuits (RFIC) Symposium*, (Long Beach, CA), pp. 671–674, June 2005.

[52] L. B. Michael, M. Ghavami, and R. Kohno, "Multiple pulse generator for ultra-wideband communication using Hermite polynomial based orthogonal pulses," in *IEEE Conference on Ultra Wideband Systems and Technologies, UWBST*, (Baltimore, Maryland), pp. 47–51, May 2002.

[53] N. C. Beaulieu and B. Hu, "A pulse design paradigm for ultra-wideband communication systems," *IEEE Transactions on Wireless Communications*, vol. 5, pp. 1274–1278, June 2006.

[54] A. F. Molisch, J. Zhang, and M. Miyake, "Time hopping and frequency hopping in ultrawideband systems," in *IEEE Pacific Rim Conference on Communications, Computers and Signal Processing, PACRIM*, vol. 2, (Victoria, Canada), pp. 541–544, August 2003.

[55] M. Hamalainen, J. Iinatti, I. Oppermann, M. Latva-aho, J. Saloranta, and A. Isola, "Coexistence measurements between UMTS and UWB systems," in *IEE Proceedings in Communications*, vol. 153, pp. 153–158, February 2006.

[56] M. L. Welborn, "System considerations for ultra-wideband wireless networks," in *IEEE Radio and Wireless Conference, RAWCON*, (Waltham, MA), pp. 5–8, August 2001.

[57] M. Welborn and J. McCorkle, "The importance of fractional bandwidth in ultra-wideband pulse design," in *IEEE International Conference on Communications, ICC*, vol. 2, (St.-Petersburg, Russia), pp. 753–757, April–May 2002.

[58] J. A. N. da Silva and M. L. R. de Campos, "Performance comparison of binary and quaternary UWB modulation schemes," in *Global Telecommunications Conference, GLOBECOM*, vol. 2, (San Francisco, CA), pp. 789–793, December 2003.

[59] G. Durisi and S. Benedetto, "Performance evaluation and comparison of different modulation schemes for UWB multiaccess systems," in *IEEE International Conference on Communications, ICC*, vol. 3, (Anchorage, Alaska), pp. 2187–2191, May 2003.

[60] M. Hamalainen, R. Tesi, J. Iinatti, and V. Hovinen, "On the performance comparison of different UWB data modulation schemes in AWGN channel in the presence of jamming," in *IEEE Radio and Wireless Conference, RAWCON*, (Boston, MA), pp. 83–86, August 2002.

[61] S. Erkucuk and D. I. Kim, "Power spectral density characteristics of MCSK based impulse radios in UWB communications," in *IEEE 61st Vehicular Technology Conference, VTC-Spring.*, vol. 2, (Melbourne, Australia), pp. 1391–1395, May–June 2005.

[62] A. Batra, J. Balakrishnan, G. R. Aiello, J. R. Foerster, and A. Dabak, "Design of a multiband OFDM system for realistic UWB channel environments," *IEEE Transactions on Microwave Theory and Techniques*, vol. 52, pp. 2123–2138, September 2004.

[63] M. Sablatash, "Pulse Shaping, Modulation and Spectrum Shaping for UWB Wireless Communications and the Effects on Interference for Single and Multiband Transmission of UWB Signals," in *Canadian Conference on Electrical and Computer Engineering*, (Ottawa, Ont.), pp. 1640–1645, May 2006.

[64] C. J. L. Martret and G. B. Giannakis, "All-digital PPM impulse radio for multiple-access through frequency-selective multipath," in *IEEE Proceedings of the Sensor Array and Multichannel Signal Processing Workshop. 2000*, (Cambridge, MA), pp. 22–26, March 2000.

[65] C. N. Georghiades, "On PPM sequences with good autocorrelation properties," *IEEE Transactions on Information Theory*, vol. 34, pp. 571–576, May 1988.

[66] F. Ramirez-Mireles, "Performance of ultrawideband SSMA using time hopping and M-ary PPM," *IEEE Journal on Selected Areas in Communications*, vol. 19, pp. 1186–1196, June 2001.

[67] F. Ramirez-Mireles, "Multiple access with ultra wideband impulse radio modulation using spread spectrum time hopping and block waveform pulse position modulated signals," *Ph.D. Dissertation,Communication Sciences Institute Electrical Engineering Department,University of Southern California*, 1998.

[68] A. A. D'Amico, U. Mengali, and L. Taponecco, "Impact of MAI and channel estimation errors on the performance of rake receivers in UWB communications," *IEEE Transactions on Wireless Communications*, vol. 4, pp. 2435–2440, September 2005.

[69] C. J. L. Martret and G. B. Giannakis, "All-digital PAM impulse radio for multiple-access through frequency-selective multipath," in *IEEE Global Telecommunications Conference, GLOBECOM*, vol. 1, (San Francisco, CA), pp. 77–81, November–December 2000.

[70] M. D'Souza and A. Postula, "Novel ultra-wideband pulse spectrum modulation scheme," in *IEEE Conference on Ultra Wideband Systems and Technologies, UWBST*, (Reston, VA), pp. 240–244, November 2003.

[71] X. Chu and R. D. Murch, "Multidimensional modulation for ultra-wideband multiple-access impulse radio in wireless multipath channels," *IEEE Transactions on Wireless Communications*, vol. 4, pp. 2373–2386, September 2005.

[72] L.-L. Yang and L. Hanzo, "Residue Number system assisted fast frequency-hopped synchronous ultra-wideband spread-spectrum multiple-access: a design alternative to impulse radio," *IEEE Journal on Selected Areas in Communications*, vol. 20, pp. 1652–1663, December 2002.

[73] M. Z. Win, R. A. Scholtz, and L. W. Fullerton, "Time-hopping SSMA techniques for impulse radio with an analog modulated data subcarrier," in *IEEE 4th International Symposium on Spread Spectrum Techniques and Applications Proceedings*, vol. 1, (Mainz, Germany), pp. 359–364, September 1996.

[74] D. C. Laney, G. M. Maggio, F. Lehmann, and L. Larson, "Multiple access for UWB impulse radio with pseudochaotic time hopping," *IEEE Journal on Selected Areas in Communications*, vol. 20, pp. 1692–1700, December 2002.

[75] M. J. Sushchik, N. Rulkov, L. Larson, L. Tsimrin, H. Abarbanel, K. Yao, and A. Volkovskii, "Chaotic pulse position modulation: a robust method of communicating with chaos," *IEEE Communications Letters*, vol. 4, pp. 128–130, April 2000.

[76] B. M. Sadler and A. Swami, "On the performance of UWB and DS-spread spectrum communication systems," in *IEEE Conference on Ultra Wideband Systems and Technologies, UWBST*, (Baltimore, Maryland), pp. 289–292, May 2002.

[77] K. Siwiak, P. Withington, and S. Phelan, "Ultra-wide band radio: the emergence of an important new technology," in *IEEE 53rd Vehicular Technology Conference, VTC-Spring*, vol. 2, (Rhodes), pp. 1169–1172, 2001.

[78] J. R. Foerster, "The performance of a direct-sequence spread ultrawideband system in the presence of multipath, narrowband interference, and multiuser interference," in *IEEE Conference on Ultra Wideband Systems and Technologies, UWBST*, (Baltimore, Maryland), pp. 87–91, May 2002.

[79] V. S. SoMayazulu, "Multiple access performance in UWB systems using time hopping vs. direct sequence spreading," in *IEEE Wireless Communications and Networking Conference, WCNC*, vol. 2, (Orlando, FL), pp. 522–525, March 2002.

[80] N. Boubaker and K. B. Letaief, "Ultra wideband DSSS for multiple access communications using antipodal signaling," in *IEEE International Conference on Communications, ICC*, vol. 3, (Anchorage, Alaska), pp. 2197–2201, May 2003.

[81] K. Takizawa and R. Kohno, "Low-complexity rake reception and equalization for MBOK DS-UWB systems," in *IEEE Global Telecommunications Conference, GLOBECOM*, vol. 2, (Dallas, Texas), pp. 1249–1253, November–December 2004.

[82] Y. Kawashima, S. Sasaki, and H. Kikuchi, "Fractionally Spaced Selective Rake Reception for MBOK DS-UWB Systems," in *International Symposium on Intelligent Signal Processing and Communications, ISPACS*, (Yonago, Japan), pp. 187–190, December 2006.

[83] S. Verdu, "Wireless bandwidth in the making," *IEEE Communications Magazine*, vol. 38, pp. 53–58, July 2000.

[84] M. Hamalainen, V. Hovinen, J. Iinatti, and M. Latva-aho, "In-band interference power caused by different kinds of UWB signals at UMTS/WCDMA frequency bands," in *IEEE Radio and Wireless Conference, RAWCON*, (Waltham, MA), pp. 97–100, August 2001.

[85] M. Hamalainen, J. Iinatti, V. Hovinen, and M. Latva-aho, "In-band interference of three kinds of UWB signals in GPS L1 band and GSM900 uplink band," in *12th IEEE International Symposium on Personal, Indoor and Mobile Radio Communications, PIMRC*, vol. 1, (San Diego, CA), pp. 76–80, September–October 2001.

[86] H. Sato and T. Ohtsuki, "Frequency domain channel estimation and equalisation for direct sequence ultra wideband (DS-UWB) system," in *IEE Proceedings-Communications*, vol. 153, pp. 93–98, February 2006.

[87] M. A. Rahman, S. Sasaki, J. Zhou, and H. Kikuchi, "Simple-to-evaluate error probabilities for impulse radio UWB multiple access systems with pulse-based polarity randomization," *IEEE Communications Letters*, vol. 9, pp. 772–774, September 2005.

[88] M. A. Rahman, S. Sasaki, J. Zhou, and H. Kikuchi, "Error analysis for a hybrid DS/TH impulse radio UWB multiple access system," in *IEEE International Conference on Ultra-Wideband, ICU*, (Zurich, Switzerland), September 2005.

[89] R. Tesi, M. Hamalainen, J. Iinatti, J. Oppermann, and V. Hovinen, "On the multi-user interference study for ultra wideband communication systems in AWGN and modified Saleh-Valenzuela channel," in *Joint Conference on Ultrawideband Systems and Technologies with International Workshop on Ultra Wideband Systems,UWBST & IWUWBS*, (Kyoto, Japan), pp. 91–95, May 2004.

[90] Q. Li and L. A. Rusch, "Multiuser detection for DS-CDMA UWB in the home environment," *IEEE Journal on Selected Areas in Communications*, vol. 20, pp. 1701–1711, December 2002.

[91] B. Hu and N. C. Beaulieu, "Accurate BER of time-hopping and direct-sequence UWB systems in multi-user interference," in *IEEE Pacific Rim Conference on Communications, Computers and signal Processing, PACRIM*, (Victoria, Canada), pp. 25–28, August 2005.

[92] L. Piazzo, "Performance analysis and optimization for impulse radio and direct-sequence impulse radio in multiuser interference," *IEEE Transactions on Communications*, vol. 52, pp. 801–810, May 2004.

[93] N. Boubaker and K. B. Letaief, "Performance analysis of DS-UWB multiple access under imperfect power control," *IEEE Transactions on Communications*, vol. 52, pp. 1459–1463, September 2004.

[94] Z. Ye, A. S. Madhukumar, and F. Chin, "Power spectral density and in-band interference power of UWB signals at narrowband systems," in *IEEE International Conference on Communications, ICC*, vol. 6, (Paris, France), pp. 3561–3565, June 2004.

[95] M. Z. Win, "Spectral density of random time-hopping spread-spectrum UWB signals with uniform timing jitter," in *IEEE Military Communications Conference Proceedings, MILCOM*, vol. 2, (Atlantic City, NJ), pp. 1196–1200, October–November 1999.

[96] M. Z. Win, "Spectral density of random UWB signals," *IEEE Communications Letters*, vol. 6, pp. 526–528, December 2002.

[97] A. Taha and K. M. Chugg, "A theoretical study on the effects of interference UWB multiple access impulse radio," in *Thirty-Sixth Asilomar Conference on Signals, Systems and Computers*, vol. 1, (Pacific Grove, CA), pp. 728–732, November 2002.

[98] S. Villarreal-Reyes and R. M. Edwards, "Spectral line suppression in TH-IR ultra wideband systems," in *Fifth IEE International Conference on 3G Mobile Communication Technologies*, (London, UK), pp. 614–618, 2004.

[99] L. Piazzo and J. Romme, "Spectrum control by means of the TH code in UWB systems," in *IEEE 57th Vehicular Technology Conference, VTC-Spring*, vol. 3, (Jeju, Korea), pp. 1649–1653, April 2003.

[100] H. Khani and P. Azmi, "Performance analysis of TH-UWB radio systems using proper waveform design in the presence of narrow-band interference," in *European Transactions on Telecommunications*, vol. 17, pp. 111–123, April 2005.

[101] J. Romme and L. Piazzo, "On the power spectral density of time-hopping impulse radio," in *IEEE Conference on Ultra Wideband Systems and Technologies, UWBST*, (Baltimore, Maryland), pp. 241–244, May 2002.

[102] N. H. Lehmann and A. M. Haimovich, "The power spectral density of a time hopping UWB signal: a survey," in *IEEE Conference on Ultra Wideband Systems and Technologies, UWBST*, (Reston, Virginia), pp. 234–239, November 2003.

[103] R. A. Scholtz, R. Weaver, E. Homier, J. Lee, P. Hilmes, A. Taha, and R. Wilson, "UWB radio deployment challenges," in *11th IEEE International Symposium on Personal, Indoor and Mobile Radio Communications, PIMRC*, vol. 1, (London), pp. 620–625, September 2000.

[104] R. D. Wilson, R. D. Weaver, M. H. Chung, and R. A. Scholtz, "Ultra wideband interference effects on an amateur radio receiver," in *IEEE Conference on Ultra Wideband Systems and Technologies, UWBST*, (Baltimore, Maryland), pp. 315–319, May 2002.

[105] A. Batra, J. Balakrishnan, and A. Dabak, "Multi-band OFDM: a new approach for UWB," in *International Symposium on Circuits and Systems, ISCAS*, vol. 5, (Vancover, Canada), pp. 365–368, May 2004.

[106] J. Balakrishnan, A. Batra, and A. Dabak, "A multi-band OFDM system for UWB communication," in *IEEE Conference on Ultra Wideband Systems and Technologies, UWBST*, (Reston, Virginia), pp. 354–358, November 2003.

[107] K. Mandke, H. Nam, L. Yerramneni, C. Zuniga, and T. Rappaport, " The Evolution of Ultra Wide Band Radio for Wireless Personal Area Networks," in *High Frequency Electronics, Summit Technical Media LLC, www.highfrequencyelectronics.com/Archives/Sep03/HFE0903_TechReport.pdf*, pp. 22–32, September 2003.

[108] B. Muquet, Z. Wang, G. B. Giannakis, M. de Courville, and P. Duhamel, "Cyclic prefixing or zero padding for wireless multicarrier transmissions?," *IEEE Transactions on Communications*, vol. 50, pp. 2136–2148, December 2002.

[109] D. Falconer, S. L. Ariyavisitakul, A. Benyamin-Seeyar, and B. Eidson, "Frequency domain equalization for single-carrier broadband wireless systems," *IEEE Communications Magazine*, vol. 40, pp. 58–66, April 2002.

[110] P. Runkle, J. McCorkle, T. Miller, and M. Welborn, "DS-CDMA: The modulation technology of choice for UWB communications," in *IEEE Conference on Ultra Wideband Systems and Technologies, UWBST*, (Reston, Virginia), pp. 364–368, November 2003.

[111] G. Durisi and S. Benedetto, "Performance of coherent and noncoherent receivers for UWB communications," in *IEEE International Conference on Communications, ICC*, vol. 6, (Paris, France), pp. 3429–3433, 2004.

[112] D. Cassioli, M. Z. Win, F. Vatalaro, and A. F. Molisch, "Performance of low-complexity RAKE reception in a realistic UWB channel," in *IEEE International Conference on Communications, ICC*, vol. 2, (St.-Petersburg, Russia), pp. 763–767, April–May 2002.

[113] Z. Tian and G. B. Giannakis, "BER sensitivity to mistiming in ultra-wideband impulse Radios-part I: nonrandom channels," *IEEE Transactions on Signal Processing*, vol. 53, pp. 1550–1560, April 2005.

[114] B. Sklar, "Rayleigh Fading Channels in Mobile Digital Communications Systems Part 1: Characterization," *IEEE Communications Magazine*, vol. 35, pp. 102–109, July 1994.

[115] H. Lee, B. Han, Y. Shin, and S. Im, "Multipath characteristics of impulse radio channels," in *IEEE 51st Vehicular Technology Conference, VTC-Spring*, vol. 3, (Tokyo, Japan), pp. 2487–2491, May 2000.

[116] P. A. Bello, "Sample size required in error-rate measurement on fading channels," *Proceedings of the IEEE*, vol. 86, pp. 1435–1441, July 1998.

[117] J. Karedal, S. Wyne, P. Almers, F. Tufvesson, and A. F. Molisch, "Statistical analysis of the UWB channel in an industrial environment," in *IEEE 60th Vehicular Technology Conference, VTC*, vol. 1, (Los Angeles, CA), pp. 81–85, September 2004.

[118] S. S. Gassemzadeh, R. Januarya, C. Rice, W. Turin, and V. Tarokh, "Measurement and modeling of an ultra-wide bandwidth indoor channel," *IEEE Transactions on Communications*, vol. 52, pp. 1786–1796, October 2004.

[119] M. Z. Win and R. A. Scholtz, "On the robustness of ultra-wide bandwidth signals in dense multipath environments," *IEEE Communications Letters*, vol. 2, pp. 51–53, February 1998.

[120] M. Z. Win and R. A. Scholtz, "On the energy capture of ultrawide bandwidth signals in dense multipath environments," *IEEE Communciations Letters*, vol. 2, pp. 245–247, September 1998.

[121] S. S. Ghassemzadeh, L. J. Greenstein, A. Kavcic, T. Sveinsson, and V. Tarokh, "UWB indoor delay profile model for residential and commercial environments," in *IEEE 58th Vehicular Technology Conference, VTC-Fall*, vol. 5, (Orlando,Florida), pp. 3120–3125, October 2003.

[122] S. S. Ghassemzadeh, L. J. Greenstein, A. Kavcic, T. Sveinsson, and V. Tarokh, "UWB indoor path loss model for residential and commercial buildings," in *IEEE 58th Vehicular Technology Conference, VTC-Fall*, vol. 5, (Orlando, Florida), pp. 3115–3119, October 2003.

[123] S. S. Ghassemzadeh, L. J. Greenstein, T. Sveinsson, and V. Tarokh, "An impulse response model for residential wireless channels," in *IEEE Global Telecommunications Conference, GLOBECOM*, vol. 3, (San-Francisco, CA), pp. 1211–1215, December 2003.

[124] D. Cassioli, M. Z. Win, and A. F. Molisch, "The ultra-wide bandwidth indoor channel: from statistical model to simulations," *IEEE Journal on Selected Areas in Communciations*, vol. 20, pp. 1247–1257, August 2002.

[125] M. Z. Win and R. A. Scholtz, "Characterization of ultra-wide bandwidth wireless indoor channels: A communication theoretic view," *IEEE Journal on Selected Areas in Communications*, pp. 1613–1627, December 2002.

[126] M. M. Cramer, R. A. Scholtz, and M. Z. Win, "Evaluation of an ultra-wide band propagation channel," *IEEE Transactions on Antennas and Propagation*, vol. 50, pp. 561–570, May 2002.

[127] J. Kunisch and J. Pamp, "Measurement results and modeling aspects for the UWB radio channel," in *IEEE Conference on Ultra Wideband Systems and Technologies, UWBST*, (Baltimore, Maryland), pp. 19–23, May 2002.

[128] J. Keignart and N. Daniele, "Subnanosecond UWB channel sounding in frequency and temporal domain," in *IEEE Conference on Ultra Wideband Systems and Technologies, UWBST*, (Baltimore, Maryland), pp. 25–30, May 2002.

[129] H. Zhang, T. Udagawa, T. Arita, and M. Nakagawa, "A statistical model for the small-scale multipath fading characteristics of ultra wideband indoor channel," in *IEEE Conference on Ultra Wideband Systems and Technologies, UWBST*, (Baltimore, Maryland), pp. 81–85, May 2002.

[130] W. Turin, R. Januarya, S. S. Ghassemzadeh, C. W. Rice, and T. Tarokh, "Autoregressive modeling of an indoor UWB channel," in *IEEE Conference on Ultra Wideband Systems and Technologies, UWBST*, (Baltimore, Maryland), pp. 71–74, May 2002.

[131] Z. Irahhauten, H. Nikookar, and G. J. M. Januaryssen, "An Overview of Ultra Wide Band Indoor Channel Measurements and Modeling," *IEEE Microwave and Wireless Components Letters*, vol. 14, pp. 386–388, August 2004.

[132] A. Durantini, W. Ciccognani, and D. Cassiolo, "UWB Propagation Measurements by PN-Sequence Channel Sounding," in *IEEE International Conference on Communications, ICC*, vol. 6, (Paris, France), pp. 3414–3418, June 2004.

[133] A. A. M. Saleh and R. A. Valenzuela, "A Statistical Model for Indoor Multipath Propagation," *IEEE Journal on Selected Areas in Communications*, vol. 5, pp. 128–137, February 1987.

[134] W. Ciccognani, A. Durantini, and D. Cassioli, "Time domain propagation measurements of the UWB indoor channel using PN-sequence in the FCC-compliant band 3.6-6 GHz," *IEEE Transactions on Antennas and Propagation*, vol. 53, pp. 1542–1549, April 2005.

[135] A. F. Molisch, K. Balakrishnan, D. Cassioli, C. C. Chong, S. Emami, A. Fort, J. Karedal, J. Kunisch, H. Schantz, and K. Siwiak, "A Comprehensive Model for Ultrawideband Propagation Channels," in *IEEE Global Telecommunications Conference, GLOBECOM*, vol. 6, (St. Louis, Missouri), pp. 14–21, November–December 2005.

[136] C. C. Chong, Y. Kim, and S. S. Lee, "A modified S-V Clustering Channel Model for the UWB Indoor Residential Environment," in *IEEE 61st Vehicular Technology Conference, VTC*, vol. 1, (Stockholm, Sweden), pp. 58–62, June 2002.

[137] S. Venkatesh, J. Ibrahim, and R. M. Buehrer, "A New 2-Cluster Model for Indoor UWB Channel Measurements," in *IEEE International Symposium on Antennas and Propagation Society, ISAP*, vol. 1, (Monterey, CA), pp. 946–949, June 2004.

[138] L. J. Greenstein, S. S. Ghassemzadeh, S.-C. Hong, and V. Tarokh, "Comparison study of UWB indoor channel models," *IEEE Transactions on Wireless Communications*, vol. 6, pp. 128–135, January 2007.

[139] D. Cassioli, M. Z. Win, and A. F. Molisch, "A statistical model for the UWB indoor channel," in *IEEE 53rd Vehicular Technology Conference, VTC-Spring*, vol. 2, (Rhodes, Greece), pp. 1159–1163, May 2001.

[140] S. H. Song and Q. T. Zhang, "Dimension Diversity for the Enhancement of UWB Signal Detection," in *IEEE 63rd Vehicular Technology Conference, VTC-Spring*, vol. 3, (Melbourne, Vic.), pp. 1450–1454, 2006.

[141] D. Cassioli, M. Z. Win, F. Vatalaro, and A. F. Molisch, "Effects of Spreading Bandwidth on the performance of UWB Rake receiver," in *IEEE International Conference on Communications, ICC*, vol. 5, (Anchorage, Alaska), pp. 3545–3549, May 2003.

[142] L. L. Yang and L. Hanzo, "Performance of generalized multicarrier DS-CDMA over Nakagami-m fading channels," *IEEE Transactions on Communications*, vol. 50, pp. 956–966, June 2002.

[143] E. Fishler and H. V. Poor, "On the tradeoff between two types of processing gains," *IEEE Transactions on Communications*, vol. 53, pp. 1744–1753, October 2005.

[144] B. Hu and N. C. Beaulieu, "Comparison of direct-sequence impulse radio and direct-sequence ultra-wide bandwidth in multi-user interference," *IET Communications*, vol. 2, pp. 266–271, February 2008.

[145] E. Geraniotis, "Coherent hybrid DS-SFH spread-spectrum multiple-access communications," *IEEE Journal on Selected Areas in Communications*, vol. 3, pp. 695–705, September 1985.

[146] S. R. Aedudodla, S. VijayakuMarchan, and T. F. Wong, "Timing acquisition in ultra-wideband communication systems," *IEEE Transactions on Vehicular Technology*, vol. 54, pp. 1570–1583, September 2005.

[147] S. R. Aedudodla, S. VijayakuMarchan, and T. F. Wong, "Ultra-wideband signal acquisition with hybrid DS-TH spreading," *IEEE Transactions on Wireless Communications*, vol. 5, pp. 2504–2515, September 2006.

[148] Q. Z. Ahmed and L.-L. Yang, "Performance of hybrid direct-sequence time-hopping ultrawide bandwidth systems in nakagami-m fading channels," in *IEEE 18th International Symposium on Personal, Indoor and Mobile Radio Communications, PIMRC*, (Athens, Greece), pp. 1–5, September 2007.

[149] S. Verdu, *Multiuser Detection*. Cambridge University Press, 1998.

[150] L. Hanzo, L.-L. Yang, E.-L. Kuan, and K. Yen, *Single- and Multi-carrier DS-CDMA*. John Wiley and IEEE Press, 2003.

[151] E. G. Strom and S. L. Miller, "Properties of the single-bit single-user MMSE receiver for DS-CDMA systems," *IEEE Transactions on Communications*, vol. 47, pp. 416–425, March 1999.

[152] S. Moshavi, "Multi-user detection for DS-CDMA communications," *IEEE Communications Magazine*, vol. 34, no. 10, pp. 124–136, 1996.

[153] Z. D. Lei and T. J. Lim, "Simplified polynomial-expansion linear detectors for DS-CDMA systems," *Electronics Letters*, vol. 34, pp. 1561–1563, August 1998.

[154] B. Widrow and S. D. Stearns, *Adaptive Signal Processing*. Prentice Hall, 1985.

[155] Q. Z. Ahmed, W. Liu, and L.-L. Yang, "Least mean square aided adaptive detection in hybrid direct-sequence time-hopping ultrawide bandwidth systems," in *IEEE Vehicular Technology Conference, VTC Spring*, (Singapore), pp. 1062–1066, May 2008.

[156] L.-L. Yang, *Multicarrier Communications*. John Wiley & Sons Ltd., 2009.

[157] G. Woodward and B. S. Vucetic, "Adaptive detection for DS-CDMA," *Proceedings of the IEEE*, vol. 86, pp. 1413–1434, July 1998.

[158] K. C. Hwang and K. B. Lee, "Performance analysis of low processing gain DS/CDMA systems with random spreading sequences," *IEEE Communications Letters*, vol. 2, pp. 315–317, December 1998.

[159] W. A. Hamouda and P. J. McLane, "A fast adaptive algorithm for MMSE receivers in DS-CDMA systems," *IEEE Signal Processing Letters*, vol. 11, pp. 86–89, February 2004.

[160] C. N. Pateros and G. J. Saulnier, "An adaptive correlator receiver for direct-sequence spread-spectrum communication," *IEEE Transactions on Communications*, vol. 44, pp. 1543–1552, November 1996.

[161] A. K. Dutta and S. Kiaei, "Adaptive multiuser detector for asynchronous DS-CDMA in rayleigh fading," *IEEE Transactions on Circuits and Systems II: Analog and Digital Signal Processing*, vol. 44, pp. 468–472, June 1997.

[162] S. L. Miller and A. N. Barbosa, "A modified MMSE receiver for detection of DS-CDMA signals in fading channels," in *IEEE Military Communications Conference, MILCOM*, vol. 3, (McLean, VA), pp. 898–902, October 1996.

[163] A. N. Barbosa and S. L. Miller, "Adaptive detection of DS/CDMA signals in fading channels," *IEEE Transactions on Communications*, vol. 46, pp. 115–124, January 1998.

[164] Z. Liang, S. Zhu, and S. Wang, "A novel adaptive transmit-receive architecture for indoor DS-UWB systems," in *IEEE International Conference on Ultra-Wideband, ICU*, (Zurich, Switzerland), pp. 385–390, September 2005.

[165] V. Lottici, A. D'Andrea, and U. Mengali, "Channel estimation for ultra-wideband communications," *IEEE Journal on Selected Areas in Communications*, vol. 20, pp. 1638–1645, December 2002.

[166] S. Zhao, H. Liu, and Z. Tian, "Decision directed autocorrelation receivers for pulsed ultra-wideband systems," *IEEE Transactions on Wireless Communications*, vol. 5, pp. 2175–2184, August 2006.

[167] S. Zhao, H. Liu, and Z. Tian, "A decemberision-feedback autocorrelation receiver for pulsed ultra-wideband systems," in *IEEE Radio and Wireless Conference, RAWCON*, pp. 251–254, September, address=Atlanta, GA 2004.

[168] B. M. Sadler and A. Swami, "On the performance of episodic UWB and direct-sequence communication systems," *IEEE Transactions on Wireless Communications*, vol. 3, pp. 2246–2255, November 2004.

[169] M. L. Honig, S. L. Miller, M. J. Shensa, and L. B. Milstein, "Performance of adaptive linear interference suppression in the presence of dynamic fading," *IEEE Transactions on Communications*, vol. 49, pp. 635–645, April 2001.

[170] S. L. Miller, M. L. Honig, and L. B. Milstein, "Performance analysis of MMSE receivers for DS-CDMA in frequency-selective fading channels," *IEEE Transactions on Communications*, vol. 48, pp. 1919–1929, November 2000.

[171] J. Kusuma, I. Maravic, and M. Vetterli, "Sampling with finite rate of innovation: channel and timing estimation for UWB and GPS," in *IEEE International Conference on Communications, ICC*, vol. 5, pp. 3540–3544, May 2003.

[172] M. Honig and M. K. Tsatsanis, "Adaptive techniques for multiuser CDMA receivers," *IEEE Signal Processing Magazine*, vol. 17, pp. 49–61, May 2000.

[173] R. Kumar, "Convergence of a decision-directed adaptive equalizer," in *The 22nd IEEE Conference on Decision and Control*, vol. 22, pp. 1319–1324, December 1983.

[174] Z. Tian, L. Wu, and S. A. Zekavat, "Blind v.s. training-based UWB timing acquisition with effective multipath capture," in *Thirty-Seventh Asilomar Conference on Signals, Systems and Computers*, vol. 2, (Pacific Grove, CA), pp. 1771–1775, November 2003.

[175] Z. Tian and G. B. Giannakis, "A GLRT approach to data-aided timing acquisition in UWB radios-part i: algorithms," *IEEE Transactions on Wireless Communications*, vol. 4, pp. 2956–2967, November 2005.

[176] Z. Tian and G. B. Giannakis, "A GLRT approach to data-aided timing acquisition in UWB radios-part II: training sequence design," *IEEE Transactions on Wireless Communications*, vol. 4, pp. 2994–3004, November 2005.

[177] J. J. Shynk, "Frequency-domain and multirate adaptive filtering," *IEEE Signal Processing Magazine*, vol. 9, pp. 14–37, January 1992.

[178] C. Breining, P. Dreiscitel, E. Hansler, A. Mader, B. Nitsch, H. Puder, T. Schertler, G. Schmidt, and J. Tilp, "Acoustic echo control. an application of very-high-order adaptive filters," *IEEE Signal Processing Magazine*, vol. 16, pp. 42–69, July 1999.

[179] C. Paleologu and C. Vladeanu, "On the behavior of LMS adaptive algorithm in MMSE receivers for DS-CDMA systems," in *International Multi-Conference on Computing in the Global Information Technology*, (Guadeloupe, French Caribbean), pp. 12–12, March 2007.

[180] S. L. Miller, "An adaptive direct-sequence code-division multiple-access receiver for multiuser interference rejection," *IEEE Transactions on Communications*, vol. 43, no. 234, pp. 1746–1755, 1995.

[181] M. Montazeri and P. Duhamel, "A set of algorithms linking NLMS and block RLS algorithms," *IEEE Transactions on Signal Processing*, vol. 43, pp. 444–453, February 1995.

[182] S. C. Douglas, "Mean-square analysis of the multiple-error and block LMS adaptive algorithms," in *IEEE International Conference on Acoustics, Speech and Signal Processing, ICASSP*, (Adelaide, SA), April 1994.

[183] T. Aboulnasr and K. Mayyas, "A robust variable step-size LMS-type algorithm: analysis and simulations," *IEEE Transactions on Acoustics, Speech and Signal Processing*, vol. 45, pp. 631–639, March 1997.

[184] R. H. Kwong and E. W. Johnston, "A variable step size LMS algorithm," *IEEE Transactions on Acoustics, Speech and Signal Processing*, vol. 40, pp. 1633–1642, July 1992.

[185] R. Harris, D. Chabries, and F. Bishop, "A variable step (VS) adaptive filter algorithm," *IEEE Transactions on Acoustics, Speech and Signal Processing*, vol. 34, pp. 309–316, April 1986.

[186] M. Tarrab and A. Feuer, "Convergence and performance analysis of the normalized LMS algorithm with uncorrelated gaussian data," *IEEE Transactions on Information Theory*, vol. 34, pp. 680–691, July 1988.

[187] A. L. Swindlehurst, "Normalized adaptive decemberision directed equalization," *IEEE Signal Processing Letters*, vol. 5, pp. 18–20, January 1998.

[188] S. C. Douglas and T. H. Y. Meng, "Normalized data nonlinearities for LMS adaptation," *IEEE Transactions on Signal Processing*, vol. 42, pp. 1352–1365, June 1994.

[189] Y.-C. Liang and F. P. S. Chin, "Coherent LMS algorithms," *IEEE Communications Letters*, vol. 4, pp. 92–94, March 2000.

[190] M. Fukumoto, H. Kubota, and S. Tsujii, "Improvement in stability and convergence speed on normalized LMS algorithm," in *IEEE International Symposium on Circuits and Systems, ISCAS*, vol. 2, (Seattle, WA), pp. 1243–1246, April–May 1995.

[191] S. C. Douglas, "A family of normalized LMS algorithms," *IEEE Signal Processing Letters*, vol. 1, pp. 49–51, March 1994.

[192] G. O. Glentis, K. Berberidis, and S. Theodoridis, "Efficient least squares adaptive algorithms for FIR transversal filtering," *IEEE Signal Processing Magazine*, vol. 16, pp. 13–41, July 1999.

[193] J. G. Proakis, C. M. Rader, F. Ling, C. L. Nikias, M. Moonen, and I. K. Proudler, *Algorithms for Statistical Signal Processing*. Pearson Education, 2003.

[194] G. V. Moustakides, "Study of the transient phase of the forgetting factor RLS," *IEEE Transactions on Signal Processing*, vol. 45, pp. 2468–2476, October 1997.

[195] L. J. Zhu and U. Madhow, "Adaptive interference suppression for direct sequence CDMA over severely time-varying channels," in *IEEE Global Telecommunications Conference, GLOBECOM*, vol. 2, (Phoenix, AZ), pp. 917–922, November 1997.

[196] H. L. V. Trees, *Optimum Array Processing*. Wiley Interscience, 2002.

[197] X. Wang and H. V. Poor, *Wireless Communication Systems Advanced Techniques for Signal Reception*. Prentice Hall, 2004.

[198] M. L. Honig, "A comparison of subspace adaptive filtering techniques for DS-CDMA interference suppression," in *IEEE Military Communications Conference, MILCOM*, vol. 2, (Monterey, CA), pp. 836–840, November 1997.

[199] S. Burykh and K. Abed-Meraim, "Reduced-rank adaptive filtering using krylov subspace," *Eurasip Journal on Applied Signal Processing*, no. 12, pp. 1387–1400, 2002.

[200] J. S. Goldstein, I. S. Reed, and L. L. Scharf, "A multistage representation of the wiener filter based on orthogonal projections," *IEEE Transactions on Information Theory*, vol. 44, pp. 2943–2959, November 1998.

[201] L.-L. Yang, "Reduced-rank MMSE detection in space-time coded space-division multiple-access systems," in *IEEE 17th International Symposium on Personal, Indoor and Mobile Radio Communications, PIMRC*, (Helsinki), pp. 1–5, September 2006.

[202] J. S. Goldstein and I. S. Reed, "Reduced-rank adaptive filtering," *IEEE Transactions on] Signal Processing*, vol. 45, pp. 492–496, February 1997.

[203] M. L. Honig and J. S. Goldstein, "Adaptive reduced-rank residual correlation algorithms for DS-CDMA interference suppression," in *Thirty-Second Asilomar Conference on Signals, Systems & Computers*, vol. 2, (Pacific Grove, CA), pp. 1106–1110, November 1998.

[204] K. A. Byerly and R. A. Roberts, "Output power based partially adaptive array design," in *23rd AsiloMarch Conference on Signals, Systems and Computers*, (Pacific Grove, CA), pp. 576–580, November 1989.

[205] P. Thanyasrisung, I. S. Reed, and X. Yu, "Reduced-rank MMSE multiuser receiver for synchronous CDMA," in *21st Century Military Communications Conference Proceedings MILCOM*, vol. 1, (Los Angeles, CA), pp. 569–573, October 2000.

[206] A. J. Thorpe and L. L. Scharf, "Data adaptive rank-shaping methods for solving least squares problems," *IEEE Transactions on Signal Processing*, vol. 43, pp. 1591–1601, July 1995.

[207] P. A. Zulch, J. S. Goldstein, J. R. Guerci, and L. S. Reed, "Comparison of reduced-rank signal processing techniques," in *Thirty-Second Asilomar Conference on Signals, Systems & Computers*, vol. 1, (Pacific Grove, CA), pp. 421–425, November 1998.

[208] S. Moshavi, E. G. Kanterakis, and D. L. Schilling, "A new multiuser detection scheme for DS-CDMA systems," in *IEEE Conference on Military Communications, MILCOM*, vol. 2, (San Diego, CA), pp. 518–522, November 1995.

[209] E. G. Strom, S. Parkvall, S. L. Miller, and B. E. Ottersten, "Complexity reduction of direct-sequence code division multiple access receivers," in *IEEE International Conference on Communications, ICC*, (New Orleans, LA), pp. 1643–1647, May 1994.

[210] M. L. Honig and J. S. Goldstein, "Adaptive reduced-rank interference suppression based on the multistage wiener filter," *IEEE Transactions on Communications*, vol. 50, pp. 986–994, June 2002.

[211] J. Cioffi, "Limited-precision effects in adaptive filtering," *IEEE Transactions on Circuits and Systems*, vol. 34, pp. 821–833, July 1987.

[212] M. L. M. L. Honig and W. Xiao, "Performance of reduced-rank linear interference suppression," *IEEE Transactions on Information Theory*, vol. 47, pp. 1928–1946, July 2001.

[213] X. Wang and H. V. Poor, "Blind adaptive multiuser detection in multipath CDMA channels based on subspace tracking," *IEEE Transactions on Signal Processing*, vol. 46, pp. 3030–3044, November 1998.

[214] Z. Tian, H. Ge, and L. L. Scharf, "Low-complexity multiuser detection and reduced-rank wiener filters for ultra-wideband multiple access," in *IEEE International Conference on Acoustics, Speech and Signal Processing, (ICASSP)*, vol. 3, (Philadelphia, PA), March 2005.

[215] P. Strobach, "Low-rank adaptive filters," *IEEE Transactions on Signal Processing*, vol. 44, pp. 2932–2947, December 1996.

[216] B. Yang, "Projection approximation subspace tracking," *IEEE Transactions on Signal Processing*, vol. 43, pp. 95–107, January 1995.

[217] J. S. Goldstein and I. S. Reed, "Theory of partially adaptive radar," *IEEE Transactions on Aerospace and Electronic Systems*, vol. 33, pp. 1309–1325, October 1997.

[218] J. S. Goldstein, S. M. Kogon, I. S. Reed, D. B. Williams, and E. J. Holder, "Partially adaptive radar signal processing: the cross-spectral approach," in *Twenty-Ninth Asilomarh Conference on Signals, Systems and Computers*, vol. 2, (Pacific Grove, CA), pp. 1383–1387, October–November 1995.

[219] S. Moshavi, E. G. Kanterakis, and D. L. Schilling, "Multistage linear receivers for ds-cdma systems," *International Journal of Wireless Information Networks*, vol. 3, pp. 1–17, January 1996.

[220] G. M. A. Sessler and F. K. Jondral, "Low complexity polynomial expansion multiuser detector for CDMA systems," *IEEE Transactions on Vehicular Technology*, vol. 54, pp. 1379–1391, July 2005.

[221] G. M. A. Sessler and F. K. Jondral, "Rapidly converging polynomial expansion multiuser detector with low complexity for CDMA systems," *IEEE Electronics Letters*, vol. 38, pp. 997–998, August 2002.

[222] J. Y. Pan, C. B. Soh, and E. Gunawan, "Reduced-complexity iterative multiuser detection scheme for CDMA," *IEEE Electronics Letters*, vol. 36, pp. 839–840, April 2000.

[223] A. Dua, "Adaptive implementation of polynomial expansion detector for multi-user detection in DS-CDMA systems," *IEEE Electronics Letters*, vol. 37, pp. 1384–1386, November 2001.

[224] Z. Li and W. Ser, "An adaptive WPE multiuser detector," *IEEE Signal Processing Letters*, vol. 12, pp. 305–308, April 2005.

[225] W. Chen and U. Mitra, "Reduced-rank detection schemes for DS-CDMA communication systems," in *IEEE Military Communications Conference, MILCOM*, vol. 2, (Washington, D.C.), pp. 1065–1069, October 2001.

[226] P. Comon and G. H. Golub, "Tracking a few extreme singular values and vectors in signal processing," *Proceedings of the IEEE*, vol. 78, pp. 1327–1343, August 1990.

[227] G. H. Golub and C. F. V. Loan, *Matrix Computations*. North Oxford Academic Publishing Company Limited, 1983.

[228] S. Chen, S. Tan, L. Xu, and L. Hanzo, "Adaptive minimum error-rate filtering design: A Review," *IEEE Transactions on Signal Processing*, vol. 88, no. 7, pp. 1671–1679, 2008.

[229] Q. Z. Ahmed and L. L. Yang, "Reduced-rank detection for hybrid direct-sequence time- hopping UWB systems in nakagami-m fading channels," in *IEEE 68th Vehicular Technology Conference, VTC-Fall*, (Calgary, Canada), pp. 1–5, September 2008.

[230] G. H. Dunteman, *Principal components analysis.* Newbury Park, 1989.

Index

M

N

O

P

Q

R

S

T

U

W

Z

Author Index

C

D

E

F

G

H

I

J

K

L

M

N

O

P

Q

R

S

T

U

V

W

X

Y

Z